UNIVERSITAT DE BARCELONA

Inversion Tectonics in the Alpine Foreland, Eastern Alps (Austria)

Pablo Martínez Granado

Institut de Recerca Geomodels

Departament de Dinàmica de la Terra i de l'Oceà

Grup de Recerca de Geodinàmica i Anàlisi de Conques

Universitat de Barcelona

Inversion Tectonics in the Alpine Foreland, Eastern Alps (Austria)

Memòria de Tesi Doctoral -com a compendi d'articles- presentada per **Pablo Martínez Granado** per optar al grau de Doctor en Ciències Geològiques per la Universitat de Barcelona.
Aquesta memòria ha estat realitzada dintre del Programa de Doctorat de "Ciènces de la Terra" (R.D. 99/2011) sota la direcció del **Dr. Josep Anton Muñoz i de la Fuente.**

Pablo Martínez Granado
Març 2017

Dr. Josep Anton Muñoz i de la Fuente

This PhD thesis has been carried out at the Departament de Dinàmica de la Terra i de l'Oceà (formerly Departament de Geodinàmica i Geofísica), within the Institut de Recerca Geomodels and the Grup de Recerca de Geodinàmica i Anàlisi de Conques (2014SGR467SGR) from the Agència de Gestió d'Ajuts Universitaris i de Recerca (AGAUR) and the Secretaria d'Universitats i Recerca del Departament d'Economia i Coneixement de la Generalitat de Catalunya and the Fundació Bosch i Gimpera. Pablo Martínez Granado benefited from the financial support provided by OMV Exploration and Production GmbH (Austria) under the project FBG307451 entitled "Inversion tectonics in the Höflein area". Sandbox analogue models were carried out at the SIMGEO-Geomodels Analogue Modelling Laboratory supported by a Scientific Infrastructure (UNBA08-4E-006) and co-funded by Statoil and the European Regional Development Fund of the Ministerio de Ciencia e Innovación of the Spanish Government.

A los mis padres y al Edu

Ackwoledgements

In the first place I want to thank the financial support provided by OMV Exploration and Production GmbH through the project FBG307451 "Inversion tectonics in the Höflein area". This thesis could not have been possible without their funding. I want to express my gratitude to OMV for the permission to publish the data used and the interpretations carried out during this thesis. I also take this chance to thank the OMV staff from the exploration and production offices in Vienna and Gäserndorf. I specially thank the support from Philipp Strauss and Wolfgang Thöny, for triggering this project as well as for their trust during these years. Similarly, I want to express my gratitude to a part of the OMV staff that, in one way or another, have contributed to this thesis, including: Andreas Beidinger, Michael Bierbaumer, Evelina Burghelea, Rudolf Dellmuor, Rudolf Finsterwalder, Oliver Gratzer, Ralph Hinsch, Wolfgang Hujer, Christian Kling, Michael König, Anna Kruk, Friedrich Kucher, Johannses Loisl, Herwig Peresson, Gabor Tari and Andras Zamolyi.

I also thank the Department of Earth Dynamics and Ocean Sciences (formerly Department of Geodynamics and Geophysics), the Administration and Services staff of the Faculty of Earth Sciences from the University of Barcelona, the Geomodels Research Institute, the Geodynamics and Basin Analysis Group (2014SGR467SGR) for their direct or indirect participation in this thesis. I also genuinely thank the administrative work from Teresa Beamud Amorós from the Geomodels Research Institute.

This theis has been made by a compilation of two articles in which several people have been involved. I think it is fair to dedicate a few words for them. I want to thank the co-authors, and specially my supervisor Josep Anton Muñoz, for the suggestions and discussions that arose during the completion of thesis and the production of the articles. I also want to express my gratitude to two anonymous reviewers that participated on the reviews of the first article, along with Dennis Brown (Institut Jaume Almera, CSIC-Barcelona) and Olivier Lacombe (Université Pierre et Marie Curie - Paris VI) as co-editors of the special volume in which the article was finally published. My gratitude as well for João C. Duarte (Universidade de Lisboa), Stephane Dominguez (Université de Montpellier) and Philippe Agard (Université Pierre et Marie Curie - Paris VI) for their roles as reviewers, and editor-in-chief, respectively, of the analogue modelling article.

I obviously have a few words for my PhD supervisor Josep Anton Muñoz. He has been my boss for about 8 years now, and almost 4 years as PhD supervisor. As the Director of the Geomodels Research Institute, Josep Anton has supervised my scientific and consultancy work in the Pyrenees, the Cantabrian Mountains, the Bolivian Andes, the Western Mediterranean, and ultimately, in the Alpine-Carpathian fold-and-thrust belt. During this time, I recognise I have critised Josep Anton for being probably too laid back (kind of common for PhD supervisors I presume), or for not being around when needed in desperate project deadlines. On the other hand, I admire him not just only for his knowledge on Earth Sciences, or his technical skills, his ability for getting to the point of things, and for turning things around. I genuinely respect Josep Anton for being a fund raiser, for making his vision for real, and for keeping it alive.

I also have some words of gratitude to my "fish-tank" co-workers Núria Carrera, Marco de Matteis, Oscar Gratacós, Joana Mencos, Mireia Butille, Roger Clavera, Anna Carmona, Oriol Ferrer, Oriol Pla, Maria Roma, and Frederic Escosa. I have special thanks to Pau Arbués for his friendship, for introducing me into the Pyrenean turbidites and growth strata, and for completing those drill holes in the boiling Tabernas summer; no one would have bet a nickel on us! I want to express my most sincere gratitude to my friend Stefano Tavani for becoming the "problem makers" and to Luis Valero for his support and counsel in these last years. I also want to thank Marco Snidero for his unique spirit during these years, and for his help with the analogue models time-lapse videos. I also thank Esther Izquierdo and Pablo Santolaria for their feedbakcs regarding the scaling of the sandbox models.

Finally I want to thank you, Esther, for your understanding during these years, for your help in the proof reading of this thesis, but most importantly, for your care and loving support in the good and the bad times. I also have to thank a very long list of friends, either here, or in the distance. I genuinely thank my parents, and in particular my father, for their continuos support, and for their restless and active role in providing love and respect.

Thank you very much to all of you!

Table of Contents

Figure List

Chapter 2

Chapter 3

Chapter 4

Table List

Chapter 2

PREFACE AND DESCRIPTION OF THE MEMOIR

This memoir is presented as a compilation of two scientific articles published on citation index journals. This thesis spins off from a 2-year industry project entitled "Inversion tectonics in the Höflein area" funded by the Austrian-based company OMV Exploration and Production GmbH. The project aimed at re-appraising a large compilation of vintage industry data from the prolific Alpine-Carpathian foreland fold-and-thrust belt, and assessing whether any structural traps related to positive inversion tectonics may remain undiscovered in the deeply buried sub-thrust region. This thesis benefited from a wealth of 2D and 3D seismic data, geophysical logs as well as a detailed chronostratigraphic framework from the numerous wells drilled in the area. The study has allowed gaining additional understandings into the deformation processes that occur at collisional foredeeps and the deep roots of the external parts of fold-and-thrust belts. This line of research has been complemented with the realization of a series of scaled sandbox analogue models of tectonic wedges incorporating buried half-graben basins in sub-thrust and foreland settings.

Chapter 2 provides an introduction to the Alpine-Carpathian-Pannonian geodynamical framework, from its Mesozoic paleogeography to the present day. The chapter introduces the structure, stratigraphy and timing of key events that affected the Neo-Tethys, Alpine Tethys and Para-Tethys realms. In this chapter, definitions, examples and the fundamental importance of basin inversion on the evolution orogenic systems is provided. This introduction is followed by an overview on the impacts of inversion tectonics on the prospectivity of natural resources. The fundamental diagnostic characteristics and tools for the proper assessment and definition of positively inverted rifts are also summarised. A brief note on the mechanics of fault reactivation inherent to basin inversion is also given. An introduction to the published articles is provided with the intention of linking the main parts of the research carried out. The data and methodology used are also briefly provided.

In **Chapter 3** the general results of this thesis are described. The first part summarises the processes of basement-involved deformation recorded in the Alpine-Carpathian Junction, its foredeep and its sub-thrust. The regional 3D structure of the Lower Austria Mesozoic Basin is illustrated as well as the timing and structural styles related to the extensional and compressional reactivation of its basement fault array. The processes are contextualised within its European geodynamic framework. On a second part, **Chapter 3** also describes the general results of inversion tectonics within brittle and

brittle-viscous tectonic wedges simulated by sandbox analogue models. In this section, the objectives, experimental set ups, results and implications are stated.

Chapter 4 provides a summary for the discussions that have been provided in the published articles. The chapter integrates the outcome from the two separate articles -from nature and models- into a discussion with local and general implications for the general understanding of foredeep and sub-thrust deformation patterns.

Chapter 5 lists the summary of the conclusions of this thesis.

Chapter 6 lists all the references mentioned throughout the text.

The published articles and the videos generated from time-lapse photography of the sandbox models are also provided in the **Appendix** and the attached **DVD**, respectively.

CHAPTER 1. SUMMARY

In this thesis, the 3D structure and kinematics of the locally and mildly inverted Lower Austria Mesozoic Basin beneath the Alpine-Carpathian fold-and-thrust belt is described. This study has been carried out by the integrative interpretation of 2D and 3D seismic surveys, well and geophysical logs data and gravity maps. A basin-scale, 3D structural model has been carried out, focused on the sub-thrust and foreland zones. The Late Eocene to Early Miocene Alpine–Carpathian fold-and-thrust belt resulted from the subduction of the European plate beneath the Adriatic one, and the subsequent continental collision between both plates. The Alpine–Carpathian foredeep and fold-and-thrust belt recorded the long-lasting involvement of the European crystalline basement in several deformation events: from late Variscan transtension, to Jurassic rifting, and Cretaceous to Neogene shortening. In this thesis, two additional basement fault reactivation events have been defined in relation to the Alpine-Carpathian Cenozoic shortening: an extensional reactivation event related to the bending of the European plate coeval with Egerian to Karpatian (*ca.* 28–16 Ma) thin-skinned thrusting; followed by the selective positive inversion of the basement faults in the sub-thrust and in the foreland during Karpatian to Badenian times (*ca.* 16-12.5 Ma). The flexural bending of the European plate and the associated extensional fault reactivation were promoted by high lateral gradients of lithospheric strength in addition to the slab pull forces associated with subduction. Delamination of the European lithosphere during the final stages of collision around Karpatian times (*ca.* 16 Ma) promoted a large-wavelength uplift and an excessive topographic load. This topographic load was compensated by broadening the orogenic wedge through the compressional reactivation of the inherited fault array in the Euroepan plate beneath and ahead of the thin-skinned thrust system. Ultimately, collapse and deep burial of the Alpine-Carpathian tectonic wedge took place by the formation of the Pannonian basins system.

To gain further insights in the deformational processes in sub-thrust and foreland settings, sandbox analogue models of brittle and brittle-viscous sand wedges have been carried out. The models aimed testing the influence of different topographic loads (i.e., thrust wedges) on the sub-thrust inversion of extensional basins, as well as the influence of the initial orientation of the extensional basins, and the presence or absence of weak detachment layers. Segmented half-graben basins -striking at 90º, 45º and 15º to the extension direction- were created first, and then shortened using different angles for the

basal detachment and topographic slope. A shallow layer of viscous polymer over the half-graben basin was included in one of the models. The experiments were analysed using time-lapse photography, topography laser scans and image-based 3D voxels. The modelling results indicate a deformation sequence characterised by layer-parallel compaction, fault reactivation, thrust propagation and related folding. Fault reactivation and basin inversion were associated with layer-parallel compaction accomplished by slip along the basal detachment, prior to and in between pulses of thrusting. The results of the sandbox analogue models reveal a fundamental control imposed by the vertical load of the tectonic wedge and its integrated strength profile in the inversion of sub-thrust basins. Small vertical loads or strong gradients of vertical load have revealed as fundamental factors aiding in the inversion of buried, sub-thrust basins. The integrated strength profile resulted from the combination of inherited, strain-softened fault zones, as well as the presence or absence and distribution of weak, viscous horizons. The results of the sandbox models carried out indicate that the vertical load, its gradient over the sub-thrust basins and the inherited, strain-softened faults, are more important than the obliquity between the direction of shortening and the orientation of pre-existing fault systems. As indicated by the results of sandbox analogue models, the recurrent and long-lasting frictional reactivation of the Lower Austria basement fault array may have been favoured by fault-weakening mechanisms, as well as by steep gradients of vertical loads generated by thin-skinned out-of-sequence stacking of the Rhenodanubian Flysch located south of the inverted basement fault array.

CHAPTER 2. GENERAL INTRODUCTION

2.1 INTRODUCTION

The involvement of basement has been widely recognised in collisional foredeeps and underneath active deformation belts. Basement-involved deformation in these settings commonly encompasses the inversion of former sedimentary basins inherited from previous rifting episodes. The understanding of the processes controlling this type of deformation is important due to their economic and social impact in terms of the exploration and management of natural resources, or the associated seismic risk within the margins and interiors of plates. This thesis arises from a hydrocarbon exploration assessment carried in the Alpine-Carpathian fold-and-thrust belt (NE Austria) in a collaboration between the Institut de Recerca Geomodels (University of Barcelona) and the Austrian company OMV Exploration and Production GmbH. The company provided the funds and a wealth of seismic and well data to carry out the study. The study of these data has allowed investigating the processes of basement-involved deformation in the collisional foredeep and the deeply-buried sub-thrust setting of the Alpine-Carpathian fold-and-thrust belt. The results of this study have implications for the yet-to-find hydrocarbons of the area, but are also relevant to the understanding of the geological evolution of the Alpine-Carpathian-Pannonian area and orogenic systems in general.

The main objective of this thesis is to document, explain and contextualise the processes of fault reactivation and basin inversion, and the interplay between shallow thin-skinned tectonics and deeper thick-skinned deformation in fold-and-thrust belts. The first documentation of basement-involved basin inversion in the studied area was compiled by Ziegler (1987) but exclusively referred to a Lower Cretaceous intraplate shortening event that affected the European plate at the onset of the Alpine orogenesis. During this thesis, the first evidences for a Cenozoic extensional and compressional basement-involved reactivation encompassing basin inversion in the foreland and in the sub-thrust of the Alpine-Carpathian Junction have been recognised and described.

The Alpine-Carpathian fold-and-thrust belt is a mature hydrocarbon province where production and hydrocarbons dates back to the XIX century (Janoschek et al. 1996). In particular, the Höflein field is the only commercial hydrocarbon accumulation sitting on the former Jurassic continental margin of Europe, in the so-called Autochthonous Mesozoic (Wessely, 1987) of Lower Austria. It was discovered in the early 1980's using 2D seismic profiles, and subsequently appraised and developed with 3D seismic data and

additional wells. Hydrocarbons are trapped in the Jurassic post-rift cover and in thin syn-rift deposits on a structural high known as the Höflein high (Zimmer and Wessely, 1996). Although this structure is significantly elevated above any other basement high of the Lower Austria Mesozoic Basin, it was traditionally perceived as the tilted footwall of a purely extensional half-graben. Recent drilling results on the hanging-wall of the Höflein half-graben intersected post-rift and thick syn-rift units above the regional expected depths. These results challenged the traditional purely-extensional interpretation, and suggested that the Höflein high may be the result of positive inversion tectonics, thus indicating the potential existence of a new exploration concept for the deep sub-thrust "Autochthonous" Mesozoic.

To validate this new exploration approach, and to probe whether it could be applied to the rest of the Lower Austria acreage, a detailed 3D structural model of the Höflein high from seismically mapped horizons and faults had to be built. The tectonic model derived from this 3D model of the Höflein high had to be extended to the whole Lower Austria Mesozoic Basin beneath the Alpine-Carpathian foreland basin, the fold-and-thrust belt and, to some extent, beneath the middle to late Miocene Vienna Basin.

The regional tectonic model had to be brought and explained within the European Alpine-Carpathian geodynamical context. The Alpine-Carpathian Junction has an astonishing and long-lived geological history, spanning from Jurassic rifting through subduction and accretion followed by continental collision and collapse of the orogenic edifice by extensional and strike-slip tectonics accommpained by intense volcanic activity. It is in such a complicated setting that the inversion of the deeply buried continental margin basins had to contextualised and explained. This study has provided the opportunity for gaining additional understanding in the deformation processes in collisional foredeeps and sub-thrust settings within fold-and-thrust belts.

2.2 BRIEF INTRODUCTION TO THE EUROPEAN ALPS, THE WESTERN CARPATHIANS AND THE PANNONIAN BASINS

A brief introduction to the tectonics and paleogeography of the European Alps and the Western Carpathians is provided to contextualise this thesis. Given the inherent complexity of the European Alpides as a whole and the clearly stated objectives of this thesis, only the most relevant aspects will be summarised in the following to provide the unfamiliar reader a paleogeographic and tectonic context. The reader should be aware of the many unresolved issues regarding, amongst others, the paleogeographical affinity of different tectonic units, the pre orogenic boundary conditions, as well as the deep lithospheric structure of the European Alpine system. Although a throughout review of the Alpine evolution is not intended in this introduction, emphasis has been given to cover those aspects considered fundamental for understanding of this complicated orogenic system. The reader can refer to concise historical reviews of Alpine studies provided by Trümpy (2001) and Dal Piaz (2001), as well as to the many references that will be provided along.

The European Alps are probably the most studied orogenic system on Earth. It was in this mountain belt where the first "mobilistic" ideas involving large horizontal displacements and related crustal deformations were proposed (e.g. Suess, 1875; Argand, 1911, 1924). These ideas were soon discarded by Alpine scientists in favour of the Earth's shrinking or gravitational gliding models. On the contrary, the thrust tectonics models were accepted in the Carpathian region between the latest 18th and early 19th centuries, as this tectonic concept was proven by early exploratory drilling (see Picha et al. 2006 for a synthesis). However, it was not until the late 1960's and the early 1970's that modern plate tectonics -earlier postulated by marine geophysicists in the late 1950's- was applied to the European Alps (e.g. Laubscher, 1969, 1971; Dewey and Bird, 1970; Smith, 1971; Dal Piaz et al. 1972; Dewey et al. 1973). These were the first authors that interpreted the Alpine chain as the result of oceanic subduction followed by continental collision. In more recent years, significant efforts from the European scientific community have contributed to improving the understanding of the Alpine belt. Paramount advances came from regional seismic refraction studies such as the ECORS-CROP (ECORS-CROP Deep Seismic Sounding Group, reviewed by Roure et al. 1996), the EUROPEAN GEOTRAVERSE (Blundell et al. 1992), the National Research Program NPR-20 profiles (Pfiffner et al. 1997), the TRANSALP (TRANSALP Working Group, 2002), CELEBRATION 2000

(Guterch et al. 2003), ALP 2002 (Brückl et al. 2007), the NESTMK (Graßl et al. 2004) and global seismic tomography imaging (Bijwaard and Spackman, 2000; Cavazza et al. 2004). The current understanding of the Alpine belt has been summarised on several review publications including Coward and Dietrich (1989), Schmid et al. (1989, 1990, 1996, 2004, 2008), Froitzheim et al. (1996), Schmid and Kissling (2000), Rosembaun et al. (2002), Cavazza et al. (2004), Rosembaun and Lister (2005), Golonka and Picha (2006), Dumond et al. (2008), Froitzheim et al. (2008), Beltrando et al. (2010), Handy et al. (2010, 2015), DeGraciansky et al. (2011), Malusà et al. (2011), Carminati and Doglioni (2012), Schlunegger and Kissling (2015), amongst many others. Regional seismic profiles and global tomography studies integrated with decades of surface geology mapping and radiometric dating of tectono-metamorphic events (i.e., P-T-t-d paths) have defined the current understanding of the Alps.

Broadly speaking, the geological units of the European Alps and the Western Carpathians have registered the break-up of Gondwana following the Variscan orogeny, the opening and closure of several oceanic basins belonging to the Neo-Tethys and the Alpine Tethys realms in the Cretaceous Eo-Alpine and the Cenozoic Neo-Alpine orogenies, as well as the subsequent formation of the Para-Tethys realm. On a more local scale, but somehow significantly important for this thesis, key concepts of basin inversion were also developed for the first time from fieldwork studies on the external parts of the Alps (Gillcrist et al. 1987; Ziegler, 1987; Grand, 1988; Butler, 1989; DeGraciansky et al. 1989; Coward et al. 1991).

2.2.1 GEOGRAPHICAL OUTLINE OF THE ALPS, CARPATHIANS AND PANNONIAN BASIN

The European Alps and the Western Carpathians are located in south-central Europe and belong to the northern Circum-Mediterranean Alpine orogenic belt (**Fig. 2.1**). The European Alps and the Western Carpathians constitute a mountain chain of *ca.* 1500 km in length and about 120 to 300 km wide. At their western termination, the Alps describe a westward-convex arc around which the strike of the belt turns about 180°. At its central parts, the mountain belt widens and displays a rather straight ENE-WSW orientation. To the east, the Western Carpathians also describe a northward-convex arc, less pronounced than the western end of the chain. As a whole, the Carpathians describe a

wide arc that surrounds the Neogene Pannonian Basin system. This large basin is bound by the Dinarides chain to the SW and by the Balkan ranges to the S (**Fig. 2.1**).

Geographically speaking, the European Alps have been divided into the Western, Central, Eastern and Southern Alps (**Fig. 2.1**). The boundary between the Western and the Central Alps runs from Lake Geneva to the north, to the Rhone Valley over the Grand St. Bernard Pass in Switzerland, along the Aosta Valley down south to the Po Plain in Italy. The boundary between the Central and the Eastern Alps is defined from Lake Constance in Switzerland southward along the Rhine Valley, the Splügen Pass and the Lake Como in Italy. The boundary between the Southern Alps and the other parts of the European Alps is defined by a trend of roughly E-W oriented valleys, namely the Valtellina, Pustertal and Gaital. These valleys are the geomorphological expression of a major Cenozoic right-lateral fault known as the Periadriatic Fault or Insubric Line (**Fig. 2.1**).

The boundary between the Eastern Alps and the Western Carpathians is represented by a roughly N-S striking imaginary line running southwards from the city of Vienna (**Fig. 2.1**). This area south of the Bohemian massif is referred to as the Alpine-Carpathian Junction. There, the Alpine relief disappears eastwards of this N-S imaginary line beneath the low-lying Hungarian plains and their thick Neogene cover (**Fig. 2.1**). Further to the east and northeast, relief is regained in the Western Carpathians. The Western Carpathians include the high relief northern mountains but also include the subsurface of the wide low-lying plains of the Pannonian Basin (**Fig. 2.1**). The Western Carpathians extend from the easternmost Eastern Alps up to the Eastern Carpathians. The boundary between the Western and the Eastern Carpathians is conventionally given by the roughly N-S trending Polish and Slovakian border with Ukraine. From a geographical point of view, the Western Carpathians are divided into the properly mountainous Western Carpathians, the lowlands of the north-westerly Vienna and Danube basins and the NW part of the Great Hungarian Plain. The mountainous Western Carpathians are subdivided into the Outer Western Carpathians and the Inner Western Carpathians, partly separated by the Pieniny klippen Belt. The External Western Carpathians extend along NE Austria, the SE part of Moravia (i.e., in the Czech Republic), the north of Slovakia and SE Poland, whereas the Internal Western Carpathians are restricted to Slovakia, and to local inselbergs in northern Hungary.

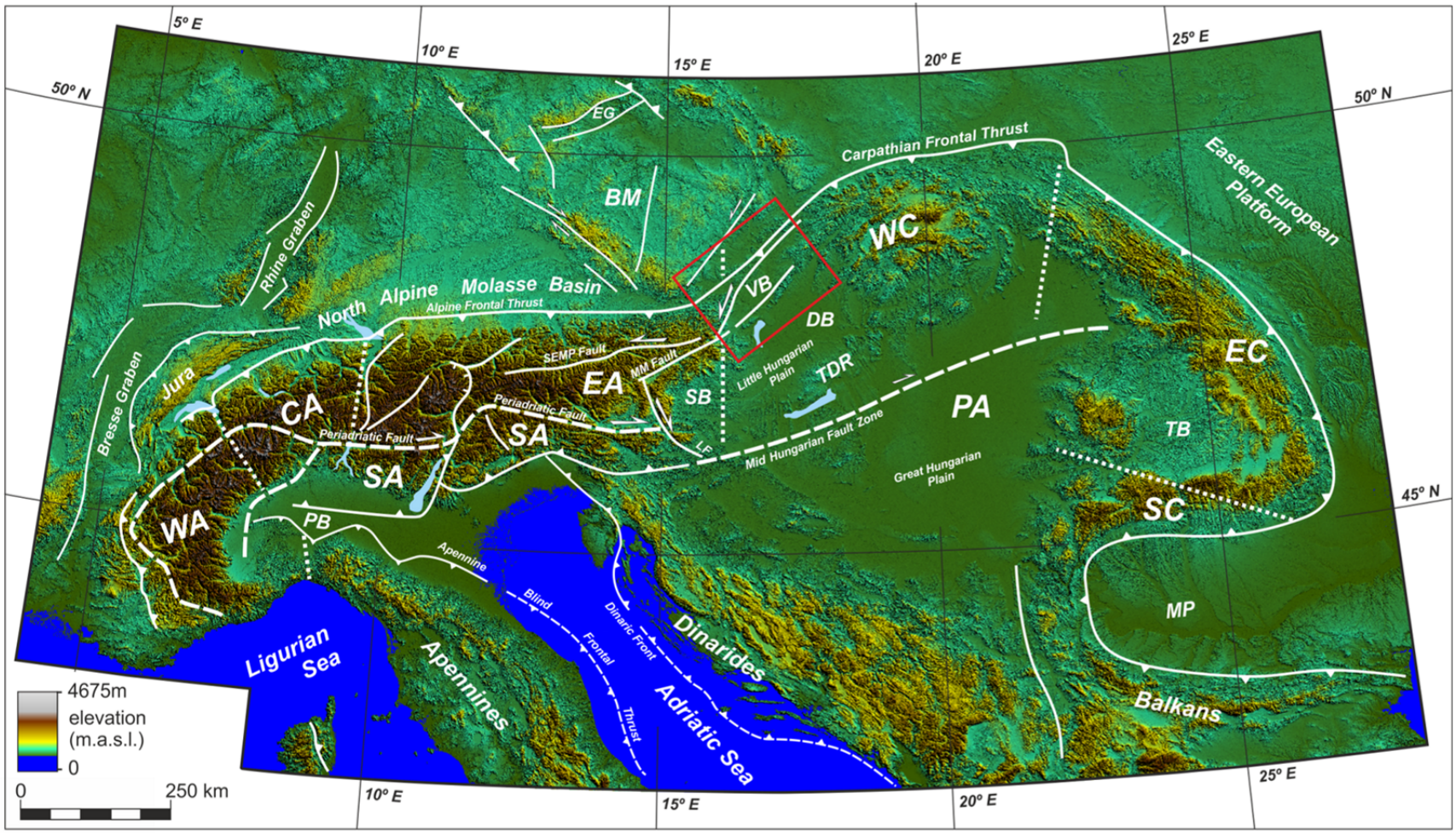

FIGURE 2.1. Digital elevation model of South Central Europe with the major geographic subdivisions of the Alps, Apennines, Carpathians, Dinarides and Balkan ranges. CA: Central Alps; DB: Danube Basin; EA: Eastern Alps; EC: Eastern Carpathians; EG: Egger Graben; LF: Lavanttal fault; MP: Moesian Platform; Mur-Mürz fault; PB: Po Basin; SA: Southern Alps; SC: Southern Carpathians; SEMP fault: Salzach–Ennstal–Mariazell–Puchberg fault; SB: Styrian Basin; TB: Transylvanian Basin; TDR: Transdanubian Ranges; VB: Vienna Basin; WA: Western Alps; WC: Western Carpathians.

Geographically speaking, the Pannonian Basin forms a topographically low-lying plain surrounded by the reliefs of the Carpathians, the Eastern Alps, the Dinarides and the Balkan mountains **(Fig. 2.1**). The basin covers the whole territory of Hungary, parts of Serbia, Croatia, Slovakia and the southwestern tip of Ukraine along northern Bosnia-Herzegovina and easternmost Slovenia and Austria. It is crossed by the Danube River and its tributary the Tisza which divide it into the Western Pannonian Plain and Eastern Pannonian provinces. The former is further subdivided into the Vienna Basin and the Little Hungarian Plain, whereas the eastern province is subdivided into the Great Hungarian Plain, the Pannonian Island Mountains, the Transdanubian Mountains and the Drava-Mura lowlands. The Great and the Little Hungarian plains are separated by the Transdanubian Ranges. A series of sub-basins constitute the great Pannonian Basin namely the Korneuburg and Vienna Basin to the NE, the Danube and the Styrian basins to the south and southwest of Vienna, respectively, and the Transylvanian Basin to the ESE, west and north of the Central and South Carpathians, respectively (**Fig. 2.1.**).

2.2.2 TECTONIC AND PALEOGEOGRAPHICAL UNITS OF THE EUROPEAN ALPS

From a paleogeographical point of view, the European Alps have been traditionally divided into four major tectonic zones: the Helvetic, Penninic, Austro-Alpine and South Alpine Zones (**Fig. 2.2**). These tectonic zones are further subdivided into sub-zones - sometimes referred to as *nappes*- which carry intrinsic paleogeographic significance. Although these zones are characterised by distinct facies associations and deformational histories, their original relative boundaries may have not been necessarily parallel to the actual tectonic boundaries. The terminology used by Schmid et al. (2004), Froitzheim et al. (2008) and Handy et al. (2015) will be used in the following as it is widely accepted by the Alpine community. Where appropriate, the used correlations between the Alpine and the Western Carpathian realms are those compiled from Golonka et al. (2006), Picha et al. (2006), Schmid et al. (2008), Ustaszewski et al. (2008) and Handy et al. (2015).

Albeit still debated, it is broadly accepted that the following Mesozoic paleogeographic domains were arranged in a NW to SE fashion:

a. The European Shelf and its continental margin, constituted by the External Massifs, the Helvetic and Ultra-Helvetic Nappes and the Sub-Penninic Nappes.

b. The northern Valais oceanic basin, commonly referred to as the Lower Penninic Nappes.
c. The Briançonnais Terrane, commonly referred to as the Middle Penninic Nappes. This terrane would have been an elongated discontinuous continental fragment of possible Iberian affinity (i.e., similar to Corsica and Sardinia). Its Western Carpathian equivalent could have been the Czorsztyn Ridge.
d. The southern Piedmont-Liguria oceanic basin is commonly referred to as the Upper Penninic Ophiolite Nappes.
e. The Cervinia Terrane, a discontinuous continental terrane within the Piedmont-Liguria Ocean. It is commonly referred to as the Upper Penninic Continental Nappes.
f. The Adriatic (or Apulian) Plate, which includes the Austro-Alpine and the South Alpine zones.
g. A southern ocean referred to as the Meliata Ocean belonging to the larger Neo-Tethys realm. The remnants of the Meliata Ocean are broadly exposed in the Inner Western Carpathians but only preserved as slivers in the Eastern Alps Austro-Alpine Zone.

2.2.2.1 TECTONIC UNITS DERIVED FROM THE EUROPEAN CONTINENTAL MARGIN

The External Massifs are Alpine structural culminations constituted by Variscan crystalline basement of the European Plate. These are particularly well exposed on the external parts of the Western Alps, and fundamentally consist of gneisses, amphibolites and granitoids. Along the strike of the Western Alps from SW to NE these massifs are known as the Argentera, Pelvoux, Grandes Rousse, Belledonne, Aiguilles Rouges, Mont Blanc and Aare (**Fig. 2.2**). It is in the Pelvoux, Grandes Rousse and Belledone massifs where significant advances in the understanding of positive basin inversion tectonics were developed (see Gillcrist et al. 1987; Grand, 1988; DeGraciansky et al. 1989; Coward et al. 1991). In the Eastern Alps and the Western Carpathians, the crystalline basement of the Jurassic continental margin of Europe is buried beneath the foreland basin sediments or has been overridden by the north-directed fold-and-thrust belt. North of the North Alpine Foreland Basin, the Vosges, Black Forest and the Bohemian massifs constitute the exposed European crystalline basement equivalents. Strongly-metamorphosed and deformed European crystalline basement is also exposed in the Tauern tectonic window of the Eastern Alps (Schmid et al. 2004). However, on the large Bohemian massif the Jurassic

continental margin sedimentary cover has been strongly eroded (Wessely, 1987). It is underneath and ahead of the thin-skinned Alpine-Carpathian fold-and-thrust belt where the Jurassic continental margin basins are best preserved.

The Helvetic and Ultra-Helvetics comprise the autochthonous and para-autochthonous cover of the European crystalline basement and were defined *sensu stricto* in Switzerland. There, the Helvetic cover comprises Upper Carboniferous to Permian half-graben fills, a Triassic and Jurassic cover of variable thickness related to rifting, Cretaceous to Paleocene shelf sediments, and Eocene to Oligocene deep-water clastics (Froitzheim et al. 2008). During the Cretaceous, the Helvetic constituted the shelf of the European continental margin, whereas the Ultra-Helvetic series were deposited on the distal continental margin, between the Helvetic shelf and the Valais Ocean to the SE. In the northern foreland of the Eastern Alps and the Alpine-Carpathian Junction, a significantly thinner Helvetic and Ultra-Helvetic cover is buried beneath the foreland sediments and the fold-and-thrust belt. There, the limited outcrops of Helvetic and Ultra-Helvetic units consist of Upper Jurassic and Lower Cretaceous carbonates and marls hosted within thrust slices. These materials were scrapped off from their basement and imbricated within the Waschberg-Ždánice Zone. The Ultra-Helvetic and Helvetic can be correlated to the Western Carpathian Silesian and Sub-Silesian units, which were once located to the north of the Magura Basin (Picha et al. 2006; Beidinger and Decker, 2014, 2016).

2.2.2.2 TECTONIC UNITS DERIVED FROM THE VALAIS OCEAN

Units from this domain are considered to be derived from an oceanic domain or the immediately adjacent distal continental margin. These units consist of monotonous series of calcareous shales and sandstones referred to the *Bündnerschiefer*, the *Schistes Lustrés* or the *Calcescisti* and usually lack their pre-Mesozoic basement (Schmid et al. 2004). Similar facies are, however, reported on the Piedmont-Liguria oceanic units, hampering a straightforward paleogeographic assignation. Sedimentation of the Valais *Bündnerschiefer* probably started around the Jurassic-Cretaceous boundary and continued into the Tertiary under the sedimentation of the Rhenodanubian Flysch in the Eastern Alps and Alpine-Carpathian Junction. These should be equivalent to the Magura Flysch units located in the Outer Western Carpathians (Picha et al. 2006).

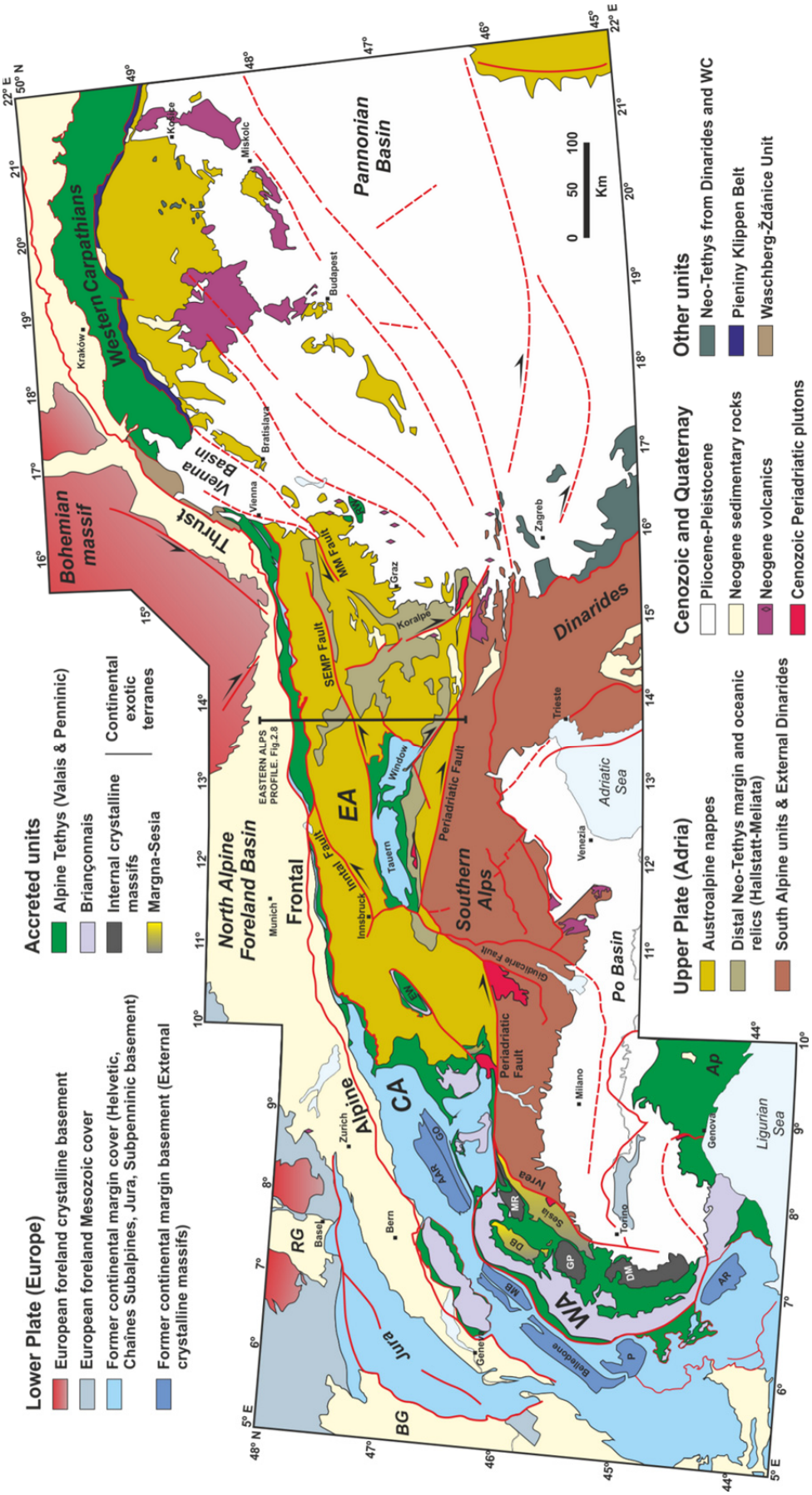

Figure 2.2. Tectonic map of the Alps and the Western Carpathians. Modified from Froitzheim et al. (1996); Schmid et al. (2004); Horváth et al. (2006); Froitzheim et al. (2008); Handy et al. (2015). BG: Bresse graben; RG: Rhine graben; AAR: Aare massif; AR: Argentera massif; P: Pelvoux massif; MB: Mont Blanc massif; GO: Gothard; DM: Dora Maira massif; GP: Gran Paradiso massif; DB: Dent Blanche massif; MR: Monte Rossa massif; Ap: Apennines; RW: Rechnitz Window; EG: Engadine Window; SEMP fault: Salzach–Ennstal–Mariazell–Puchberg fault; MM fault: Mur-Mürz fault.

As no evidences of the Briançonnais terrane are present east of the Central Alps some authors associate the Rhenodanubian Flysch with the Piedmont-Liguria Ocean instead (i.e., with the Upper Penninic Ophiolite Nappes). In addition, controversy still exists whether the Valais basin was a true oceanic basin floored by oceanic crust or not (see contrasting arguments provided by Schmid et al. 2004 and references therein, and those provided by Beltrando et al. 2007).

2.2.2.3 TECTONIC UNITS DERIVED FROM THE BRIANÇONNAIS TERRANE

The Briançonnais continental fragment was a block of continental crust that is thought to have represented the continental margin of Europe prior to the opening of the Valais Ocean. It also includes those units that were formerly adjacent to the Piedmont-Liguria Ocean and the Valais Ocean. It is widely accepted that the Briançonnais block consisted of a promontory of Iberian crust wedging out from the SW to the NE into the Alpine realm, as originally proposed by Frisch (1979) and Stampfli (1993). The acceptance of this model has strong implications for the lateral correlation of the Valais and Piedmont-Liguria oceanic basins (i.e., the Upper and Lower Penninic Nappes). In fact, the Briançonnais terrane disappears somewhere in between the Engandine and the Tauern tectonic windows (**Fig. 2.2**), and is no more present in the Eastern Alps.

In the Western Alps a series of continental crystalline massifs registered high-pressure (HP) and ultra high-pressure (UHP) metamorphism related to subduction of continental crust during the Eo-Alpine and/or the Neo-Alpine orogenies. These terranes are known as the Monte Rossa, Gran Paradiso and Dora Maira (**Fig. 2.2**) terranes. In fact, their paleogeographic origin has been a long-lived matter of debate, and have been assigned to Europe, Briançonnais, intra Penninic or even belonging to the Adriatic margin (see Schmid et al. 2004; Froitzheim et al. 2008; Beltrando et al. 2010 for discussions).

2.2.2.4 TECTONIC UNITS DERIVED FROM THE PIEDMONT-LIGURIA

The Piedmont-Liguria is thought to have been located in between the Briançonnais continental terrane and the distal continental margin of the Adriatic plate. These units currently occupy the structurally highest position within the Penninic nappe stack (Schmid

et al. 1990). These Upper Penninic Ophiolite Nappes encompass relics of true oceanic lithosphere and/or exhumed sub-continental lithospheric mantle. A Middle Jurassic age for sea floor spreading has been proposed based on the presence of deep water facies such as radiolarites and *Aptychus*-bearing limestones. These facies associations are considered diagnostic of the Piedmont-Liguria Ocean and the nearby parts of the Adriatic continental margin and have not been reported in the northerly Valais Ocean (see Schmid et al. 2004 for a discussion). Several tectonic windows exposing ophiolites of Penninic affinity also occur in the eastern margin of the Eastern Alps. The largest of these windows is known as the Rechnitz window (**Fig. 2.2**), where Lower to Upper Cretaceous fauna has been found within metasediments.

Cretaceous trench deposits found in the Upper Penninic Ophiolite Nappes are considered as evidence for the early development of an accretionary prism to the SE, therefore indicating the onset of an active plate boundary north of the Adriatic continental margin (i.e., Austro-Alpine Zone). The Rhenodanubian Flysch outcrops along the northern border of the Alpine-Carpathian Junction (**Fig. 2.2**) and is considered to have, at least to some point, developed in such accretionary prism. Although some authors assign a Valais affinity to this strongly imbricated and deformed deep marine units (Kurz et al. 2001; Schmid et al. 2004), some others consider these as deposited onto the Piedmont-Ligurian Ocean (Faupl and Wagreich, 2000; Wagreich, 2001). This differentiation may be irrelevant if no intervening "Briançonnais" block was present nevertheless. In fact, a substantial agreement exists in that some parts of the Rhenodanubian Flysch were once deposited onto true Jurassic oceanic basement as preserved on the Ybbsitz klippen, whereas others were deposited on thinned continental crust (Decker, 1990; Egger, 1990, 1992; Schnabel, 1992). In these klippen, serpentinites are in contact with Jurassic radiolarites and *Aptychus*-bearing limestones of Piedmont-Liguria affinity, as those reported from the Upper Penninic Ophiolite Nappes of the Western and Central Alps (Schmid et al. 2004). In Upper Austria, the well Grünau1 intersected a thick serpentinite body within a strongly imbricated thrust zone between the Northern Calcareous Alps, the Ultra-Helvetics and the Rhenodanubian Flysch units (Hamilton et al. 2000; Beidinger and Decker, 2014). According to this, the Rhenodanubian Flysch was detached from its original oceanic basement during subduction and imbricated into an accretionary prism at the front of the Austro-Alpine nappes. At the Alpine-Carpathian Junction, the Rhenodanubian Flysch marks the tectonic suture between the Austro-Alpine Zone (i.e., juxtaposed to the Northern Calcareous Alps) and the former European continental margin.

2.2.2.5 TECTONIC UNITS DERIVED FROM THE CERVINIA TERRANE

These units are referred by Frotizheim et al. (2008) as to the Upper Penninic Continental Nappes. These authors assign a Penninic affinity to these continental nappes, belonging to another microcontinent in between the Briançonnais and the Adriatic margins named Cervinia (Pleuger et al. 2007) or Margna-Sesia fragment (Schmid et al. 2004). Other authors affirm these terranes could belong to former extensional allochthons derived from the hyperextended continental margins of Adria (i.e., Austro-Alpine Zone) or even Europe (Froitzheim and Manatschal, 1996; Dal Piaz, 1999; Froitzheim, 2001; Schmid et al. 2004; Beltrando et al. 2010), casting serious doubts on their paleogeographical affinity (see Schmid et al. 2004; Froitzheim et al. 2008; Beltrando et al. 2010). At the Central Alps these continental fragments are the Sesia Nappe (or Sesia-Lanzo zone), the Dent Blanche Nappe, the Margna Nappe and the Monte Rosa Nappe. These continental blocks display HP- to UHP-metamorphism dated as Cretaceous in age (see Beltrando et al. 2010 for a review on the published Alpine isotopic ages and the interpretation of related tectono-metamorphic events).

2.2.2.6 TECTONIC UNITS DERIVED FROM THE ADRIATIC PLATE

Units derived from the Adriatic plate are presently located north and south of the Periadriatic fault (**Figs. 2.1** and **2.2**). These are the Austro-Alpine Zone, north of the Periadriatic fault, and the South Alpine Zone to the south of the Periadriatic fault (**Fig. 2.2**). The Austro-Alpine Zone records a long-lived geological history spanning for most of the Phanerozoic Eon. It contains a large variety of sedimentary, metasedimentary, and igneous rocks affected by Variscan, Permian-Triassic, Eo-Alpine, Gossau, and Neo-Alpine tectono-metamorphic events (see Froitzheim et al. 2008 for a review). These units are arranged into the so-called Austro-Alpine nappes.

According to the review by Schmid et al. (2004), the Austro-Alpine Zone is divided into the Lower and Upper Austro-Alpine units. The Lower Austro-Alpine formed the northern margin of the Adriatic plate facing the Piedmont-Ligurian Ocean from Jurassic to Early Cenozoic times. These units were affected by the opening and closure of this continental margin, as it has been recognised by an inherited extensional architecture and related sedimentation (Häusler, 1987; Manatschal and Nievergelt, 1997, amongst others), as

well as the subsequent subduction-related deformation and metamorphism (Schuster, 2004). The Upper Austro-Alpine units are better represented by far than the Lower Austro-Alpine ones. The Upper Austro-Alpine constitutes a structurally complex stack of thrust sheets formed during the Cretaceous Eo-Alpine orogeny. During the Cretaceous to Eocene these nappes were affected by significant extensional faulting and related sedimentation registered in the so-called Gosau Basins. Nevertheless, these basins developed in a regional compressional tectonic setting, locally associated with a subduction zone accretionary wedge (Wagreich, 1993). The Upper Austro-Alpine stack remained in an upper-plate position during subsequent Cenozoic Neo-Alpine shortening, accommodating severe thrusting and folding. A significant part of these nappes (and the Rhenodanubian Flysch) became deeply buried beneath the Neogene cover of the Vienna Basin from middle Miocene onwards. In more detail, the Upper Austro-Alpine nappes are constituted by the Northern Calcareous Alps (including the Bajuvaric, Tirolic and Juvavic nappes), the Greywacke zone, the Silvretta-Seckau nappe system, the Koralpe-Wölz nappe system, the Ötztal-Bundschuh nappe system and the Drauzug-Gurktal nappe system. Due to the inherent complexity and the still poorly understood tectonic correlation between the many nappes that constitute the Austro-Alpine, a detailed description of the Austro-Alpine Zone is considered to be out of the scope of this thesis. The reader can refer to Tollman (1959, 1977), Frank (1987), Mandl (2000), Neubauer et al. (2000), Schmid et al. (2004) and Froitzheim et al. (2008) for more detailed descriptions.

The South Alpine Zone is located only south of the Periadriatic Fault and can be traced into the Dinarides to the SE of the Eastern Alps (**Fig. 2.2**). Tectonically speaking, the South Alpine Zone is divided into the Lombardic-Giudicaric fold-and-thrust belt to the west, and the eastern South Alpine units of the Dolomites, Carnio and Julian Alps. As opposed the Austro-Alpine Zone, the South Alpine is devoid of any significant Alpine metamorphism. In more detail, the Lombardic-Giudicaric fold-and-thrust belt is a south-directed basement-involved system that can be further subdivided into the Canavese, Ivrea, Strona-Ceneri, the Val Colla zones, the Orobic basement and its Variscan cover. The eastern parts of the fold-and-thrust belt were intruded by Eocene to Oligocene granitoids, dated at 43 to 34-32 Ma according to Del Moro et al. (1983) and Stipp et al. (2004), respectively. These intrusions are commonly referred to as Adamello-type intrusive bodies (**Fig. 2.2**). On the other hand, SE of the Margna-Sesia fragment, lower crustal and upper mantle rocks have been exposed as a result of the above mentioned thick-skinned thrusting (Lanza, 1982).

2.2.2.7 TECTONIC UNITS DERIVED FROM THE MELIATA OCEAN

The Meliata Ocean was an oceanic basin that belonged to the larger Neo-Tethys realm. In the Alps, only small remnants of this ocean are preserved within the Eastern Alps. Conversely, in the Western Carpathians larger units of basement and cover belonging to the Meliata Ocean have been reported (i.e., the so-called Meliaticum). The Meliata Ocean existed from Triassic to Jurassic (and possibly during the beginning of the Cretaceous) until its subduction and partial obduction. However, the paleogeography of the Meliata oceanic realm remains poorly constrained, and some authors propose it was closed in Jurassic times (see Channel and Kozur, 1997; Mandl, 2000; Stampfli and Borel, 2004). Strongly sheared zones hosting units of Meliata-affinity have been found in the eastern Northern Calcareous Alps (i.e., in the Upper Austro-Alpine nappes of the Austro-Alpine Zone). These include serpentinites, basic volcanic rocks and Jurassic metasediments such as mass-flows including resedimented radiolarites, limestones, cherts shales and marls of Triassic age. Other potential Meliata remnants have been found as basic volcanic rocks and serpentinites included into Permian evaporitic melanges at the base of the Juvavic nappes of the Northern Calcareous Alps, as detrital serpentinites and heavy minerals within Cretaceous syn-orogenic strata from Berriasian onwards (Kozur and Mostler, 1992), and within the Upper Cretaceous of the Gosau Basins (Gruber et al. 1992).

2.2.3 TECTONIC AND PALEOGEOGRAPHICAL UNITS OF THE WESTERN CARPATHIANS

The Western Carpathians can be subdivided into three main zones: the External, Central and Internal Western Carpathians (**Fig. 2.2**). The External Western Carpathians have been interpreted as corresponding to a Cenozoic accretionary complex related to the southwards subduction of the Penninic oceanic basin. In Western Carpathians paleogeographic terms, the Lower Penninic Ocean or Piedmont-Liguria Ocean is sometimes also referred to as the Magura Ocean. This Cenozoic accretionary complex may also have incorporated an additional oceanic basin known as the Moldavide (Golonka et al. 2006; Picha et al. 2006). The External Western Carpathians are separated from the Central Western Carpathians by a narrow and steeply-dipping transpressional zone known as the Pieniny klippen Belt (**Fig. 2.2**). Units within this belt also correspond to the Penninic and Austro-Alpine zones in the Western Carpathians. The Pieniny Klippen Belt is thought to

represent a sutured plate boundary, although no proper ophiolite remnants have ever been reported within. The Central and the Internal Western Carpathians represent a crustal stack formed during the latest Jurassic to mid-Cretaceous 'oceanic' subduction and continental collision. In this collision the Central Western Carpathians may have represented the pro-wedge, whereas the retro-wedge would have been constituted by the Internal Western Carpathians (Froitzheim et al. 2008). The following paleogeographical domains were arranged in a north to south fashion (Froitzheim et al. 2008):

a. The European continental margin.
b. The Moldavide basins, of unclear oceanic affinity.
c. The Silesian ridge, representing an elongated continental fragment.
d. The Magura Flysch basin, in an equivalent Lower Penninic position (i.e., Valais).
e. The Czorsztyn (or Oravic) ridge, constituted by an elongated continental fragment in a position that somehow would be equivalent to the Briançonnais block (i.e., in a Middle Penninic position).
f. An Upper Penninic Ocean known as the South Penninic or Vahic Ocean (i.e., equivalent to the Piedmont-Liguria Ocean).
g. The Adriatic continental margin which includes the Slovako-Carpathian units (i.e., equivalent to the Austro-Alpine Zone of the Alps) and the Pelso units (equivalent to the Upper Austro-Alpine –South-Alpine– Dinaric units in broad terms).

In very broad terms, during the Triassic and Jurassic, the units belonging to the present External and Central Western Carpathians represented the European rifted continental margin of the Meliata Ocean. Conversely, those units presently constituting the Internal Western Carpathians formed the southern continental margin of Meliata and correspond to the northern parts of the Adriatic lithosphere. The Central and Internal Western Carpathians collided by the transition between the Jurassic and Cretaceous following the closure of the Meliata Ocean. At this point onwards, the evolution of the Western Carpathians is considered to be similar to that of the Alps, and also included the sedimentation of Gosau-type sediments in Upper Cretaceous-Eocene times. The Carpathians and the Alps can be considered as belonging to the same orogenic belt, but strongly differ to one another. The Carpathians are characterised by an extensive and a locally very thick cover of Neogene Basins (i.e., the Pannonian Basins), and widespread acidic to basic calc-alkaline and alkaline volcanism are also present (**Fig. 2.2**).

2.2.4 TECTONIC AND PALEOGEOGRAPHICAL UNITS BENEATH THE PANNONIAN BASINS

Beneath the thick sedimentary cover of the Pannonian and the Transylvania basins (**Fig. 2.1**), three large Mega Units are present, namely the ALCAPA, Tisza and Dacia Mega Units (**Fig. 2.3**). These Mega Units have been defined based on the paleogeographic and tectonic reconstructions of the Alpine-Carpathian-Dinaric systems provided by Csontos and Vörös (2004), Haas and Péró (2004), Schmid et al. (2008) and Ustaszewski et al. (2008), amongst others. Ustaszewski et al. (2008) define a Mega unit as an assembly of tectonic units with a common paleogeographic origin distinct from adjacent tectonic units or other mega units from which is separated by faults. In contrast to a microplate, its original lithospheric underpinnings are either lacking or unknown.

In the Alps, the ALCAPA Mega unit is referred to the Austro-Alpine Zone *sensu* Schmid et al. (2004), and corresponds to the Central and Inner Western Carpathians according to Plašienka et al. (1997a, b). Hence, ALCAPA is fundamentally derived from Adriatic units and the continental margins bordering the Triassic Meliata Ocean (Ustaszewski et al. 2008). The Dacia Mega unit is interpreted as the Carpathian equivalent of the Europe-derived Helvetic, Ultra-Helvetic and Sub-Penninic Nappes, and the Briançonnais. Some units belonging to the Dacia Mega unit would have separated from Europe during the opening of the Valais-Magura Basin in Lower Cretaceous times (Csontos and Vörös, 2004; Schmid et al. 2008), whereas others may in fact have been scrapped off the Moesia foreland (i.e., European margin; **Figs. 2.1** and **2.3**) during the Miocene collision (Ziegler et al. 1995). In a similar fashion to Dacia, the Tisza Mega unit was also separated from Europe during the Middle Jurassic as the eastern Alpine Tethys propagated eastwards, and would have been in a position equivalent to the Piedmont-Liguria Ocean (Haas and Péró, 2004). Based on its stratigraphy and faunal associations, it has been suggested that spreading of the Piedmont-Liguria Ocean may have moved the Tisza Mega unit into a paleogeographic position comparable to that of the Adriatic plate. The nappe systems that constitute the Tisza Mega unit are only exposed as inselbergs in the Pannonian plains (Haas, 2001).

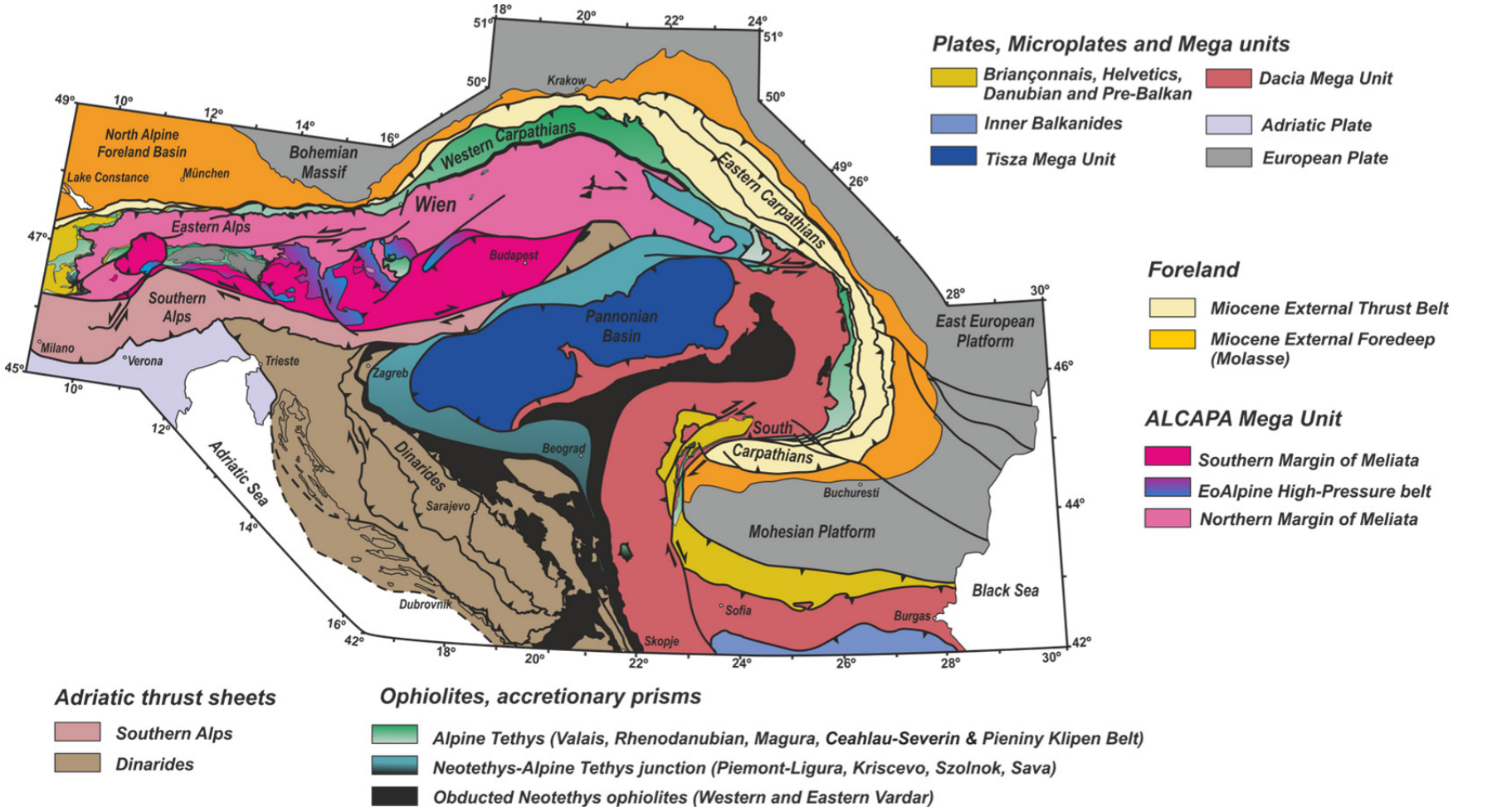

FIGURE 2.3. Tectonic map of the Pannonian region, including the Eastern Alps, Southern Alps, Dinarides and Carpathians beneath the Pannonian Basin Neogene cover. Modified from the compilation of Ustaszewski et al. (2008).

2.2.5 OVERALL TECTONIC AND PALEOGEOGRAPHICAL EVOLUTION

The European Alpides are a doubly-vergent orogenic wedge that resulted from the Cretaceous to recent convergence and collision between a series of microplates (i.e., Adria, Iberia, Alcapia, Alkapecia and Tiszia-Dacia) located in between and related to the European and Adriatic lithospheres (Froitzheim et al. 1996, 2008; Schmid et al. 1996, 2004, 2008; Ustaszewski et al. 2008; Handy et al. 2010, 2015). The Adriatic plate or micro-plate, also known as the Adriatic Indenter, or Apulian plate (Schmid et al. 2004) is considered to be a northern promontory belonging to the African plate or a microplate located to the north of the African one (Dewey et al. 1989; Rosembaum et al. 2002). The Helvetic, Penninic and Austro-Alpine zones north of the Periadriatic Fault locate on the north-directed pro-wedge. The South Alpine Zone, conversely, sits on the south-directed retrowedge south of the Periadriatic Fault (**Fig. 2.2**). It forms a basement-involved fold-and-thrust belt where Adriatic lower crustal rocks and lithospheric mantle have been imbricated and brought up to the surface. In contrast, the Helvetic, Penninic and the Austro-Alpine zones are arranged in three major thrust sheets -or nappes- where the Austro-Alpine zone is the structurally higher unit, the Helvetic is the structurally lower and the Penninic one lies in between. The Eastern Alps, where the Austro-Alpine Zone outcrops extensively, correspond to the upper plate of the orogenic wedge. In contrast, the Central and Western Alps where the European units are widely exposed correspond to the lower plate of the Alpine orogen. The Tauern and Engadine windows of the Eastern and Central Alps (**Fig. 2.2**) expose European lower plate and Penninic units, respectively. In between, units of Valais and Piedmont-Liguria as well as Briançonnais and Cervinia terranes correspond to accreted units marking the orogenic suture between the upper and the lower tectonic plates. Although the Austro-Alpine Zone is presently located to the north of the Periadriatic Fault and on the pro-wedge of the orogen, paleogeographically speaking corresponds to the colliding upper plate.

The Alps were formed upon the closure of the Neo-Tethys (which included at least, the Meliata and the Vardar oceans) and the Alpine Tethys realms concomitant with the opening of the Atlantic oceanic basin (Stampfli and Borel, 2002; **Fig. 2.4**). According to Froitzheim et al. (2008), magmatic crystallisation ages (i.e., U-Pb in zircon) have indicated progressively younger ages for oceanic spreading from SE to the NW (i.e., from the Neo-Tethys Meliata and Vardar oceans to the Alpine Tethys southern and northern branches; **Fig. 2.4**). Radiometric dating has also allowed constraining the ages of high-pressure (HP)

and ultra-high-pressure (UHP) metamorphism related to two distinct Alpine orogenies: the Cretaceous Eo-Alpine and the Cenozoic Neo-Alpine orogenies. The Meliata oceanic basin opened around Middle Triassic at 237-228 Ma according solely to stratigraphic dating (Channel and Kozur, 1997) and was closed by Late Jurassic times (160-150 Ma, according to radiometric dating provided by Froitzheim et al. 2008). The Piedmont-Liguria ocean opened between the Middle Jurassic and the earliest Cretaceous (166-142 Ma) and closed during the Paleocene to middle Eocene (70-40 Ma), also according to this radiometric dating compiled by Froitzheim et al. (2008). These authors also provide two magmatic crystallization ages for the Valais Ocean, one at *ca.* 163-155 Ma and another at *ca.* 93 Ma, suggesting a "re-rifting" event on pre-existing oceanic crust. They report a 40-37 Ma age of HP metamorphism related to the closure of the basin. However, these isotopic ages have been challenged by Beltrando et al. (2010), suggesting alternative spreading and tectonic burial histories in relation with the opening and closure of the Penninic basins (**Fig 2.5**). In an earlier work, Beltrando et al. (2007) provided Permian magmatic crystallization ages for the Valais igneous basement, and attribute the *ca.* 93 Ma magmatic crystallization ages compiled in Froitzheim et al. (2008) to thermal and metasomatic events. In fact, the *ca.* 93 Ma age for magmatic crystallization is coincident with the thermal metamorphic peak recorded in the Pyrenees (Clerc et al. 2014). These radiometric ages should be therefore regarded with caution.

According to the review provided by Handy et al. (2010) subduction of mainly continental lithosphere led to the formation of the Upper Cretaceous (dated as around 110-90 Ma) Eo-Alpine HP eclogite-facies metamorphic belt of the Eastern Alps (**Fig. 2.4**). This belt shows NW- to W-directed nappe-stacking and exhumation. Conversely, the Western Alps display Cenozoic Neo-Alpine high-pressure metamorphism and top-to-the N and NW tectonic transport direction associated with S- to SE-directed subduction. As recorded in the Eastern Alps, in between these two orogenic episodes a period of orogenic collapse took place. This collapse is represented by the formation of the Gosau Basins from which no record is present in the Western Alps (Faupl and Wagreich, 1996, 2000; Froitzheim et al. 2008). Progressive drowning of the Gosau Basins from Upper Cretaceous (post-Turonian) to Eocene times has been interpreted from the shallow to deep marine sedimentary record. Formation and deformation of the Gosau Basins is thought to have taken place in an accretionary prism, coevally with the southwards subduction of the Piedmont-Liguria Ocean (i.e., the southern oceanic branch of the Alpine Tethys) beneath the northern continental margin of the Adriatic Plate (Wagreich, 2001). The Neo-Alpine

orogeny continued with the imbrication of the Rhenodanubian Flysch in an accretionary prism. It is important to note that the temporal division between the Eo-Alpine and Neo-Alpine tectono-metamorphic events separated by the Upper Cretaceous to Eocene collapse is only strictly documented in the Austro-Alpine nappes of the Eastern Alps and its Carpathian counterparts. Convergence and accretion of Penninic units and the Sesia-Margna continental fragments in the Western Alps seem to have taken place continuously, from Cretaceous to Paleogene, without any orogenic collapse in between (Cortiana et al. 1998; Dal Piaz, 1999; Dal Piaz et al. 2001; Schmid et al. 2004; Beltrando et al. 2010). Conversely, the Western Carpathians reconstruction compiled by Picha et al. (2006) describe a series of extended fore-arc-type basins –time equivalent to the Penninic basins- soled by thinned European crust northwards of the oceanic subduction zone. These basins were subsequently incorporated into the accretionary prism from Upper Cretaceous to late Miocene (**Fig. 2.6**). The Penninic oceanic basins most probably wedged out eastwards as Jurassic oceanic basement is preserved on the Ybbsitz klippen of the Eastern Alps (Decker, 1990), although significant controversy still exists regarding the paleogeographic evolution of the Penninic basins and the continental terranes in between. Although it still receives a lot of attention from the Alpine geoscience community, further discussion on this issue is regarded as out of scope. To summarise, it is generally agreed that the age trends for both oceanic spreading and UHP- and HP-metamorphism young from SE to NW, indicating the migration of subduction and collision from SE to the NW (Schmid et al. 1996, 2004, 2008; Froitzheim et al. 2008).

The collision and partial subduction of the European continental lithosphere beneath the Adriatic one formed large Cenozoic fold-and-thrust belts and related peripheral foreland basins (Beaumont, 1981; Jordan, 1981; DeCelles and Giles, 1996). The Eocene to Miocene North Alpine Foreland Basin (i.e., the Molasse Basin; Heim, 1921) was part of the Alpine-Carpathian foredeep. The basin can be traced from the Rhône River in France, along Bavaria and Austria into the Western Carpathian's foredeep of Slovakia and Poland (**Figs. 2.1** and **2.2**). It developed on the European plate as an E-W-striking depocenter in front of the N-directed thrust sheets. The basin is characterised by a generally regressive infill arranged in several transgressive-regressive cycles deposited over a regional unconformity. This unconformity can be trace from as far as the Jura (**Fig. 2.2**) towards the south in the Helvetic domain, eroding the pre-deformational stratigraphic section down into the Variscan basement. This unconformity reflects the flexural bending of the European lithosphere as a response of the Alpine loading forces. At the North

Alpine Foreland Basin progressive N- to NW-directed thrusting incorporated the Ultra-Helvetic and the Helvetic units (i.e., the European continental margin sequences) as well as foreland sediments onto the European Platform (Decker et al. 1987; Wessely, 1987; Decker and Peresson, 1996; Wagner, 1996; Beidinger and Decker, 2014). On the retrowedge, the Eocene to Present Po Basin developed on the Adriatic plate and represents the foreland basin of the Southern Alps and that of the Apennines (**Figs. 2.1** and **2.2**).

Concomitant with Oligocene and Miocene foreland sedimentation and thrusting, counter-clockwise rotation and oblique indentation of the Adriatic plate into the European one took place. As a result, the European and Penninic metamorphic basements of the Alps were uplifted and basement exhumation was favoured along E- and W-dipping low-angle extensional faults (**Fig. 2.7**) such as those in the Lepontine Dome and the Tauern and Engadine windows (Selverstone, 1988; Genser and Neubauer, 1989; Mancktelow et al. 1995). At the transition between the Eastern Alps and the Carpathian embayment (**Fig. 2.5c**), extension along a large early to middle Miocene SE-dipping extensional fault exhumed the Rechnitz Penninic metamorphic core complex (Koller, 1985; Ratsbacher et al. 1991b; Tari et al. 1992). Significant lithospheric extension and magmatism occurred ahead of the northward-propagating Alpine orogen, forming the NNE-SSW striking Rhine, Bresse and Rhône grabens (**Fig. 2.1**) and the Provençal and Tyrrhenian back-arc basins of the Western Mediterranean (**Fig. 2.7**). The opening of these back-arc basins is also synchronous to the development of the Apennine chain (Morley, 1993; Carminati and Doglioni, 2012). As shortening continued on the Eastern Alps during the Oligocene and Miocene, N-S to NNE-SSW extension in the Bohemian massif was responsible for the opening of the WSW-ENE striking Ohře (or Egger) Graben (**Fig. 2.7**) which was also accompanied by alkaline volcanism (Špičáková et al. 2000).

In the Alpine-Carpathian Junction, the ages of the imbricated foreland sediments indicate the diachronic termination of thrusting, becoming younger front west to east from the easternmost Alps and along the Carpathian's arc. Active thrusting is still ongoing in the Eastern and Southern Carpathians transition (Roure et al. 1993; Roca et al. 1995; Decker and Peresson, 1996; Beidinger and Decker, 2014). The easternmost parts of the Eastern Alps underwent lateral extrusion encompassing both lateral escape and dismantling of the orogenic edifice as defined by the seminal papers of Ratschbacher et al. (1991a, b). Lateral extrusion was induced by the northward collision and indentation of the Adriatic plate into the European margin (Schmid and Kissling, 2000), favoured by the unconstrained

eastward-migrating boundary at the Carpathian embayment (Royden, 1985; Ratschbacher et al. 1991b; Tomek and Hall, 1993; Decker and Peresson, 1996; **Fig. 2.5c**). There, subduction roll-back of the European oceanic lithosphere and retreat of the subduction zone allowed for the back-arc extension of the upper plate, followed by active rifting and widespread extension. Intense magmatic activity encompassed the subduction of the oceanic lithosphere and the back-arc rifting of the Pannonian Basin (**Fig. 2.6**).

The transition from subduction, collision and rifting is supported by the geochemical evolutionary trends of magmatic occurrences in the Pannonian region: a progressive eastward migration of calk-alkaline magmatic centres from *ca.* 20 to 11 Ma evolved towards a more widespread alkaline magmatism (*ca.* 9-1 Ma) has been observed in the voluminous lavas present in the Pannonian Basin (Embey-Isztin et al. 1993; Seghedi et al. 2004; **Figs. 2.1** and **2.6**). The ages of calk-alkaline (i.e., subduction-related) magmatism broadly young from west to east following the Carpathian arc in a similar fashion as the ages of thrusting (Nemčok et al. 1998). As a result of the European slab roll-back and the retreat of the subduction zone, the Eastern Alpine and Western Carpathian orogenic edifice collapsed, leading to the formation of a series of thick middle to late Miocene extensional, transtensive, and transpressive and pull apart basins. The largest of these are the Vienna, Danube, Styrian and Pannonian basins (Royden et al. 1985; Ratschbacher et al. 1991b; Csontos et al. 1992; Horváth, 1993; Tomek and Hall, 1993; Csontos, 1995; Fodor, 1995; Horváth, 1995; Decker and Peresson, 1996; Kováč et al. 1997; Fodor et al. 1999; Huismans et al. 2001; Strauss et al. 2001; Linzer et al. 2002; Cloetingh et al. 2006; Horváth et al. 2006; Matenco and Radivojevic, 2012; Balázs et al. 2016). These middle to late Miocene basins underwent complex sedimentary and deformational histories and have recorded significant uplift during latest Miocene-Quaternary (Dunkl and Frisch, 2002). The causes for such uplift have been strongly debated as well, and have been interpreted in different ways: either related to a change in plate kinematics leading to fault reactivation and basin inversion (Horvárth, 1995; Decker and Peresson, 1996; Horváth and Cloetingh, 1996; Fodor et al. 1999; Strauss et al. 2001), or in relation with rift push forces associated with the asthenospheric doming during active rifting (Huissmans et al. 2001), or as a result of isostatic rebounds accommodating asymmetric extension (Matenco and Radivojevic, 2012).

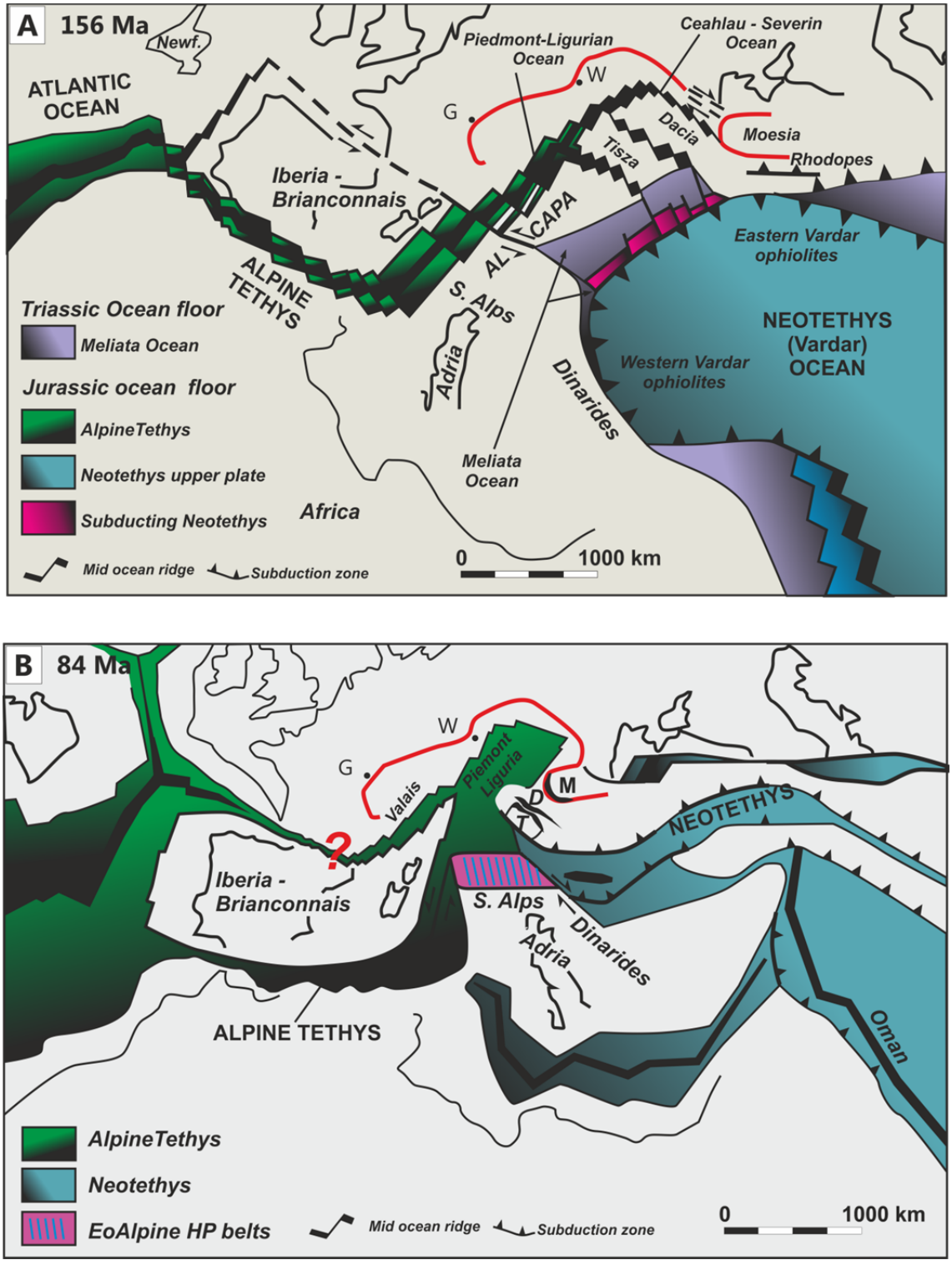

FIGURE 2.4. Schematic palinspastic reconstruction for (A) Oxfordian (*ca.* 156 Ma) and (B) Santonian (*ca.* 84 Ma) times illustrating the evolution of the Neo-Tethys, Alpine Tethys and Atlantic realms. On Santonian times, significant re-arrangement of plate kinematics took place, marking the onset of Pyrenean shortening. The question mark indicates the controversial connexion between the Valais and the Bay of Biscay via the Pyrenean Rift System. Modified from Schmid et al. (2008), from the ideas of Frisch (1979), Frank (1987), Dercourt et al. (1993), Stampfli (1993), Săndulescu (1994), Marroni et al. (2002), Stampfli and Borel (2002) and Schmid et al. (2004). The red line represents the outline of the future Alpine-Carpathian-Balkan orogenic belt. G: Geneva; W: Vienna; T: Tisza; D: Dacia; M: Moesia; Newf: Newfoundland (Canada).

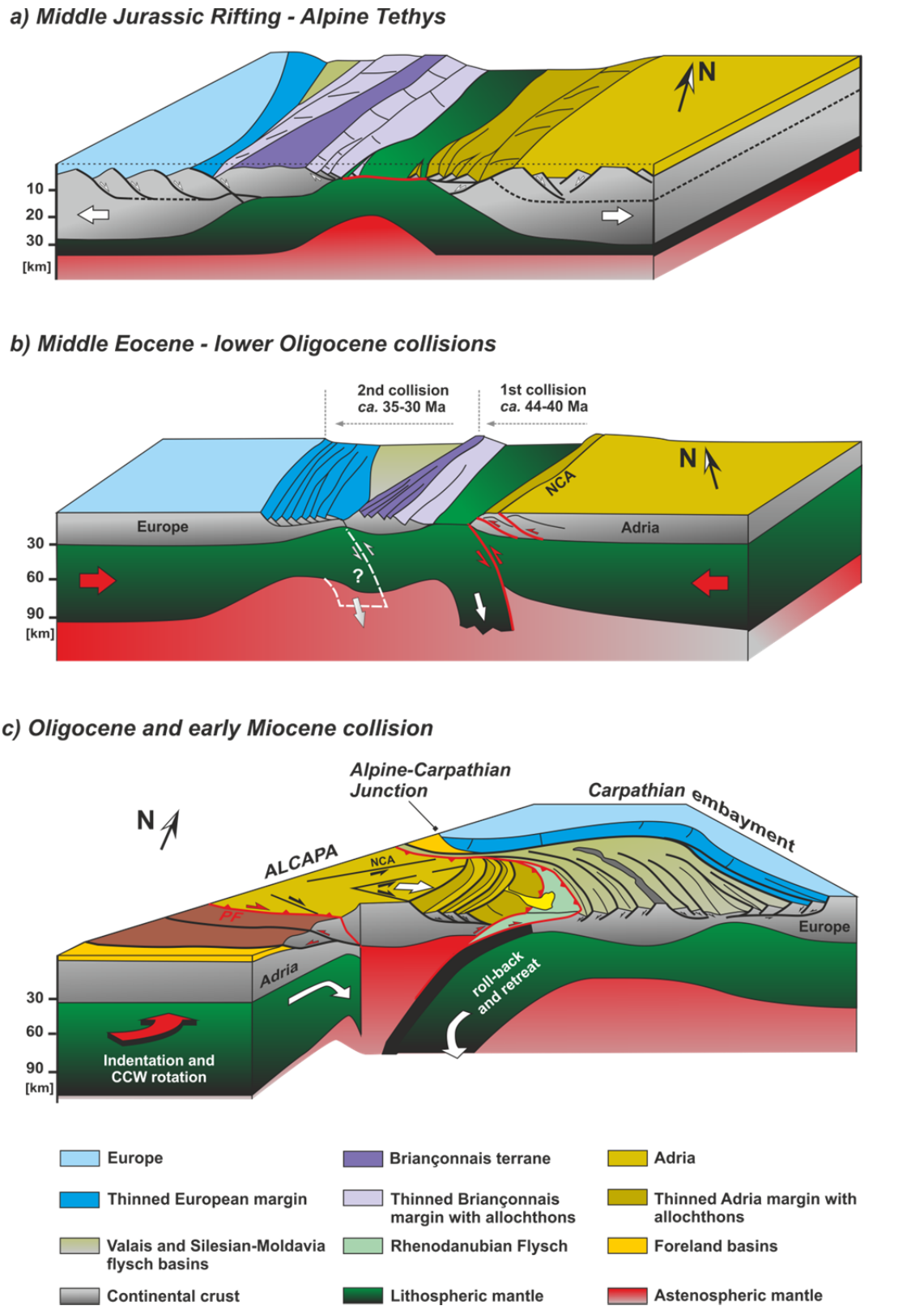

FIGURE 2.5. Synoptic 3D models illustrating the arrangement of plates and terranes in the Alpine Tethys realm during the Mesozoic and Cenozoic. A) Middle Jurassic rifting. B) Middle Eocene to lower Oligocene Neo-Alpine collisions. C) Early Miocene lateral extrusion accompanied by subduction zone retreat and roll-back of the European-Vrancea slab. A and B are modified from Faupl and Wagreich (2000) and Beltrando et al. (2010) whereas C is modified from Horvárth et al. (2006).

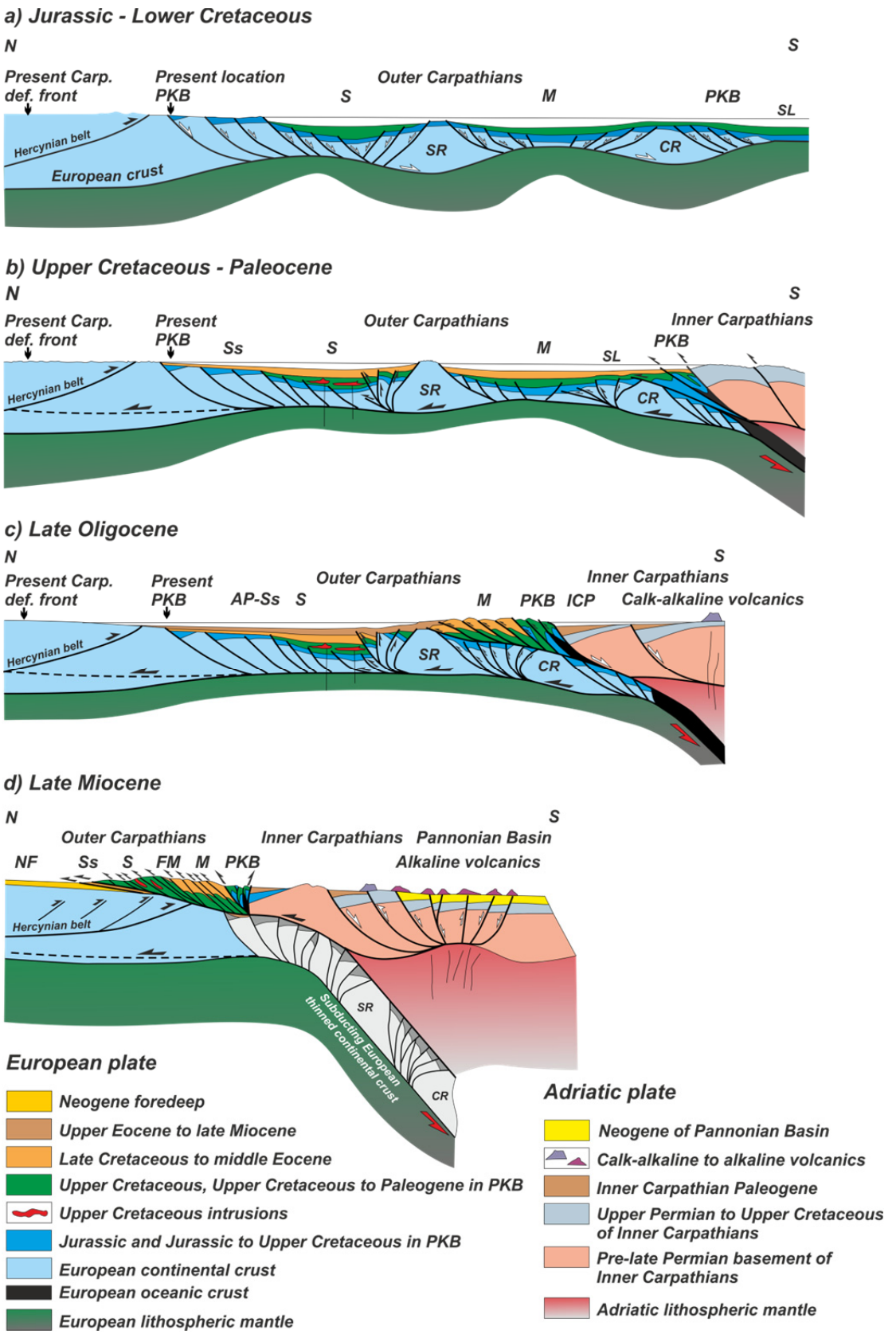

Figure 2.6. Jurassic to late Miocene evolution of the Western Carpathians. AP: autochthonous Paleocene; CR: Czorstyn (Oravic) ridge; ICP: Inner Carpathian Paleogene; M: Magura Flysch; NF: Neogene foredeep; PKB: Pieniny Klipen Belt; S: Silesian unit; SR: Silesian ridge; Ss: SubSilesian unit; SL: Sea level. Modified from Picha et al. (2006).

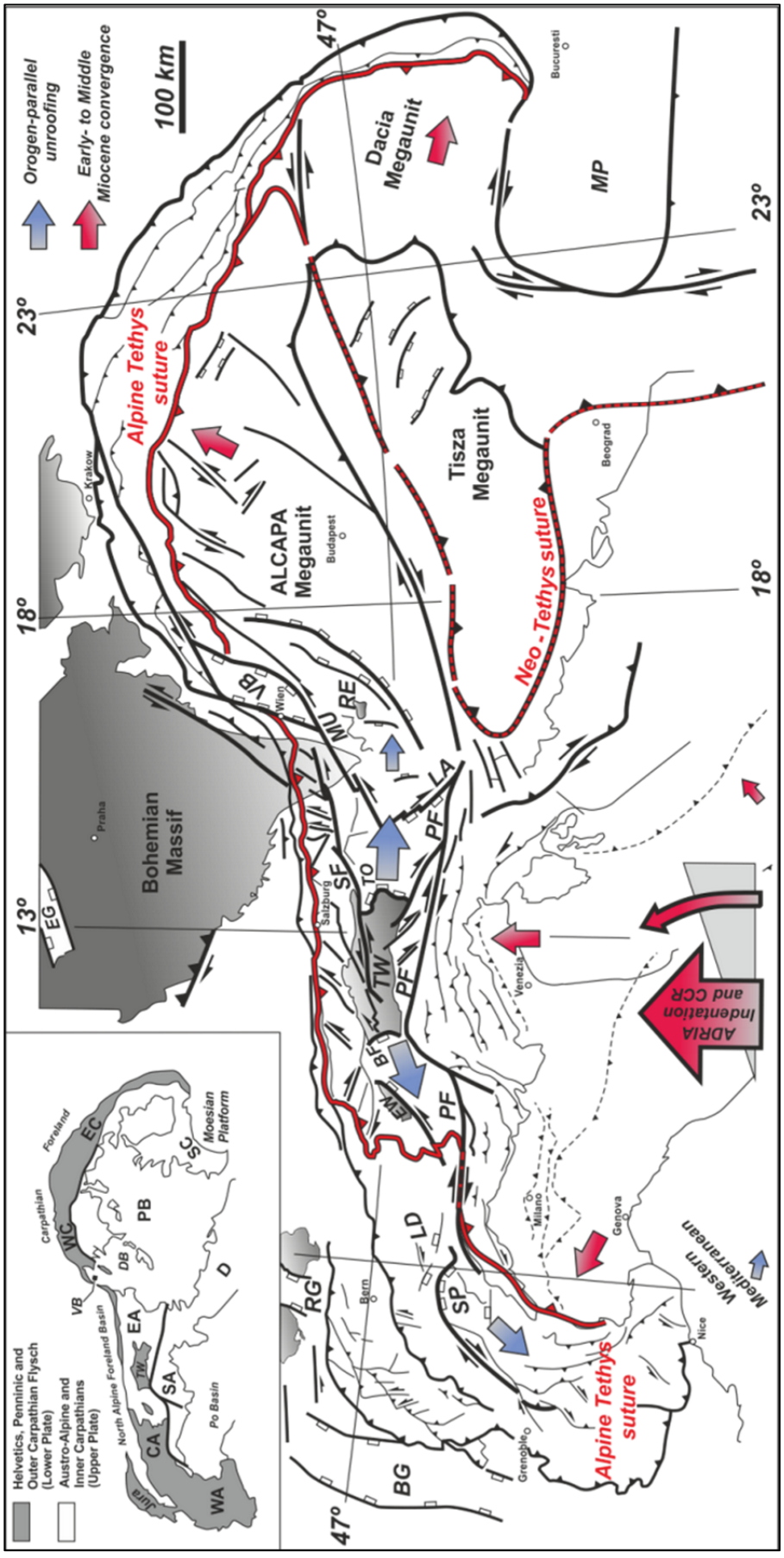

FIGURE 2.7. Early to middle Miocene tectonic framework and kinematics of the Alpine-Carpathian-Pannonian region. BF: Brenner fault; BG: Bresse graben; CA: Central Alps; D: Dinarides; DB: Danube basin; EA: Eastern Alps; EC: Eastern Carpathians; EG: Egger (or Ohře) graben; EW: Engadine window; LA: Lavanttal fault; LD: Lepontine dome; MP: Moesian platform; MU: Mur-Mürz fault; PF: Periadriatic fault; RE: Rechnitz window; RG: Rhine graben; SA: Southern Alps; SC: Southern Carpathians; SF: Salzachtal-Ennstal fault; SP: Simplon fault; TO: Tauernostrand fault; TW: Tauern window; VB: Vienna basin; WA: Western Alps; WC: Western Carpathians. Modified from Decker and Peresson (1996).

The Alpine orogeny also had significant effects north of the Alpine belt, reaching as far as the North Sea. The Cenozoic tectonic evolution of Europe has been largely governed by the far-field transmission of stress resulting from the continental collision in the Alpine belt, the ridge push effect of the Mid Atlantic spreading ridge, the rise of mantle plumes and the northwards retrieve of the glacial ice cap. Alpine tectonics ahead of the Alps started as early as Upper Cretaceous (about Santonian times) times with the Pyrenean collision between the Iberian and the European plates (Muñoz, 2002). The effects of this early shortening propagated northwards through the European crust, reactivating and inverting Permian and Triassic basins inherited from the break-up of Gondwana, as well as the Upper Jurassic to Lower Cretaceous European rift systems (Ziegler, 1987) such as the North Sea Rift (Thomas and Coward, 1995), or the Harz Mountains of Germany (Malz and Kley, 2012). In the Alpine-Carpathian Junction and the Bohemian massif, a Cretaceous to Paleocene shortening event has been proposed (Wessely, 1987; Ziegler, 1987; Picha et al. 2006) as responsible for the large erosion of the 'Helvetic' Lower Cretaceous and Jurassic cover of the Bohemian massif and the present foredeep. Coubal (1990) reported up to 1000 meters of elevation in the basement units of the Bohemian massif associated with the revers reactivation of a NE-dipping, NW-striking fault. On the western (i.e., German) side of the Bohemian massif, Schröder (1987) and Zulauf (1993) also reported uplift and transpression along steeply-dipping basement-involved faults. Lower Cretaceous reverse slip and related sedimentation of similar basement structures have been reported for the foreland of Upper Austria beneath the North Alpine Foreland Basin (Nachtmann and Wagner, 1987; Wagner, 1998).

2.2.6 Deep Structure of the European Alps, the Western Carpathians and the Pannonian Basin.

Early geophysical evidence for the southwards subduction of the European lithosphere beneath an Adriatic lithosphere was provided by the distribution of regional gravity profiles (Karner and Watts, 1983) and magnetic anomalies (Lanza, 1982). The gravity lows in the profiles indicated the down warping of the European Moho beneath the North Alpine Molasse Basin and the Alpine edifice. Positive gravity and magnetic anomalies were found close to the Periadriatic Fault in the Western-Central Alps, and are associated with the Lanzo and Ivrea ultramafic bodies. These imbricated lower crust and

mantle units resulted from the indentation and southwards overthrusting of the Adriatic lithosphere onto the South-Alpine zone along the Periadriatic Fault. More recent regional seismic profiling studies (Blundell et al. 1992; Roure et al. 1996; Pfiffner et al. 1997; TRANSALP Working Group, 2002; Guterch et al. 2003; Brückl et al. 2007, Graßl et al. 2004) and global seismic tomography (Bijwaard and Spackman, 2000; Cavazza et al. 2004) have provided fundamental observations regarding the deep structure of the European Alps (**Fig. 2.8**) and overall agree in the subduction of the European lithosphere underneath the Adriatic one, at least as the initial driving force for the Alpine continental collision.

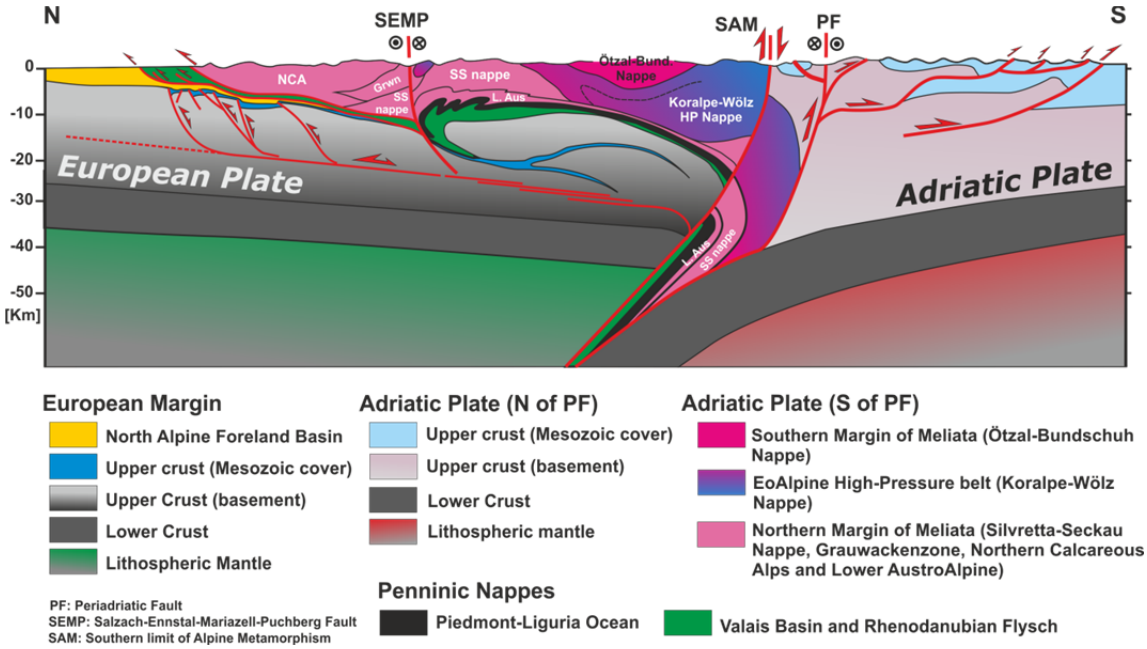

FIGURE 2.8. Lithospheric cross section along the Eastern Alps, east of the Tauern window. Grwn: Grauwacken Zone; L. Aus: Lower AustroAlpine; NCA: Northern Calcareous Alps; SS: Silvretta-Seckau Nappe; SEMP: Salzach–Ennstal–Mariazell–Puchberg fault; SAM: southern limit of alpine metamorphism; PF: Periadriatic fault. Simplified and modified from Schmid et al. (2004) and Ustaszewski et al. (2008). These authors propose the current subduction of the Adriatic lithosphere beneath the European one after the break-off of the later and a subsequent reversal of subduction polarity. See figure 2.2 for location.

Nevertheless, geophysical evidence for subduction polarity changes arose from more recent seismic tomography and mantle seismic anisotropy studies (Bijwaard and Spackman, 2000; Lippitsch et al. 2003). These studies suggested a south-dipping European lithosphere subducting beneath Adria in the Western-Central Alps in agreement with the ECORS-CROP, NPR-20 and TRANSALP studies, but also highlighted a sub-vertical to N-dipping Adriatic lithosphere beneath the Eastern Alps. Based on these works, a model where the Adriatic Plate is undergoing subduction underneath the European lithosphere was proposed, implying a change in the subduction polarity (in space) along the strike of

the orogenic belt from the Western-Central Alps to the Eastern Alps. More recent works based on the upper mantle's seismic anisotropy are in agreement with the former original models with an initial southwards-subduction of Europe beneath Adria (e.g., Bianchi et al. 2014; Qorbani et al. 2014). The most recent integrative models proposed by Handy et al. (2015) and Schlunegger and Kissling (2015) suggest that a change of subduction polarity may have taken place in space but also, in time. Schlunegger and Kissling (2015) have integrated geophysical observations and isostatic mass balance with the stratigraphic record of the North Alpine Molasse Basin, proposing that the apparent absence of elevation in the northern Alpine foreland since 30 Ma argues for an extra loading mechanism in addition to the topographic, subduction and foreland sediment loads (Beaumont, 1981; Jordan, 1981; DeCelles and Giles, 1996; Beaumont et al. 2000). Schlunegger and Kissling (2015) state that break-off of the oceanic section of the subducting European lithosphere was followed by the roll-back, local tearing and delamination of the thickened portion of the European continental lithosphere in order to balance the accommodation space recorded by the North Alpine Foreland Basin. In the Eastern Alps, the continuation of collision between Adria and Europe after the removal of the subducting European continental lithosphere (Bianchi et al. 2014; Qorbani et al. 2014) could have been followed by the northward subduction of the Adriatic lithosphere. This subduction polarity change in space and time reconciliates with the seismic tomography studies that indicate the north-eastwards subduction of the Adriatic lithosphere beneath the Dinarides and the Pannonian area (Cavazza et al. 2004; Horvárth et al. 2006; Brückl et al. 2010; Carminati and Doglioni, 2012; Matenco and Radivojevic, 2012).

2.2.7 THE ALPINE-CARPATHIAN JUNCTION

The Alpine-Carpathian Junction is located in the transition between the easternmost Eastern Alps and the westernmost Western Carpathians. The Junction is characterised by three key structural and physiographical features (**Fig. 2.9**):

1. A strong structural bend in the strike of the orogen from the ENE-WSW-striking Eastern Alps to the NE-SW-striking Alpine-Carpathian Junction and the ESE-WNW- to E-W-striking Western Carpathians.
2. A foreland basin as narrow as 9 km in front of the Bohemian Spur between the frontal thrust and the outcropping crystalline basement of the Bohemian massif.

3. The disappearance of the Alpine structural relief beneath the Neogene cover of the Vienna Basin between the cities of Vienna and Bratislava.

The Alpine-Carpathian Junction spreads from the Lower Austria region of NE Austria (i.e., Niederösterreich), to the Moravian and Silesian regions of the eastern Czech Republic, the western Slovak Republic, and north-western Hungary. The strong structural bend of the Alpine-Carpathian Junction is roughly coincident with the disappearance of the relief beneath the Neogene cover. It is through this low relief junction where the Danube River crosses from the North Alpine Foreland Basin to the NW across the buried Alpine structures into the plains of Slovakia and Hungary, up to its sink in the Black Sea further east.

Another relevant characteristic of the Alpine-Carpathian Junction is its Miocene chronostratigraphy. Based on the occurrence of rare Oligocene and Miocene mollusc fauna in the Pannonian Basin, Laskarev (1924) proposed that remnants of the former Alpine Tethys persisted in a large isolated sea known as the Euro-Asiatic Para-Tethys. This sea spread as far as from the Rhône Basin in France towards Inner Asia, and was individuated into three paleogeographic and tectonic entities: the Western, Central and Eastern Para-Tethys (Rögl and Steininger, 1983). The Central Para-Tethys includes the Eastern Alpine-Carpathian foreland basins, from Lower Austria to Moldavia, as well as the Pannonian basin system. The stratotypes of the Central Para-Tethys realm have been defined in Austria, Hungary, and Czech Republic (see Piller et al. 2007 for a review), where a Central Para-Tethys chronostratigraphy is applied as well as to the Slovak Republic. The Central Para-Tethys chronostratigraphy will be used thereof when referring to the late Oligocene and Miocene stages. The Central Para-Tethys chronostratigraphy and its equivalence to the Western European one are illustrated on **figure 2.10.**

FIGURE 2.9. *Slope-shader* image extracted from a 30m-resolution digital elevation model. The low-relief Miocene basins (i.e., Vienna, Danube and Pannonian) stand out from the rugged relief of the Eastern Alps and the Western Carpathians. Note also how the strike of the Alpine-Carpathian deformation front is significantly controlled by the Bohemian massif salient, where the foredeep becomes as narrow as 9 km. The large rectilinear valleys of the Eastern Alps correspond to the major strike-slip faults related to the Miocene lateral extrusion. Digital elevation model from Shuttle Radar Topography Mission (SRTM) downloaded from http://staff.glcf.umd.edu/sns/branch/htdocs.sns/data/srtm/. V: Vienna; B: Bratislava.

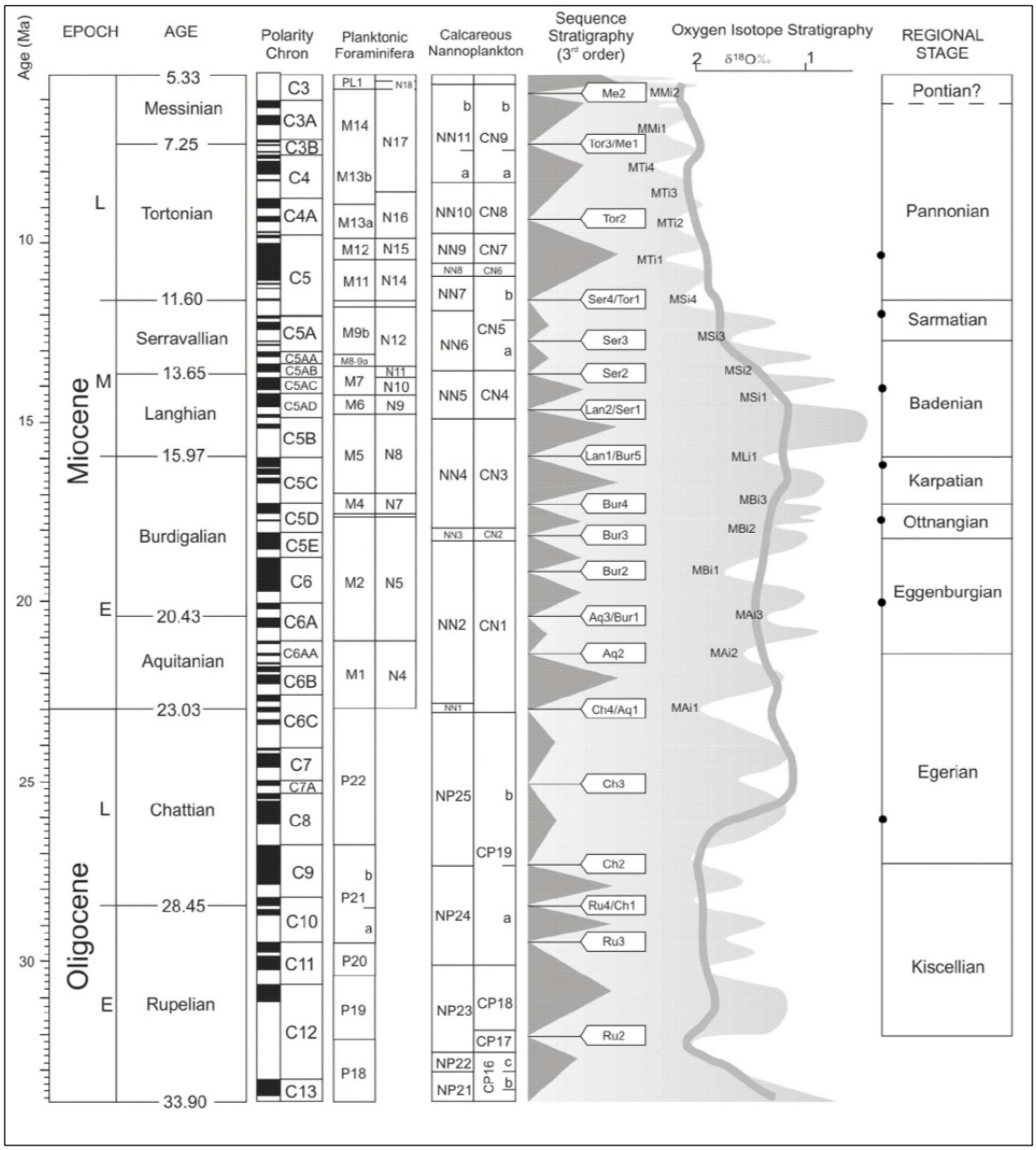

FIGURE 2.10. Oligocene-Miocene Central Para-Tethys stages and their correlation with the Western European ones, the magnetic polarity chrons, planktonic foraminifera, nannoplankton biozones and oxygen isotope curve. From Piller et al. (2007).

From NW to SE, the Alpine-Carpathian Junction displays the following geological units (**Fig. 2.11a**):

a. The European crystalline basement.
b. The Lower Austria Mesozoic Basin, beneath the foreland and in the sub-thrust.
c. The Alpine-Carpathian foreland basin (or Molasse Basin).
d. The Roseldorf-Waschberg-Ždánice Zone.

e. The (Rhenodanubian-Outer Carpathian/Magura) Flysch Zone.
f. The Pieniny Klippen Belt (Western Carpathians only).
g. The Northern Calcareous Alps (and its Carpathian equivalents).
h. The Korneuburg and the Vienna Basins.

In the Alpine-Carpathian Junction, parts of the Rhenodanubian-Magura Flysch and the Northern Calcareous Alps are covered by the Neogene sediments of the Korneuburg, Vienna and Danube Basins (Wessely, 2006; **Fig. 2.11**). Miocene subcrop maps made from subsurface data (i.e., wells and seismic data) reveal a significantly complex framework developed previous to and reworked by the formation of these middle to late Miocene basins (**Fig. 2.12**)

2.2.7.1 THE CRYSTALLINE BASEMENT OF THE ALPINE-CARPATHIAN JUNCTION

The Bohemian massif represents the outcropping crystalline basement of the European plate (**Fig. 2.13**). This crystalline massif was assembled during the Variscan orogeny and consists of Precambrian to Paleozoic medium- to high-grade metamorphic rocks and Variscan granitoids (Kröll and Wessely, 2001; Wessely, 2006). It is cross-cut by major NW-SE and NE-SW fault systems, and to a lesser extent by N-S and E-W striking faults (Wagner, 1998). The Bohemian massif forms a SSE-elongated spur that divides the Lower Austrian Mesozoic Basin to the east from the Upper Austria Mesozoic Basin to the west (Wessely, 1987). No Mesozoic units are preserved on top of the spur (**Fig. 2.14**). The broadly triangular shape of the Bohemian Spur is controlled by the NW-SE and NE-SW fault systems which are as old as late Paleozoic and relate with the collapse of the Variscan orogenic edifice (Wagner, 1998). The Bohemian basement fault array became partly reactivated during the Jurassic rifting and during the Lower Cretaceous to Paleocene shortening (Nachtmann and Wagner, 1987; Schröder, 1987; Wessely, 1987; Coubal, 1990; Zulauf, 1993), but also during the Cenozoic in the Upper Austria (Wagner, 1998) and the Lower Austria Mesozoic basins (Granado et al. 2016).

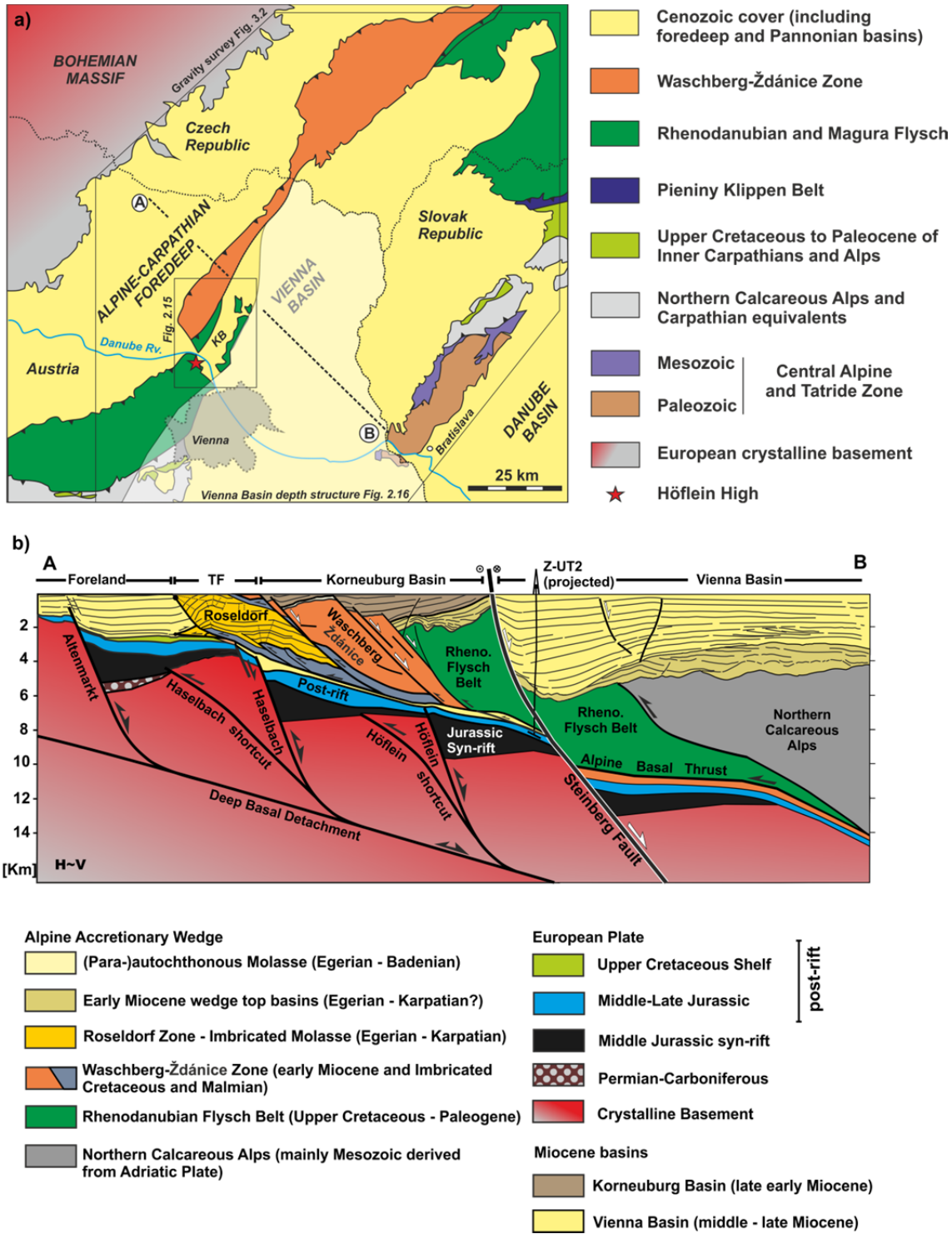

FIGURE 2.11. A) Simplified geological map of the Alpine-Carpathian Junction. Modified from Zimmer and Wessely (1996). B) NW-SE striking geological cross section along the studied area. Modified from Granado et al. (2016) and based on previous works by Zimmer and Wessely (1996), Wessely (2006), Roeder (2010), Beidinger and Decker (2014). KB: Korneuburg Basin.

Well and seismic data have shown that the top of the Bohemian crystalline basement dips gently southwards, and extends beneath the Alpine-Carpathian foredeep and the fold-and-thrust belt as far as 50 km south of the thrust front (e.g., Wessely, 1987; Wagner, 1998; Graßl et al. 2004). Most of the crystalline rock types drilled by hydrocarbon exploration wells had been previously described from the Bohemian massif. The buried spur and the massif are constituted by crystalline rocks of Moldanubikum affinity, whereas the basement of the Lower Austria Mesozoic Basin consists fundamentally of rocks with a Moravikum paleogeographic affinity (Kröll and Wessely, 2001; Wessely, 2006). These two basement domains were assembled during the Variscan orogeny, and their boundary has been interpreted to represent a major orogenic suture (Neubauer and Handler, 2000). In this sense, the Moldanubikum is a higher metamorphic grade, more internal part of the Variscan orogen than the Moravikum. The boundary between the Lower Austria Mesozoic Basin and the Bohemian massif hence corresponds to a major reactivated structure. According to the interpretations from these wells, the basement drilled on the Höflein high belongs to the higher-grade Moldanubikum basement such as the Bohemian Spur (see Höflein1 well, number 50 in **Fig. 2.13**).

2.2.7.2 THE LOWER AUSTRIA MESOZOIC BASIN (LAMB)

From the SW to the NE along the Alpine-Carpathian Junction, the sedimentary cover of the crystalline basement consists of Late Paleozoic and Jurassic to Cretaceous units (Wessely, 1987). Conversely, towards the NE in the Western Carpathians foreland, the Variscan frontal tectonic wedge in found on top of the crystalline basement (Picha et al. 2006; Beidinger and Decker, 2016; see **Fig. 2.6**). The LAMB defines a large, concave-to-the-SE segment belonging to the European Jurassic to Cretaceous continental margin of the Alpine Tethys (Frisch, 1979; Wagner, 1998). It developed upon the Jurassic stretching and rifting of poly-deformed European crystalline basement. In the LAMB, the oldest rocks unconformably overlying the crystalline basement are represented by clays, sandstones, breccias, and coal seams of Carboniferous to Permian age; local volcanic intercalations associated with the latest Variscan cycle and orogenic collapse are also found (Kroner et al. 2008). These igneous units have been drilled in several wells, including the Mailberg1 and Holabrunn1 (i.e., wells 45 and 36, respectively in **Fig. 2.13**) associated with the NE-SW-striking basement fault array.

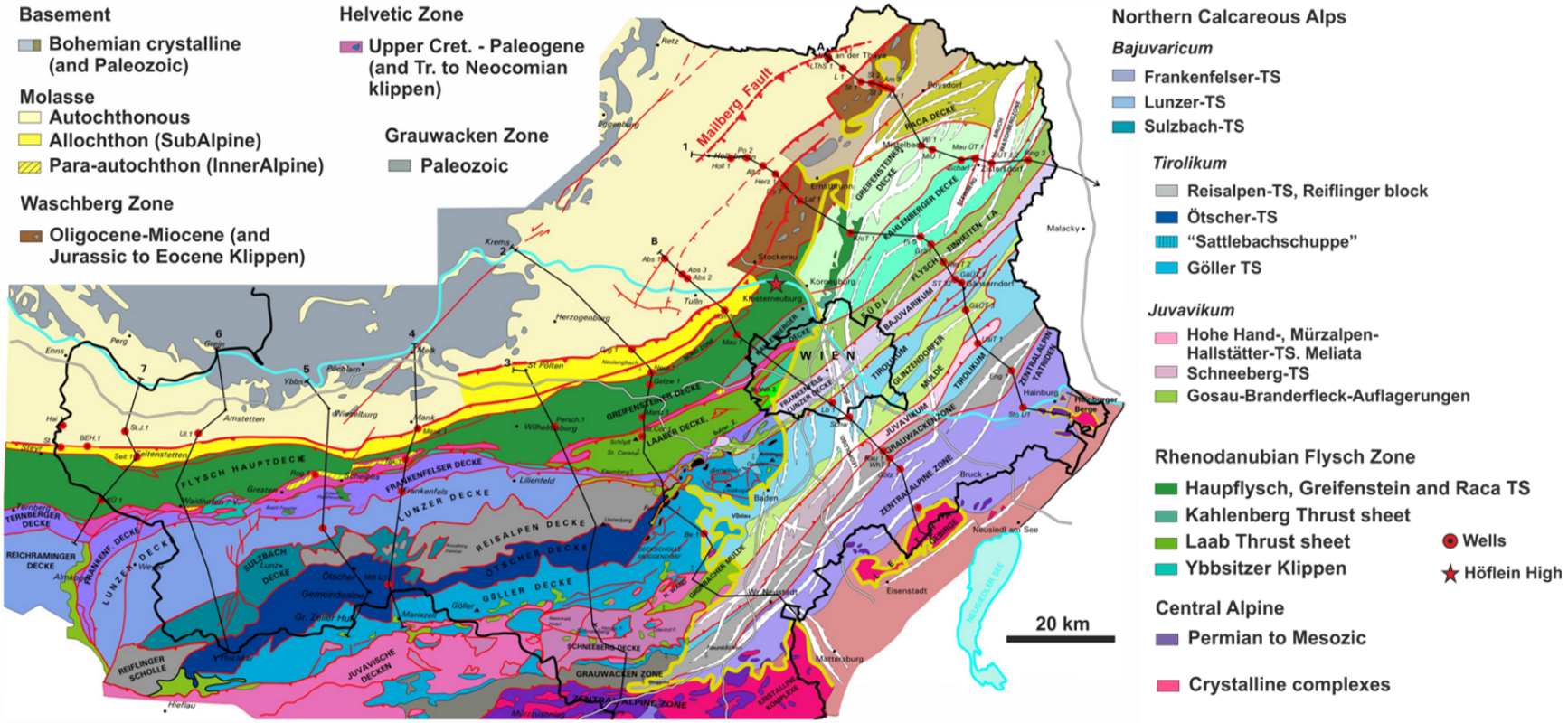

FIGURE 2.12. The Eastern Alps and their correlation beneath the Vienna Basin in Austria. Note the large extensional fault heaves of the middle to late Miocene extensional faults of the Vienna Basin. Modified from Wessely (2006). TS: Thrust sheet (i.e., nappe).

The Lower Austria Mesozoic Basin is controlled by a large, mainly NE-SW striking and SE-dipping basement fault array. The spacing between these faults is about 10 km perpendicular to their strike, indicating that these faults must sole deep in the crust into the brittle-plastic transition (Rutter, 1986; Scholz, 1988) as suggested by Granado et al. (2016). Large, fault-bound syn-rift wedges of Middle Jurassic fluvial to deltaic sediments are found associated with the NE-SW-striking basement faults. These deposits record the onset of Jurassic rifting in the area. These Middle Jurassic syn-rift deposits are extensively covered by a post-rift carbonate platform to slope system starting in Callovian times and lasting for the whole Upper Jurassic (**Fig. 2.14**). These syn-rift and post-rift units are commonly referred to as the Autochthonous Mesozoic series (Wessely, 1987). In Lower Austria, these units have been fundamentally defined based on the geological results of drilling activities in the search for hydrocarbons (Grün, 1984; Ladwein, 1988; Sauer et al. 1992; Brix and Schultz, 1993; Sachsenhofer et al. 2006).

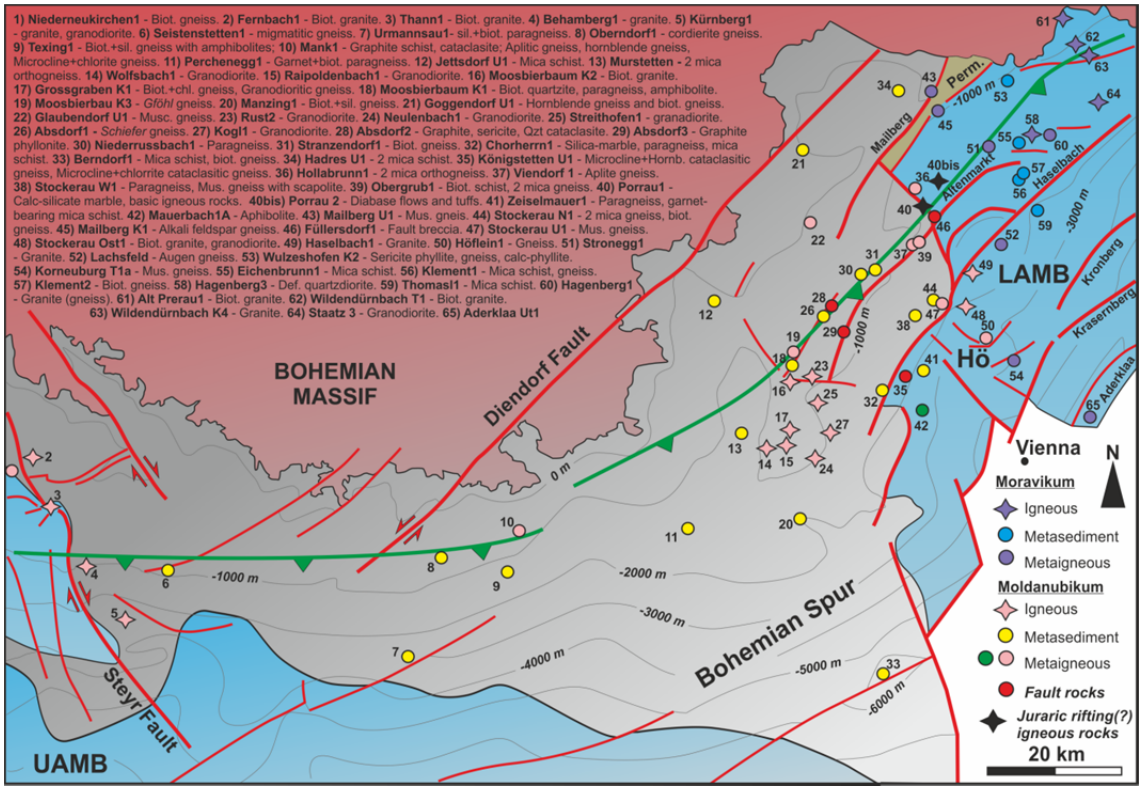

FIGURE 2.13. Subcrop map compiled from well intersections of the crystalline basement. Note the different paleogeographic assignation of the crystalline basements of the Bohemian massif (and its spur) and the Lower Austria Mesozoic Basin. Modified from Wessely (2006) but compiled from Kapounek et al. (1967), Kröll and Wessely (2001). The green line depicts the approximate present-day location of the Alpine-Carpathian thrust front (from Beidinger and Decker, 2014). LAMB: Lower Austria Mesozoic Basin. UAMB: Upper Austria Mesozoic Basin. Well numbers and their names are provided at the top. The Höflein1 well (Hö) is number 50.

The Jurassic sediments ascribed to the Lower Austria Mesozoic Basin have been found by ultra-deep exploratory drilling (Zimmer and Wessely, 1996) beneath the Vienna Basin and the underlying tectonic wedge. The Aderklaa ÜT-1 (well 65, **Fig. 2.13**) near the city of Vienna bottomed in crystalline basement at 6245 meters after drilling trough 173 meters of Upper Jurassic marls and 22 meters of a carbonate section. The well Zistersdorf ÜT2A north of Vienna drilled 145 meters of Tithonian carbonates and almost 900 meters of marls assigned to the Upper Jurassic, bottoming at 8553 meters. A twin well, Zistersdorf ÜT1 finished into upper Oligocene and Eocene Molasse sediments at 7544 meters, interpreted to lie above the Mesozoic section. The well Maustrenk ÜT1 drilled a similar section between 6050 and 6563 meters depth. From the available data, the post-rift basin apparently had a semi-circular shape where marginal carbonate platforms were fringed by a deeper water basin area opened to the east toward the Alpine Tethys (Wessely, 1987, 2006).

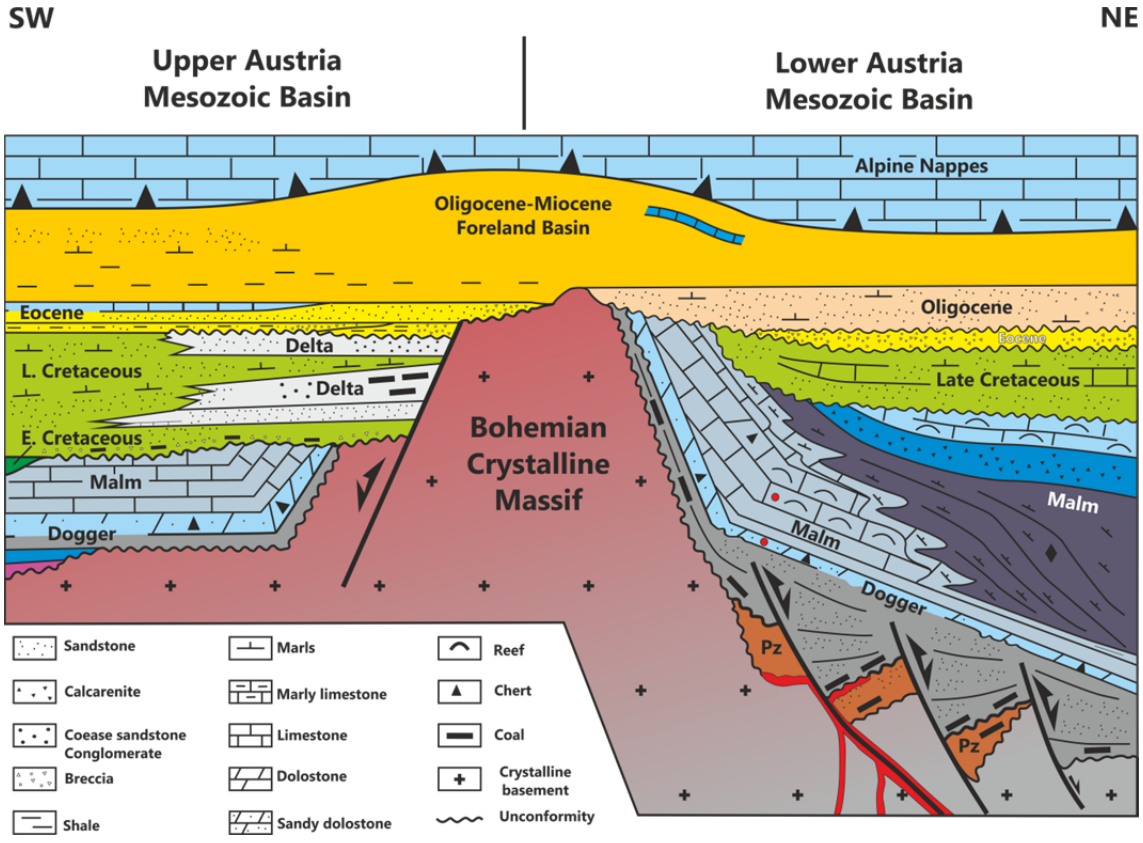

FIGURE 2.14. The Bohemian spur and the Mesozoic basins of Upper and Lower Austria. Note the absence of Mesozoic units on the Spur, as well as the different stratigraphy of both basins. The Triassic, Lower Jurassic and Lower Cretaceous are represented in the Upper Austria Mesozoic Basin, whereas they are not represented in the Lower Austria Mesozoic Basin. The Lower Austria Mesozoic Basin also displays coal-bearing Middle Jurassic syn-rift wedges bound by faults, whereas the post-rift is represented by a Upper Jurassic carbonate platform to slope system. Modified from Wessely (1987).

As the Lower Austria Mesozoic Basin remains covered beneath thick foreland deposits, the fold-and-thrust belt and the Vienna Basin, the distribution of the post-rift facies in regards to that of the syn-rift and the underlying basement fault array is poorly constrained. In fact, the reconstruction of this Jurassic-Cretaceous basin is also hampered by the strong Cretaceous and Paleocene erosion that affected the Bohemian massif and its sedimentary cover (Wessely, 1987), as well as by the Cenozoic syn-collisional extensional and compressional reactivation of the basement fault array (Granado et al. 2016). The syn-rift and post-rift units were largely sourced from the Bohemian massif, in particular the Middle Jurassic and Upper Cretaceous materials according to their facies associations (Wessely, 1987). In this thesis, the sedimentary infill of the LAMB has been grouped into a pre- to syn-rift and a post-rift megasequence division and is explained in more detail the following sections.

2.2.7.2.1 PRE- TO SYN-RIFT MEGASEQUENCE

The pre- to syn-rift megasequence is constituted by the Middle Jurassic Gresten Group (Sachsenhofer et al. 2006). Its thickness varies significantly as a result of Jurassic rifting and it has been reported to be as thick as 1500 meters in the literature (Wagner, 1998). However, according to this study it can be as much as twice these figures (Granado et al. 2016). In well Porrau2 (i.e., well 40bis, **Fig. 2.13**) volcanoclastic diabase flows and tuffites of probably Aalenian-age (i.e., lowermost Middle Jurassic, *ca.* 174-170 Ma) occur below the base of the Gresten Group, close to the western margin of the Lower Austria Mesozoic Basin.

The Gresten Group is constituted from base to top by four units: the Lower Quartzarenite Formation, the Lower Claystone Formation, the Upper Quartzarenite Formation and the Upper Claystone Formation (Wessely, 1987; Sachsenhofer et al. 2006). The Lower Quartzarenite Formation is constituted by coal-bearing arkoses, quartzarenites coaly-shales and shales with plant remains. It has been dated as Aalenian, and interpreted as deposited on a braided river system and deltaic to coastal plain environments. On seismic data it is characteristically shown as bright continuous reflections associated with the coal measures. It is considered as belonging to the pre-rift megasequence as it displays a rather even thickness on the hanging-wall of the rift faults.

The following formations are hosted within thick fault-bound wedges revealed by seismic and well data and have been ascribed to the syn-rift megasequence. The Lower Claystone Formation is constituted by dark claystones and is dated as Bajocian with ammonite fauna. It is interpreted as deposited in a prodeltaic marine environment. Above, the Upper Quartzarenite Formation is constituted by quartzarenites with dolomitic cement, interpreted as shallow-marine to deltaic, and dated as Bathonian with ammonite fauna as well. The Upper Claystone Formation is constituted by thin, dark marine shales which grade laterally into calcarenite coastal facies and is dated as well as Bathonian in age. As a whole, the syn-rift megasequence represents a transgressive clastic system (Wessely, 1987). The quartzarenite beds of the Gresten Group have been targeted as gas reservoirs in Lower Austria (i.e., at the Höflein field), whereas the coal measures of the Lower Quartzarenite Formation are thought to be a CO_2 and H_2S-rich gas source rock (Sachsenhofer et al. 2006).

2.2.7.2.2 POST-RIFT MEGASEQUENCE

The post-rift megasequence is represented by a carbonate platform to slope system (Wessely, 1987; Sauer et al. 1992; Adámek, 2005; **Fig. 2.14**). The post-rift megasequence commences with the Callovian (*ca.* 165 Ma) Höflein Formation. The Höflein Formation is significantly extensive and is present throughout the Lower Austria Mesozoic Basin expanding over the Gresten Group up to the rift shoulder represented by the Bohemian Spur. The deep well Kronberg was drilled on the footwall block of a basement rift fault (i.e., the Kronberg high), where the Höflein Formation was missed (see Zimmer and Wessely, 1996 and Granado et al. 2016, for different interpretations of the well results). The Höflein Formation is reported to be around 250 meters thick (Wessely, 1987; Wagner 1998; Adámek, 2005), but alternative estimates lower this figure down to only about 55 meters (Sauer et al. 1992). The Höflein Formation is made up of light to dark grey sandy dolostones to greenish-grey glauconite-rich sand beds and chert nodules, sometimes porous, sometime tight. It frequently occurs fractured, sometimes with solution-enlarged fractures (Sauer et al. 1992). It also occurs as variably silicified and dolomitized chert-nodule-bearing, glauconite-rich medium to coarse-grained (even conglomeratic) polymictic sandstones (i.e., commonly referred to as the "doloquartzarenite"). Characteristically, the

porous chert nodules are irregular in shape and irregularly distributed, but always associated with the sandy dolostones (Sauer et al. 1992).

The Höflein Formation constitutes the most important reservoir in the Alpine–Carpathian sub-thrust region (Sauer et al. 1992; Zimmer and Wessely, 1996). The chert nodules are mainly constituted by microcrystalline quartz, with inclusions of detrital quartz grains, glauconite, feldspar and dolomite rhombohedra. The source of silica to form the chert nodules may have originated from resedimented sponges with silica spicules. Primary porosity is macroscopic in the porous cherts, and is enhanced by a secondary fracture porosity whose abundance is directly proportional to that of the chert nodules. Effective porosities are in between 1.3 and 24%, with a 16% mean value, whereas permeability values are from 0.1 to 1119 md, with a mean value of 30.2 md (Sauer et al. 1992).

The Höflein Formation is overlain by Oxfordian to Kimmeridgian platform carbonates fringed by slope to deeper water facies. The platform carbonates are commonly referred to as the Altenmarkt Formation (Ladwein, 1976) or Altenmarkt Group (Adámek, 2005). This unit consists of thin-bedded, cherty carbonates grading upwards into bioclastic limestones, overlain by algal- and sponge-bearing carbonates with abundant detritus. The whole sequence is usually topped by reef build-ups of sponge-algal bioherms at the base and corals reefs above (Sauer et al. 1992). These reef build-ups grade laterally into oolitic and bioclastic limestones. These carbonate platform facies are fringed laterally by marly limestones and re-sedimented carbonates known as the Falkenstein Formation. All these platform facies associations grade basinwards (i.e., to the SE) into deeper water facies represented by the dark basinal marls of the Mikulov Marls (Adámek, 2005). The Mikulov marls range in thickness from 600 to 1000 meters and constitute the most important source rock and the basal detachment of the Alpine–Carpathian fold-and-thrust (**Fig. 2.11b**).

Sediment by-passing and progradation followed as represented by coarsening-upwards terrigenous and bioclastic turbidite sedimentation (i.e., Kurdejov Formation). The age of the Kurdejov Formation has been recently updated as Kimmeridgian to early late Tithonian based on ammonite biostratigraphy and micropaleontology (Schneider et al. 2013). The Kurdejov Formation is partially covered by the Ernstbrun Formation. According to recent work by Schneider et al. (2013), the transition between both units is gradual, and the Ernstbrun Formation is constituted by lagoonal to patch reef facies, fringed by ooid-oncoid bars deposits. The age of the Ernstbrun Formation is middle Tithonian to Berriasian (Hauterivian?). Both the Kurdejov and Ernstbrun formations have

been reported in wells (Wessely, 1987; Zimmer and Wessely, 1996; Wessely, 2006), but also occur as tectonic slices with the Waschberg-Ždánice Zone (Schneider et al. 2013).

In Upper Austria and on the Bohemian massif the Cretaceous is widely represented, either covering large parts of the Jurassic sequences, or being directly deposited onto the crystalline basement, respectively (Klein et al. 1979; Wessely, 1987; Hamilton et al. 2000). Conversely, in Lower Austria an Upper Cretaceous cover was unconformably deposited in a marine shelf environment over the Upper Jurassic to Lower Cretaceous and the crystalline basement. This Upper Cretaceous cover is unevenly distributed, and most of the Lower Cretaceous is regarded as a hiatus of regional extent (Wessely, 1987, 2006; Sauer et al. 1992; Hamilton et al. 2000; Adámek, 2005). In Lower Austria, the autochthonous Cretaceous is restricted to the Cenomanian-Maastrichtian unconformably deposited onto the Tithonian to Berriasian carbonates. The Upper Cretaceous starts with a basal marine transgressive unit of glauconite-rich sandstone, grading upwards to bioturbated marly sandstones and siltstones, and locally, into Turonian age limestones. Above, *Senonian* marine sandy marls are present. The whole Upper Cretaceous sequence has never been penetrated in a single well, but its cumulative thickness has been calculated to be about 900 meters thick (Fuchs and Wessely, 1977; Wessely, 1987, 2006).

2.2.7.3 THE ALPINE-CARPATHIAN FOREDEEP

The sedimentary infill of the Alpine-Carpathian foredeep is commonly referred to in the literature as the Autochthonous Molasse (Sauer et al. 1992; Wagner, 1998; Zimmer and Wessely, 1996; Wessely, 2006). It locates at the fold-and-thrust belt deformation front, between the Bohemian crystalline massif to the NW and the Roseldorf-Waschberg-Ždánice Zone to the SE (**Figs. 2.11** and **2.12**). As proven by deep exploratory drilling (wells Zisterdorf ÜT1a and ÜT2a, Zimmer and Wessely, 1996), the Autochthonous Molasse extends further SE for several tens of kilometres beneath the thrust belt and the Vienna Basin. It consists of Egerian to Karpatian age siliciclastic units that remained in the footwall of the main thin-skinned Alpine Basal Thrust (Beidinger and Decker, 2014). As illustrated by Granado et al. (2016), these sediments are actually deformed by the late early Miocene to earliest middle Miocene reactivation of the basement fault array beneath and ahead of the thin-skinned thrust front (**Figs. 2.12** and **2.13**). Evidence for these reactivation

episodes has been reported by Granado et al. (2016) based on the interpretation of seismic data covering the foreland, and its integration with the Badenian sediment distribution reported by Mandic (2004). For this reason, Granado et al. (2015) originally referred to the autochthonous Molasse as the para-autochthonous Molasse.

2.2.7.4 THE ROSELDORF-WASCHBERG-ŽDÁNICE ZONE OR IMBRICATED MOLASSE

The Roseldorf-Waschberg-Ždánice Zone is located north of the Danube River (**Figs. 2.11** and **2.12**) and represents the external NE-SW-striking leading edge of thin-skinned deformation in the Alpine-Carpathian Junction. The Roseldorf Zone is also referred in the literature as the Imbricated Molasse, and corresponds to the truly thin-skinned deformation front of the Alpine-Carpathian fold-and-thrust belt. The Waschberg-Ždánice Zone is the immediately more internal unit of the fold-and-thrust belt. This NE-SW-striking thin-skinned deformation front is offset by a series of perpendicular (i.e., NW-SW-striking) tear-like faults. The larger of these faults juxtaposes the Rhenodanubian Flysch Zone to the south of the Danube River with the Waschberg- Ždánice Zone to the north, and corresponds as well with the southwestern boundary of the early Miocene Korneuburg Basin (**Fig. 2.11**). The Roseldorf-Waschberg-Ždánice Zone is constituted by a series of NW-directed thrust imbricates involving Egerian to Karpatian Molasse clastic sediments, along with exotic blocks of Mesozoic and Paleogene units (i.e., commonly referred in the local literature as *klippen*) sheared off from the underlying autochthonous. These Mesozoic to Paleocene units can be considered equivalent to the Swiss Helvetic nappes. The Helvetic imbricates are significantly thinner than their Western and Central Alps equivalents due to the significant erosion of the Helvetic cover as a result of the Cretaceous and Paleocene intra-plate shortening; in addition, an originally thinner sequence cannot be excluded. Therefore, these thin imbricate slices were formed from the erosional remnants of a thin Helvetic sedimentary prism (Wessely, 1987; Schmid et al. 2004). Geological maps have also revealed the presence of crystalline blocks of uncertain affinity within these imbricated sheets, probably scrapped off from the European and the Penninic basements as well. Beneath the Vienna Basin sediments correlatable with the Waschberg-Ždánice Zone have been found (**Fig. 2.11b**) in the deep wells Zisterdorf ÜT and Maustrenk ÜT (Sauer et al. 1992).

2.2.7.5 THE RHENODANUBIAN-OUTER CARPATHIAN FLYSCH ZONE

The Flysch Zone is sandwiched between the Waschberg-Ždánice Zone to the NW and the Northern Calcareous Alps thrust stack to the SE (**Fig. 2.11a**). The Flysch Zone consists of a long strip of mostly Lower Cretaceous to middle Eocene imbricated turbidites. The Flysch Zone runs from the Eastern Alps towards the Western Carpathians for about 500 km. This accretionary wedge also incorporated parts of the former Penninic Ocean as well as the distal units of the European margin (i.e., the Ultra-Helvetics). To the NE of the city of Vienna, the Flysch Zone is buried beneath the thick Neogene cover of the Vienna Basin, where these thrust imbricates have attained significant extensional faulting (**Figs. 2.11b** and **2.12**). The Rhenodanubian Flysch sediments were deposited on a trench developed in between the European and the advancing Adriatic plate, probably on oceanic crust of the Penninic domain of the Eastern Alps (i.e., Ybbsitz klippen), and on thinned continental crust further east into the Carpathian embayment (compare **figures 2.5** and **2.6**). In Lower Austria, the age of the Flysch Zone sediments ranges from Hauterivian to Eocene, overall becoming younger to the east. Four large tectonic units have been defined for the Rhenodanubian Flysch Zone in the easternmost Eastern Alps: the Haupt Flysch, Greifenstein, Laab and Kahlenberg thrust sheets (**Fig. 2.12**). The cumulative thickness for each of these main thrust sheets is in excess of 1000 meters (Sauer et al. 1992). The Ybbsitz klippen is interpreted as imbricated true oceanic basement and in the Alpine-Carpathian Junction has been correlated with the Kahlenberg nappe (Decker, 1990; Egger, 1990, 1992; Schnabel, 1992). The Ybbsitz klippen consists of Jurassic deep-sea facies with radiolarites, mafil/ultramafic rocks, pillow basalts, serpentinites and ophicalcites, along with a flysch sedimentary cover of Cretaceous age. Beneath the Vienna Basin, the Rhenodanubian Flysch Zone has also been described and consists of the Raca, Greifenstein, Kahlenberg and Südliche Flysch Einheiten units (Sauer et al. 1992; Wessely, 2006; **Fig. 2.12**). In the Alpine-Carpathian Junction, the Flysch Zone records important NE-, N- to NW-directed shortening. Cross-sections restorations and fission track thermochronology have indicated significant out-of-sequence thrusting and strike-slip deformation (Trautwein et al. 2001; Andreucci et al. 2013; Casteluccio et al. 2015; Beidinger and Decker, 2016). Thrust-related shortening in the Flysch Zone has been calculated to be in the order of several hundreds of kilometres (Roure et al. 1993; Decker and Peresson, 1996; Beidinger and Decker, 2016).

2.2.7.6 THE NORTHERN CALCAREOUS ALPS

The Northern Calcareous Alps (NCA) form a *ca.* 500 km long by 20 to 50 km wide complexly deformed fold-and-thrust belt. The NCA strike ENE along the Eastern Alps, continue beneath the Vienna Basin and outcrop again at the Western Carpathians. The NCA comprise Permian to Eocene sedimentary rocks -including the Upper Cretaceous to Eocene Gosau units- with only local and poor metamorphic overprint, but are fundamentally dominated and known by the abundant Triassic carbonate units. The most widely accepted view for the NCA is that they were sedimented during the Permian-Triassic on the northern continental margin of the Neo-Tethys realm facing the Meliata Ocean (**Fig. 2.4a**). From north to south, and structurally from bottom to top, the NCA have been divided as follows: the northern frontal parts are represented by the Bajuvaric Nappes which are deformed into narrow and tight folds. Toward the south, the Bajuvaric Nappes are overthrusted by the Tyrolic Nappes. The Tyrolic Nappes are dominated by stiff faulted and thrusted dolostones. The Juvavic Nappes are structurally above. In broad terms, these nappes were arranged from a proximal (i.e., Bajuvaric) to a more distal (i.e., Tyrolic-Juvavic) position along the Triassic continental margin facing the Meliata Ocean (Mandl, 2000). The arrangement of the Northern Calcareous Alps nappes in the Eastern Alps and beneath the Vienna Basin is represented in **figure 2.12**. However, the evolution and paleogeographical correlations of the NCA are still strongly debated (see Mandl, 2000). Additional details on their stratigraphy and tectonic evolution are available from Tollmann (1959, 1977, 1985, 1986) and Wessely (2006).

2.2.7.7 THE KORNEUBURG AND VIENNA BASINS

The Korneuburg and Vienna Basins developed over the Alpine-Carpathian fold and thrust belt on the western margin of the Bohemian massif. The opening of these basins was partly synchronous with the late stages of early Miocene thin-skinned shortening, and buried the Rhenodanubian Flysch Zone and the Northern Calcareous Alps (**Figs. 2.11a** and **2.12**) beneath as much as 6000 meters of middle to late Miocene sediments. The Korneuburg Basin is located west of the larger Vienna Basin (**Fig. 2.16**). The Korneuburg Basin developed slightly before the Vienna Basin over the Waschberg-Ždánice Zone to the NE and over the Flysch Zone to SW (i.e., slightly oblique to the underlying fold-and-thrust

belt). The Korneuburg Basin forms an asymmetrical sedimentary wedge that thickens towards the NE-SW-striking and SE-dipping Schliefberg fault. It runs for 20 km along strike and is 7 km wide (**Fig. 2.15**). The SE-dipping Schliefberg fault accommodated up to 800 meters of Karpatian sediments arranged in two isolated depocenters separated by a fault-perpendicular ridge (Wessely, 1988; Harzhauser and Wessely, 2003; Wessely, 2006). The basin can be regarded as a strictly 'thin-skinned' feature in the sense that the bounding Schliefberg fault soles within the shallow thrust imbricates with no structural connexion with the crystalline basement. The Karpatian infill of the Korneuburg Basin is constituted by grey to yellow marly silts and fine- to medium-grained sandstones belonging to the Korneuburg Formation (Wessely, 1988). The Karpatian units were deposited on top of Eggenburgian sediments assigned to the Ritzendorf unit (Harzhauser and Wessely, 2003). These Eggenburgian sediments are similar in age to those sediments found beneath the thick middle to late Miocene fill of the Vienna Basin (see cross section in **Fig. 2.11c**). In addition, the Karpatian age of the Korneuburg Basin is coincident with that of the youngest growth strata of the thin-skinned deformation front (Harzhauser and Wessely, 2003; Hölzel et al. 2010; Beidinger and Decker, 2014). The Korneuburg Basin hence developed synchronous to or immediately after the cessation of late early Miocene thin-skinned thrust deformation at the Roseldorf Zone. The Höflein basement high locates immediately to the south of the Korneuburg Basin boundary beneath the NW-SE-striking transfer fault that juxtaposes the Waschberg-Ždánice Zone with the Rhenodanubian Flysch Zone. Additional hydrocarbon accumulations (i.e., Stockerau and Roseldorf fields) are present in the area associated with the thin-skinned deformation front but arranged on a N-S-striking trend (**Fig. 2.15**).

The Vienna Basin is located to the SE of the Korneuburg Basin (**Figs. 2.9** and **2.11**) and is a considerably larger and more complicated basin from a structural and sedimentological point of view. It roughly strikes NNE-SSW for about 200 km and is as much as 60 km wide. It has been described as a classical rhombohedral pull-apart basin formed over an active left-lateral pattern of strike-slip faults (Royden, 1985; Wessely, 1988). The Vienna Basin is considered to have developed coevally to the late stages of shortening in this region of the Alpine-Carpathian fold-and-thrust belt (Kapounek et al. 1965).

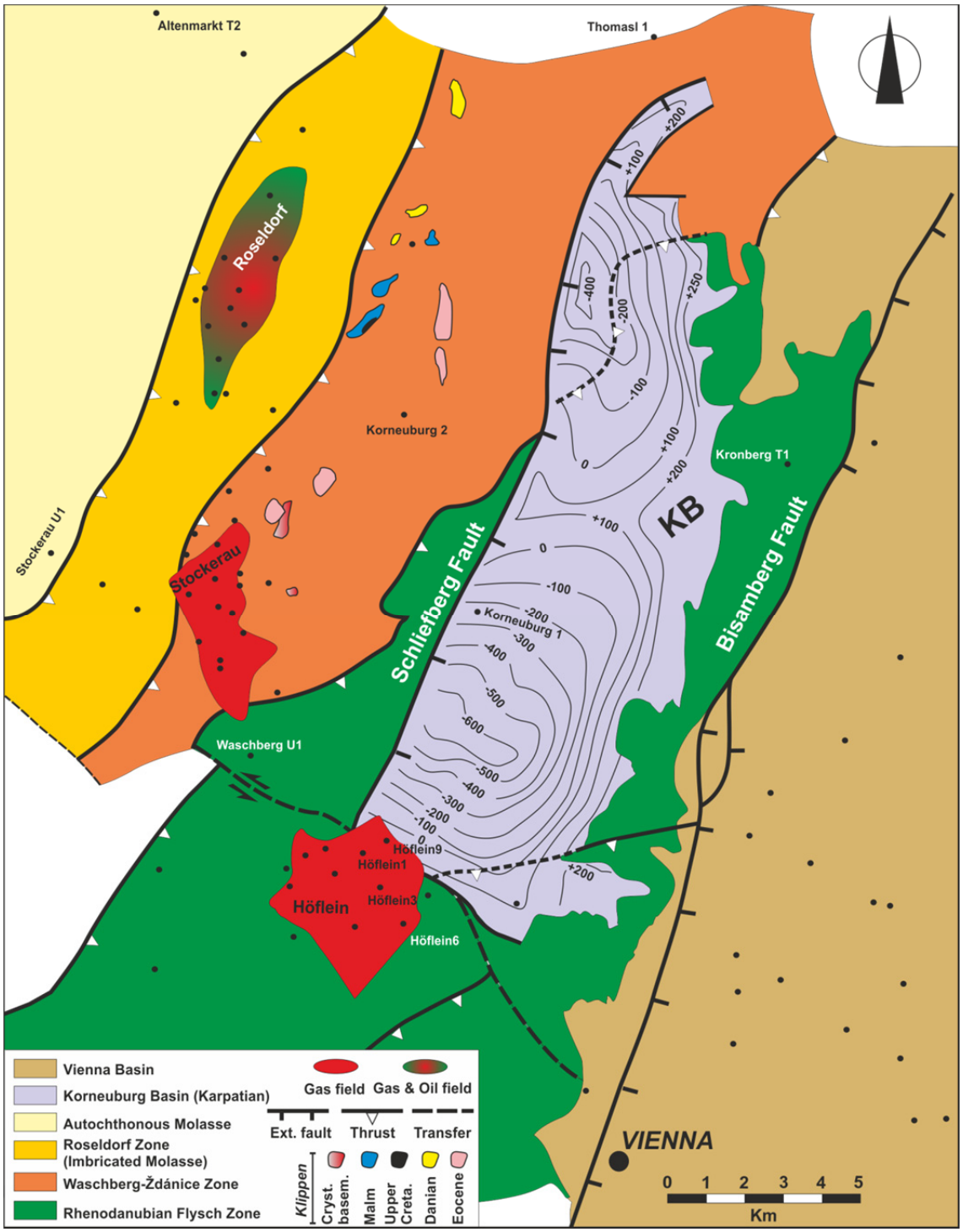

FIGURE 2.15. The Korneuburg Basin. The contour lines indicate the elevation of the basin's floor to sea level reference, indicating up to 800 meters of Karpatian age sediments. The Waschberg-Ždánice Zone includes '*klippen*' blocks of Mesozoic and Cenozoic units as well as crystalline basement. The Höflein field is located deep beneath the thrust belt whereas the Stockerau and Roseldorf fields are hosted in the thrust front imbricates. See **figure 2.11a** for location. The Schliefberg and Bisbanberg faults are late early to middle–late Miocene extensional faults related to the Pannonian extension. Modified from Wessely (2006).

The widely accepted models for the formation of the Vienna Basin propose an interaction between thrust-related shortening and the lateral extrusion of the Alpine belt towards the Carpathian embayment (Royden, 1985; Wessely, 1988; Ratschbacher et al. 1991b; Linzer et al. 2002). These models highlight the significant control imposed by the shape of Bohemian Spur on the kinematics and propagation of thrusting and the associated formation of the Vienna Basin. The shape of the spur (and the lack of an efficient detachment) blocked the propagation of thin-skinned thrusting in the easternmost Eastern Alps and the Alpine-Carpathian Junction, but allowed for its propagation toward the unconstrained foreland of the Western Carpathians. As a consequence, left-lateral tearing of the thin-skinned thrust system favoured the opening of the Vienna Basin as a rhombohedral pull-apart (Royden, 1985; Wessely, 1988). Internally, the Vienna Basin consists of a series of horst and grabens bordered by anastomosing faults and relays, broadly striking NE-SW and NNE-SSW. In fact, the approximate axis of the basin is delineated by a series of horsts arranged in a slightly sigmoidal fashion and bound by curvilinear faults (Wessely, 1988). The main structural elements of the Vienna Basin were defined by Sauer et al. (1992), Wessely (1988, 1992, 2006) and Arzmüller et al. (2006). The western boundary of the basin consists of the Schrattenberg-Steinberg-Bisamberg-Leopoldsdorf fault system. These faults, some of which display normal offsets ranging from hundreds of meters to several kilometres (i.e., throw values of ~5.6 km for the Steinberg fault and ~4.2 km for the Leopoldsdorf fault; Decker et al. 2005; Hinsch et al. 2005a, b), bound a central system of depocenters where up to 6000 meters of Miocene sediments were deposited. In a median position, several fault-bound highs are present such as the Matzen-Aderklaa high (**Fig. 2.16**). The Vienna Basin has received considerable attention given the large amount of hydrocarbons discovered within its recent infill and beneath within the Rhenodanubian Flysch and the Northern Calcareous Alps (Zimmer and Wessely, 1996; Hamilton et al. 2000; Arzmüller et al. 2006; Wessely, 2006). More recently, the basin has been the focus of several neotectonic studies, as some of its bounding and internal faults are regarded as sources for potentially large earthquakes (Decker et al. 2005; Hinsch et al. 2005a, b).

The stratigraphy of the Vienna Basin is regarded as a classic example of the Central Para-Tethys Miocene. It has been compiled and summarised on several monographs and publications such as Buday and Cicha (1968), Papp et al. (1973), Janoschek and Matura (1980), Kröll (1980), and Jiřiček and Tomek (1981). The basin displays two well-differentiated stages of subsidence and deformation (Royden, 1985; Decker and Peresson,

1996). The earlier phase is dated as early Miocene (i.e., Eggenburgian to Karpatian, *ca.* 18.5 – 16 Ma) and corresponds to the formation of a wedge-top or piggy-back basin (DeCelles and Giles, 1996). This phase was followed by the middle to late Miocene (i.e., Badenian to Pannonian, *ca.* 16-8 Ma) pull-apart phase (Hölzel et al. 2010). Both 'megasequences' are separated by a large basin-wide angular unconformity (**Fig. 2.11b**) that resulted from significant out-of-sequence thrusting promoting uplift, tilting and erosion. This deformation was followed by extensional faulting, marking the transition between the piggy-back and pull-apart stages. One remarkable element developed in the Alpine-Carpathian foreland during the Karpatian-Badenian transition is a large, erosive 'channelised' feature, referred to by Dellmuor and Harzhauser (2012) as the Iváň Canyon. At least, an additional "canyon" has been imaged by 3D seismic data in the footwall of the Steinberg fault (**Fig. 2.16**). This feature is about 20 km wide and exploration drilling has shown a Karpatian-Badenian infill several hundreds of meters thick affecting the Rhenodanubian Flysch imbricated units. This channelised feature is referred to as the Mistelbach system whose origin and evolution are currently being investigated.

The early Miocene sedimentation of the Vienna and the Korneuburg Basins marks the final stages of thin-skinned thrusting in the Waschberg-Ždánice Zone and out-of-sequence thrusting within the more internal Penninic and Austro-Alpine units (Hölzel et al. 2010; Beidinger and Decker, 2014). In the Vienna Basin, these early Miocene strata reach up to 1500 meters in thickness and were deposited in fluvial, deltaic, lacustrine to brackish-littoral and shallow-marine environments. From the facies distribution and paleogeographical reconstructions, Seifert (1992) suggested that the original areal distribution of the early Miocene sediments extended over the present day limits of the Vienna Basin. In this sense, the lowermost Eggenburgian sediments of the Korneuburg Basin (Harzhauser and Wessely, 2003) are interpreted as remnants of a former wedge-top system (Hölzel et al. 2010), correlatable with the early Miocene strata of the Vienna Basin (**Fig. 2.11c**). These depocenters are now separated by half-graben and pull apart basins located over releasing segments of strike-slip faults (Ratschbacher et al. 1991b; Fodor, 1995; Strauss et al. 2001). These observations raised a long-lived discussion of whether the buried early Miocene basins are solely fault-controlled structures, or remnants of a once larger, and more extensive, wedge-top basin (Hölzel et al. 2010).

The middle to late Miocene pull-apart stage of the Vienna Basin buried and down-faulted the former early Miocene sediments as well as the underlying Rhenodanubian Flysch and Northern Calcareous Alps. The stratigraphic and subsidence record of the Vienna Basin has been studied and compiled from previous studies by Lankreijer et al. (1995), Strauss et al. (2006), Wessely (2006), and more recently by Lee and Wagreich (2016). At the Karpatian/Badenian boundary, a major regressive event that affected the Central Para-Tethys realm has been interpreted also in the Vienna Basin (Rögl et al. 2002). A major change in the sediment dispersal pattern occurred, from an originally northwards direction towards and along the Alpine-Carpathian foredeep to a dramatic eastwards to south-eastwards change into the developing Vienna Basin. During the Badenian, several fault blocks became individuated and controlled the sediment input: from proximal fluvial to deltaic clastics to distal shallow water systems, along with carbonate platforms in those areas sheltered from clastic inputs. In the transition between the Badenian and the Sarmantian a sea level drop took place producing the erosion of the former Badenian platforms. A transgression followed during the Sarmantian, producing further reworking of the platforms and allowing for additional sandy and carbonate facies sedimentation. The Pannonian stage recorded a transgressive period (Harzhauser et al. 2004) that covered most of the Sarmantian sediments with lacustrine clays and sands (i.e., Lake Pannon) and alluvial deposits. In latest Pannonian times, a change in the regional stress field (Decker and Peresson, 1996; Huismans et al. 2001) led to an E-W directed shortening that resulted in mild uplift and inversion of the Vienna Basin (Decker and Peresson, 1996). In recent times, but probably starting in the Pleistocene, renewed subsidence seems to have been controlled by a sinistral transtensional regime that seems to be the cause of some of the recent seismicity observed in the area (Decker et al. 2005; Hinsch et al. 2005a, b; Hinsch and Decker, 2011).

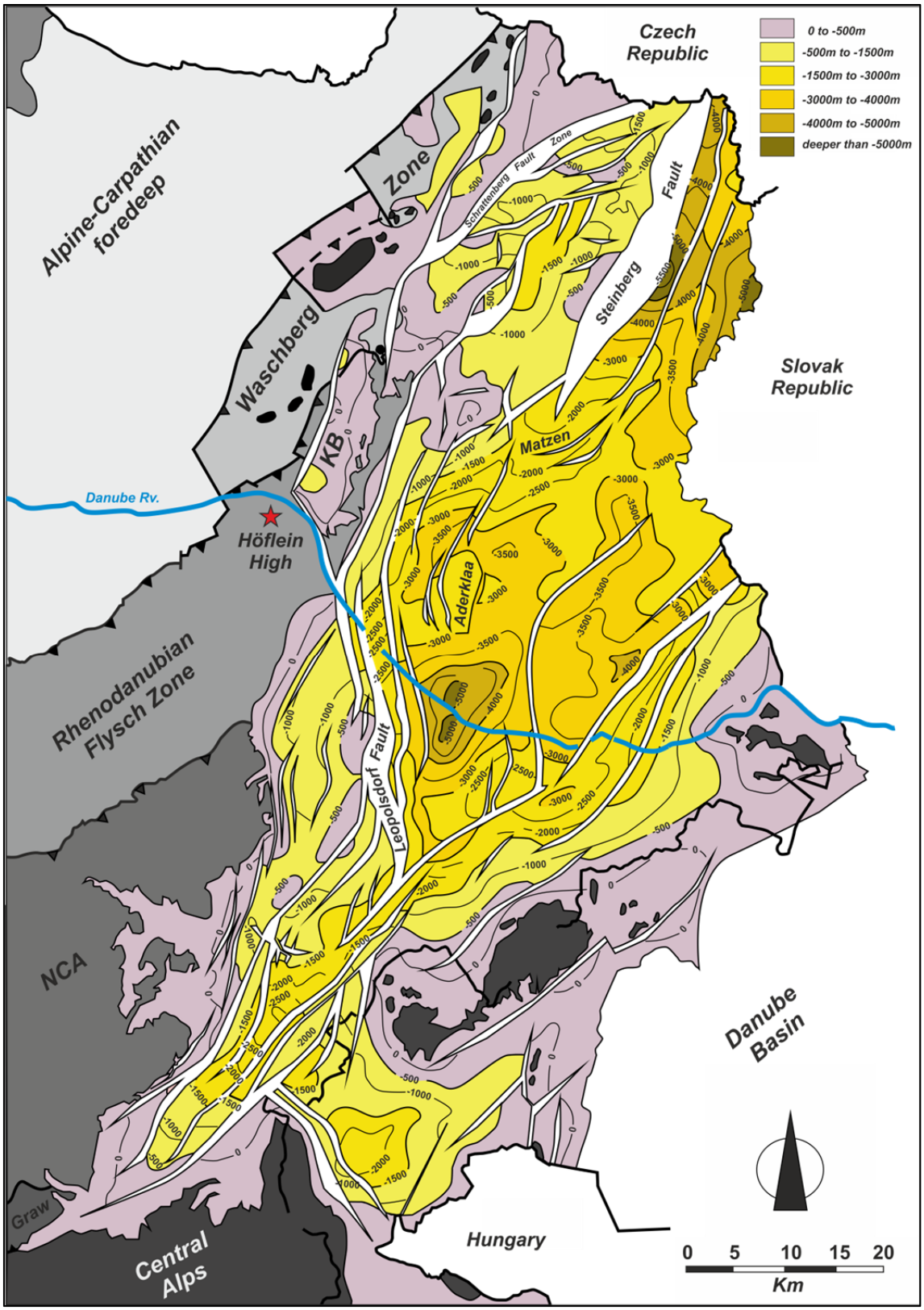

Figure 2.16. Depth-structure map showing the depth to the basement of the Vienna Basin in Austria. See location in **figure 2.11a** and compare with gravity maps in **figure 3.2**. Based on the work by Wessely (2006) and references therein. KB: Korneuburg Basin; NCA: Northern Calcareous Alps; Graw: Grauwacken Zone.

The thin- vs. thick-skinned nature of the Vienna Basin is a remarkable and still debated issue. Whether the larger bounding faults of the basin (i.e., Steinberg and Leopoldsdorf faults; **Fig. 2.16**) sole within the flat-lying Alpine Basal Thrust, or are kinematically linked with the deeper basement fault array is not yet resolved. The early models of Royden (1985) proposed that the Vienna Basin is a "typical" example of thin-skinned pull-apart tectonics that caused the extension of the tectonic wedge along the sole thrust of the Alpine-Carpathian fold-and-thrust belt. For these authors, this thin-skinned style is supported by generally low heat flow of the basin, and proposed a gradient from thin-skinned extension to the NW to a thick-skinned extension to the SE in the Pannonian Basin based on calculated thermal subsidence curves (Royden and Dövényi, 1988). The thin-skinned model has also been adopted in recent works by Decker et al. (2005), Hinsch et al. (2005a, b) and Hölzel et al. (2010). On the other hand, the early model by Wessely (1988) provided a thick-skinned interpretation for the bounding Steinberg and Leopoldsdorf faults based on the evidence from wells and a large database of seismic profiles. In this sense, Lankreijer et al. (1995) proposed that the Vienna Basin underwent thick-skinned extension in its central and southern parts (i.e., the Austrian part) also involving the lithosphere in order to produce the observed tectonic and thermal subsidence patterns reflecting cooling of extended lithosphere (Morley, 1993). The results of Lankreijer et al. (1995) were also supported by numerical forward modelling, and seem to be in agreement with the early structural interpretations of Wessely (1988) and the 65mW/m^2 heat flow data earlier reported by Royden and Dövényi (1988).

2.2.8 HYDROCARBON RESOURCES OF THE ALPINE-CARPATHIAN JUNCTION

In the Alpine-Carpathian-Pannonian area, the presence of hydrocarbons has been recognised for many years. In fact, previous to the discovery of prolific Middle East hydrocarbon provinces by the westerners, the Alpine-Carpathian-Pannonian region hosted the largest accumulations of hydrocarbons known to the western world. For these reasons, the area underwent special interest and endured large conflicts before, during and after the first and second world wars, given that the area belonged the former Austro-Hungarian Empire, was then seized by Germany, and then by the Allies and the USSR blocks until 1955, when the territory was returned to the Austrian authority. The first hydrocarbons in the region were produced in the Carpathian foreland of today's Poland and Ukraine since

the 1860's. In Austria the first discoveries of hydrocarbons were made by water wells in the Molasse Zone of Upper Austria between 1891 (gas) and 1906 (oil). The first commercial exploration and production of hydrocarbons from the Vienna Basin dates from about the 1930's (Janoschek et al. 1996). Since then, thousands of exploration wells have been drilled, and extensive seismic profiling and 3D surveys have been acquired. Exploration and production are taking place as today in the Miocene fill, the Alpine-Carpathian fold-and-thrust belt and the Lower Austria Mesozoic Basin. Campaigns of deep drilling favoured the discovery of large gas accumulations in the Northern Calcareous Alps as early as the 1960's. Drilling in the sub-thrust led to the discovery of the Höflein field in 1981, whereas ultradeep exploration wells such as Zisterdorf ÜT, Maustrenk ÜT and Aderklaa ÜT confirmed the existence of gas-bearing imbricated Jurassic as well as the presence of the Autochthonous Molasse and Mesozoic beneath the Vienna Basin. An extended summary of the oil and gas acreage of Austria has been provided by the monograph of Wessely and Liebl (1996), and more recently by the summaries of Hamilton et al. (2000), and the works of Arzmüller et al. (2006) and Picha et al. (2006).

During this thesis two additional plays have been added to the portfolio of the Lower Austria region. These include structural traps related to the inversion of the rift basement faults belonging to the Lower Austria Mesozoic Basin. Two potential kinds of traps have been defined (in red in **Fig. 2.17**): deeply-buried sub-thrust inversion traps, and foreland inversion anticlines.

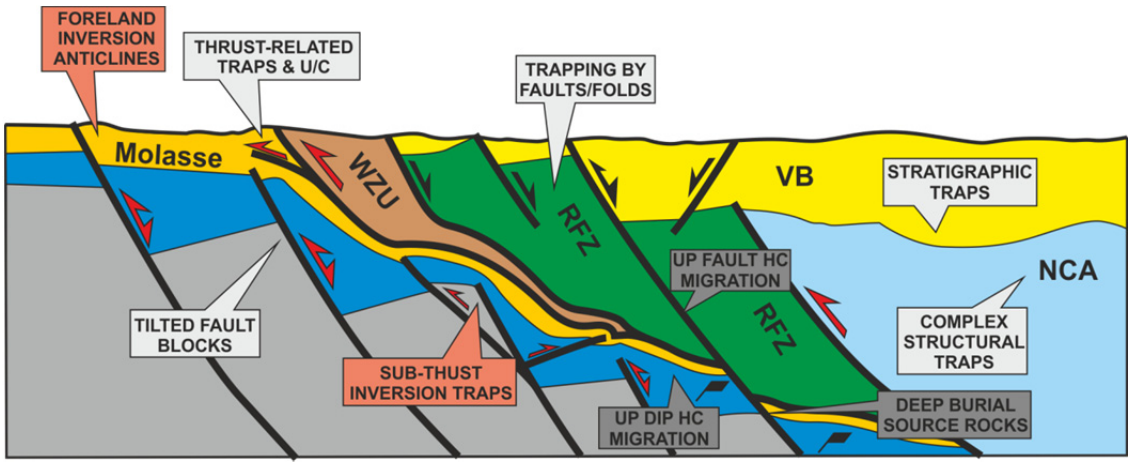

FIGURE 2.17. Hydrocarbon plays of the Alpine-Carpathian Junction. The inversion-related plays have been included as a result of this thesis. Modified from Janoschek et al. (1996) and Hamilton et al. (2000).

2.3 Basin Inversion and Basement-involved Deformation in Fold-And-Thrust Belts and Collisional Foredeeps

2.3.1 Introduction and Main Controls

The concept of basin inversion refers to a change in the tectonic regime from extension to compression, so that extensional basins become positive structural features by the compressional reactivation of extensional faults (e.g., Bally, 1984; Cooper and Williams, 1989). Alternatively, negative inversion occurs when extensional basins are developed by the reactivation of previously developed thrusts or reverse faults (**Fig. 2.18**). In its original definition, there are two fundamental features associated with basin inversion. First, significant reactivation of pre-existing fault systems must take place, and second, uplift associated with fault reactivation must be focused on the hanging-wall rather than on the footwall for positively inverted basins. If negative inversion takes place, it is subsidence that needs to be preferentially focused on the hanging-wall. It is essential therefore to constrain a chronostratigraphic framework to properly recognise and assess inversion tectonics, so syn-rift or syn-extensional sedimentary sequences should be correlated across the studied fault systems. Ideally, pre-, syn- and post-rift sequences -including growth strata- should be characterised to define the geological history of any inverted basin. In addition, it is necessary to portrait these sedimentary sequences within their present structural elevation, and to compare it with their corresponding regional elevation.

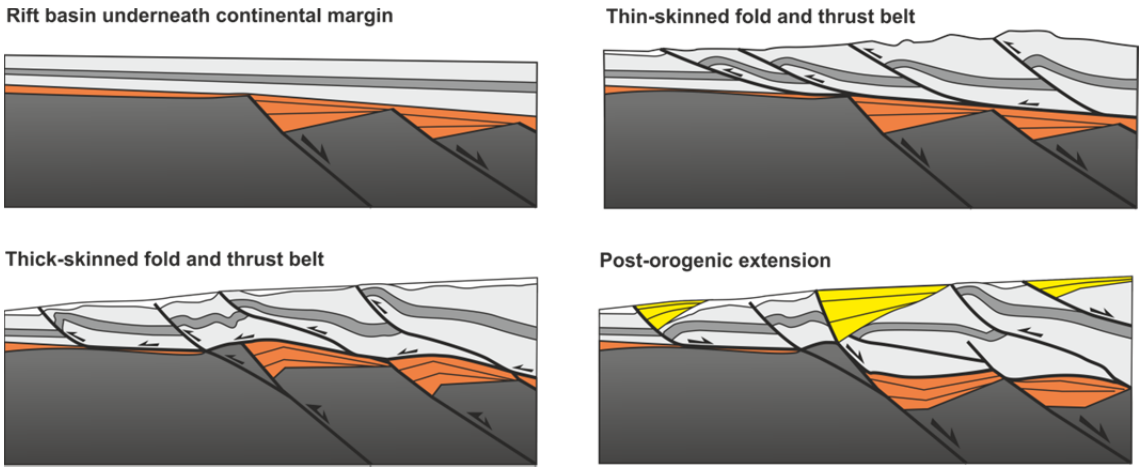

Figure 2.18. Synoptic examples of positive and negative inversion tectonics in the evolution of a ritfted margin to a fold-and-thrust belt. Thin- and thick-skinned deformation examples are shown.

Positively inverted basins have been recognised at different scales and within different tectonic scenarios such as the Circum-Mediterranean Alpine system (e.g., Gillcrist et al. 1987; Butler, 1989; Williams et al. 1989; Huyghe and Mugnier, 1995; Lowell, 1995; Guiraud, 1998; Muñoz, 2002), the Andes (e.g., Uliana et al. 1995; Carrera and Muñoz, 2013), the Sundaland basins of Indonesia (e.g., Letouzey et al. 1990; Hall and Morley, 2004), Taiwan (e.g., Álvarez-Marrón et al. 2014), the Los Angeles Basin within the San Andreas fault system of the U.S.A. (e.g., Bjorklund and Burke, 2002), the North Sea (e.g., Ziegler et al. 2001) or Japan (Panayotopoulos et al. 2016). Conversely, negative inversion has probably received less scientific attention although it has been recognised affecting large areas such as the Devonian Basins of western Norway (e.g., Fossen, 1992), the Sevier orogen of Western U.S.A. (e.g., Kloppenburg et al. 2010) and the huge Pannonian Basin (Horváth, 1993; Matenco and Radivojevic, 2012).

Bally (1984) proposed a classification of the amount of inversion related to the recovery of extensional displacement along basin bounding faults. If fault activity governed growth sedimentation during extension, the fault will display a downwards increasing displacement gradient. Upon positive inversion, if there is no extensional offset across the fault for the pre-rift section so the basement is returned to its pre-extensional configuration, then the basin is described as totally inverted. Prior to this stage, when pre-rift beds in the basement are in net extension and the post-rift beds are in net shortening, the basin is considered to be only partially inverted. The amount of inversion can be assessed therefore using an imaginary point -the null point- at which there is no net offset of beds. The null point separates net contraction above from net extension below and migrates down the fault plane during progressive compressional reactivation of the fault. If reactivation goes beyond the stage of total inversion (Bally, 1984) the null point will no longer exist. In a 3D analysis, the null point is referred to as the null line. Cooper et al. (1989) suggested a similar terminology of mild, moderate, strong and total inversion (**Fig. 2.3**). If additional shortening occurs along the basin bounding fault after total inversion has been achieved, the pre-, syn- and post-rift sequences will be in net shortening.

In a larger scale of observation, MacGregor (1995) divided simple rifts from locally inverted rifts and regionally inverted rifts. Fold-and-thrust belts would represent the end member of such increasing deformation trend. These three types of inverted rift basins should be considered as merely representative cases, as a continuum trend is to be expected between different basins and within one single inverted rift basin as well. Some basins may

show varying degrees of inversions as well as different structural styles at different areas. Other basins may in fact display complex structural histories involving multiple episodes of extension and inversion. Inverted basins fully incorporated onto fold-and-thrust belts can still display evidences of their extensional history in terms of fault displacements and stratigraphic record across inherited fault systems. When fault reactivation has surface or near-surface expression, changes in the distribution of sedimentary depocenters from the extensional to the compressional phases -and *vice versa*- can be diagnostic to recognise and assess inversion tectonics. Conversely, the assessment of inversion can be significantly hampered if it takes place in deeply-buried regions such as the sub-thrust zones beneath fold-and-thrust belts or beneath thick foreland basins. This also imposes the problem of dating the absolute age of inversion, as it would have to be exclusively constrained by cross-cutting relationships. Indirect evidence for active deep-seated inversion may be gathered from earthquake focal mechanisms solutions (Brown et al. 2012; Álvarez-Marrón et al. 2014).

But, why is basin inversion that important anyway for the Earth Sciences? Plate tectonics theory states that the Earth's lithosphere is composed of a series of plates which are in motion with respect to each other, with basins opening and closing within such a framework. Extension of the lithosphere leads to the formation of rift basins and continental margins and ultimately, the opening of oceanic basins. Relative plate motion produces deformation along the boundaries of plates but also the development of new plates and new boundaries. It is along these boundaries where tectonic stresses are generated and concentrated. But in addition, the nature of the tectonic plates allow for the transmission of stress from their boundaries into their interiors, establishing what is referred to as intraplate stress fields. Intraplate stress fields are also responsible for the inversion of basins and the involvement of basement in the deformation sequence far away from any plate boundary. Changes in the movement of tectonic plates can therefore deform and close former extensional basins, a process in which strain is localised at pre-existing weak crustal volumes (i.e., including rocks and fault zones). If shortening proceeds, continental margin basins may become shortened, and eventually, become incorporated into thrust sheets to form fold-and-thrust belts. In most cases, inversion tectonics is easier to recognise in the external parts of orogens, as at the internal areas strong deformation and metamorphism may significantly obliterate the inherited continental margins architecture. In a similar fashion, extensional tectonics can occur synchronous with tectonic shortening in the foreland regions of collisional foredeeps. This process has been termed

"flexural extension" (Bradley and Kidd, 1991) as resulting from bending-related extension of the orogenic lower lithospheric plate. As documented in this thesis, extensional reactivation of the basement fault array in the Alpine-Carpathian Junction has been observed, taking place synchronous to the forelandward propagation of thin-skinned thrust sheets and before the positive inversion of the basement faults.

At this point, a brief review on the major controls of basin inversion, fault reactivation and the involvement of basement in collisional foredeeps is needed. A significant amount of work regarding the first order controls on basin inversion dynamics following rifting and the mechanical controls on compressional intraplate deformation has been already published. These include theoretical studies based on observations at different scales, spanning from a lithospheric scale, single half-graben structures, and laboratory deformation experiments. However, how the combination of these key parameters influences or controls the involvement of basement in collisional foredeeps still remains the focus of very recent works (Nemčok et al. 2013; Lacombe et al. 2016). The following factors are recognised to have an important effect on the deformation in orogenic systems:

- The lithosphere's integrated strength, its Equivalent Elastic Thickness (or EET) and its variation through time, which are strongly dependent on its composition and thermal history. These two factors should be regarded as a function of the time spam between the end of rifting and the onset of shortening (e.g., Ziegler et al. 1998, 2001, 2002; **Fig. 2.19**), but also as collision and subduction of the orogenic lithosphere take place (e.g., Butler and Mazzoli, 2006; Lacombe and Bellahsen, 2016; **Fig. 2.20**).
- The regional geometry of the rift basin or system of rift basins (e.g., Macedo and Marshak, 1999; **Fig. 2.21**), where it can be included the geometry of the extensional fault system and its mechanical properties (e.g., Sibson, 1985; Holdsworth, 2004), as well as its orientation relative to the direction of tectonic shortening (e.g., Sibson, 1985; Gillcrist et al. 1987)
- The depth of burial, which controls whether the deformation mechanisms are limited to the shallow frictional field (i.e., pressure-dependent mechanisms), or controlled by deeper temperature-activated processes (e.g., Rutter, 1986; Scholz, 1988; Holdsworth et al. 2001; Lafosse et al. 2016; Pfiffner, 2016; **Fig. 2.20**).
- The rheological contrast between the basin infill and its basement (e.g., Buiter et al. 2009; Bauville and Schmalholz, 2015; Lacombe and Bellahsen, 2016), or the

presence and distribution of weak layers such as salt or overpressured formations within the sedimentary basin (e.g., Davis and Engelder, 1985). This last point is of particular importance as it has strong implications for the timing of inversion, burial and uplift, structural styles and thermal regimes (**Fig. 2.22**).

- The ingression of fluids (e.g., Wibberley, 2005), either hydrous, related to the maturation and migration of hydrocarbons or magmatic (**Fig. 2.20**). Of particular importance for fault reactivation is the pore-fluid pressure that can reduce the effective stress necessary for reactivating misoriented faults (e.g., Sibson, 1985, 1990; Cox et al. 2001).

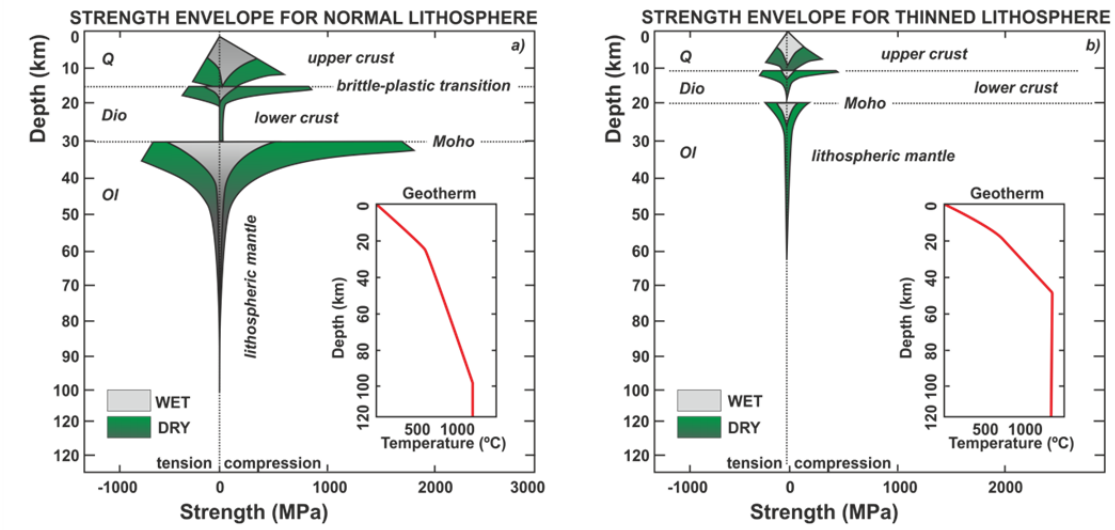

FIGURE 2.19. Idealised depth-dependent strength envelopes for dry and wet lithosphere asuming a quartz(Q)/diorite (Dio)/olivine (Ol) rheology. A) Applicable for unextended, cratonic lithosphere with a 30 km thick crust and 70 km thick lithospheric mantle. B) Applicable for stretched and thermally unstabilised cratonic lithosphere thinned to a 20 km thick crust and 45 km lithospheric mantle. These rheological models indicate that the response of the lithosphere to stresses (in extension and compression) depends on its thickness, strength and spacing of the rigid layers, stress magnitude, strain rate and thermal regimes, as well as the orientation of rheological discontinuites in respect to the prevailing stress trajectories. Modified from Ziegler et al. (2001, 2002).

To summarise, the deformation of orogenic systems typically include the inversion of sedimentary basins and the involvement of basement to larger or lesser degrees. One of the fundamental controls on basin inversion and basement-involvement deformation can be resumed in one big concept known as rheological inheritance. This term embraces the geometry and mechanical properties of basins and their bounding fault systems, their orientation in respect to the prevailing stress trajectories, and the rheological contrast between and within the sedimentary cover and its basement. Another fundamental point is that such inherited rheology is suitable to changes through space and time, from a pre-rifting configuration, during rifting and along orogenic build up.

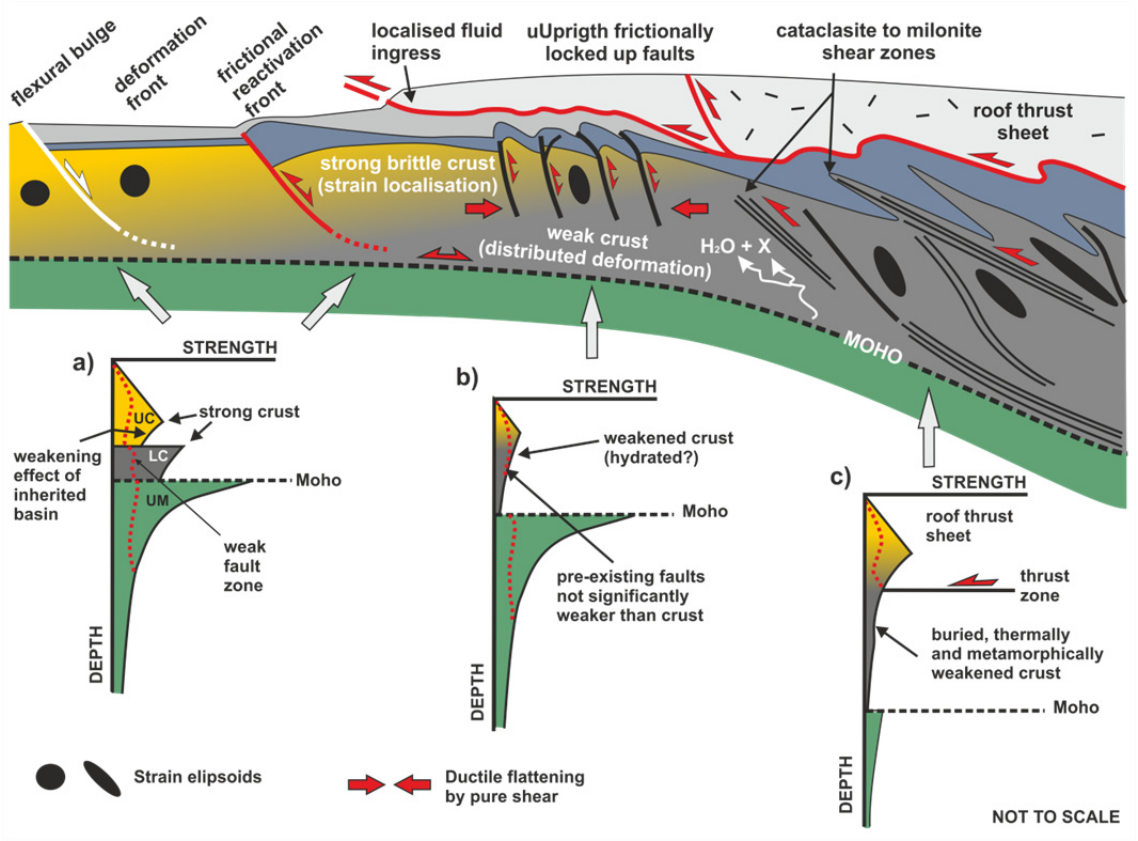

FIGURE 2.20. Conceptual profile showing the rheological variations of the crust and its propensity for structural reactivation as strength envelopes for the external, mid and internal regions of an orogenic system. A) The external regions are prone to tectonic inversion (positive and negative) as deformation is localised onto inherited basins and fault systems, assumming strong surrouding crust and weak faults. B) Other parts of the orogenic wedge may display crustal volumes not stronger than inherited faults or discontinuities, hence faults are less prone to reactivation and strain is distributed. C) At the internalmost and deeper sections of the orogenic wedge burial by overthrusting and subduction weakens the crust aided by metamorphic reactions. Frictional reactivation of faults is not expected to occur so pre-existings faults are unlikely to reactivate. An continuum spectrum for these three situations in space but also in time can be envisaged for any particular orogen. Based on Butler and Mazzoli (2006), Butler et al. (2006), Lacombe and Bellahsen (2016).

On a more local scale of observation, the reactivation of inherited fault systems is inherent to the concept of basin inversion. In shallow crustal levels this process is controlled by frictional processes which are basically pressure-dependent (Rutter, 1986). The main factors controlling the frictional reactivation of faults are: the cohesion, the coefficient of friction, the orientation of the fault (i.e., dip and direction of dip) in respect to the stress trajectory and the pore-fluid pressure (Jaeger and Cook, 1979; Zoback, 2010). In this sense, the cohesive strength of a fault plays a major role in the angle at which shear failure occurs upon reactivation. The reduction in cohesive strength increases the range of possible fault orientations for shear failure for a given stress field (i.e., that stress field required for intact rock failure).

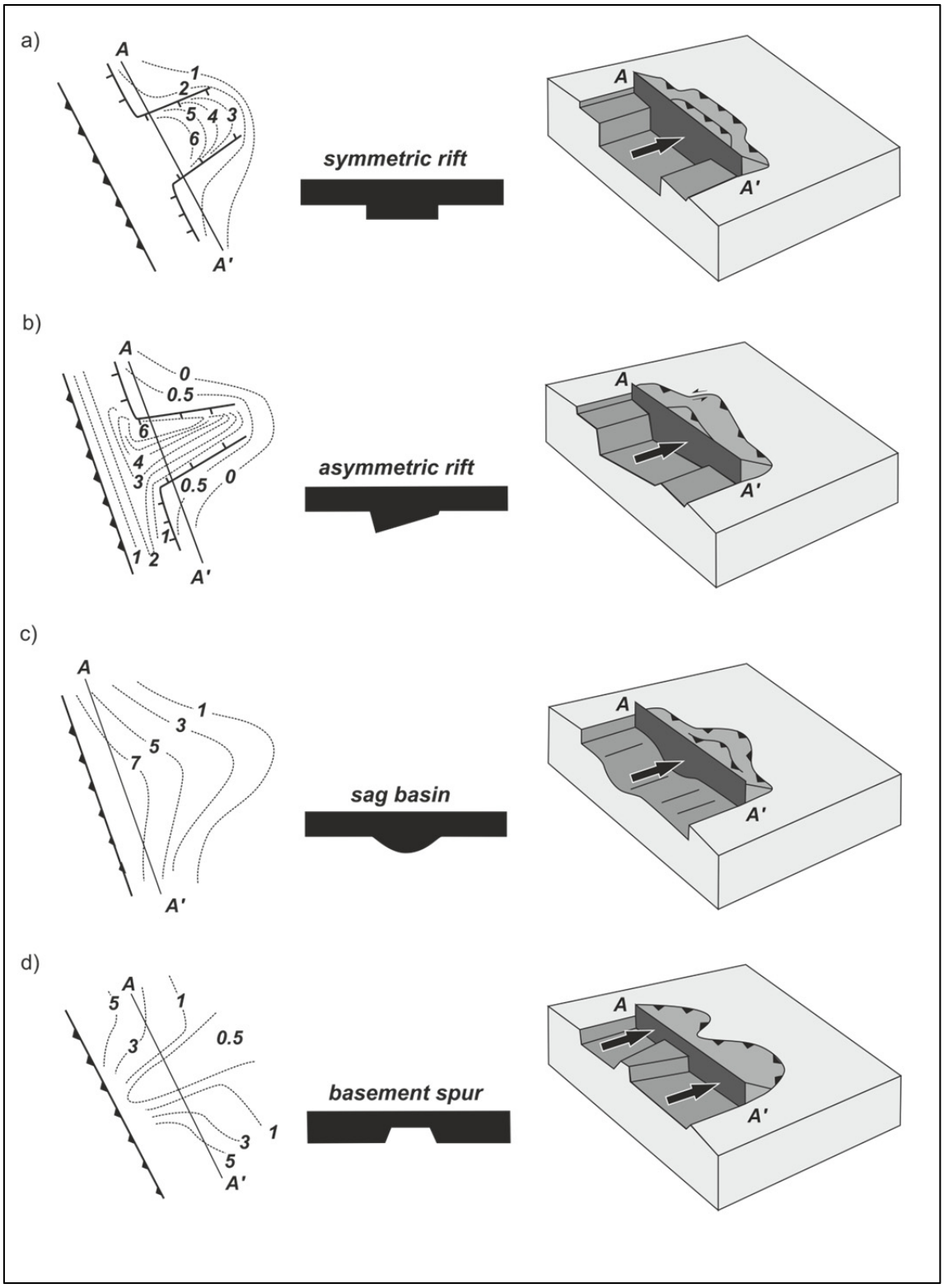

FIGURE 2.21. Different basin geometries displaying thickness variations and irregular basement topographies. The numbers indicate sediment isopachs. Basement topography as well as the sediment thickness distribution of the basin infill control the depth of the detachment and also shape of the propagating thrust front either as a roughly linear feature or arranged into salients and recesses (i.e., syntaxes). A) Symmetric rift basin. B) Asymmetric rift basin. C) Sag basin. D) Basement salient example, similar to the Bohemian Spur of the Alpine-Carpathian Junction. Modified from Macedo and Marshak (1999).

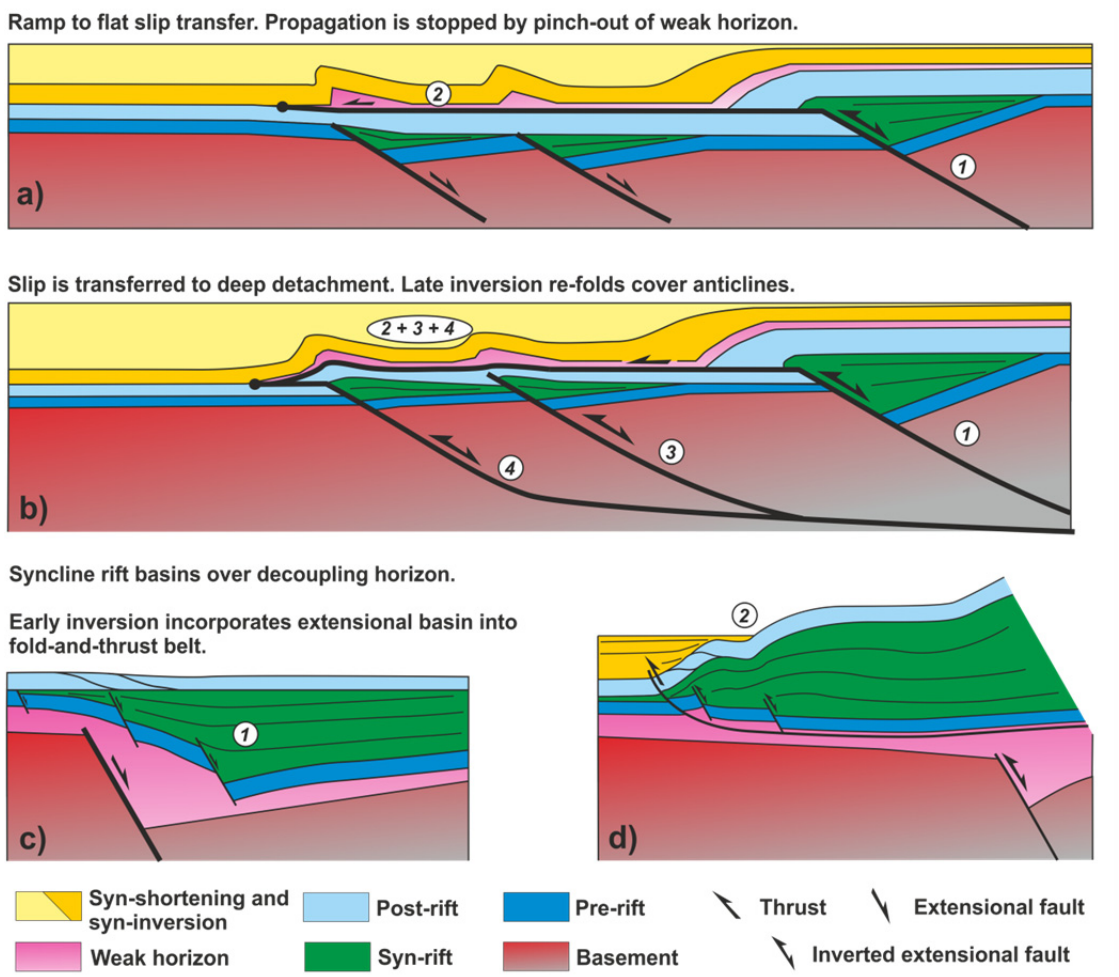

FIGURE 2.22. Examples of naturally inverted basins with intervening weak detachments. A and B depict a fold-and-thrust belt where the weak horizon is located on a post-rift position. C and D display a thick weak horizon in a pre-rift positicion. The first two examples are inspired in the Malargüe fold-and-thrust belt of Argentina (modified from Kozlowski et al. 1993), whereas C and D are inspired from the Organyà Basin in the South Central Pyrenees (from Mencos et al. 2015). The encircled numbers indicate the sequence of deformation. Note how the inherited pre-shortening location of the weak horizon controls deformation styles but also the timing of inversion, burial and uplift.

Different rock types can display different values of friction along fault planes as compared to friction values for intact rock. This has been proven empirically, as lowering the angle of internal friction within the fault surface increases the range of fault plane orientations that can be reactivated under the stress field required for intact rock failure (Jaeger and Cook, 1979). Fault-weakening process (Rutter et al. 2001) involving chemical reactions between circulating fluids and the host fault-rocks can induce the formation of low-friction phyllosilicate-bearing paragenesis. Fault-weakening allows faults sustaining significant slip under theoretically anomalous orientations in respect to the prevailing stress field (Colletini et al. 2009). As faults accommodate slip, both the cohesive strength and the

angle of friction generally become lower within fault zones, but precipitation of certain hydrothermal fluids or quenching of melts may induce the frictional lock-up of faults due to a significant increase on the fault zone coefficient of friction and cohesion (Etheridge, 1986; Cox et al. 2001).

Fault orientation relative to the inversion stress field is an important factor as well (**Fig. 2.23**). Broadly speaking, dip-slip positive inversion of high angle extensional faults or dip-slip negative inversion of low-angle thrust faults is not favoured under simple idealised stress conditions in the frictional field (Etheridge, 1986). Sibson (1985) outlined the mechanical requirements for fault reactivation in its simplest 2D case. He defined R as the ratio between the principal stresses (SH_{MAX} or σ1 and SH_{MIN} or σ3) which will generate frictional reactivation of a particular fault plane with an orientation (α) to the maximum stress direction, thus:

$$R = \left(\frac{\sigma 1}{\sigma 3}\right) = (1 + \mu Cot\alpha) \,/\, (1 - \mu Tan\alpha)$$

This relationship can be plotted as the stress ratio against fault plane angle for reactivation (**Fig. 2.23d**). From this equation it can be drawn that the most efficient orientation of a cohesionless fault plane for frictional reactivation is about 26.5º to the principal stress direction for a coefficient of friction μ = 0.75 (i.e., an empirically derived value for upper crustal rocks). Angles above and below 26.5º require an increase in R, such that R = ∞ when α = 0º or 53º. For an extensional fault developed with dips above 53º to become frictionally reactivated in compression, the least principal stress (SH_{MIN} or σ3) needs to become tensile. On the other hand, elevated pore fluid pressures lower the effective normal stress across failure planes. The shear stress remains unchanged thus permitting fault movement at lower resolved shear stresses on the fault plane. Hence, for a given stress system, high pore fluid pressure will increase the range of possible fault angles that can be reactivated, both in compressional and extensional frictional reactivation (Sibson, 1985). Although significant, the approach made by Sibson (1985) is two-dimensional only. In fact, fault reactivation is also strongly dependent on the magnitude and orientation of the intermediate stress, SH_{INT} or σ2 (e.g., Jaeger and Cook, 1979; Gillcrist et al. 1987; Zoback, 2010; Peacock et al. 2016), and this needs to be considered when the inversion-related principal stress (σ1) is not perpendicular to the extensional fault or when the fault is not rectilinear. In such cases, σ2 will not be contained by the fault plane, meaning that it will also have its normal and the shear stress components acting on the fault plane, thus

facilitating frictional reactivation. It is readily apparent that oblique inversion will permit a wider range of possible fault angles to be reactivated than pure dip-slip inversion. That is why many inversion features have been reported in strike-slip settings where oblique slip tectonics is common (Letouzey, 1990; Bjorklund and Burke, 2002; Peacock et al. 2016). For the possible combinations of all these parameters, the frictional reactivation of faults is known to be selective.

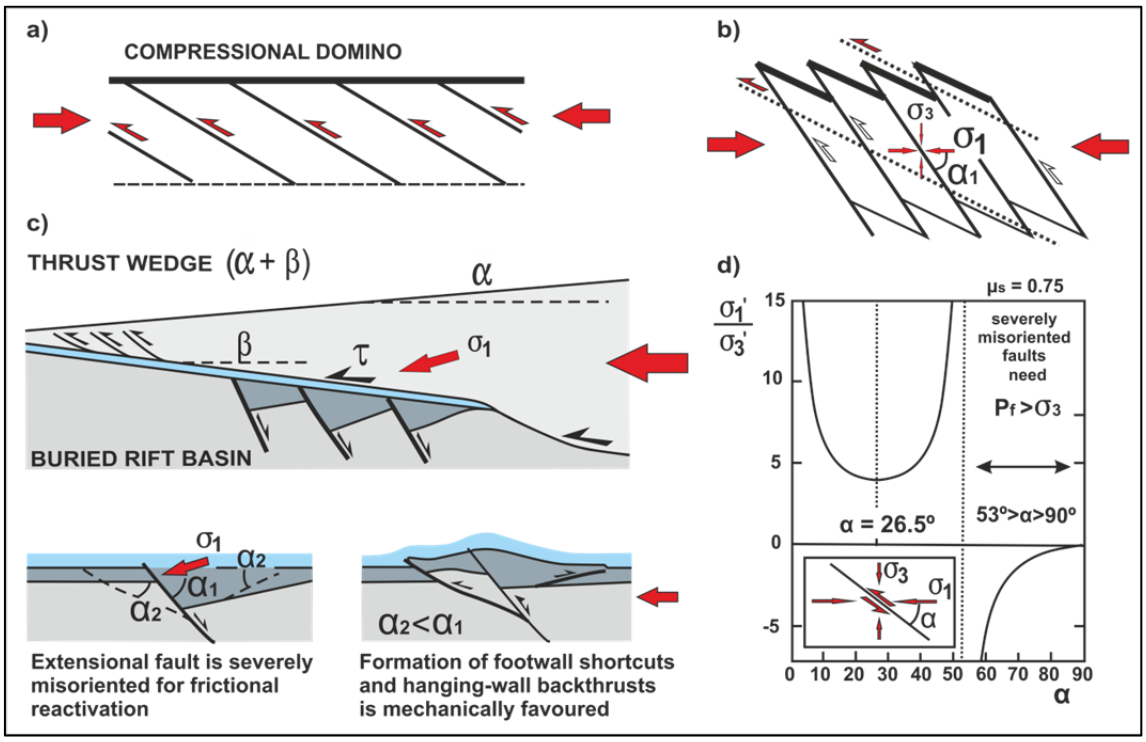

FIGURE 2.23. A) and B) display the frictional lock-up of a steeply-dipping rotated compressional domino fault array (from Sibson, 2001). C) Steeply-dipping of sub-thrust rift faults become misoriented for frictional compressive reactivation upon tectonic burial. In these cases, formation of footwall shortcuts and/or hanging-wall backthrusts is mechanically favored (modified from Gillcrist et al. 1987). D) Alternatively, steeply-dipping (>53°) faults (for μ_s=0.75 faults) will only be frictionally reactivated in compression when the pore-fluid pressure (P_f) exceeds the lower principal stress (σ_3). From from Sibson (2001).

2.3.2 SOCIAL AND INDUSTRIAL IMPLICATIONS OF BASIN INVERSION

The concept of tectonic inversion and crustal fault reactivation has also been applied to explain the involvement of basement and related seismicity at plate boundaries and within intraplate interiors (Sibson, 1990). Some relatively recent earthquakes that caused significant human and economic loses have been related to the activity of deeply-seated basement-involved fault systems. In fact, some fairly intense seismic events have been interpreted as resulting from the compressional reactivation of former extensional

fault systems such as 21st September 1999 M7.7 Chi Chi earthquake in Taiwan (Brown et al. 2012; Chuang et al. 2013), the 22nd November 2014 M6.7 Northern Nagano earthquake (Panayotopoulos et al. 2016) or the 23rd October 2004 M6.8 Mid-Niigata (Sibson, 2007) both in Japan. In addition to the large socio-economic implications of seismicity, it has been recognised that the processes involved in the positive inversion of basins and the negative inversion of contractional systems can have a strong role in the accumulation, exploration and management of natural resources such as mineral deposits (e.g. McClay et al. 1989; Cox et al. 2001; Kloppenburg et al. 2010) or hydrocarbons (e.g., MacGregor, 1995; Thomas and Coward, 1995; Bjorklund and Burke, 2002). The recognition of inversion tectonics needs to be considered for a series of reasons:

- It affects the burial history of basins, and hence their thermal evolution having a direct implication on the maturation of source rocks and the migration of hydrocarbons.
- It can enhance or decrease the petrophysical properties of geological reservoirs due to the structural and diagenetic processes involved (i.e., burial, uplift, fracturation, chemical dissolution, circulation and precipitation of fluids, etc.).
- It modifies the attitude of sedimentary layers, allowing for different directions of fluid migration trough time.
- It can reactivate pre-existing fault systems, changing their sealing properties, breaching traps, and re-pumping fluids.
- When inversion has surface expression, it can strongly influence the distribution of sediments, environments and ecosystems.
- The structures developed during inversion may be used as conduits for magma intrusion and hydrothermal/meteoric fluid circulation, modifying the seismic cycle of active fault systems.

Based on the review provided by MacGregor (1995), the frequency of hydrocarbon exploration success is relatively high for simple and locally inverted rift basins. Local and mild positive inversion is frequently a favourable factor for the development of major hydrocarbon provinces. The most important factor is the timing relationship between trap formation and hydrocarbon generation and migration, albeit the presence of effective seals and reservoirs. Apparently, many locally inverted rifts (particularly those without pre-rift reservoirs), would contain no or few large traps if it was not for the effects of local inversions. Hydrocarbon accumulations in regionally inverted rifts are less frequent and

often relay to special criteria such as the reactivation of kitchens by syn- to post-inversion burial, or by the occurrence of unbreached evaporite seals which preserved hydrocarbons during inversion. Regionally inverted rift basins are characterised by proportionally lower hydrocarbon reserves due to the destruction of pre-existing hydrocarbon systems during inversion and/or thrusting. Simple rifts are characterised by dispersed field size distributions, with rarely more than 25% of basin reserves in the largest field. This can be attributed to a high degree of structural segmentation that characterises rift basins in terms of trap and kitchen geometries. On the contrary, locally and regionally inverted rift basins tend to show a higher degree of concentration of reserves in the largest field. According to MacGregor (1995), two hypotheses can be proposed to explain this:

- One inversion structure has formed a migration focus accessing the majority of the basin's kitchen area.
- A more dispersed field size distribution once existed but has been altered as a result of the destruction of many of the original fields.

The first hypothesis seems more applicable to the cases of high reserves concentration in a single field in locally inverted rifts, particularly in those cases in which uplift has focused on a predominant structure. On the other hand, the second hypothesis is more applicable to regionally inverted rifts where abundant evidence for trap destruction in the form of seeps and surface impregnations can be found and where reserves are concentrated in a surviving palaeostructure. The lower reserves and exploration success rates in regionally inverted rifts are often accompanied by considerable direct evidence for loss of hydrocarbons at surface. This is particularly evident for those systems that have suffered recent tectonic inversion. Loss of hydrocarbons at surface may be either in the form of flowing seeps, generally concentrated along reverse fault planes, or as exposed oil impregnations representing eroded oil accumulations or former migration pathways. The critical point at which inversion begins to have a negative impact on petroleum productivity is when previously existing accumulations are uplifted into zones where shallow degradation processes may occur and/or fault connections are established to surface.

To conclude, depending on its severity and its relationships to the phases of hydrocarbon generation, positive inversion may have beneficial or detrimental effects on the hydrocarbon systems at any given basin. Former kitchen areas may become uplifted and brought to the surface along with traps if inversion is large. On the positive side, the uplift and overthrusting of inverted basins can induce the burial of formerly uplifted areas,

and the formation of new kitchens. Renewed migration can then occur synchronously with, or shortly after, the formation of inversion structures and traps. Mild inversions clearly play a positive role in creating large anticlinal traps. Regional inversions, particularly those associated with compressional surface breaching faults and non-evaporitic seals, frequently cause significant losses from pre-existing petroleum systems. These losses result in lower exploration success rates and on smaller field sizes. However, successful examples of regionally inverted rifts (MacGregor, 1995), demonstrate that if the right conditions are met, success can be obtained. Areas of surviving palaeotraps or traps near kitchens that may have been reactivated post-inversion are clearly areas where exploration effort should be better concentrated.

2.4 DATA AND METHODOLOGY

2.4.1 DATA USED IN THIS THESIS

For this thesis 3D and 2D seismic data along with a large database of wells (**Fig. 2.24**) and related downhole logs and well tops were used. Unless stated, all the data described here were provided by OMV Exploration and Production GmbH. The data was handed in a Petrel® Exploration & Production modelling (Schlumberger) project or as separate files that were imported afterwards into this platform. Along the development of this thesis, several seismic volumes were handed by OMV in time-migrated and depth-migrated versions as well as with different geophysical processing workflows of varying quality. As significant differences on imaging and well-to-seismic occur between these datasets, an agreement between both parts was achieved to concentrate the interpretation work on the 3D seismic survey Donau_Nord_CRS_D_unscaled_2010 cube (hereinafter Donau_Nord). The Donau_Nord 3D seismic data is a post-stack depth-migrated merge of several seismic cubes covering around 550 km^2 north of the city of Vienna (**Fig. 2.24**). The depth-migrated version has a maximum recorded depth of around 7 km. It has a 15 meters line spacing for the NE-SW-trending inlines (i.e., strike lines), and 30 meters spacing for the NW-SE trending cross-lines. In terms of quality, the 3D seismic data is generally good but decreases significantly at structurally-complicated zones. Seismic velocity inversions associated with the unevenly distributed post-rift carbonate units and artifacts related to seismic data processing result in noisy areas, artifacts and locally limited resolution. All these issues had to be considered for the interpretation.

An additional 3D dataset covering the Vienna Basin has also been used to gather additional insights into the regional evolution of the Alpine-Carpathian Junction. This cube is named Vienna Basin Supermerge and covers an area of around 1900 km^2 (**Fig. 2.24**). A depth-migrated version was used which displays a total recording depth of 9.5 km. For the same reasons as for the Donau_Nord cube, the data displays better imaging in the shallower parts (i.e., the middle to late Miocene basins and the shallow parts of the fold-and-thrust belt), and becomes poorer downwards. Deep exploration well data were fundamental to aid on the interpretation.

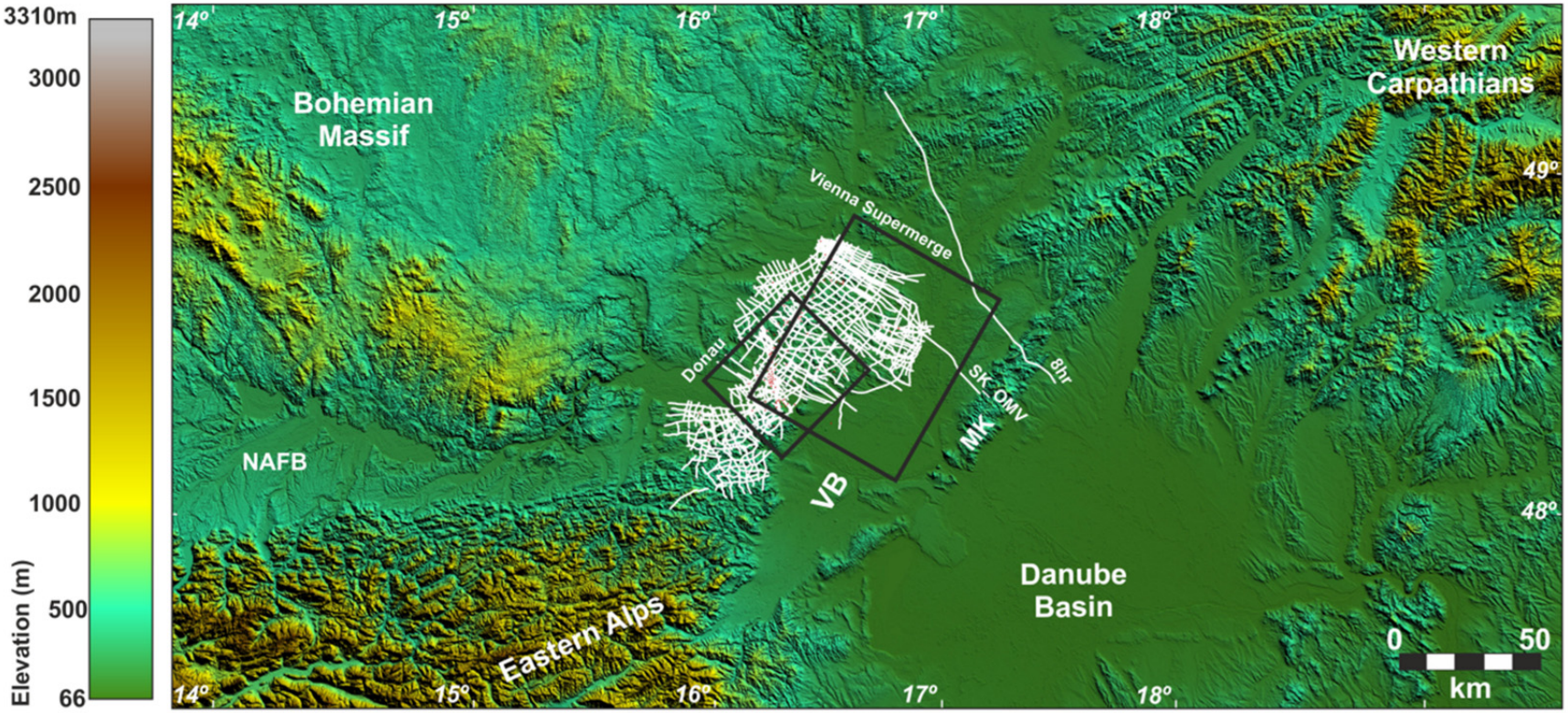

FIGURE 2.24. Digital elevation model of the Alpine-Carpathian Junction showing the location of the data used in this thesis. The rectangles show the area ocupied by the 3D seismic survey (Donau_Nord) and the Vienna Basin Supermerge (Vienna Supermerge). White lines are the time-migrated seismic profiles. The largest seismic profile to the north is the 8hr_8586 crs080001 (8hr), whereas the second largest inmediately to the south is the SK_OMV_2009 OMV_mergeline_AT_SK (SK_OMV). Red dots are wells. MK: Malé Karpaty; NAFB: North Alpine Foreland Basin; VB: Vienna Basin.

The studied area is also covered by a dense network of around 650 2D time-migrated seismic profiles (**Fig. 2.24**) belonging to several vintages including Wasch2D, Andrae-Woerdem, Duern2D, and Waschberg Zone. These profiles display a large overlap with the 3D seismic surveys described above but also cover large parts of the foreland, the Bohemian massif spur, the Lower Austria Mesozoic Basin, the fold-and-thrust belt and Miocene basins where 3D seismic data is not available. Two regional NW-SE-striking time-migrated seismic profiles were also provided by OMV to be integrated into the study; these surveys are the SK_OMV_2009 (OMV_mergeline_AT_SK) and the 8hr_8586 (crs080001) profiles. The SK_OMV_2009 runs for 60 km along the northern sector of the Vienna Basin Supermerge 3D survey and covers the Alpine-Carpathian foreland and fold-and-thrust belt to the NW and the Vienna Basin to the SE. On the other hand, the 8hr_8586 (crs080001) profile runs for around 100 km north of the Vienna Basin Supermerge 3D survey within Slovakian territory. The seismic profile also covers the Alpine-Carpathian foreland and fold-and-thrust belt to the north and the Vienna Basin, stretching further south over the Malé Karpaty horst block and the northern boundary of the Danube Basin. These time-migrated profiles were studied to aid on the interpretation of the Donau_Nord 3D dataset, and to gain further insights into the geodynamical evolution of the area. These two regional lines as well as the Vienna Basin Supermerge were fundamental for the construction of a regional synthetic cross-section (**Fig. 2.11b**).

A total of 151 wells with a downhole suite of gamma ray, sonic, resistivity, spontaneous potential and checkshots surveys were provided by OMV Exploration and Production GmbH. These well data had about 2800 biostratigraphically-constrained formation tops. Out of these 151 wells, about 65 wells intersected autochthonous or para-autochthonous units below the Alpine Basal Thrust and bottomed at the crystalline basement. These wells provided useful constraints to tie well to seismic and decipher the regional structure in those areas poorly imaged by seismic data.

Regional maps of gravity data were also provided by OMV Exploration and Production GmbH. These maps were used as an aid to regionally constraining the shape and structural trends of the NW basin boundary of the Lower Austria Mesozoic Basin. The extent and strike of Jurassic half-graben basins beneath and ahead of the Basal Alpine thrust as well as the overlying middle to late Miocene basins were also regionally constrained using these Bouger and residual gravity maps.

2.4.2 DATA INTERPRETATION

The seismic data was also interpreted using Petrel® modelling software. All data were integrated to identify and constrain the regional structure with an emphasis on the Lower Austria Mesozoic Basin margin and its basement fault array. The Middle Jurassic syn-rift megasequence was defined by interpreting the top of the autochthonous (or para-autochthonous) crystalline basement and the base of the post-rift. The syn-rift megasequence is spatially associated with the basement rift faults and occurs as fault-bound wedges exclusively. The base of the post-rift megasequence happens to be the Höflein Formation and is the main reservoir in the sub-thrust region of Lower Austria (Sauer et al. 1992). These horizons were defined based on well intersections and formation tops, as well as their geometry, internal architecture, truncations and seismic facies. All these features and their relationships with the major structures of the basin were also assessed. Delimiting the syn-rift and post-rift megasequence boundaries allowed for: 1) constraining the geometry of the Jurassic rift basin in the studied area, 2) constraining the stratigraphic thickness and distribution of the syn-rift megasequence and, 3) the bases of these two megasequences are the best geological markers to constrain the type and magnitude on any fault reactivation events following rifting (e.g., Williams et al. 1989; Turner and Williams, 2004).

Cross-lines were interpreted every 10 lines (i.e., every 300 meters), whereas Inlines were interpreted every 20 lines (i.e., every 300 meters too) for all the Donau_Nord seismic dataset. As to faults, these were interpreted using both Cross-lines and Inlines every 10 and 20 lines, respectively. The kinematic evolution of the basement fault array and the overlying thrust system was studied by documenting the observed structural styles and the relative timing of cross-cutting relationships within and between the basement and its thrust-related cover. In addition, a quantitative approach was taken by computing fault-displacement profiles (i.e., fault length vs. throw) for the top basement and the base of the post-rift megasequence. This procedure is supported by the assumption that during the post-rift, subsidence is mostly controlled by the thermal re-equilibration of the lithosphere after rifting as opposed to the syn-rift subsidence which is fundamentally fault controlled (e.g., Allen and Allen, 2005). Hence, large offsets affecting the post-rift megasequence are indicative for fault reactivation once rifting had ceased (i.e., post-rift and onwards). Fault-displacement profiles illustrate the along strike variation of throw but can also indicate

which faults (or fault segments) undergo extensional reactivation and positive inversion (e.g., Thomas and Coward, 1995; Willemse et al. 1996).

The structure around the Höflein high is poorly constrained given the lack of 3D seismic data around the field, the large uncertainties related to the limited quality of the seismic imaging, beside the local mismatch between key well formation tops and the depth-converted seismic data. In addition, the Höflein Formation at the Höflein field happens to change laterally its seismic reflection polarity. For these reasons, the density of seismic interpretation was increased around the Höflein high to every 5 cross-lines and every 10 inlines (i.e., every 150 meters) to better constrain the 3D structure of the structural high. A fundamental approach for constraining such zones has been the use of structural concepts related to inversion tectonics as summarised on **Chapter 2**. In this sense, the interpretation of the Donau_Nord 3D data provided in this study is strongly based on the data used for the study, but has been significantly aided by the use structural concepts and insights from sandbox analogue models of inversion tectonics to reduce uncertainty. The presented models are supported by field studies in inverted extensional basins such as those from the Pyrenees, the Western Alps, the Argentinian Andes, the North Sea, or Papua-New Guinea amongst others.

2.4.3 3D MODEL CONSTRUCTION AND STRUCTURAL VALIDATION

The interpreted faults and horizons were used to generate a 3D basin-scale structural model in Petrel®. Several unsuccessful attempts were made with this software. Most of the problems encountered were associated with the modelling of horizon cut-offs for hanging-wall and footwall blocks. Greatest errors were found for constructing the cut-offs of multi-evaluated surfaces (i.e., overthrust surfaces displaying several Z coordinates with the same X and Y coordinates), but also significant problems were found for building surfaces affected by purely extensional faults. Seismic interpretations were imported into SKUA® software (by Paradigm Subsurface Modelling) which provided faster and better 3D modelling results for a basin-wide model.

The procedure for constructing 3D static structural models with SKUA® is similar to that of Petrel®. To start with, the model's boundaries have to be defined. A preliminary stratigraphy has to be generated stating the relative ages between geological surfaces, the

type of horizons and their mutual geological contacts (i.e., erosional, conformable, etc.). A fault framework has to be created as well, where each fault is classified according to its geometry and offset type (i.e., planar or listric, thrust, extensional, undefined). Once the boundary conditions are set, the user is guided through a 3D modelling workflow. As the 3D modelling is set to run, the software highlights any problems encountered during the construction of the surfaces and faults' cut offs with the fault network. If problems are encountered during construction, the software provides potential solutions or if any modifications to the boundary conditions or the interpretations need to be carried out for a geometrically correct 3D solution. Several tens of iterations were run in SKUA® before obtaining the final positive results.

A structural restoration of the Höflein high was carried out to validate the seismic interpretation and the 3D model. For this matter, Move® structural restoration software (by Midland Valley) was used. Structural restoration is a geometric and mechanical technique where geological units and structures are progressively retrodeformed to validate the interpretations inherent to the construction of any cross section. It can be used to elucidate the geometry, the space and time distribution of geological units, their burial and uplift histories. Originally, a 3D structural restoration was planned for validating the interpretation of the sub-thrust inversion structures. Once the structural complexity of the area was revealed, the 3D restoration was discarded. This is due to the fact that Move® restoration tools use a vertical restoration plane along which horizons are moved backward/forward. The 3D unfolding of the Höflein structure along such a vertical plane will undoubtedly generate space problems on the hanging-wall layers such as voids and overlapping of horizons, rendering the 3D model unbalanced and non-viable.

For these reasons, a 2D restoration approach was taken. Firstly, a NW-SE striking section was chosen as this is considered to be the prevailing directions for both Jurassic rifting and subsequent Alpine shortening. The chosen NW-SE section passes along two key structures: the Höflein high to the SE and the Stockerau anticline to the NW. This section was also chosen because the extent of seismic coverage of the Höflein structure is laterally limited. In fact, each of these structures is associated with a Jurassic rift fault and both structures display evidences of positive inversion. As both structures are inverted, they have to kinematically linked along the same basal detachment in the crystalline basement.

The model built in SKUA® was imported into Move® for section construction, restoration and validation. The structural restoration was carried out sequentially, from the present day inverted structure, to the pre-rift stage based on the observed cross-cutting relationships and relative timing-constraints. For the shortening structures, a SE to NW forward-breaking sequence of basement fault reactivation and shortcut thrusts propagation was assumed. Slip along thrusts was restored using the fault-parallel-flow algorithm whereas folded horizons not offset by faults were restored using flexural-slip-unfolding to a datum using a fault-parallel pin line. Extensional displacements were restored using antithetic-simple-shear (with shear angles of 70º and 87.5º). For kinematic compatibility and to ease in the restoration procedures, all faults were soled at depth into a SE-dipping detachment within the crystalline basement and below seismic coverage. For geometric validation, the geometry of the Haselbach and Höflein faults had to be modified during the restoration, from an originally steeply-dipping, planar geometry to slightly listric at depth. In addition, two footwall shortcut thrusts associated with the Höflein extensional fault were added to the original interpretation of an imbricate fan consisting of solely two shortcut thrusts. Before restoration, the offset of these two additional shortcuts was interpreted as related to antithetic extensional faults in the Haselbach hanging-wall. Both interpretations are not mutually exclusive though, as these extensional faults could have been thrusted and transported by subsequent slip associated with the footwall shortcut thrusts.

According to the structural restoration carried out, the Höflein high was uplifted about 545 meters by the formation of footwall shortcut thrusts. A horizontal displacement of about 1.5 km was also obtained by the structural retrodeformation, accommodated by folding of the Haselbach syn-rift wedge, slip on shortcut basement-involved imbricates and the counter-clockwise rotation of the Höflein fault. The restoration indicated an 18% of area loss in the Haselbach syn-rift wedge ahead of the basement imbricate fan; this value is in agreement with internal deformation related to buttressing against the Haselbach fault. Although the structural restoration validates the folding the Alpine Basal Thrust by younger, thick-skinned thrusting, the results of this restoration remain unsatisfactory. Even after the removal of the 545 meters of uplift, the Höflein high remains significantly elevated in comparison with all the other basement highs of the Lower Austria Mesozoic Basin. Beside the limitations imposed by the software restoration algorithms at dealing with 3D structures, these results may arise from the significantly different directions of shortening since the onset of Alpine continental collision, or additional basement

reactivation since the middle Miocene onwards. Alternatively, the Höflein high may have been originally at higher elevations than the surrounding structural culminations.

2.4.4 SANDBOX ANALOGUE MODELLING OF INVERSION IN TECTONIC WEDGES

By controlling the modelling parameters sandbox analogue models can provide structurally balanced and scaled solutions aiding in the interpretation of structurally complicated regions (McClay, 1996). Despite the large amount of analogue modelling works on basin inversion to date, few have addressed the inversion of continental margins during the development of tectonic wedges (e.g., Bonnet et al. 2007). This provided an additional inspiration to carry out the second part of this thesis (**Fig. 2.25a, b**).

The analogue modelling carried out in this thesis was done using materials suitable for simulating upper crustal deformation processes (see Davy and Cobbold, 1991; Weijermars and Schmeling, 1986; Schellart, 2000; Lohrmann et al. 2003; Adam et al. 2005; Dell'Ertole and Schellart, 2013; Schellart and Strak, 2016; **Table 2.1**). The experimental programme was done at the Geomodels Analog Modelling Laboratory of the University of Barcelona. A similar set up to that described by Brun and Nalpas (1996), Smit et al. (2003), Scheurs et al. (2006), Graveleau et al. (2012) or Bonini et al. (2012) for physical analogue experiments of brittle and brittle-viscous systems was used. The experimental rig consisted on two glass-sided walls, a fixed wall, and a moving backstop wall with pre-deformation dimensions of 75 x 50 x 6 cm^3 (**Fig. 2.25c**). A strong plastic sheet was set at its base to simulate the basal detachment surface. Dry well-sorted quartz sand with an average grain size of 250 μm, a mean coefficient of friction (φ) of 0.6, an average angle of internal friction (ø) of ~34º, and a bulk density of 1600 kg/m^3 and cohesive strength of around 55 Pascals was used. The polymer used to replicate the shallow detachment of the thin-skinned fold-and-thrust belt was Rhodosil GUM FB from Bluestar Silicones, a transparent high-viscosity polydimethylsiloxane (see Dell'Ertole and Schellart, 2013). At the low velocities of deformation used in these sandbox model experiments (**Table 2.1**), this polymer behaves as a nearly-Newtonian fluid with low yield strength and a stress exponent of n~1 (e.g., Davy and Cobbold, 1991; Weijermars and Schmeling, 1986; Dell'Ertole and Schellart, 2013). Its rheological behaviour is appropriate to simulate the natural deformation of salt or overpressured shale formations in upper crustal settings (e.g., Weijermars et al. 1993; Couzens-Schultz et al. 2003; Smit et al. 2003; Santolaria et al. 2015; Schellart and Strak,

2016). In comparison with the polymer detachment, the basal detachment in our models constituted by the plastic sheet can be considered frictional as indicated by the dominant breaking-forward sequence of thrusting obtained in our models and the lack of significant back-thrusting (e.g., Couzens-Schultz et al. 2003; Smit et al. 2003; Graveleau et al. 2012).

To avoid complexity that would render the results unclear, for each sandbox model one single parameter was changed at a time whereas the rest of the parameters remained unchanged. In such a way, the role and relative importance of each parameter could be evaluated. As the role of each parameter was constrained, additional variables were added. A pre-deformational sandpack was built by pouring layers of even thickness of white-, blue- and black-coloured sand over the basal rigid plate and the plastic sheet. Sand layers of 0.4 cm thickness were laid to facilitate tracking of deformation. A total of 6 models are presented here (i.e., models 1 to 6; **Table 2.2**). All the models were subjected to 5 cm of extension parallel to the glass-sided walls of the rig at a constant rate of 1 cm/h. Deformation was carried out by a computer-controlled rolling engine that pulled the plastic sheet away from the fixed basal plate (**Fig. 2.25d**). This forced an asymmetric velocity discontinuity at the base of the sandpack and the consequent development of a half-graben. At the same time, the moving backstop wall was pulled by a worm screw attached as well to a computer-controlled engine. Both engines worked synchronously at the same rate to avoid differential shortening or extension of the sandpack. The accommodation space created during extension was filled with alternating layers of poured red-, white- and black-coloured sand simulating syn-rift deposits.

Extension was halted every 30 minutes to add each new layer of syn-rift sand. The syn-rift sand was only poured inside the developing half-graben basin to fill the accommodation space created during each step of extension. For this, the top of the undeformed pre-rift layers was used as a regional reference of elevation. These steps were repeated until a total of 5 cm of extension were completed. Following extension, all models were covered with an even layer of orange-coloured sand to simulate a post-rift cover. This post-rift layer was used as a regional datum of elevation to assess the degree of shortening and uplift of the extensional basins during the subsequent phases of deformation.

For the shortening phase the rolling engine was locked and deformation was applied exclusively by pushing the backstop wall towards the 'undeformed foreland' at a constant velocity of 1.5 cm/h. For shortening, the first shortening model was kept horizontal whereas for the rest of the shortening experiments, the deformation rig was

tilted 3º towards the backstop moving wall (**Fig. 2.25d**). In such a way, a series of distinct hinterland-thickening wedges were built by pouring brown and white layers of sand. The parameters changed for our modelling were: the dip of the basal detachment (β), the topographic slope (α), the wedge angle (α+ β), and the presence or absence of a shallow viscous detachment in an equivalent post-rift position, similar to that of the post-rift overpressured Mikulov Formation. Although erosion and sedimentation are known to have a significant impact on the kinematics of tectonic wedges (e.g., Storti and McClay, 1995; Bonnet et al. 2007; Malavieille, 2010; Graveleau et al. 2012), these were omitted in our approach for the sake of simplicity.

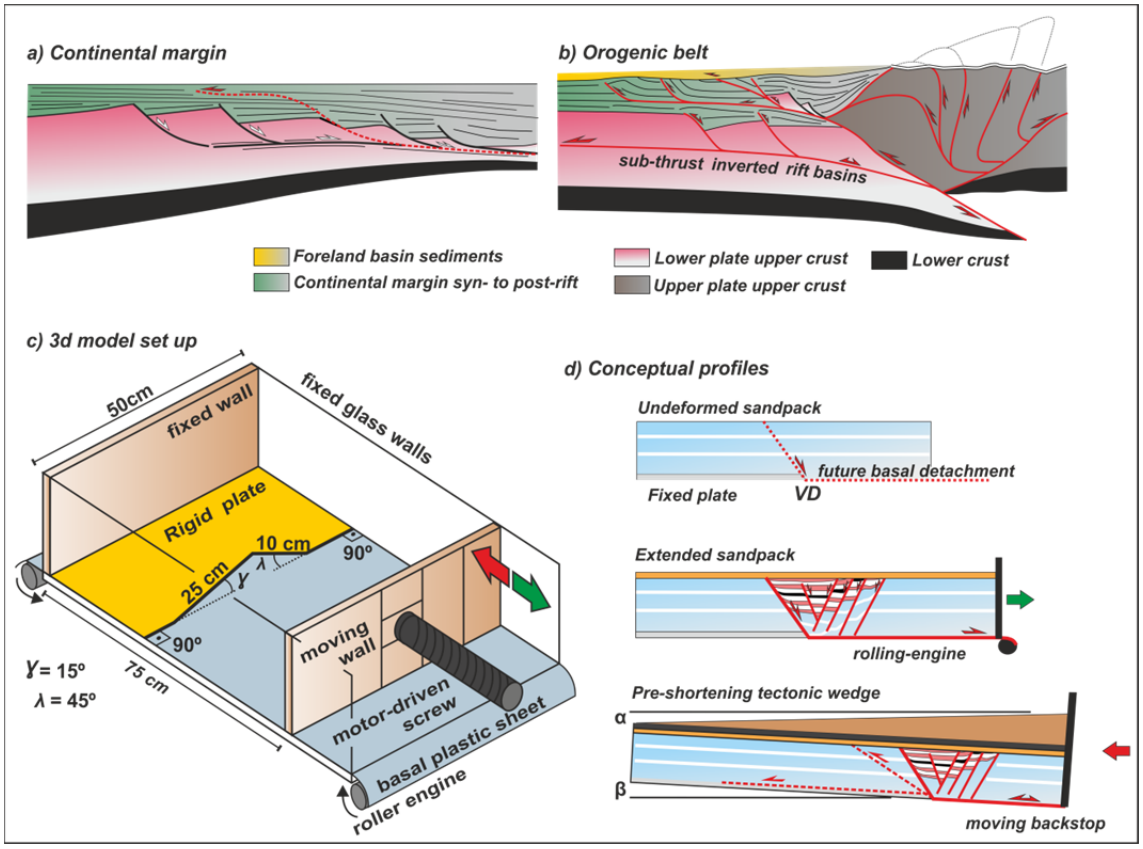

FIGURE 2.25. Concept behind the analogue modelling carried out in this thesis. A) Continental margin. B) Orogenic shortening inverts and incoporates the margin's basins in a fold-and-thrust belt. C) Conceptual design for the analogue modelling of a segmented half-graben basin and its inversion in sub-thrust setting within a thrust wedge. D) Profiles for some of the pre-extension, post-extension and pre-shortening configurations tested in the modelling carried out. The objectives were to test the influence of the Ɣ and λ angles in the formation of segmented half-grabens and their subsequent inversion using different tectonic wedges configurations based on the topography angle (α), the dip of the basal detachment (β) and the presence or absence of viscous detachments.

TABLE 2.1. Scaling and materials' properties

Parameter	Experiment	Nature	Model/Nature
Length (L)	1 cm	1 km	1.10^{-5}
Gravity (g)	9.81 m/s^2	9.81 m/s^2	1
Dry quartz sand Density (ρ)	1.6 g/cm^3	2.6 g/cm^3	0.61
Polymer Rhodosil GUM FB Density (ρ)	0.97 g/cm^3	2.2 g/cm^3	0.44
Polymer Rhodosil GUM FB Viscosity (η)	$1.18x10^4$ Pa·s	$5x10^{18}$ Pa·s	$2.3x10^{-15}$
Time (t)	1 h	258270 yrs.	$4.42x10^{-10}$
Velocity (V)	1.5 cm/h	5 mm/yrs.	$2.24x10^4$

In order to keep record of our experiments during extension and shortening, time-lapse high-resolution digital photographs were taken from the lateral sides of the model, from an oblique point of view and from the top of the model at 15 seconds intervals. Videos from these time-lapse photos were generated for kinematic analysis of deformation (see **attached DVD**). A white-light scanner was also used to record the topographical evolution of the models. During extension, these scans were carried out after stopping the deformation rig and before adding each corresponding syn-rift layer (i.e., after each 0.5 cm increments of extension). During shortening, scans were made after stopping the rig and for each 3 cm deformation increments. At the end of each experiment, the models were preserved and then longitudinally sectioned at 3 mm spacing. A 4 cm wide section along each side of the experiments was discarded to remove any border effects. High-resolution photographs of each longitudinal cross-section were taken and then imported as seeds to generate 3D voxel models. Image-processing software was used to generate mutually orthogonal crosslines, inlines and depth-slices that allowed for better visualization and interpretation of the experimental results.

2.5 INTRODUCTION TO THE PUBLISHED ARTICLES

The main objectives of this thesis were to asses and describe the basement-involved deformation observed in the sub-thrust beneath the Alpine-Carpathian fold-and-thrust belt. During this study, basement-involved deformation in extensional and shortening modes have been observed affecting the European foreland plate. In addition, extension affecting the upper colliding plate has been also and documented in Granado et al. (2016) as well. Although attention was focused on the involvement of the orogenic lower plate in the deformation, the late dismantling of the Alpidic edifice by extensional and strike-slip tectonics was also included in the discussion of the first article, thus providing a full geodynamic contextualization of the compressive involvement of the basement.

The first paper of this thesis was focused on compiling, describing and integrating observations at different scales from subsurface data of the Alpine-Carpathian Junction. On a first step, detailed maps from seismic interpretation of the top of the crystalline basement and the base of the post-rift were created. Surfaces for the Lower Austria Mesozoic Basin faults, the Alpine Basal Thrust and the main middle to late Miocene extensional faults were also generated. These interpretations allowed documenting the geometry of a large part of the Lower Austria Mesozoic Basin, its fault systems, the distribution of Jurassic syn-rift deposits, and in particular the geometry of the Höflein high. Cross-cutting and relative timing constrains were obtained from seismic mapping. A large biostratigraphically-constrained well database allowed constraining the chronology of fault activity, sedimentation and the evolution from rift, fold-thrust-belt and orogenic collapse. These results were summarised on a tectono-chrono-stratigraphic chart (**Fig. 2.26**). Fault-displacement profiles (e.g., Willemse et al. 1996) for the basement fault array were built to decipher the existence of several episodes of fault reactivation in the Lower Austria Mesozoic Basin. Based on the seismic mapping and the generated fault-displacement plots, almost all the Jurassic rift faults beneath and ahead of the fold-and-thrust belt underwent several episodes of reactivation, in extension and in compressive modes. The relative timing of deformation between the shallow thin-skinned fold-and thrust-belt and the underlying thick-skinned basement-involved system was constrained by documenting the cross-cutting relationships underneath the fold-and-thrust belt, whereas in the foreland it was constrained with the aid of published maps and paleontological data of the early to middle Miocene foreland sediments (Mandic, 2004).

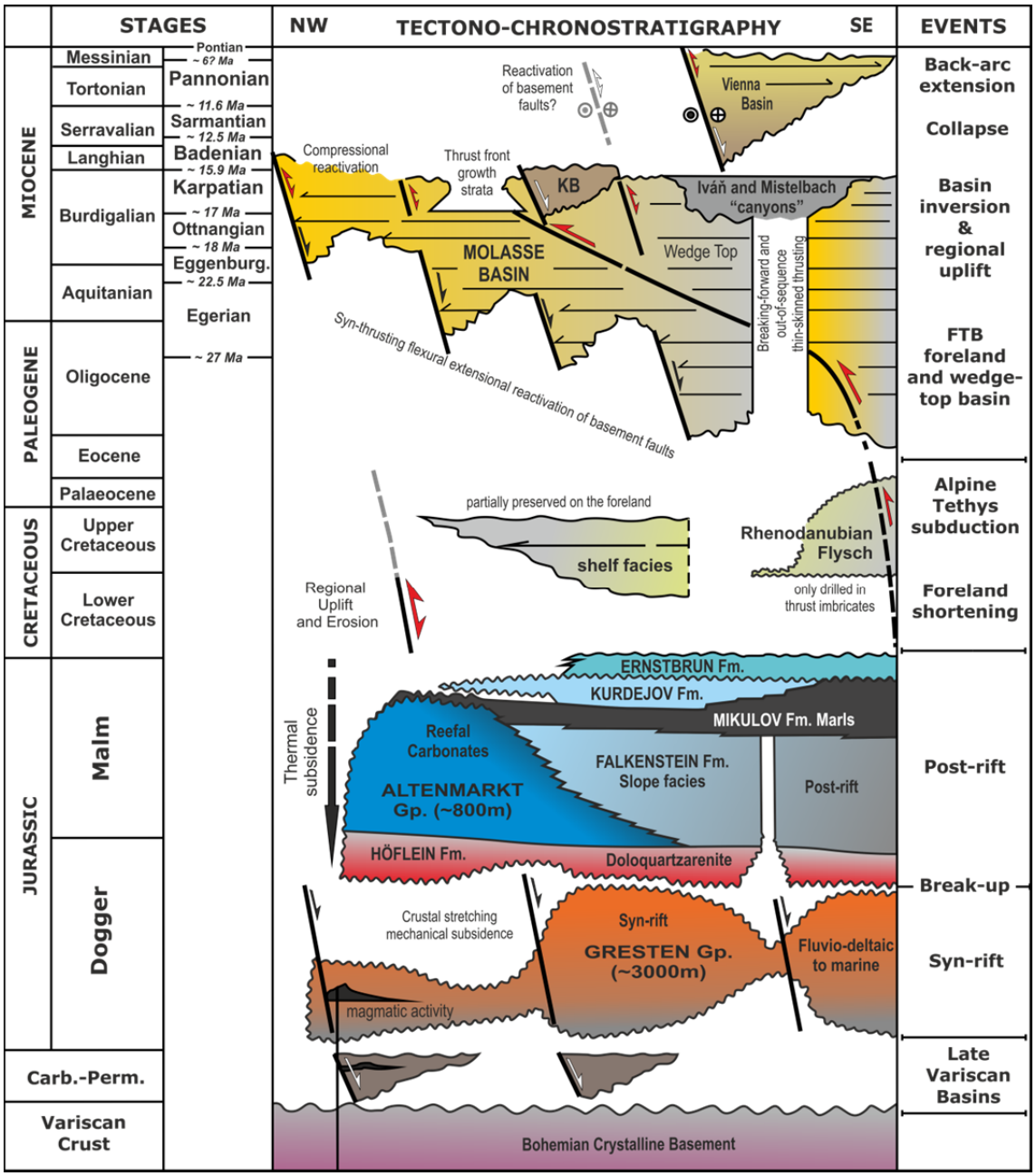

Figure 2.26. Tectono-chrono-stratigraphic chart for the Alpine-Carpathian Junction of Lower Austria. Modified from OMV Exploration and Production. Miocene Central Para-Tethys stages are from Piller et al. (2007). Chart modified from unpublished OMV Exploration and Production internal literature. KB: Korneuburg Basin.

The second part of the thesis included the modelling of inversion tectonics in sub-thrust settings by the use of sandbox analogue modelling techniques. Despite the large amount of analogue modelling works on basin inversion to date few have addressed the inversion of continental margins during the development of tectonic wedges (e.g., Bonnet et al. 2007). In the sandbox experiments carried out a non-cylindrical (i.e., 3D) approach to simulate the inversion and imbrication of segmented half-graben basins beneath and ahead of developing fold-and-thrust belts was used. These experiments aimed at investigating how the geometry of the tectonic wedge and its strength profile impact such inversion processes by using distinct configurations of pre-shortening tectonic wedges and the combination of several analytical techniques. In addition, the modelling also aimed at obtaining insights into the structural styles developed during shortening, the deformation sequence, and the timing of basin inversion vs. thrust propagation.

To accomplish these objectives the deformation of distinct tectonic wedges using different basal detachment dips and topographic slopes (i.e., β and α angle, respectively) over a frictional basal detachment was modelled (**Fig. 2.27**). **Table 2.2** summarises the main parameters of our experimental programme. The interpretative work was focused on two models sharing the same tectonic wedge configuration but one with a shallow viscous polymer detachment and one without it. These two models aimed at representing end members in terms of structural coupling. Image-based 3D voxel reconstructions (see Dooley et al. 2009) were used to aid in the interpretation of our results we have applied. Using longitudinal serial cross-sections as seeds, the technique allowed correlating along-strike the extensional and compressional architecture of the models by means of mutually-orthogonal virtual depth-slices and inline-sections. The experimental results are compared with the Höflein high natural prototype, discussing the competing factors that may influence the role of inheritance in natural systems.

The main results indicate that the pre-deformation geometry of the tectonic wedge and its related vertical load has a fundamental role on the inversion of buried extensional basins. The distribution of weak horizons within the tectonic wedge (i.e., the strength profile) has also proven to be a key factor on the kinematics of deformation and on the coupling-decoupling relationships between 'basement and cover' and very importantly, in the timing of sub-thrust basin inversion. Time-lapse videos indicated that inversion of the sub-thrust basins was associated with the compaction of sand related to slipping along the basal detachment of the model.

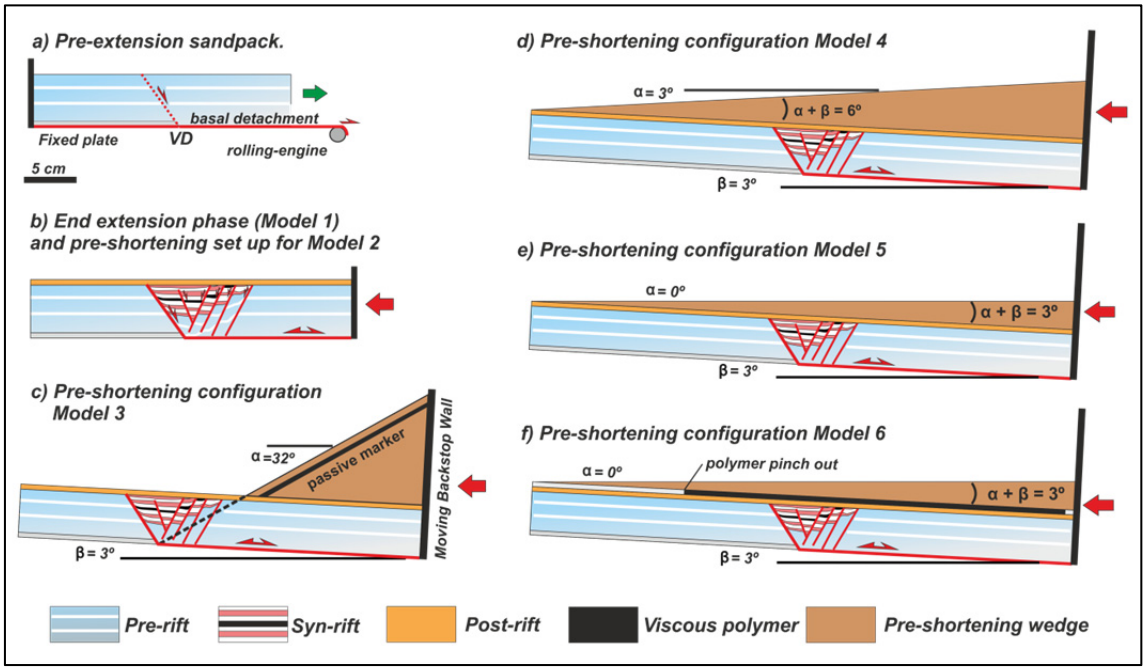

FIGURE 2.27. Summary of the pre-deformation configuration of the sandbox analogue models carried out.

TABLE 2.2. Main parameters of the experimental programme

	Basal detach.	Dip (β)	Shallow Detach.	Topo. slope (α)	(α + β)	Total ext.	Ext. rate	Total short.	Short. rate
Model 1	Frictional	0°	-	0°	-	5 cm	1 cm/h	-	-
Model 2	Frictional	0°	-	0°	0°	5 cm	1 cm/h	6 cm	1.5 cm/h
Model 3	Frictional	3°	-	32°	35°	5 cm	1 cm/h	15 cm	1.5 cm/h
Model 4	Frictional	3°	-	3°	6°	5 cm	1 cm/h	15 cm	1.5 cm/h
Model 5	Frictional	3°	-	0°	3°	5 cm	1 cm/h	15 cm	1.5 cm/h
Model 6	Frictional	3°	Viscous	0°	3°	5 cm	1 cm/h	15 cm	1.5 cm/h

CHAPTER 3. GENERAL RESULTS

3.1 INTRODUCTION

The general results of this thesis have been summarised in two scientific manuscripts entitled "Basement-involved reactivation in foreland fold-and-thrust belts: the Alpine-Carpathian Junction" and "Basin inversion in tectonic wedges: insights from analogue modelling and the Alpine-Carpathian fold-and-thrust belt". The first article was submitted to a special issue of the Geological Magazine journal devoted to the tectonic evolution and mechanics of basement-involved fold-and-thrust belts. The second article was submitted to the journal Tectonophysics, and was focused on the analogue modelling of fold-and-thrust belts involving inherited rift basins using different wedge configurations. The sandbox modelling was aimed at gaining insights on the deformation of collisional foredeeps and sub-thrust settings in fold-and-thrust belts. Both journals are enlisted within the international Journal Citation Index (JCI). The main results of each of these articles are summarised in the following sections.

3.2 BASEMENT-INVOLVED REACTIVATION IN FORELAND FOLD-AND-THRUST BELTS: THE ALPINE-CARPATHIAN JUNCTION

During this thesis, work was focused on documenting and explaining the kinematic evolution of the Alpine-Carpathian Junction foredeep and sub-thrust region, with an emphasis on fault reactivation and basin inversion tectonics. For the fulfillment of these objectives, a large dataset of subsurface data was used including 2D and 3D seismic surveys tied to tens of deep exploration wells by biostratigraphically-constrained well tops and geophysical logs. A particular emphasis on defining the 3D structure of the Lower Austria Mesozoic Basin in the sub-thrust region has been given, describing the structural styles associated with the basement fault array as well as with the timing of basin inversion. The studied foredeep deformation pattern mostly relates with a system of inherited steeply-dipping NE-SW-striking basement-involved faults, and to a lesser extent NW-SE-, E-W- and N-S-striking ones. These faults occur beneath and ahead of the Alpine-Carpathian fold-and-thrust belt and display a long-lived history of reactivation:

- A first Late Carboniferous to Permian extensional to transtensional event related to the dismantling of the Variscan orogenic edifice (Wessely, 1987; Wagner, 1998).

- A Cretaceous-Paleocene syn-collisional compressional/transpressional reactivation responsible for the large erosion of the Mesozoic cover in the foredeep and the Bohemian massif (Wessely, 1987; Nachtmann and Wagner, 1987; Schröder, 1987; Ziegler, 1987)
- A late Oligocene and early Miocene extensional reactivation ahead of the propagating fold-and-thrust belt (firstly defined in this study).
- A latest early Miocene to earliest middle Miocene compressional/transpressional mode (also defined in this study for the first time).

Evidence for these reactivation episodes comes from the sediment wedges and facies distribution associated with the basement faults (i.e., providing absolute time-constraints), and cross cutting relationships (i.e., providing relative time-constraints), their structural styles, the comparison between regional and structural elevations and the presence of erosional unconformities and calculated fault-displacement profiles. Regarding the Lower Cretaceous to Paleocene compressional or transpressional reactivation, unequivocal evidences are only present in the Bohemian massif; within the Lower Austria Mesozoic Basin, the autochthonous Cretaceous is unevenly distributed and poorly constrained by seismic and well data to provide any unequivocal constraints on the Cretaceous fault reactivation event. In fact, the Cretaceous units are strongly eroded in their preserved autochthonous (or para-autochthonous) position or have been strongly imbricated in the thin-skinned fold-and-thrust belt (Wessely, 1987; Zimmer and Wessely, 1996; Wessely, 2006; Beidinger and Decker, 2014).

The most important basement fault system is NE-SW-striking and steeply SE-dipping. One of the most striking features associated with these faults is that they consistently show large extensional offsets for the post-rift carbonate megasequence (Granado et al. 2016). To properly constrain these extensional displacements and their reactivation episodes, a dense seismic interpretation of the 3D depth-migrated and 2D time-migrated data was carried out. Given the generally poor data resolution beneath any strongly imbricated fold-and-thrust belt, the accomplishment of these objectives required extremely detailed and careful seismic interpretation for the sub-thrust region. As the Höflein Formation (i.e., the main reservoir at the base of the post-rift megasequence) is about 55 meters thick (Sauer et al. 1992) the well to seismic tie was problematic. In some cases, seismic interpretation had to rely on the critical assessment of the well to seismic tie, aided by structural concepts.

3.2.1 3D STRUCTURE OF THE LOWER AUSTRIA MESOZOIC BASIN

The model presented here corresponds to the Lower Austria sub-thrust region within the Donau_Nord 3D volume. Given the interpretation disadvantages stated above, the full stretch of the 3D depth-converted Donau_Nord dataset was interpreted four times for the top of the Basement and the Höflein Formation horizons, until a final interpretation was chosen. A total of 37 faults, including basement faults, thin-skinned thrusts, and extensional faults affecting the cover were interpreted.

Within the Donau_Nord dataset, the Lower Austria Mesozoic Basin is constituted by a crystalline basement, syn-rift and post-rift megasequences and a series of basement-involved faults. From NW to SE, the main faults defined in this thesis are the Mailberg, Altenmarkt, Stockerau, Haselbach, Höflein, Kronberg and Kasernberg faults. The Mailberg fault is imaged by several NW-SE striking 2D time-migrated profiles in the foreland region and is not covered by the seismic cubes. For this reason it was not included in the 3D structural model (see Granado et al. 2016 for further details and analysis). The Lower Austria Mesozoic Basin basement fault array is constituted by steeply to moderately SE-dipping extensional faults and minor synthetic and antithetic steeply to moderately NW-dipping faults. These basement-involved faults are arranged in segments with slightly different orientations, striking from NNE-SSW, to E-W and NW-SE, but overall configuring a general NE-SW trend (**Fig. 3.1**). The less abundant NW-SE-striking fault trend could correspond to transfer fault systems segmenting the regional NE-SW-striking basement fault trend along the former Jurassic continental margin. The largest of these transfer faults has been named Roseldorf transfer fault, and links the Stockerau fault with Altenmarkt fault, beneath the Roseldorf hydrocarbon field (**Fig. 3.1**). Shallower, tear-like faults with a similar NW-SE orientation occur along the thrust front at the Waschberg-Ždánice Zone. Other NW-SE striking faults in the order of tens to hundreds of meters long (i.e., up to two orders of magnitude shorter that the major basement faults) occur within the basement and pre-rift to early syn-rift sections.

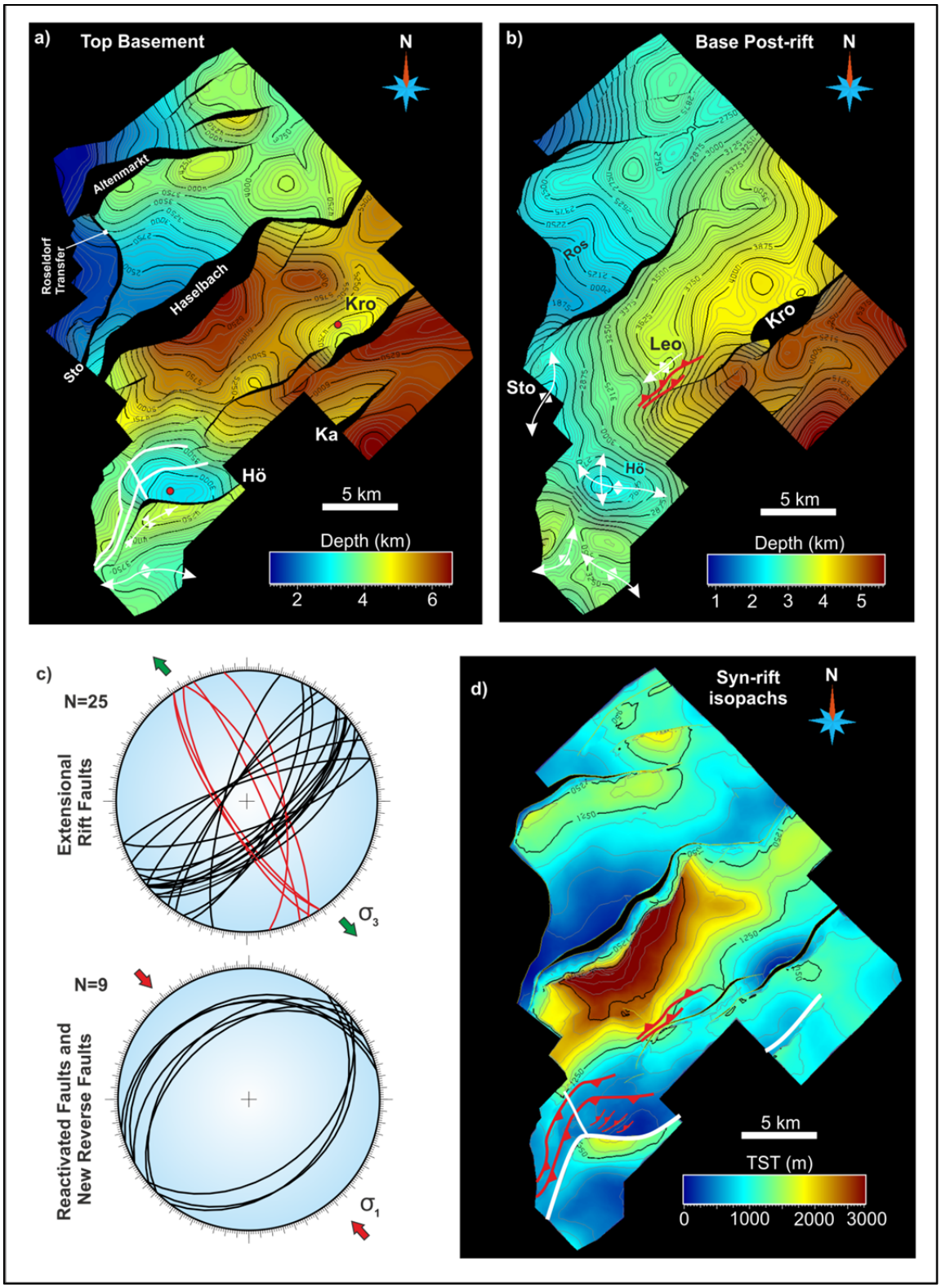

Figure 3.1. 3D structural model of the Lower Austria Mesozoic Basin from the Donau_Nord survey A) Top crystalline basement. B) Base post-rift (Höflein Formation). C) Sub-thrust fault orientations. D) True stratigraphic thickness map for the syn-rift megasequence. Sto: Stockerau anticline; Kro: Kronberg high; Leo: Leobendorf; Hö: Höflein high; Ros: Roseldorf transfer zone; Ka: Kasernberg fault.

These faults are depicted in red in **figure 3.1**, and display significantly lower throw values than the master faults and are interpreted as release faults (Destro, 1995). This type of fault accommodates the along-strike stretching of the hanging-wall layers during regional extension and may partly account for the other NW-SE striking fault sets revealed by the fault orientation stereoplots.

In the studied area, the general trend of the basement fault array is roughly parallel to the strike of the overlying thin-skinned thrust front. Major basement faults display lengths in excess of 10 km along strike and their full stretch is not completely covered by the 3D seismic data. Gravity anomaly maps (Geofyzika, 1999; **Fig. 3.2**) were used in an attempt to qualitatively characterise the shape and dimensions of the basement fault array and related half-graben basins. The Bouger anomaly map defines the general shape of the Vienna Basin as a large, NNE-SSW-striking gravity low. This map shows that Vienna Basin displays one large gravity low in the triple junction of the Austrian, Slovakian and Czech Republic borders. Such gravity low is associated with the hanging-wall depocenter of the Steinberg fault (**Figs. 2.16** and **3.2**). The Bouger gravity map also illustrates the shape of the eastern margin of the Bohemian massif and the south-elongated Bohemian spur (**Fig. 3.2a**). The eastern margin of the spur appears dissected by NW-SE-striking lineaments juxtaposing contrasting gravity readings. These lineaments are parallel to the shallow tear faults that affect the frontal thin-skinned fold-and-thrust belt (i.e., Waschberg-Ždánice Zone), and may actually reflect the presence of rift-inherited hard-linked transfer fault systems (**Fig. 3.2**). In the southern part of the Vienna Basin, the residual gravity maps indicate a shallower basement that broadly corresponds with the location of the Matzen and Aderklaa horst blocks. A roughly N-S striking lineament bounds this shallower area to the Bohemian spur, probably corresponding with the footwall of the Leopoldsdorf fault (**Figs. 2.16** and **3.2)**.

On a more detailed scale of observation, residual gravity maps (Geofyzika, 1999) were also used to study the basement structure. Only the most external half-graben (i.e., Mailberg fault) and its sediment wedge are well illuminated as a gravity low in this map. The residual gravity map indicates a large >30 km long half-graben with a thick sediment wedge (Granado et al. 2016). The other half-graben basins are poorly defined by the data as they are buried beneath the fold-and-thrust belt. The Kronberg high is shown as a significant residual gravity high that corresponds to the elevated footwall of the Kronberg fault (**Figs. 3.1** and **3.2**). On the other hand, the Höflein high (which sits significantly

higher that the Kronberg high) is not characterised by such a local residual gravity high. In fact, the higher residual gravity readings at Höflein are spread over the hanging-wall and footwall, suggesting that the basement may have been involved over a large area in the Höflein half-graben.

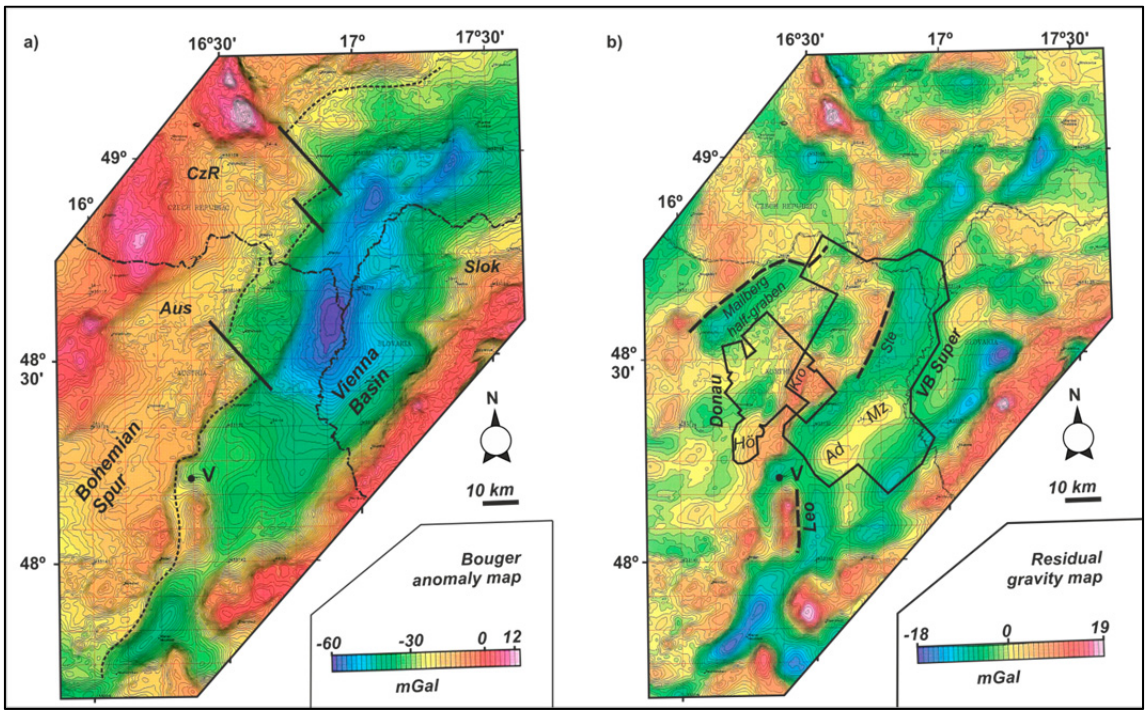

FIGURE 3.2. Gravity anomaly maps from the Alpine-Carpathian Junction. A) Bouger gravity map. B) Residual gravity map. The boundaries of the Donau_Nord and Vienna Basin Supermerge 3D surveys are indicated. Ad: Aderklaa; Aus: Austria; CzR: Czech Republic; Hö: Höflein gravity high; Kro: Kronberg gravity high; Leo: Leopoldsdorf fault; Mz: Matzen; Slok: Slovakia; Ste: Steinberg fault; V: Vienna. Data from Geophyzika (1999) and provided by OMV Exploration and Production GmbH.

In the Donau_Nord 3D seismic data, the top of the basement in the hanging-wall of the major basement-involved faults forms either a straight panel dipping into the fault or slightly kinked panels indicating that the underlying extensional faults display a planar to slightly kinked geometry. For the major faults, the top of the crystalline basement displays fault-parallel hanging-wall synclines which trend parallel to slightly oblique to the orientation of the immediate fault segment. The Altenmarkt fault, for instance, displays two of these synclines separated by a fault perpendicular ridge. The average spacing of the basement-involved faults is around 10 km measured normal to their strike, indicating that their basal detachment should be located at about the local brittle-plastic transition. The syn-rift megasequence sediment distribution was calculated by subtracting the depth to the basement and the depth of the base of the post-rift and is represented as a True

Stratigraphic Thickness map (**Fig. 3.1d**). This map shows several syn-rift depocenters juxtaposed to the major basement faults as well as true stratigraphic thickness lows associated with the uplifted footwalls of the basement faults. The largest syn-rift depocenter is associated with the Haselbach fault where the thickness of the megasequence is in excess of 2750 meters. It should be pointed out that the thickest syn-rift in the Höflein half-graben is related to its E-W striking segment, which is strongly oblique (i.e., about 45º) to the other main faults of the Lower Austria Mesozoic Basin.

In summary, the Lower Austria Mesozoic Basin is characterised by a well-preserved inherited extensional architecture corresponding to a series of tilted fault blocks and associated half-graben basins. The observed displacements along the basement-involved faults of the basin die out upwards by developing fault-propagation folds. These folds also affect the post-rift megasequence, the upper Oligocene to Miocene foreland sediments of the Molasse Basin, and locally, the overlying thin-skinned thrust system (Granado et al. 2016). The observations made above suggest that the Lower Austria Mesozoic Basin basement faults grew to a certain point by the lateral linkage of isolated fault segments, but also account for significant fault reactivation after the post-rift, first in extension and then in shortening modes.

3.2.2 3D FAULT REACTIVATION AND BASIN INVERSION IN THE LAMB

A quantitative approach was taken to provide further constraints to the regional structure and evolution of the Lower Austria Mesozoic Basin. Fault-displacement profiles (i.e., fault length vs. throw values) were calculated for the top basement and the base of the post-rift megasequence (**Fig. 3.3**) given their fundamental role in constraining the magnitude and timing of fault reactivation (e.g., Williams et al. 1989; Turner and Williams, 2004). Hence, large offsets affecting the post-rift megasequence are indicative for fault reactivation following rifting. Fault-displacement profiles illustrate the along strike variation of throw but can also indicate which faults (or fault segments) underwent reactivation (e.g., Thomas and Coward, 1995; Willemse et al. 1996). Except for the Höflein fault, the calculated profiles indicate that the net displacement is extensional for the top Basement and the Höflein Formation. As commonly observed in other extensional fault systems, the displacement maxima occur slightly shifted sideways from the central position of the faults (Willemse et al. 1996).

3.2.2.1 THE MAILBERG FAULT

The Mailberg fault is located in the foreland region ahead of the thin-skinned fold-and-thrust belt. It is covered by 17 unevenly spaced NW-SE-striking 2D time-migrated seismic profiles. The Mailberg fault runs for about 30 km striking NE-SW and displays a large hanging-wall depocenter which is significantly well constrained by residual gravity data (**Fig. 3.2b**) and the fault-displacement profile (**Fig. 3.3a**). The fault displays a thick hanging-wall sedimentary wedge that has been penetrated by the exploration well Gross-Harras1 down to the Paleozoic. This wedge includes Carboniferous strata, overlaid by the syn-rift Middle Jurassic Gresten Group and the Upper Jurassic carbonates of the post-rift megasequence. The latter is significantly downthrown in the hanging-wall and is eroded to the SW in the footwall. In addition, Egerian-Badenian (i.e., upper Oligocene to middle Miocene) foreland sediments are significantly thicker on the hanging-wall than in the footwall, indicating the extensional activity of this fault during these times. The top of the crystalline basement is folded into an open syncline, and the associated extensional displacement has formed a fault-propagation fold affecting the post-rift and overlying foreland units.

On the other hand, the uppermost and younger hanging-wall layers just above the Mailberg fault are dated as Karpatian to Badenian (Mandic, 2004) and are folded into a gentle, open fold. This fold is slightly asymmetric and has been named the Mailberg anticline (Granado et al. 2016). This fold lies slightly above regional elevation and seismic data has revealed a thin compressional growth sequence of mainly Badenian in age. In fact, according to the facies distribution in the foreland of the Alpine-Carpathian Junction reported by Mandic (2004), a Badenian coralline-algal reef developed onto this growing anticline, surrounded by and interfingering with deeper water siliciclastic-dominated facies of the Mailberg Formation (Granado et al. 2016). These observations have allowed dating the two Cenozoic events of basement fault reactivation and related basin inversion. The reverse displacement associated with the compressional reactivation of the Mailberg fault may be in fact responsible for the flat-lying distribution of throw identified in fault-displacement profile (**Fig. 3.3a**).

3.2.2.2 THE ALTENMARKT FAULT AND THE ROSELDORF TRANSFER SYSTEM

The Altenmarkt fault is located just ahead of the thin-skinned thrust front of the Alpine-Carpathian fold-and-thrust belt. This fault runs along strike for at least 15 km, and dies out toward the NE where it is relayed by a system of two smaller SE-dipping rift faults. The Altenmarkt fault is constituted by several segments of differing orientation ranging from NNE- to NE-SW to E-W-striking (**Fig. 3.1**). The fault-displacement profile for the Altenmarkt fault indicates that the top of the basement and the base of the post-rift (i.e., Höflein Formation) are in net extensional displacement with a displacement maximum strongly shifted toward the SW (**Fig. 3.3b**). This displacement maximum is sharply reduced to the SW, where the base of the post-rift is eroded. At this position the Altenmarkt fault is structurally hard-linked to the NW-SE striking Roseldorf transfer fault (**Fig. 3.1**)

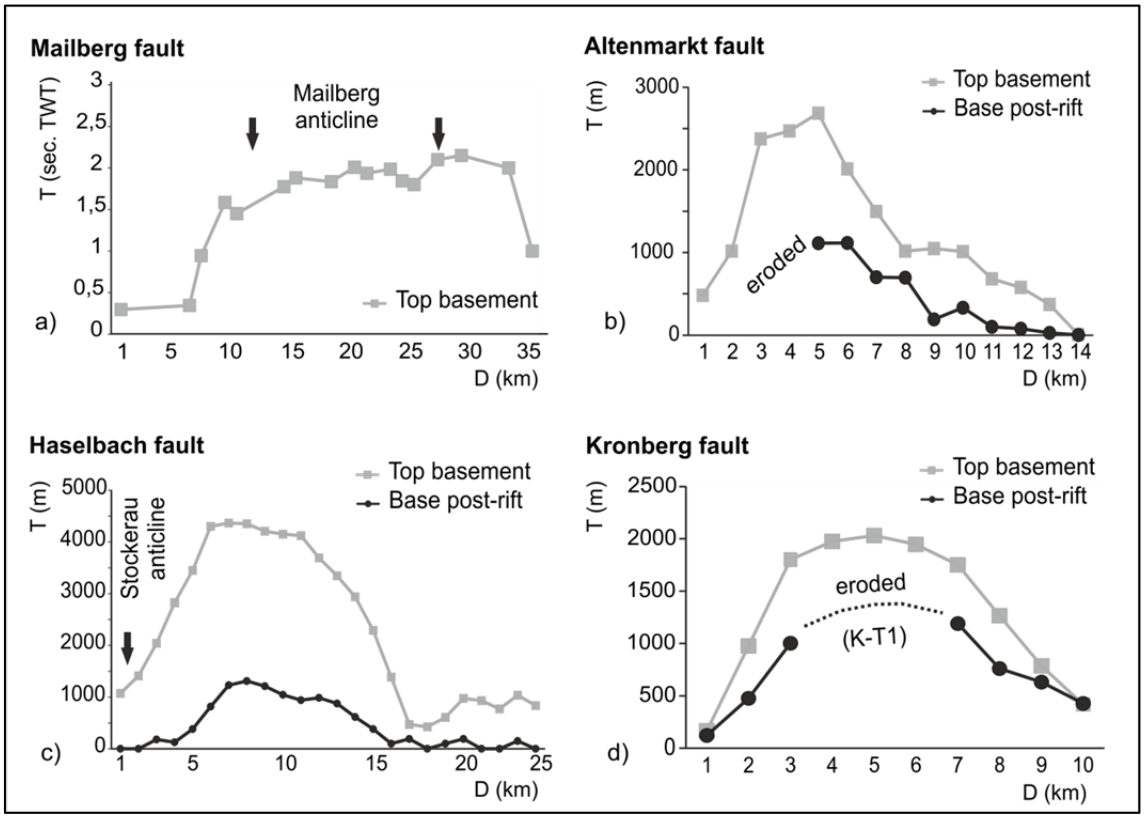

FIGURE 3.3. Fault displacement profiles for the Mailberg, Altenmarkt, Haselbach and Kronberg basement faults. Note that the Mailberg fault throw is in two-way time, whereas it is in meters for the other major faults. D is distance along the fault's strike and T is throw (i.e., vertical offset) for the given horizons. K-T1 indicates the position of the deep well Kronberg-T1.

Seismic interpretation and well data indicate that the post-rift megasequence is missing to the west and SW on the footwalls of the Altenmarkt and the Roseldorf transfer faults. On their footwalls, Egerian strata are unconformably overlying the top of the crystalline basement. The base of the post-rift megasequence is also downthrown in the hanging-wall of these two faults, where a thick post-rift carbonate sequence remains preserved beneath the erosive Egerian. A series of observations derived from the combined study of inlines and cross-lines provide fundamental evidences of thick-skinned reactivation of the Altenmarkt fault and the Roseldorf transfer fault system, first in extension and then in compression:

- No post-rift is preserved on the Altenmarkt and Roseldorf footwalls to the NW of Roseldorf fault where the Egerian foreland strata are unconformable over the crystalline basement.

- Thick Upper Jurassic units are preserved on the hanging-wall of these two faults beneath the erosional Egerian foreland strata. The Upper Jurassic carbonates are preserved due to the early Miocene extensional reactivation of the basement fault.

- The unconformity at the base of the Egerian strata is folded into several panels beneath the Alpine Basal Thrust, forming a NE-SW striking anticline directly above the Roseldorf transfer fault. A syncline axial surface propagates from and is sub-parallel to the underlying Roseldorf transfer fault.

- The Upper Jurassic on the hanging-wall of Altenmarkt fault / Roseldorf transfer is above regional elevation. This observation accounts for the significant reduction of extensional offset shown by the Altenmarkt fault to the SW.

Additional evidence for positive inversion is shown by a low angle offset at the top of the crystalline basement in the hanging-wall of the Altenmarkt fault. At the hanging-wall, the top of the basement is divided into two slightly offset panels. The NW panel dips toward the fault more steeply than the SE panel. The units above this basement kink (i.e., syn-rift and post-rift megasequences and the overlying Molasse basin sediments) are folded into a broad open anticline, above which the Roseldorf hydrocarbon field is located. This anticline and the low angle offset affecting the top of the basement are interpreted to be related to a NW-directed SE-dipping basement-involved shortcut thrust emanating from and kinematically-linked to the steeply-dipping Haselbach fault (Granado et al. 2016). The inversion of this faults system includes the Altenmarkt fault, the Roseldorf transfer and the

Haselbach fault and its footwall shortcut. Whether the Roseldorf anticline is exclusively related to the thin-skinned thrust front or with the positive inversion of the underlying rift fault system is not yet clear, but the compiled evidence suggests a mix-mode deformation style of thin-skinned imbrication followed by open folding developed by basement-involved positive inversion.

3.2.2.3 THE HASELBACH FAULT AND RELATED INVERSION STRUCTURES

The Haselbach fault is located in the middle of the Donau_Nord 3D survey (**Fig. 3.1**). The fault is steeply dipping to the SE and runs NE-SW in excess of 20 km along strike below the Waschberg-Ždánice thin-skinned imbricates. The Haselbach fault displays the largest observed throw values of the basement fault array (i.e., >4000 meters for the top of the crystalline basement; **Fig. 3.3c**) and the thickest syn-rift depocenter. In a cross section corresponding to the fault's displacement maximum, the top of the crystalline basement dips toward the NW (i.e., towards the Haselbach fault). Towards the NE, the seismic imaging becomes poorer but well data indicates that the top of the basement is folded into a hanging-wall syncline. On the other hand, in the Stockerau area to the SW, the top of the basement displays a down-to-the-SE terraced geometry. This terraced geometry is in agreement with the existence of several planar extensional faults (Granado et al. 2016).

The observed lateral variation in the geometry of the hanging-wall's basement top may suggest a slightly kinked geometry for the Haselbach fault at depth, with the hanging-wall syncline developed for those layers with less extensional displacement and still above the fault's kink (Xiao and Suppe, 1992). Nevertheless, the fault's kink is not observed in the seismic data and if it exists at all, it would be located below the recorded depth of the seismic data. In addition, the base of the post-rift megasequence in the hanging-wall is downthrown in excess of 1000 meters. Such extensional offset is also accompanied by a thick Egerian to Ottnangian (i.e., upper Oligocene to early Miocene) sedimentary wedge (Granado et al. 2016). Well and seismic data also suggests that the sedimentation of this wedge is responsible for the partial erosion of the underlying post-rift section. In addition, the post-rift section above the Haselbach fault is folded into an open anticline in the Stockerau area. This anticline, which hereafter will be referred to as the Stockerau anticline, folds the para-autochthonous foreland units and the overlying thrust-imbricated foreland strata of the Roseldorf Zone. The Stockerau anticline is related to the positive inversion of

the Haselbach basement-involved extensional faults system. The constructed 3D model indicates that the structural culmination of the anticline may be located further to the SW, but additional 3D seismic coverage is needed to fully constrain this.

Further east but still on the hanging-wall of the Haselbach fault the post-rift section is folded into a km-scale anticline with a large shallowly NW-dipping limb and a shorter SE-dipping limb. This structure has been named the Leobendorf anticline which folds gently the overlying post-rift strata and structural units above. The Leobendorf anticline is interpreted as related to a NE-SW striking SE-directed back-thrust nucleated from the Haselbach fault along the basal pre-rift section or the pre-rift and top basement interface (i.e., most probably within the coal-bearing section of the Middle Jurassic Gresten Group). According to the geometries described, the steeply dipping Haselbach fault seems to have acted as a buttress upon shortening (e.g., Butler, 1989), promoting the development of the basement-involved Haselbach shortcut fault mentioned above, and the Leobendorf hanging-wall back-thrust.

3.2.2.4 THE KRONBERG FAULT AND RELATED STRUCTURAL HIGH

The Kronberg fault and its related structural high locate to the eastern part of the 3D model from the Donau_Nord seismic data (**Fig. 3.1**). The Kronberg basement high strikes also NE-SW and corresponds to the elevated footwall of the Kronberg extensional fault. The Kronberg fault is steeply-dipping to the SE and runs along-strike for about 10 km. According to the seismic interpretation it seems to be relayed to the SW by another extensional fault, but this sub-thrust zone is significantly poorly imaged. The calculated fault displacement profile shows a displacement maxima located within the central part of the fault. At this position, extensional offsets for the top of the crystalline basement are in excess of 2 km. The Kronberg high locates in the immediate footwall of this fault's displacement maxima. The Kronberg structural high was drilled by Kronberg T1 well, targeting the sub-thrust post-rift and syn-rift reservoir sections (Zimmer and Wessely, 1996). The well drilled down to 4714 meters (measured depth) through the imbricated units of the Rhenodanubian Flysch and Waschberg-Ždánice zones, and found Egerian (i.e., upper Oligocene to early Miocene) Molasse sediments on top of the lower parts of the syn-rift megasequence; the post-rift basal carbonate section was not present. Fault displacement profiles calculated for the preserved base of the post-rift megasequence away from the

footwall high indicate extensional offsets in excess of 1000 meters (**Fig. 3.3d**). The fault displacement profile for the base of the post-rift displays a similar displacement distribution to that shown by the top of the crystalline basement. In addition, the Kronberg fault hanging-wall displays a Molasse sedimentary wedge above the post-rift megasequence thicker than that drilled at the footwall. These observations suggest that the basal section of the post-rift megasequence on the Kronberg high may have been eroded by the footwall uplift related to the Egerian to Ottnangian (i.e., late Oligocene to early Miocene) extensional reactivation of the Kronberg fault ahead of the forelandward propagating thrust system. An alternative interpretation was provided by Zimmer and Wessely (1996) in which the missing section is interpreted to have been sliced off by the Alpine Basal Thrust. Although the quality of the 3D seismic data is rather poor in this area, the seismic to well tie indicates that the basal thrust is located above the Egerian unconformity.

3.2.2.5 THE HÖFLEIN HIGH AND RELATED INVERSION STRUCTURES

The Höflein high is located at the southern corner of the Donau_Nord seismic cube, beneath the Rhenodanubian Flysch Zone imbricates (**Fig. 3.1**), and very close to the western margin of the Vienna Basin (**Fig. 2.16**) It is probably the most enigmatic structure in the area, albeit it hosts the most important gas and condensate field in the sub-thrust region of Lower Austria (Sauer et al. 1992; Zimmer and Wessely, 1996). This is due to poor quality of the seismic data as well as the absence of 3D seismic data coverage around the field. The Höflein field produces from the para-autochthonous post-rift carbonates and the siliciclastic section of the syn-rift in a footwall 4 way-dip closure.

Available well and seismic data were integrated to generate a 3D structural model of the Höflein half-graben. The generated model indicates that the master basement fault (i.e., the Höflein fault) extends for as much as 12 km along-strike and is constituted by three fault segments, namely segment 1, segment 2 and segment 3 (**Figs. 3.1** and **3.4a, b**) which strike NNE-SSW, E-W and NE-SW, respectively. These fault segments are steeply-dipping and slightly concave upwards (Granado et al. 2016, 2017). The Höflein high corresponds to the elevated footwall of the E-W striking fault segment located in the central position of the Höflein fault (i.e., segment 2). The E-W orientation of the footwall basement high (i.e., where the main hydrocarbon field locates) significantly departs from the regional NE-SW striking basement fault array trend. The calculated syn-rift true stratigraphic thickness (i.e.,

syn-rift isopach map, **Fig. 3.4a**) shows that the Jurassic syn-rift depocenter is associated with the central E-W-striking fault segment, which is in fact at 45º to the resolved regional direction of Jurassic rifting (Granado et al. 2016). The western end of the Höflein high is offset by a NW-SE striking basement fault, with its downthrown block located at the SW. This fault is similar in orientation to the Roseldorf transfer fault, but oppositely dipping. Lack of 3D seismic coverage hampers additional correlation, but this fault is an important feature as it compartmentalised the production from a hanging-wall three-way structural closure at the western end of the field from the major E-W-striking 4 way-dip closure.

The Höflein fault could be correlated to the NE with the Kasernberg fault (**Fig. 3.1a**) but lack of 3D seismic data hampers such correlation. The Höflein high is on a similar structural position with the Kronberg high located further to the NE based on seismic interpretation and the residual gravity maps (**Figs. 3.1** and **3.2**). However, the crystalline basement of Höflein high is located at around 2500 meters below mean sea level, and about 2000 meters above the top of the crystalline basement drilled by the Kronberg T1 well. In addition, the post-rift basal carbonate section is preserved at the Höflein high (i.e., the main hydrocarbon reservoir) whereas at the Kronberg high the drilling reported it missing. In order to illustrate the complex 3D geometry of the Höflein high and related fault systems, NW-SE-striking cross sections and a composite NE-SW-striking one were built (see sections in Granado et al. 2016). The first of these cross sections goes from the Stockerau anticline to the NW to the Höflein high to the SE. In this section, the Höflein high is characterised by the prominent footwall reflections of the post-rift carbonates. To the SE, these reflections disappear and locate on the Höflein's downthrown hanging-wall. On the footwall, the post-rift carbonates are offset and imbricated several times by a series of NE-SW striking small-displacement back-thrusts. The top of the crystalline basement is folded into two panels which relate to two roughly NE-SW striking basement-involved reverse faults emerging from the Höflein extensional fault. Displacement and folding associated with these reverse faults are, at least partially, responsible for the high elevation of the Höflein high.

Further to the SW, a section across the Höflein fault away from the elevated footwall displays a thick package of sub-horizontal reflections in the hanging-wall at *ca.* 3.5 km depth. These sub-horizontal reflections are unconformably overlain by SE-dipping continuous bright reflections. Similar relationships are shown in a roughly perpendicular section (Granado et al. 2016). Well data from the recently drilled well Höflein5b (OMV

Internal Report, 2013) indicate that these thick sub-horizontal reflections in the hanging-wall belong to the syn-rift Gresten Group whereas the SE-dipping reflections immediately above belong to the post-rift reservoir section. Well intersections in the Höflein field indicate thicker Eggenburgian to Ottnangian strata in the hanging-wall than in the footwall. These drilling intersections also revealed the presence of the Höflein Formation above the expected elevation on the hanging-wall when compared to the other half-grabens of the Lower Austria Mesozoic Basin. Additional well data also indicate a tectonic repetition of the Höflein Formation in the footwall of the Höflein fault. Above the folded post-rift carbonates, the reflections belonging to the Rhenodanubian Flysch Zone imbricates and the Alpine Basal Thrust are gently folded into an open anticline. A similar anticlinal feature can be observed on a perpendicular section suggesting that these relationships are not seismic artefacts. These cross-cutting relationships provide time-constraints on the structural evolution of the Höflein high and the deformation sequence of the Alpine-Carpathian fold-and-thrust belt.

In the hanging-wall, the basement top is folded into a plunging NE-SW striking syncline and anticline pair trending slightly oblique to the Höflein fault. The double or single plunging nature of the hanging-wall's anticlines is also obscured by the lack of 3D seismic coverage. The structure of the basement top and that of the Höflein Formation on the hanging-wall are rather different in terms of fold orientation but also wavelength-wise (**Fig. 3.1**). Such differences most probably arise from a buttressing effect of the Höflein fault on the folding of the hanging-wall sequences involving unconformable units of uneven thicknesses. Beside this, the non-rectilinear shape of the Höflein fault may have also dictated complicated patterns of folding associated with the positive inversion. In fact, the residual gravity map (**Fig. 3.2b**) suggests an elevated basement for the whole of the Höflein half-graben dipping towards the NW.

Fault displacement profiles were also calculated for the Höflein fault using the top of the crystalline basement and the base of the post-rift megasequence (**Fig. 3.4c**). The Höflein fault shows a dramatic change in the along strike throw distribution, a feature that is also indicated by the syn-rift isopach distribution (**Fig. 3.4a**). The sharp change in throw and syn-rift sediment thickness is coincident with the change in the strike of the fault, from the E-W striking segment to the NNE-SSW striking one.

In order to conciliate 3D seismic data, 3D structural modelling and analysis, in addition to well intersections and related geophysical logs, as well as the residual gravity data, the Höflein field is interpreted as harpoon structure consisting of a mildly inverted extensional fault and an imbricate fan of basement-involved footwall shortcut thrusts (Granado et al. 2016). In fact, the residual gravity data suggest that a hanging-wall by-pass structure may have also involved the crystalline basement to produce the observed residual gravity readings, as well as the folded reflections of the Rhenodanubian Flysch imbricates. In addition, a series of small-displacement thrust and back-thrusts could explain the repetitions of the reservoir carbonate section found in exploration wells, which are below seismic resolution. According to the geometries described, the Höflein extensional fault may have acted as a buttress upon late early Miocene shortening, promoting the development of the basement-involved shortcut faults and the minor back-thrusts. These shortcut faults are low displacement features with a limited amount of overthrusting. In fact the kinked nature of the crystalline basement top in the Haselbach hanging-wall (i.e., Höflein's footwall) is interpreted as due to the imbrication and folding promoted by these series of footwall shortcut thrusts, and not necessarily by a kink in the lower reaches of the Haselbach fault (section 3.2.2.3).

The 3D structural relationships documented for the Höflein high indicate a late folding of the overlying Alpine Basal Thrust and related imbricates (i.e., thin-skinned tectonics followed by thick-skinned). The Korneuburg Basin located in close proximity is a shallow feature, unrelated to basement faulting, and developed in Karpatian times (i.e., 17-16 Ma). As inversion ahead of the thin-skinned thrust front is dated is this thesis as Badenian based on the Miocene facies distribution given by Mandic (2004), an approximate Karpatian to Badenian age for the inversion and uplift of the Höflein high is proposed. On the other hand, given its proximity with the Vienna Basin western margin, and the localised uplift experienced by the Höflein high, a potential basement reactivation during the middle-late Miocene lateral extrusion should not be excluded. The recognised left-lateral strike-slip kinematics of the Vienna Basin may have imposed a restraining bend on the favourably oriented E-W striking segment of the Höflein fault. However, early Miocene (*ca.* 20-16 Ma) apatite cooling ages reported for the Rhenodanubian Flysch units overlaying the Höflein high (e.g., Trautwein et al. 2001) indicate a strong uplift previous to or very close to the opening of the Vienna Basin (16 Ma).

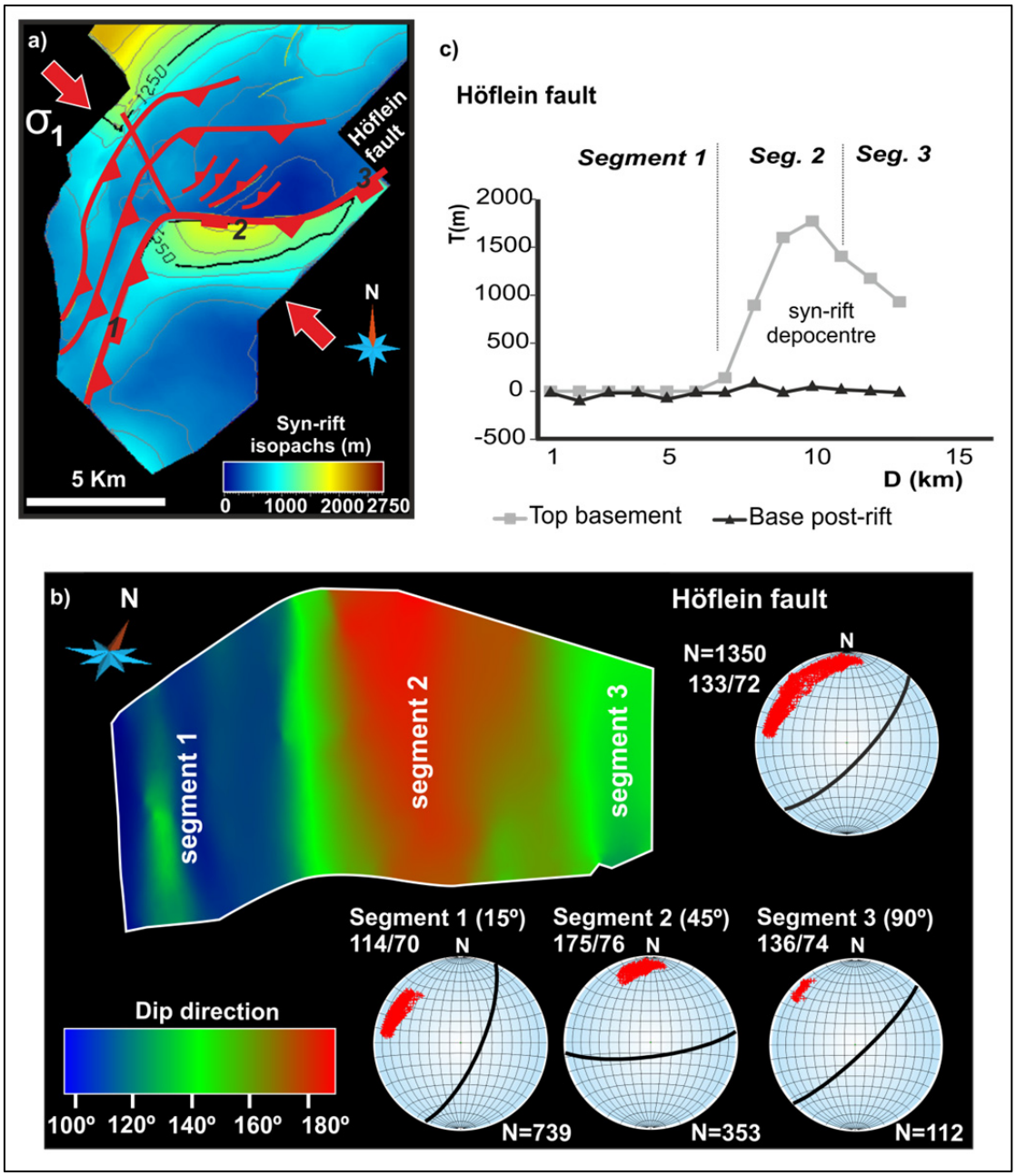

FIGURE 3.4. Summary of structural data from the Höflein half-graben derived from the seismic interpretation and 3D structural modelling. A) Syn-rift megasequence isopach distribution. B) Fault segments of the Höflein fault according to the orientation in strike and dip at 15°, 45° and 90° to the principial early Miocene compressional stress trajectory. C) Fault-displacement profile calculated for the top of the basement and the base of the post-rift megasequence (i.e., the Höflein Formation).

3.3 BASIN INVERSION IN TECTONIC WEDGES: INSIGHTS FROM ANALOGUE MODELLING AND THE ALPINE-CARPATHIAN FOLD-AND-THRUST BELT

The experimental programme was carried out at the Geomodels Analogue Modelling Laboratory of the University of Barcelona. The sandbox experiments carried out modelled the inversion and imbrication of rift basins beneath and ahead of developing fold-and-thrust belts (Granado et al. 2017). First, the effects of a segmented inherited discontinuity on the development of a half-graben basin were tested. The modelled segmentation simulated the shape of Höflein fault which had been determined from the interpretation of the Donau_Nord 3D seismic data. The segmented shape of the Höflein fault inspired the modelling, using a rigid fixed plate arranged in 3 segments striking at 15°, 45° and 90° to the directions of extension and shortening (**Fig. 2.25**), but also aimed at gaining insights on the inversion of segmented extensional basins in tectonic wedges in general.

After the development of a segmented half-graben basin, the modelling objectives were to gain insights into the structural styles and the kinematics of sub-thrust basin inversion within a fold-and-thrust belt. In order to do so, the deformation of distinct tectonic wedges using different basal detachment dips and several topographic slopes (i.e., β and α angle, respectively) over a frictional basal detachment (**Fig. 2.27**) was modelled. According to the results obtained, a model set up was selected, to be repeated adding a viscous (nearly-Newtonian) polymer layer located at the position equivalent to that of the post-rift (i.e., above the segmented half-graben basin and its infill). Adding a polymer layer allowed modelling the role of a weak horizon in the stratigraphic package of a tectonic wedge.

3.3.1 MODEL 1 RESULTS: EXTENSION ALONG A SEGMENTED BASEMENT FAULT

During the extensional deformation stage of each model a segmented half-graben basin was developed. Time-lapse photography has revealed that during the earliest stages of extension the master border fault segments at 90º and 15º to extension developed a continuous fault scarp, whereas at the fault segment trending at 45º to extension a monocline dipping into the half-graben was developed. With ongoing extension, the monocline became breached, and the upward-propagating fault segments were linked along

strike. Secondary faults, including antithetic and to a lesser extent synthetic faults, grew as initially sinuous and isolated fault segments trending parallel to the bisector of the normal to the extension direction and the corresponding velocity discontinuity segment. Initially isolated fault segments were developed on the fault segments at 90º and 15º to the extension direction, linking laterally with other isolated fault segments to produce less sinuous, longer strike faults. Overall, these faults grew migrating laterally from the 15º and 90º segments towards the 45º fault segment located in the central part of the sandbox model. The formation of additional antithetic faults always took place into the interior of the developing half-graben basin. As extension accumulated, the formerly developed antithetic fault systems progressively took less displacement, or became abandoned. At the 45º segment, all the sandbox models carried out registered the development of extensional relay ramps. With continued extension, these relay ramps were eventually breached to form longer strike extensional faults. This kinematic evolution is consistent with that derived from natural fault systems (Peacock and Sanderson, 1991; Childs et al. 1995) and has also been observed in many previous sandbox models (McClay et al. 2004). Oppositely, the master border fault displayed a continuous activity during the experiment undergoing extension, developing accommodation space immediately above the velocity discontinuity.

Serial cross sections have also shown significant differences along strike. A total of 4 narrowly-spaced antithetic faults were developed at the 90º and 15º segments, whereas only 3 widely-spaced antithetic faults were developed at the central 45º segment. A synthetic fault was also developed at the central 45º segment and is responsible for a rider block only developed at that position. The antithetic faults are planar and show similar cut-off angles at the 90º and 15º segments. On the 45º segment though, the antithetic faults steepen upwards displaying a concave upwards geometry suggesting certain degree of rotation during extension. The internal 3D architecture of the rift basin has been constrained by means of 3D voxels. The plan view geometry of the extensional basin is shown in depth-slices as a ribbon of syn-rift layers (i.e., red-, white- and black-coloured sand) that follow the shape of the basal rigid plate. The syn-rift distribution indicates along strike differences in subsidence and accommodation space, with the depocenters being relatively isolated and located at the 90º and the 15º segments. The central fault segment at 45º to extension recorded the smallest accommodation space.

As shown by time-lapse photography, the extensional displacement along the border faults was continuously concentrated in dilatant, discrete deformation zones. Within

these, sand grains underwent reorganization and disaggregation, undergoing rolling and translation by sliding along their contacts. This deformation mechanism is comparable to a particulate or granular flow (e.g., Fossen, 2010) and may have accounted for localised strain-softening. A similar deformation mechanism should be expected for the second order antithetic and synthetic faults.

3.3.2 RESULTS OF SHORTENING MODEL 2

The aim of this model was generating a model to simulate the deformation of the previously extended sandpack along a horizontal detachment ($\beta = 0^o$) and with a horizontal topography ($\alpha = 0$). The total amount of shortening was 6 cm (i.e., slightly more than the amount of extension). The resulting structure was a pop-up like symmetric anticline with no preferred sense of vergence. On plan view, the pop-up anticline and the trace of the emergent thrusts and back-thrusts broadly follow the shape of the underlying basal rigid plate, with no significant changes in the structure along strike. Time-lapse photography has shown that during the earliest stages of shortening, the push of the moving backstop wall generated sliding along the basal horizontal detachment, producing the compaction of the sandpack up to the location of the velocity discontinuity. Soon after, early surface-breaching folds were formed, mimicking the shape of the previously developed extensional fault system and hence, being indicative for the reactivation of the extensional fault system during the early stages of shortening. As shortening continued, deformation was taken up by slip along back-thrusts and thrusts.

3.3.3 RESULTS OF SHORTENING MODEL 3

This model consisted on the deformation of the previously extended sandpack with a thick sand wedge having a topographic slope $\alpha = 32^o$ along a hinterland dipping basal detachment ($\beta = 3^o$). This model aimed at simulating a near critical wedge (i.e., in the verge of failure) to test how the segmented half-graben is inverted as deformation is transferred to the toe of the wedge with the onset of shortening. The total amount of shortening was 15 cm (i.e., about three times the total value of extension). Time-lapse photography unravelled a sequence of deformation that included an initial phase of sand compaction

promoted by sliding along the hinterland-dipping basal detachment followed by the nucleation and propagation of thrusts. In more detail, early slipping along the basal detachment led to the gentle inversion of the previously developed extensional fault system as indicated by the formation surface-breaching fault-propagation folds. Inversion was followed by hanging-wall directed back-thrusting as well as by foreland-ward directed thrusting.

Although the overall kinematical evolution developed broadly in sequence towards the foreland, cross-cutting relationships shown by serial cross sections and time-lapse photography have revealed the occurrence of out-of-sequence thrusting. This out-of-sequence thrusting took place at the hinterland after the reactivation of the border extensional fault. The last deformation phase was represented by the nucleation and propagation of an emergent footwall shortcut thrust. Cross sections made at the 90º, 45º and 15º segments also showed significant along strike changes on the internal structure, as represented by footwall shortcuts at the 90º and 15º fault segments (at the borders of the sandbox), that pass laterally to the 45º segment (i.e., the central part) into a hanging-wall by-pass thrust. The by-pass thrust re-used the upper reaches of the border extensional fault in the central parts of the model, transporting and tilting the rift basin toward the foreland. The rift basin and its border fault were split in two in the central parts of the sandbox model (i.e., 45º segment), whereas in the 90º and 15º segments, the inverted basin occurs imbricated on a hanging-wall position along with the master extensional fault.

3.3.4 RESULTS OF SHORTENING MODEL 4

This model consisted on the deformation of the previously extended sandpack along a hinterland dipping basal detachment (β = 3º), with a hinterland thickening sand wedge covering the full stretch of the model. The sand wedge was built with a 6º thickening angle and a topographic slope α = 3º with the objective of simulating a large and thick tectonic wedge overlying the segmented half-graben basin. After 15 cm of shortening, the deformed tectonic wedged displayed three thrust sheets with associated surface-breaching fault-propagation folds. In a similar fashion to the models described above, the sequence of deformation commenced with a long-lasting stage of sand compaction associated with slip along the hinterland-dipping basal detachment. The deformation front of this early compaction phase migrated from the hinterland towards the foreland and

arrived ahead of the rift basin. The observed compaction affected a significantly larger section of the model in comparison to the rest of the models. Only gentle inversion of the border antithetic fault took place, and subsequent shortening was accommodated by the development of a system of forward-directed thrusts.

The cross-sections made at the 90º, 45º and 15º segments displayed a homogeneous along-strike structure dominated by a large thrust sheet. Additional thrusting propagated from beneath the inherited rift basin splitting the master extensional fault in two segments and transporting the rift basin. In this model, only the border antithetic fault underwent mild reactivation, and no unequivocal evidences for reactivation and inversion of the remaining extensional faults were observed.

3.3.5 RESULTS OF SHORTENING MODEL 5

This model consisted on the deformation previously extended sandpack along a hinterland dipping basal detachment ($\beta = 3º$) with a sand wedge covering the full stretch of model but with no surface slope ($\alpha = 0º$). The objective of this set up was to test the effect of a flat-lying tectonic wedge detached along a hinterland-dipping system in the inversion of a sub-thrust basin. Total shortening was 15 cm. As shown by time-lapse photography, topography scans and serial section, the sandbox model was deformed by a dominantly breaking-forwards sequence of thrusting forming several surface-breaching thrust faults and related splays. Prior to the nucleation of the first thrust, videos from time-lapse photography highlighted a significant amount of sand compaction by slip along the basal detachment, but with no associated surface-breaching fault reactivation. The first and second thrusts to form were responsible for the main uplift of the fold-and-thrust wedge. Conversely, the last thrust system to develop imbricated the rift basin, and was responsible for widening the tectonic wedge without causing significant uplift.

Post-deformation longitudinal sections revealed the subtle reactivation of the extensional faults (i.e., the synthetic and antithetic faults) and back-thrusting at the hinterland. Displacement along thrusts at the rear formed emergent fault-propagation folds. The last thrust faults to form nucleated also from the rear of the sandpack but propagated through the rift basin hanging-wall and footwall, and became emergent thrust fronts. As a result, the extensional basin was split into several segments and imbricated by a

footwall shortcut thrust sheet. Depth-slices revealed the shape of uplifted rift basin, the plan view geometry of the frontal thrusts and the imbricated footwall fault block. In a similar fashion to the 3D voxel of the purely extensional model, the imbricated rift basin displays its characteristic shape arranged in three 90º, 45º and 15º segments. The footwall shortcut thrust displays kinked plan view geometry, with one larger linear segment parallel to the 15º segment of the border extensional fault, and a shorter more sinuous segment striking oblique to the 45º and 90º segments of the master extensional fault, respectively. Virtual inlines taken from the foreland towards the hinterland also showed a thin sliver of syn-rift sediments in a footwall position. Thrusts can be easily correlated along strike of the sandbox model and display a characteristic concave-upwards geometry. The rift basin and the master border fault can be correlated on a hanging-wall and a footwall position along strike. The secondary extensional faults also occur both on the hanging-wall and the footwall of the thrust system.

3.3.6 RESULTS OF SHORTENING MODEL 6

In the light of the positive results from Model 5, this model consisted on the same wedge geometry (i.e., $\beta = 3º$ and $\alpha = 0º$) but included a 0.4 cm thick layer of viscous polymer pinching out in the foreland and located on a post-rift equivalent stratigraphic position. In contrast with the other models, the kinematics of thrusting and folding for Model 6 were characterised by the early decoupling of deformation between the sub-polymer layers and their cover. Contrary to Model 5, the kinematics of thrusting and folding were dominated by the presence of this weak horizon. They were characterised by the early decoupling of deformation between the sub-polymer layers and their cover. As shortening started, a first thrust was nucleated at the rear within the pre-rift layers with displacement being quickly transferred forwards and upwards in a ramp-flat transition into the cover. No early phase of sand compaction related to slipping along the basal hinterland-dipping detachment took place. In the early stages of shortening a broad cover anticline was developed above the rearmost thrust, whereas displacement along the weak detachment formed a thrust front at the foreland polymer's pinch out. Further shortening was accommodated by a breaking-forward system of thrusts affecting the sub-polymer layers, whereas deformation in the cover was represented by long-lasting deformation at the front, followed by out-of-sequence thrusting and related folding.

Gentle compaction of the sub-polymer layers took place only after a significant amount of shortening was accommodated by thrusting at the rear and shortening of the overburden along the weak polymer detachment. Topography scans have also revealed that uplift was mostly concentrated at the rear by the stacking of sub-polymer thrust sheets that folded the overlying cover. Such uplift was responsible for the development of an incipient crestal collapse graben above the frontal culmination of the sub-polymer thrust stack. Shortening accommodated by the shallow detachment widened the tectonic wedge but without generating any significant uplift.

Serial cross-sections have shown that in fact, mild inversion of the extensional fault system took place. Fault reactivation was preferentially located at the antithetic faults, although evidences for reactivation have also been found at the border and secondary synthetic extensional faults. The observed cross-cutting relationships indicate that inversion of these faults took place before the imbrication of the rift basin by the sub-polymer thrusts. At the light of these observations, compaction of the sub-polymer layers and mild inversion of the extensional faults should have taken place at least prior to the break-forward propagation of these later thrusts by slip along the basal detachment. These late thrusts formed a hanging-wall by-pass thrust, and footwall shortcut thrust.

Virtual depth-slices and inline-sections from the 3D voxel illustrated further the geometry of the sub-polymer thrust system and the inversion-related structures. The most important observations derived from the voxel are that the hanging-wall by-pass thrust was only developed at the section corresponding to the position of the 90º segment, and broadly followed the strike of the rift basin at the 45º and 15º segments in the upper parts of the model. The latest thrust to form developed as a footwall shortcut thrust parallel to the border extensional fault, particularly at the lower parts of the model. Polymer welds have also been revealed lying directly above the rift basin, on top of the anticline associated with the hanging-wall by-pass thrust, and at the frontal structural culmination of the hinterland thrust stack.

CHAPTER 4. SUMMARY OF DISCUSSIONS

4.1. INTRODUCTION

In this chapter, fault reactivation and basin inversion in foredeep and sub-thrust settings of fold-and-thrust belt settings are discussed. The chapter integrates the outcomes of the study in the Alpine-Carpathian Junction with those obtained from the sandbox analogue models carried out during this thesis. In addition, an integrative synthesis and a geodynamic contextualization for the basement fault reactivation events in the Alpine-Carpathian Junction and collisional foredeeps in general is proposed. The chapter discusses the fundamental controls on a local and regionally evolving plate-tectonic framework based on the concept of inheritance. The reactivation episodes described for the Alpine-Carpathian collisional foredeep belt are also compared with those reported for other orogenic systems.

4.2 FAULT REACTIVATION AND BASIN INVERSION IN TECTONIC WEDGES

Several episodes of basement fault reactivation have been described for the Alpine-Carpathian Junction. As shown throughout this memoir, the region has been subjected to a long-lived history of repeated basement reactivation and reworking which, at least, included: late Variscan transtension, Jurassic rifting, Lower Cretaceous to Paleocene intraplate shortening, and Cenozoic extension and shortening (e.g., Wessely, 1987; Ziegler, 1987; Coubal, 1990; Wagner, 1998; Picha et al. 2006; Granado et al. 2016). The last Cenozoic events were followed by the collapse of the orogenic edifice and the widespread rifting of the Pannonian region (e.g., Cloetingh et al. 2006 and references therein). The involvement of the Lower Austria basement faults in this middle to late Miocene event is still controversial (e.g., Royden, 1985; Wessely, 1987; Lankreijer et al. 1995; Decker et al. 2005; Hinsch et al. 2005a, b; Granado et al. 2016).

As introduced in **Chapter 2**, inheritance is one of the fundamental factors controlling deformation of the lithosphere (e.g., Holdsworth et al. 2001; Ziegler et al. 2001; Butler et al. 2006). In this study, the controls imposed by such inheritance can be related to the nature of the European lithosphere involved, as well as that of the existing fault systems. The fault systems documented in this thesis are consistently steeply-dipping, dominantly NE-SW-striking and root in the brittle-plastic transition of European crystalline basement. According the kinematic history of the area and the seismic interpretation

presented in this work, these basement faults would have been oriented almost perpendicular to the prevailing NW-directed early Miocene direction of shortening (e.g., Decker and Peresson, 1996; Beidinger and Decker, 2014). Only the Höflein fault seems to have been variably oriented to the early Miocene shortening (e.g., Granado et al. 2016, 2017).

The reactivation of inherited fault systems is inherent to the concept of basin inversion. In shallow crustal levels, fault reactivation is controlled by pressure-dependent frictional processes. Deep-seated regions are characterised by temperature-activated deformation mechanisms (Rutter, 1986). In shallow crustal levels, such as the upper reaches of the Lower Austria basement faults, the main factors controlling the frictional reactivation of faults should be the cohesion of the fault rocks, their coefficient of friction, the orientation of the fault zones with respect to the stress trajectory (i.e., both in terms of dip and direction of dip) as well as pore-fluid pressure variations (Jaeger and Cook, 1979; Zoback, 2010). Generally speaking, steeply-dipping faults tend to be frictionally locked-up for dip-slip compressional reactivation (e.g., Sibson, 1985; Etheridge, 1986). Lowering either the dip of the fault, and/or its orientation with respect to the compressive stress trajectory may result in a mechanically easier frictional compressive reactivation. Oblique shortening is thought to favour the frictional reactivation of faults as the intermediate compressive stress ($\sigma 2$) is not contained by the fault plane, and thus contributes to frictional reactivation (e.g., Jaeger and Cook, 1979; Etheridge, 1986; Letouzey et al. 1990). Low (or tensional) minimum principal stresses ($\sigma 3$) would also strongly influence in a positive manner the frictional compressional reactivation of misoriented faults. In addition, fluid overpressures are well known for lowering the effective differential stress necessary for frictional reactivation (e.g., Sibson, 1985). In Lower Austria, fluid overpressures may have developed by the generation of hydrocarbons from the syn-rift coal measures and the post-rift marl units.

As stated in **Chapter 2**, the lower the cohesive strength and the angle of friction of fault rocks, the larger the range of possible fault orientations for shear failure to occur (e.g., Jaeger and Cook, 1979). In general, as faults attain slip, the coefficient of friction and the cohesion of fault rocks tend to become lower, requiring lower effective differential stresses for any subsequent frictional reactivation. This process can be referred to as dynamic fault-weakening (e.g., see Rutter et al. 2001 and Wibberley et al. 2008 for a review) which can involve chemical reactions between fluids circulating along the fault and the host fault-

rocks. In the continental crust, these chemical reactions can induce the formation of low-friction phyllosilicate-bearing assemblages derived from the syn-kinematic breakdown of feldspars (e.g., Gueydan et al. 2003). Fault-weakening can allow faults sustaining significant slip under theoretically anomalous orientations in respect to the prevailing stress trajectories (i.e., steeply-dipping faults in compressional settings or, low-angle normal faults in extensional conditions). Such weakening mechanism permits explaining the occurrence of earthquakes under such circumstances (e.g., Colletini et al. 2009). The repeated reactivation of the Lower Austria Mesozoic Basin faults may have also been aided by these fault-weakening processes affecting the gneissic/granitic, feldspar-bearing units of the European basement. It is worth mentioning though, that precipitation of hydrothermal fluids or quenching of melts after seismic slip along the faults' displacement zone may alternatively induce the frictional lock-up of faults due to a significant increase on the fault zone coefficient of friction and/or cohesion (e.g., Etheridge, 1986; Cox et al. 2001).

The local obliquity between the inherited fault system and the early Miocene compressive stress trajectory, the potential overpressures derived from hydrocarbon generation in the Middle Jurassic syn-rift units, and the above mentioned fault zone weakening processes may have collectively favoured the selective, mild reactivation of the Höflein fault and the southwestern termination of the Haselbach fault (i.e., Stockerau anticline). Other fault segments such as the central parts of the Haselbach fault in the sub-thrust may have remained frictionally locked, as compression is strictly evidenced by the formation of footwall shortcuts and hanging-wall back-thrusts. In the absence of any proven source rock in its hanging-wall, the positive reactivation of Mailberg fault and the formation of the Mailberg anticline may have been favoured by fault-weakening processes. So, although the orientation of the basement faults has been inherited from late Variscan times, their fault zone rheology should be regarded as dynamically evolving through time.

In this line of arguments, the sandbox analogue modelling carried out during this thesis has also indicated that the presence of inherited fault systems significantly aided in the subsequent fault reactivation and related positive basin inversion (Granado et al. 2017). In these sandbox models, an equivalent fault-weakening mechanism may have taken place at the dilatant fault zones generated by extension above a pre-existing velocity discontinuity. Faulting within granular materials is characterised by reorganization and disaggregation occurring as rolling and translation by sliding along the grains' contacts takes place. This deformation mechanism can be comparable to a particulate or a granular flow

(e.g., Fossen, 2010) and may account for localised, discrete strain-softening that accounts for a frictional strength loss (e.g., Lohrmann et al. 2003). Albeit all the limitations imposed by analogue modelling techniques the experimental set up used provided a good comparison with natural collisional foredeep settings. It simulated the steepened, and thus anomalously oriented for compressional reactivation, fault system ahead of a propagating fold-and-thrust belt (**Fig. 2.23c**). As discussed above, the steepening of these faults should negatively impact the frictional compressional reactivation, particularly in dip-slip reactivation (e.g., Jaeger and Cook, 1979; Sibson, 1985; Etheridge, 1986; Gillcrist et al. 1987). Time-lapse photography has shown that reactivation of the extensional fault system was mild but affected the sandbox models rather equally along strike, independently of the steep fault dips. In fact, no substantial differences on the easiness of reactivation in regards of the obliquity between the pre-existing faults (i.e., the 15º, 45º and 90º segments) and the direction of shortening were found. Our modelling results are hence in disagreement with those reported by Brun and Nalpas (1996) or Di Domenica et al. (2014) where a fundamental role of obliquity in the easiness for reactivation is reported. The strength anisotropy provided by the strain-softened fault zones in the sandbox models has revealed significantly more important than the fault plane orientation in the reactivation process. In a similar fashion, the long-lived history of reactivation in the Alpine-Carpathian collisional foredeep may be partially explained by fault-weakening processes leading to low friction and/or low cohesion (i.e., strain-softened) fault zones.

On a larger scale of observation, the basement of the Alpine-Carpathian foredeep corresponds to the crystalline crust of the European plate. According to well data and field studies in the massif (Kröll and Wessely, 2001; Wessely, 2006) the basement for most of the Lower Austria Mesozoic Basin belongs to the Moravo–Silesian domain, whereas the Bohemian Spur (and the basement drilled at the Höflein high) belongs to the Moldanubikum domain (**Fig. 2.13**). These domains were consolidated during the Variscan orogeny and their contact broadly corresponds with the trace of Variscan deformation front (Kröll and Wessely, 2001; Wessely, 2006; Kroner et al. 2008). In more detail, the Moldanubikum basement constitutes the mechanically strong core of the Bohemian massif (**Fig. 4.1a**) where a thick and rigid lower crust is overlaid by a thin upper crust (**Fig. 4.1b**). The core of the Bohemian massif displays extreme values of lithospheric strength characterised by a large lithospheric root with a mechanically coupled continental crust. Effective elastic thickness (i.e., EET) values for the Bohemian massif core are up to 40 km. This inherited, high rigidity domain may have allowed for the transmission of stresses into

the foreland north of the Alpine orogen, favouring the compressional reactivation of misoriented weakened faults. According to these mechanical models, the strength of the European plate diminishes away from the Bohemian core towards the SE into the Alpine-Carpathian foreland fold-and-thrust belt (**Fig. 4.1a**). There, the calculated EET values are significantly lower, and constitute a sharp gradient of rigidity loss. Further to the SE, Lankreijer et al. (1999) also indicate that the EET values for the Vienna Basin basement (≈ 18-22 km) are too elevated, and most likely biased by the low heat flow values used in their calculations (i.e., values provided by Royden and Dövényi, 1988). Such low heat flow values in the Vienna Basin more likely result from the thermal insulation of its Miocene infill. Lankreijer et al. (1999) propose that the EET values may be as low as 10 km for the Vienna Basin and about 5 km for the central part of the Pannonian Basin (**Fig. 4.1a**). Beneath the Lower Austria Mesozoic Basin, rheology predictions also suggest that decoupling zones should locate at upper and lower crustal detachment levels, in agreement with the depth to detachment estimated for the Lower Austria basement fault array (i.e., 10-12 km; **Fig. 3.1**). In the Alpine-Carpathian Junction, the foreland basin is as narrow as 9 km, suggesting a large bending facilitated by the high rigidity loss gradient.

Extension in the foreland plates ahead of active fold-and-thrust belts (i.e. in the foredeep) has been reported in several orogenic systems such as the Eastern Pyrenees (Pujadas et al. 1989), the Appalachians of Eastern USA (Bradley and Kidd, 1991) or the Central Apennines (Carminati et al. 2015). In these foredeeps, kilometre-scale extensional faults have been recognised dipping towards the hinterland of the developing orogenic belts. These foreland faults systematically display steep angles and throws in the order of several hundreds of meters (**Fig. 4.2**). Bradley and Kidd (1991) proposed that such foredeep extensional faulting is related to the flexural bending of the foreland plate as it is tectonically overridden and subducted. They coined the term *flexural extension* for that matter. Conversely, the Eastern Pyrenees has provided more accurate time constraints for flexural extension as indicated by the Eocene infill of these flexural extensional basins developed coetaneous with thrust activity. The Eastern Pyrenees example of foreland flexural extension was documented by Pujadas et al. (1989) and Martínez et al. (1989), but these authors did not refer to the term flexural extension in a strict sense. In the Alpine-Carpathian Junction the observed large throws of the steeply-dipping basement faults can also be ascribed to a similar process of flexural extension provided the strong age constraints (see Beidinger and Decker, 2014 and references therein). In the Appalachian and Pyrenean examples, it seems that the flexural bending generated new foreland

extensional fault systems, whereas in the Alpine-Carpathian foredeep, the pre-existing basement fault array was reactivated instead.

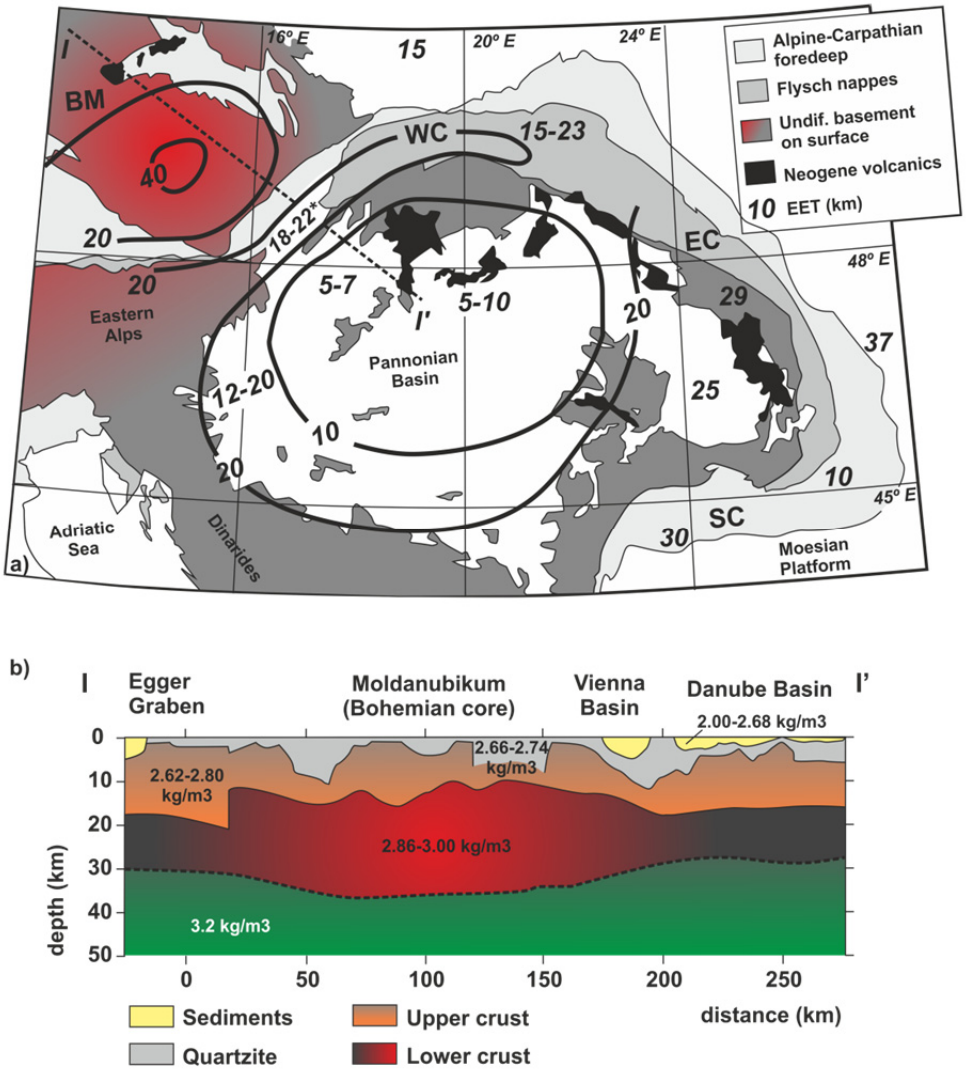

FIGURE 4.1. A) Effective elastic thickness of the lithosphere in and around the Pannonian Basin. Modified from Cloetingh et al. (2006). B) NW-SE crustal stratification along the Bohemian-Alpine-Carpathian foreland fold-and-thrust belt and the Pannonian basins. Based on gravity models and seismic profiles. All these values are derived from the rheological calculations published by Lankreijer et al. (1999).

* The elevated EET values for the Vienna Basin are due to calculations uncorrected for the thick sedimentary infill, and therefore, lower EET values are expected.

Large extensional throws in excess of 1 km for the base of the post-rift remain preserved in the hanging-wall of the Alpine-Carpathian basement faults. Such large extensional offsets may have been favoured by the strong gradient of EET observed from the Bohemian core towards the SE, which would have translated in an important gradient of flexure. These large throws in the foredeep region may have allowed for an axial sediment routing system parallel to the propagating fold-and-thrust belt as documented by Sinclair (1997) in the Western Alps, or by Bradley and Kidd (1991) in the Appalachians. Soft and hard-linked transfer faults may also have accounted for additional accommodation space creation, transversal sediment routes and erosion in tilted fault blocks (**Fig. 4.2**), as documented in rift basin settings (Morley et al. 1990).

In the Alpine-Carpathian Junction, the Egerian to Karpatian (i.e., late Oligocene to late Miocene) flexural reactivation of the basement fault array was followed by its compressional reactivation. This late shortening event was mild and not capable of removing the large extensional throws accumulated during the preceding flexural extension. However, this event should be classified as a positive basin inversion phase. The structural styles defined in this study for the late early Miocene to earliest Miocene inversion are classical inversion-related styles: imbricate fans of footwall shortcut thrusts (e.g., Höflein high imbricates, Haselbach footwall shortcut), hanging-wall back-thrusts detaching in the basement-cover interface (e.g., on the Haselbach fault hanging-wall), and hanging-wall anticlines (e.g., such as those on the Höflein and Mailberg half-grabens). In addition, a potential hanging-wall by-pass thrust may have been the responsible for the elevation of the rearmost parts of the Höflein hanging-wall basement as suggested by the depth-converted 3D seismic data and the high residual gravity readings (**Fig. 3.2b**). In the Appalachian foreland described by Bradley and Kidd (1991) no compressional reactivation of the flexural basement fault array has been recorded. Conversely, the Eastern Pyrenees flexural basins described by Pujadas et al. (1989) and Martínez et al. (1989) display evidences of full inversion and incorporation of the inverted flexural basins into the Pyrenean fold-and-thrust belt. The Montmajor antiformal stack (**Fig. 4.3**) is probably one of the best examples of flexural extension and subsequent inversion in a foredeep setting. The structure is constituted by a thrust stack of Eocene limestones that was uplifted and imbricated by the inversion of a former Eocene flexural half-graben basin. Inversion happens to have taken place in a buried sub-thrust setting as well, beneath the salt-detached Figueres-Montgrí unit (e.g., Pujadas et al. 1989; Tassone et al. 1994). The Montmajor

antiformal stack is also constituted by a series of footwall shortcuts that involved a lower Paleozoic metasedimentary succession with Variscan gneisses and granitoids.

In terms of the amount of inversion, the Alpine-Carpathian fold-and-thrust belt lies in between these two end-members provided by the Appalachian foreland (i.e., only flexural extension) and the Eastern Pyrenees (i.e., flexural extension followed by overthrusting and subsequent sub-thrust inversion). Following the nomenclatures of Bally (1984) and MacGregor (1995), the Lower Austria Mesozoic Basin should be classified as a partially and locally inverted rift basin.

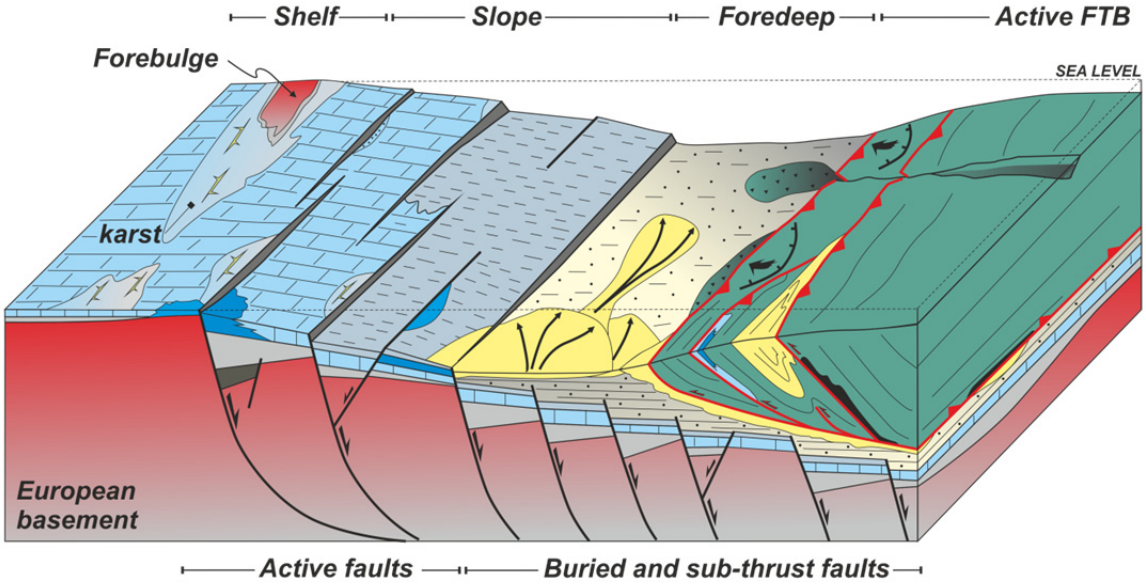

FIGURE 4.2. Conceptual geodynamic setting of flexural extension. The flexural reactivation of the basement fault array is synchronous with the forward propagation of thrusting. Additional sediment inputs may have accessed the foredeep from the Bohemian massif forebulge along a routing system provided by relay ramps and transfer faults. These sediment routes may also account for the localised erosion of carbonate banks and build-ups of the para-autochthonous Mesozoic.

In the Alpine-Carpathian fold-and-thrust belt, thin-skinned thrusting along the broadly distributed Mikulov Formation source rock was probably aided by the overpressure conditions generated by the generation of hydrocarbons (e.g., Zimmer and Wessely, 1996). As the thin-skinned system approached the Bohemian Spur salient this weak detachment was no longer present (i.e., eroded or non-deposited), and out-of-sequence thrusting took place in the thrust front, the Rhenodanubian Flysch and the Northern Calcareous Alps (e.g., Hölzel et al. 2010; Beidinger and Decker, 2014, 2016). According to the cross-cutting relationships, deformation was then transferred into a deeper detachment in the crystalline basement (Granado et al. 2016). In a similar fashion,

the presence of a broadly distributed viscous layer above the half-graben basin in the sandbox analogue models favoured the early transfer of slip and deformation into the cover (i.e., the supra polymer) sequence and the formation of a thrust front. Further shortening was accomplished by involving the sub-polymer sequence and the reactivation of the extensional fault array by slip along the basal frictional detachment (Granado et al. 2017). Conversely, natural systems with thick pre-rift salt layers are characterised by early inversion and incorporation of the extensional basins into the fold-and-thrust belt (Pujadas et al. 1989; Muñoz, 2002; Mencos et al. 2015).

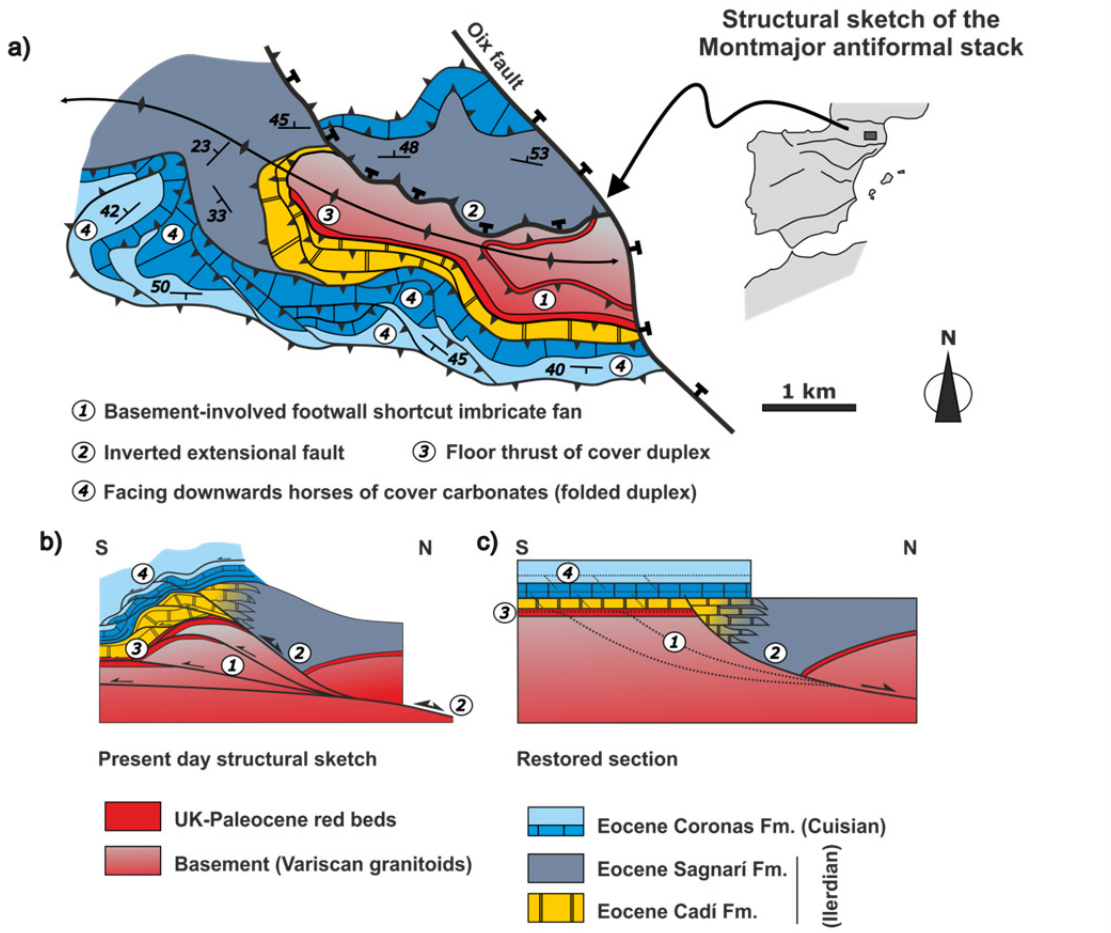

FIGURE 4.3. The Montmajor antiformal stack of the Eastern Pyrenees. This structure is constituted by the full inversion and basement-involved imbrication of a former Eocene flexural extensional basin developed ahead of the south-propagating Pyrenean thrust system. Positive basin inversion is a late feature as the reactivation of the extensional fault and the basement-involved footwall shortcut imbricate fan fold the overlying duplex affecting the Coronas Limestones. The Montmajor antiformal stack can be considered an end-member example of basement-involved deformation and positive inversion in a foredeep. Modified from Martínez et al. (1989). FW: footwall; UK: Upper Cretaceous.

Contrasting styles of thin- and thick-skinned deformation in fold-and-thrust belts are summarised on **figure 2.22** and their potential evolution is illustrated on **figure 4.4**. The deformation trend depicted by **figure 4.4** involves thin-skinned deformation along favourable weak detachments, thick-skinned deformation along crustal ramps favoured by the presence of inherited weak faults in an otherwise strong crust, development of flexural basins ahead of the shortening system, and their subsequent incorporation into the shortening sequence. This evolutionary trend can be generally applicable to foredeeps and orogenic systems and proposes the coexistence of thin-skinned and thick-skinned tectonics in single fold-and-thrust belts, based on the presence and distribution of inherited rheology in shallow and deeper crustal levels. According to this model, several deformation domains can be distinguished in the external parts of orogens: an inner belt, where basement is involved and uplifted, a shallow fold-and-thrust belt with a thin-skinned deformation front, a deeper reactivation front, a foreland deformation front characterised by pre-folding structural assemblages, flexural basins and a forebulge. In the Alpine-Carpathian Junction, the thin-skinned deformation front locates at the Imbricated Molasse Zone, whereas the shallow fold-and-thrust belt is represented by the Northern Calcareous Alps, the Rhenodanubian Flysch and the Waschberg-Ždánice Zone. The reactivation front may be localised at the Mailberg anticline, whereas the deformation front and the external most flexural basin should be located ahead, in the Bohemian massif.

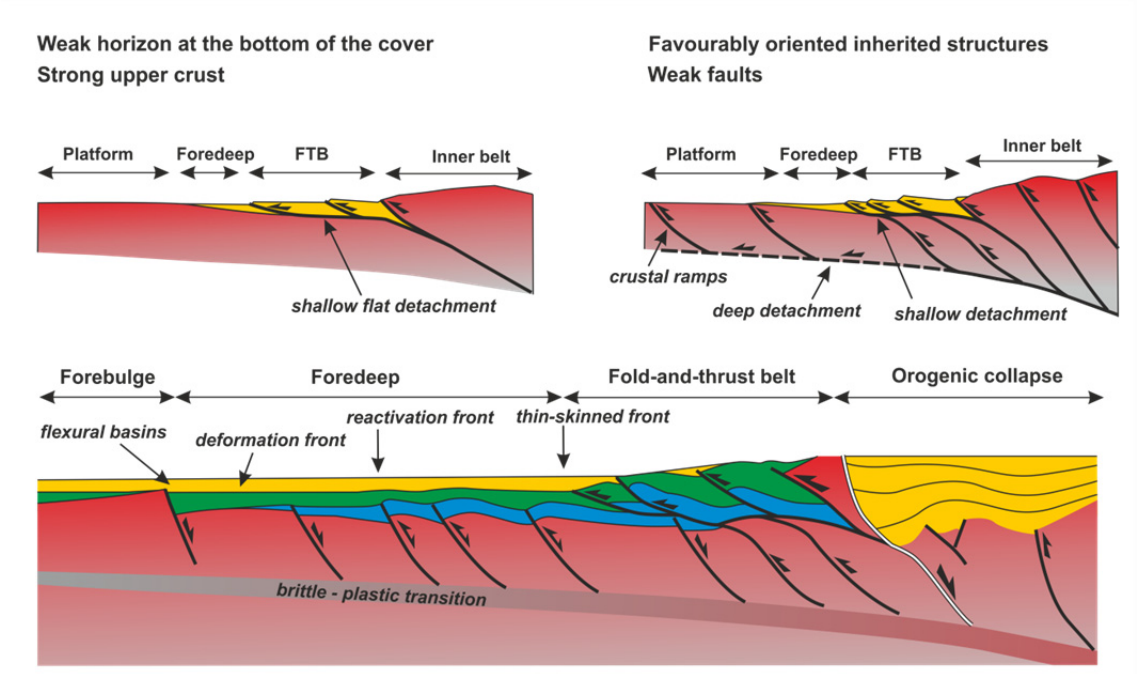

FIGURE 4.4. End-member structural styles and deformation evolution in foreland fold-and-thrust belts and sub-thrust settings. Modified from Lacombe et al. (2016). FTB: fold-and-thrust belt.

The sandbox analogue models carried out in this thesis underwent slip along the basal detachment, producing sand compaction before the onset of thrusting and in between thrust propagation pulses (Granado et al. 2017). For granular analogue materials, Koyi et al. (2004) referred to layer-parallel compaction (i.e., LPC) as the main modality of layer-parallel shortening (i.e., LPS). LPS is considered a deformation mechanism widely reported in foreland settings (e.g., Woodward et al. 1986; Mitra, 1994; Holl and Anastasio, 1995) and evidences the advancing deformation front in foreland and fold-and-thrust belts (Tavani et al. 2015). In the sandbox analogue models carried out it has been observed that the reactivation of the extensional fault system was associated with this layer-parallel compaction, before the onset of thrusting and in between thrust propagation pulses.

In addition to the presence or absence of weak detachments and strain-softened faults zones, the models carried out underwent different amounts of deformation as a function of the pre-shortening configuration of the tectonic wedge (**Figs. 3.6** and **4.5**). The influence of this parameter on the geometries and kinematics of fold-and-thrust belts has been studied by several authors already (e.g., Soto et al. 2006; Storti et al. 2007; Graveleau et al. 2012), but without including the inversion of sub-thrust basins. In the experimental results obtained for this thesis, distinctly tapered wedges (i.e., α and β angles) affected the reactivation and incorporation of the sub-thrust basins by imposing a vertical-load gradient (Granado et al. 2017). In the models where the half-graben basin was close to the surface (i.e., Models 2 and 3), inversion of the extensional fault system took place early in the deformation sequence. In these two models, the absence of any substantial vertical load (Model 2) or a large vertical load gradient (Model 3) favoured the reactivation of the extensional fault system during layer-parallel compaction. If the half-graben basin was covered by a thick wedge (i.e., Model 4), only the border antithetic fault underwent very limited reactivation by back-thrusting. Although the layer-parallel shortening propagated ahead of the half-graben basin, it seems that the large vertical load imposed by the thick wedge (i.e., large σ3) avoided the reactivation the extensional fault array. In the model where the half-graben basin was covered by a thinner wedge (i.e., Model 5), reactivation of the extensional faults took place late in the deformation sequence, following the breaking-forward propagation of thrusting. In the model where the half-graben basin was covered by a similar wedge and a shallow viscous detachment (i.e., Model 6), fault reactivation and basin inversion took place only after the propagation of thrusting over the weak detachment.

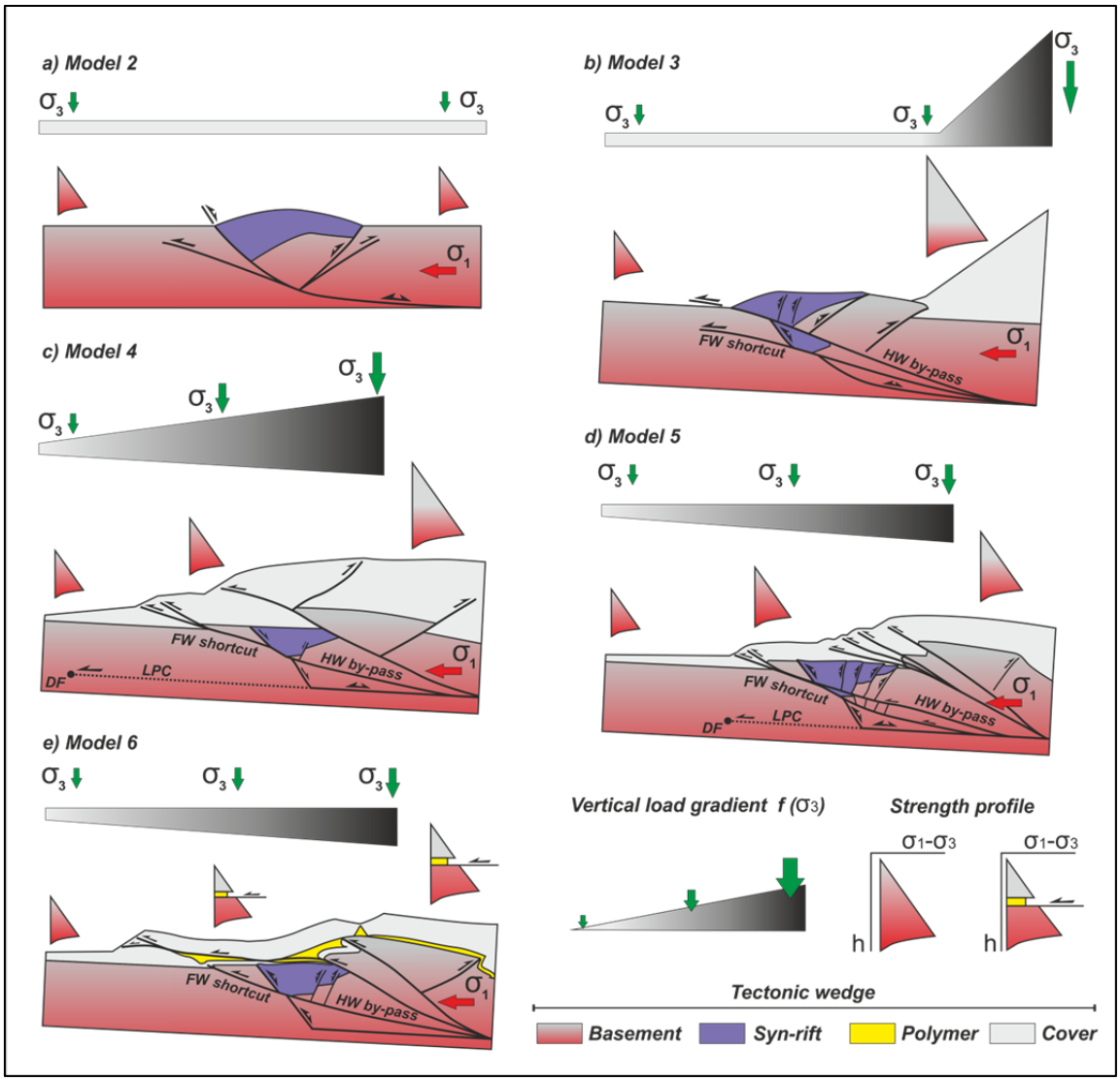

FIGURE 4.5. Summary of the shortening modelling results obtained. Note the contrasting structural styles developed as a function the pre-shortening tectonic wedge taper (i.e., α+β angles), the vertical load gradient (which is qualitatively depicted as the σ3 variation along the sandpack profile) and the tectonic wedge strength profile (which relates with the sandpack thickness and the presence or absence of the viscous polymer. A) Model 2, pop-up anticline. B) Model 3, thick nearly-critical wedge. C) Model 4, thick and large tectonic wedge. D) Model 5, thin tectonic wedge with no polymer detachment. E) Model 6, thin tectonic wedge with a polymer detachment in a post-rift equivalent position. See further explanations in the text. DF: deformation front; HW: hanging-wall; FW: footwall; LCP: layer-parallel compaction.

Recent works by Hölzel et al. (2010) and Beidinger and Decker (2014) suggest that the Alpine-Carpathian fold-and-thrust belt, which included the Rhenodanubian Flysch and the Northern Calcareous Alps, were covered by a rather continuous early Miocene wedge-top basin (see **Fig. 2.11b**). However, its original thickness distribution is still poorly understood given the large burial and offset caused by the middle to late Miocene extensional and transtensional faulting. According to the results obtained in the sandbox models (**Fig. 4.5**), the distribution of the vertical load (i.e., σ3) imposed by the tectonic wedge in the reactivation of deep seated faults is a fundamental parameter. In this sense, thermochronology can aid in the reconstruction of burial and uplift histories of fold-and-thrust belts (e.g., Beamud et al. 2011), and shed some light on the potential palaeo-vertical load distribution. Using this geochronological tools, Trautwein (2000) and Trautwein et al. (2001) pointed out that the southern units of Rhenodanubian Flysch (i.e., the Kahlenberg and Laab nappes; **Fig. 2.12**) underwent tectonic burial in between of 6 and and less than 11 km, as indicated by the total resetting of the apatite fission track ages and the undisturbed zircon ages (assuming a 20ºC/km thermal gradient). This burial was caused by the thrusting of the Northern Calcareous Alps and their wedge-top sedimentary cover onto the southern Rhenodanubian Flysch nappes. Subsequently, the Kahlenberg and Laab thrust sheets were exhumed by out-of-sequence thrusting between late Oligocene and early Miocene (i.e., between 26.7 to 18.2 Ma, or Egerian-Eggenburgian in Central Para-Tethys terms) as indicated by detrital apatite cooling ages. Although these ages should be regarded with care given the local bymodal distribution reported by Trautwein et al. (2001), they are also in agreement with the low values of vitrinite reflectance shown by the Gresten Group coals from the Höflein high wells (e.g., Gmach, 1999; Sachsenhofer et al. 2006). The tectonic burial and subsequent fast exhumation at ~20ºC/Ma by out-of-sequence thrusting must have taken place south of the Höflein half-graben. In fact, thrust stacking of the southern Rhenodanubian Flysch and the NCA nappes should have caused an important vertical load gradient on the sub-thrust basins located immediately ahead, favouring the basin inversion during subsequent Miocene shortening. The thrust kinematics inferred from the works of Gmach (1999), Trautwein et al. (2001), and Sachsenhofer et al. (2006) and the results from sandbox analogue modelling presented here are in agreement with the age and kinematics of sub-thrust and foreland basin inversion proposed for the Alpine-Carpathian Junction in this thesis (e.g., Granado et al. 2016, 2017; **Fig. 4.6**). In this sense, the overall kinematic evolution in the Alpine-Carpathian Junction is similar to that of the Western Carpathian wedge. Coupled sequential restoration and thermocronology by Castelluccio et al. (2015)

indicate thrust-related uplift and associated cooling of the Magura Flysch since *ca.* 22 Ma, with younger cooling ages between 13-4 Ma associated with uplift related to extensional faults. Compressional basement-involved basin inversion occurred slightly after in the Western Carpathians basement (by middle to late Miocene times) which is in agreement with the accepted model of eastwards deformation migration along the Carpathian arc.

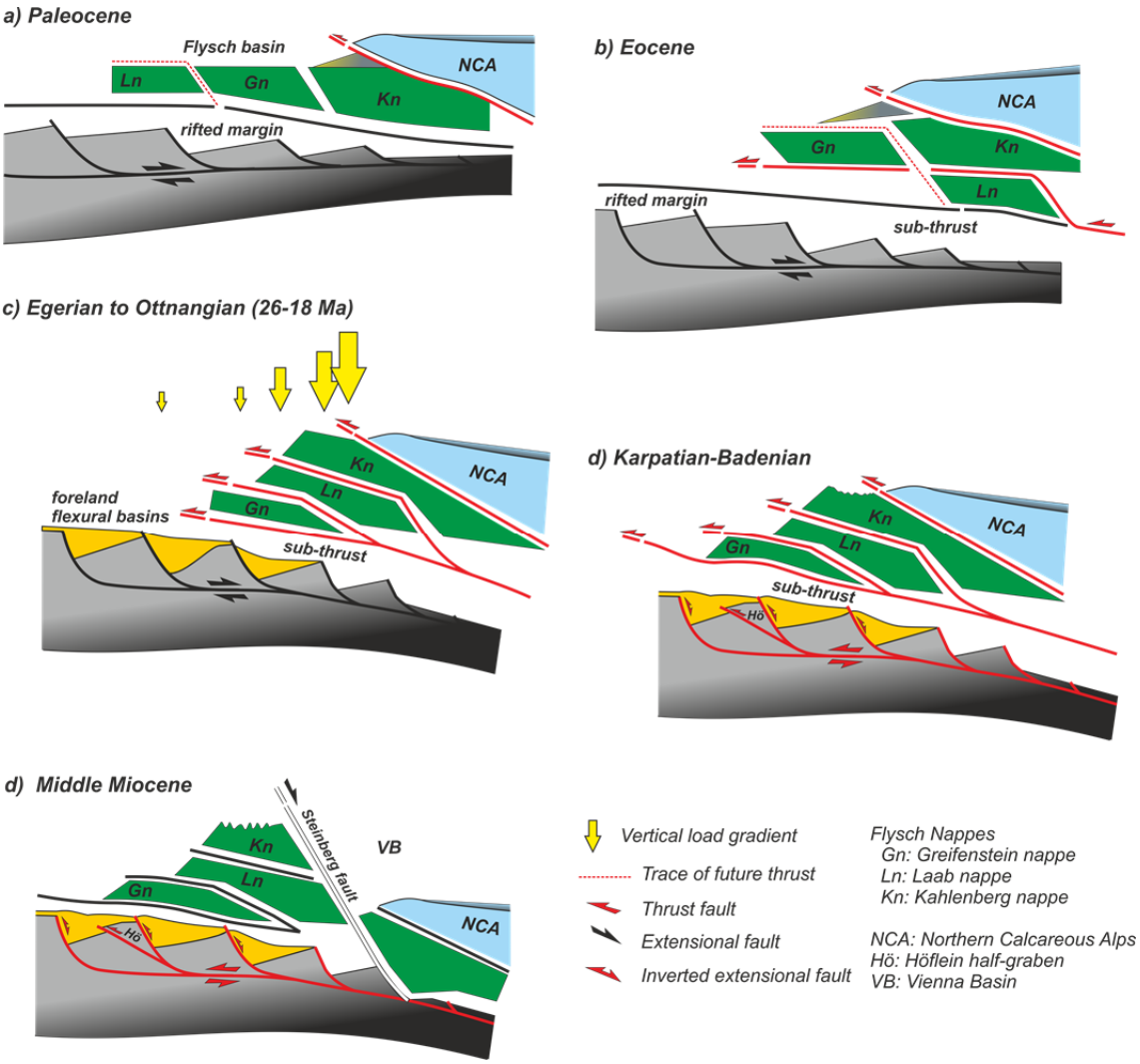

FIGURE 4.6. Proposed evolution of the Alpine-Carpathian fold-and-thrust belt based on the results of this thesis and the thrust stacking patterns derived from thermochronological results of Gmach (1999) and Trauwein et al. (2001). A) Paleocene thrusting of the NCA over the distalmost Rhenodanubian Flysch. B) Eocene overthrusting of the Northern Calcareous Alps over the Rhenodanubian Flysch caused tectonic burial in the range of 6 to 11 km (complete resetting of apatite fission tracks ages and undisturbed zircon ages). C) Egerian to Ottnangian exhumation by out-of-sequence thrusting shown by apatite cooling ages (i.e., between 26 and 18 Ma). D) This thrust stacking generated a strong vertical load gradient immediately to the south of the Höflein high, allowing for the incorporation of the sub-thrsut and foreland rift basins in the deformation sequence. E) The thrust stack was then sliced by the extensional fault system related to the opening of the Pannonian basins system.

The onset of compressional reactivation in the Alpine-Carpathian foredeep has been dated as Karpatian to Badenian times in this study (i.e., latest early Miocene to earliest middle Miocene), just coincident with the end of thin-skinned deformation, the initial extension on the shallow fold-and-thrust belt (i.e., the Korneuburg Basin) and the large erosional incisions on the Rhenodanubian Flysch and the foredeep (e.g., Mistelbach and Iváň canyons). The reasons for a change from initial extension in the foreland to generalised crustal coupling, shortening and late widespread erosion and extension in the Alpine–Carpathian Junction (e.g., the Vienna, Danube, Styrian and other Pannonian basins) must be the result of a large, lithospheric-scale processes. It is here proposed that deep-seated processes affecting the subducting European slab during the final stages of collision are the trigger mechanisms to explain the general uplift of the area as evidenced by landscape evolution, changes in the drainage and subsidence patterns, and the observed kinematics of shortening and related burial and exhumation histories (e.g. Fodor, 1995; Von Blanckenburg and Davies, 1995; Gmach, 1999; Neubauer et al. 2000; Trautwein et al. 2001; Sachsenhofer et al. 2006; Wessely, 2006; Genser et al. 2007; Qorbani et al. 2014; Legrain et al. 2015). A large-wavelength rebound is well documented by Andeweg and Cloetingh (1998) in the Molasse Basin of western Austria, whereas in the studied area such uplift is demonstrated by the presence of Karpatian to Badenian kilometer-scale canyon incisions and infill (Dellmour and Harzhauser, 2012). This broad uplift is also supported by thermochronological and field studies in the Rhenodanubian Flysch of the Alpine-Carpatian fold-and-thrust belt (e.g., Trautwein et al. 2001), and in the Western Carpathians (e.g., Danišík et al. 2010; Mazzoli et al. 2010; Zattin et al. 2011; Anczkiewicz et al. 2013; Andreucci et al. 2013, 2015; Castelluccio et al. 2015).

A large-wavelength lithospheric process can explain the flexural bending and related extension in the foreland plate by the retreat and roll-back of the subduction zone, whereas the transition into out-of-sequence thrusting and basement involvement may be explained by the delamination (see Magni et al. 2013) of the tectonically thickened European lithosphere (**Fig. 4.7**). Delamination probably started around Karpatian time (Dellmour and Harzhauser, 2012), but their effects protracted as shown by foreland subsidence analysis (Genser et al. 2007) and the ages of calc-alkaline (20–11 Ma) and late alkaline magmatic series (9–1 Ma) in the Pannonian region. These series indicate a transition from crustal contaminated magmas related to subduction to asthenosphere-derived magmas generated by lithosphere extension, respectively (Embey-Isztin et al. 1993; Nemčok et al. 1998; Seghedi et al. 2004). The fast rebound following such delamination

most probably created an excessive topographic load (**Fig. 4.7**) along with drastic changes in the stress regime and high levels of shortening (e.g., Cloetingh et al. 2004; Genser et al. 2007). The Alpine–Carpathian tectonic wedge reacted by two mechanisms: 1) the reactivation of a deep detachment and the basement-involved extensional faults in the prowedge (i.e. basin inversion in the sub-thrust and in the foreland), with the subsequent broadening of the orogen (**Fig. 4.4c**), and 2) followed by the collapse of the hinterland orogenic edifice as represented by the opening of the Pannonian basins (**Fig. 4.4d**). Independently of the dominant strike-slip or oblique-slip activity of the Vienna Basin bounding faults (i.e. Steinberg, Leopoldsdorf and Mur-Mürz faults), these faults were key structural elements for the dismantling of the orogenic edifice. The 'missing' retrowedge in the Alpine-Carpathian Junction has been extended and buried beneath the thick sedimentary cover of the middle–late Miocene basin systems. Once the topographic load was reduced, the thrust system shut off. The collapse of the orogenic wedge was ultimately driven by subduction processes (i.e. roll back, retreat and lithosphere delamination).

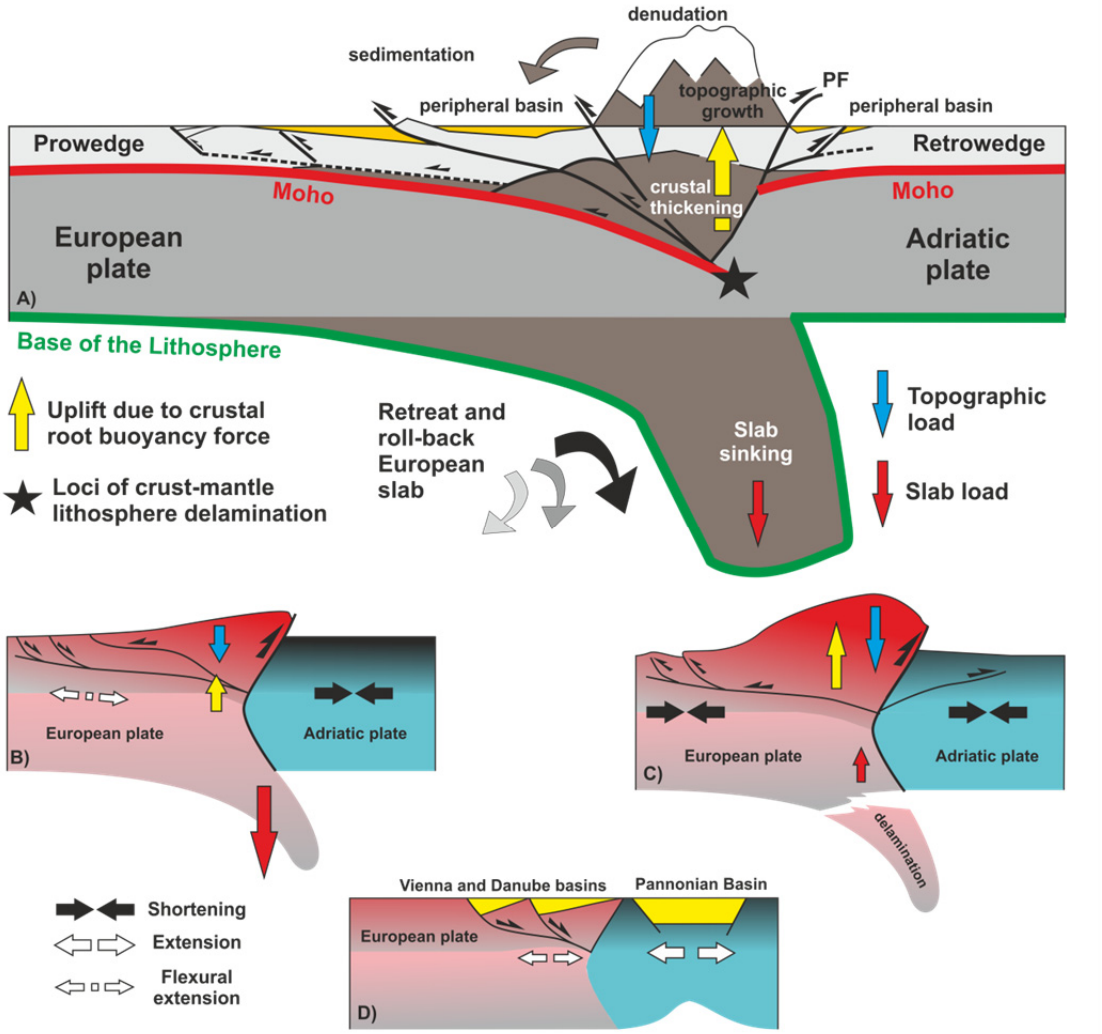

FIGURE 4.7. A) Doubly-vergent orogenic wedge and ruling forces. Based on Beaumont et al. (2000) and Schlunegger and Kissling (2015). PF: Periadriatic Fault. B) Flexural extension resulting from the bending and slab pull affecting the lower plate. C) Delamination of continental lithosphere leads to rebound, high topographic load and crustal thickening by basement-involved shortening. D) The orogenic lithospheres respond by collapse (i.e., Korneuburg and Vienna), and widespread rifting (i.e., Pannonian Basin).

CHAPTER 5. SUMMARY OF CONCLUSIONS

- Basement-involved reactivation in the foreland and sub-thrust of the Alpine-Carpathian fold-and-thrust belt has been defined using a wealth of industry data, including 2D and 3D seismic surveys tied to bio-chrono-stratigraphically-constrained wells and geophysical logs. Gravity anomaly maps were also used as an additional support to investigate the deep structure of the Alpine-Carpathian sub-thrust and foreland regions.

- At the Alpine-Carpathian Junction, reworking of the European lithosphere and related reactivation of basement fault systems is known that have taken place in several deformation episodes related to major plate tectonic reorganizations, including: a first transtensional faulting at the end of the Variscan orogenic cycle; a second fault reactivation during Jurassic rifting accompanied by fault-bound sedimentation; and a third fault reactivation episode during Cretaceous to Paleocene onset of the Alpine shortening cycle.

- In this thesis, two additional reactivation episodes have been defined in the area: an Egerian to Karpatian times (i.e., late Oligocene to latest early Miocene) flexural extensional event and related fault-bound sedimentation took place ahead of the advancing Alpine-Carpathian fold-and-thrust belt. Flexural extension was followed by the compressional, selective reactivation of the basement fault array in Karpatian to Badenian times (i.e., latest early Miocene to early middle Miocene). This last event of basement fault reactivation resulted in the mild positive inversion of the inherited Jurassic half-grabens in the sub-thrust and foreland regions.

- The late compressional involvement of the crystalline basement is indicated by the folding of the Alpine Basal Thrust over the Höflein high, the elevated regional of the Jurassic in the Roseldorf transfer zone, and the broad open folding north the the Haselbach fault. In the foreland, this positive reactivation is also indicated by the Badenian (i.e., early middle Miocene) facies distribution around the Mailberg anticline. The documented cross-cutting relationships indicate that thick-skinned reactivation took place after thin-skinned thrusting in the overlying thin-skinned fold-and-thrust belt, probably during Karpatian to Badenian times.

- The Lower Austria Mesozoic Basin can therefore be considered a locally and midly inverted continental margin.

- Given the close proximity between the Vienna Basin bounding faults, an additional phase of basement fault reactivation during middle to late Miocene cannot be excluded. The orientation of the Höflein fault segments defined in this thesis would theoretically have allowed for the left-lateral reactivation and formation of a restraining bend at its central fault segment, probably contributing to the present day elevation of this structural high.

- Only the Karpatian-Badenian fault reactivation may be properly considered as a basin inversion event (i.e., positive inversion). Lack of a well-preserved Cretaceous sedimentary record in the Lower Austria Mesozoic Basin hampers defining the magnitude of the Lower Cretaceous to Paleocene shortening.

- Typical structural styles associated with the Karpatian-Badenian positive inversion are basement-involved footwall shortcut thrusts and related imbricate fans, hanging-wall directed back-thrusts.

- Inherited domains of equivalent elastic thickness for the European plate seem to have strongly impacted the dynamics of Jurassic rifting, controlling the location and shape of the Jurassic Alpine Tethys continental margin at both sides of the Bohemian spur, as well as the magnitude of foreland bending during continental collision.

- An important component of the observed late Oligocene to latest early Miocene (i.e., Egerian to Karpatian) flexural extension could relate to the retreat of the subducting European lithospheric slab and the slab-pull forces associated with its subduction. The reported high lateral gradients of EET from the rigid Bohemian massif to the significantly softer Jurassic continental margin seems to be a fundamental cause of the large degree of bending needed to explain the observed syn-thrusting flexural extension.

- Delamination of the tectonically-thickened European lithosphere could have been the triggering mechanism for the observed regional uplift and the compressional

reactivation of the basement-involved system beneath and ahead of the fold-and-thrust belt, resulting in the overall broadening of the orogenic wedge.

- The recognition of all these fault reactivation episodes has strong implications for the management of natural resources as well as the seismicity in the foreland and sub-thrust. They also suggest that yet-to-find hydrocarbon reserves may remain undiscovered in inversion-related traps.

- Inversion of segmented half-grabens in tectonic wedges was simulated using scaled brittle and brittle-viscous sandbox analogue models. Upon shortening, the models underwent different amounts of layer-parallel compaction (i.e., equivalent to a pre-folding layer-parallel-shortening in natural fold-and-thrust belts), fault reactivation, thrust propagation and related folding. The different results were controlled by the initial pre-shortening configurations of the modelled tectonic wedges, and in particular by the wedges' vertical-load gradient and the position of this load in respect of the buried extensional basin, as well as the wedge's integrated strength profiles.

- Large vertical loads directly over buried extensional basins hamper their inversion. Conversely, lower loads, or strong gradients of hinterland loading, favour the inversion of the sub-thrust basins located ahead. The thermochronological record of the Rhenodanubian Flysch and the burial history of the syn-rift coal measures on the Höflein high also support these conclusions, and the kinematical evolution proposed for the area.

- The presence of viscous shallow detachments, their stratigraphic location and distribution within the tectonic wedge profile are key factors controlling the geometry and kinematics of compressional deformation. Viscous detachments decouple the deformation between a basement and a cover, and strongly affect the relative timing of thrust propagation vs. basin inversion. Post-rift weak detachments favour and early decoupling, with shallow thrusting overriding buried basins, and basin inversion taking place after thrust propagation. Conversely, pre-rift weak detachments may allow for early inversion of basins and their incorporation into fold-and-thrust belts early in the shortening sequence.

- Strain-softened fault zones favoured the reactivation during the compression, probably due to their inherent lower values of frictional strength. Contrary to other published sandbox models, obliquity between pre-existing fault zones and the direction of shortening had a very minor role in comparison with the parameters above. These results indicate that the recurrent frictional reactivation of the Lower Austria Mesoic Basin basement faults may have been favoured by fault-weakening mechanisms.

- Time-lapse photography, white-light scans of developing topography, serial sectioning of sandbox models and construction of imaged-based 3D voxels have revealed as fundamental tools for the study of physical analogue models.

- Our sandbox modelling results have provided additional insights into the involvement of extensional basins within fold-and-thrust belts, and add additional support for the positive inversion scenario of the Höflein high.

CHAPTER 6. REFERENCES

ADAM, J., URAI, J., WIENEKE, B., ONCKEN, O., PFEIFFER, K., KUKOWSKI, N., LOHRMANN, J., HOTH, S., VAN DER ZEE, W., SCHMATZ, J. 2005. Shear localisation and strain distribution during tectonic faulting - new insights from granular flow experiments and high-resolution optical image correlation techniques. Journal of Structural Geology 27, 283-301.

ADÁMEK, J. 2005. The Jurassic floor of the Bohemian massif in Moravia – geology and paleogeography. Bulletin of Geosciences 80 (4), 291-305.

ALLEN, P.A., ALLEN, J.R. 2005. Basins due to flexure. In: Basin Analysis. Principles and Applications, 2nd Edition (Eds. Allen, P.A. & Allen, J.R.). Blackwell Publishing, pp.116-166.

ÁLVAREZ-MARRÓN, J., BROWN, D., CAMANNI, G., WU, Y.M., HAO, K.C. 2014. Structural complexities in a foreland thrust belt inherited from the shelf-slope transition: Insights from the Alishan area of Taiwan, Tectonics 33, 1322-1339, doi: 10.1002/2014TC003584.

ANCZKIEWICZ, A.A, ŚRODOŃ, J., ZATTIN, M. 2013. Thermal history of the Podhale Basin in the internal Western Carpathians from the perspective of apatite fission track analysis. Geologica Carpathica 64, 141-151.

ANDEWEG, B., CLOETINGH, S. 1998. Flexure and 'unflexure' of the North Alpine German-Austrian Molasse Basin: constraints from forwards tectonic modelling. In: Cenozoic Foreland Basins of Western Europe (Eds. A. Mascle, C. Puigdefàbregas, H.P. Luterbacher & Fernàndez, M.). Geological Society, London, Special Publication no. 134, pp. 403-422.

ANDREUCCI, B., CASTELLUCCIO, A., CORRADO, S., JANKOWSKI, L., MAZZOLI, S., SZANIAWSKI, R., ZATTIN, M. 2015. Interplay between the thermal evolution of an orogenic wedge and its retro wedge basin: an example from the Ukrainian Carpathians. Geological Society of America Bulletin 127, 410–427.

ANDREUCCI, B., CASTELLUCCIO, A., JANKOWSKI, L., MAZZOLI, S., SZANIAWSKI, R., ZATTIN, M. 2013. Burial and exhumation history of the Polish Outer Carpathians: discriminating the role of thrusting and post-thrusting extension. Tectonophysics 608, 866-883.

ARGAND, A. 1911. Les nappes de recouvrement des Alpes pennines et leurs prolongements structuraux. Mat. Carte Geól. Suisse 31, 25.

ARGAND, A. 1924. Des Alpes et de l'Afrique. Bul. Soca. Vaudoise Sci. Nat. 55, 233–236.

ARZMÜLLER, G., BUCHTA, S., RALBOVSKÝ, E., WESSELY, G., 2006. The Vienna Basin. In: The Carpathians and Their Foreland: Geology and Hydrocarbon Resources (Eds. J. Golonka & F.J. Picha). AAPG Memoir 84, Tulsa, 191–204.

BADLEY, M.E., PRICE, J.D., BACKSHALL, L.C. 1989. Inversion, reactivated faults and related structures: seismic examples from the southern North Sea. In: Inversion Tectonics (Eds. M.A. Cooper & G.D. Williams). Geological Society, London, Special Publication no. 44, pp. 201-219.

BALÁZS, A., MATENCO, L., MAGYAR, I., HORVÁTH, F., CLOETINGH, S. 2016. The link between tectonics and sedimentation in back-arc basins: New genetic constraints from the analysis of the Pannonian Basin. Tectonics 35, doi:10.1002/2015TC004109.

BALLY, A.W. 1984. Tectogénèse et sismique reflexion. Bulleting Société Géologique de France 7, 279-285.

BARTHOLOMEW, I.D., PETERS, J.M., POWELL, C.M. 1993. Regional structural evolution of the North Sea: oblique slip and the reactivation of basement lineaments. Geological Society, London, Petroleum Geology Conference series no. 4, pp. 1109-1112.

BAUVILLE, A., SCHMALHOLZ, S.M. 2015. Transition from thin- to thick-skinned tectonics and consequences for nappe formation: Numerical simulations and applications to the Helvetic nappe system, Switzerland. Tectonophysics 665, 101-117.

BEAMUD, E., MUÑOZ, J.A., FITZGERALD, P.G., BALDWIN, S.L., GARCÉS, M., CARBRERA, L., METCALF, J.R. 2011. Magnetostratigraphy and detrital apatite fission track thermochronology in syntectonic conglomerates: constraints on the exhumation of the South-Central Pyrenees. Basin Research 23 (3), 309-331. doi 10.1111/j.1365-2117.2010.00492.x

BEAUMONT, C. 1981. Foreland basins. Geophysical Journal International 65 (2), 291-329.

BEAUMONT, C., MUÑOZ, J.A., HAMILTON, J., FULLSACK, P. 2000. Factors controlling the Alpine evolution of the central Pyrenees inferred from a comparison of observations and geodynamical models. Journal of Geophysical Research 105 (B4), 8121-8145, doi:10.1029/1999JB900390.

BEIDINGER, A., DECKER, K. 2014. Quantifying early Miocene in-sequence and out-of-sequence thrusting at the Alpine-Carpathian junction. Tectonics 33, 222-252. doi: 10.1002/2012TC003250.

BEIDINGER, A., DECKER, K. 2016. Paleogene and Neogene kinematics of the Alpine-Carpathian fold-thrust belt at the Alpine-Carpathian transition. Tectonophysics 690, partB, 263-287.

BELTRANDO, M., COMPAGNONI, R., LOMBARDO, B. 2010. (Ultra-)High pressure metamorphism and orogenesis: An Alpine perspective. Gondwana Research 18, 147-166.

BELTRANDO, M., RUBATTO, D., COMPAGNONI, R., LISTER, G. 2007. Was the Valaisian basin floored by oceanic crust? Evidence of Permian magmatism in the Versoyen unit (Valaisian Domain, NW Alps). Ofioliti 32 (2), 85-99.

BIANCHI, I., MILLER, M., BOKELMANN, G. 2014. Insights on the upper mantle beneath the Eastern Alps. Earth and Planetary Science Letters 403, 199-209.

BIJWAARD, H., SPACKMAN, W., 2000. Non-linear global P-wave tomography by iterated linearized inversion. Geophysical Journal International 141, 71–82.

BJORKLUND, T., BURKE, K., 2002. Four-dimensional analysis of the inversion of a half-graben to form the Whittier fold-fault system of the Los Angeles basin. Journal of Structural Geology 24 (9), 1369-1397.

BLUNDELL, D.J., FREEMAN, R., MUELLER, ST. 1992. A Continent Revealed: the European Geotraverse 1992 (Eds. D.J. Blundell, R. Freeman & St. Mueller). Cambridge University Press, Cambridge. 275pp.

BONINI, M. 2007. Deformation patterns and structural vergence in brittle-ductile thrust wedges: An additional analogue modelling perspective. Journal of Structural Geology 29, 141-158.

BONINI, M., SANI, F., ANTONIELLI, B. 2012. Basin inversion and contractional reactivation of inherited normal faults: A review based on previous and new experimental models. Tectonophysics 522-523, 55-88.

BONNET, C., MALAVIEILLE, J., MOSAR, J. 2007. Interactions between tectonics, erosion, and sedimentation during the recent evolution of the Alpine orogen: Analogue modelling insights. Tectonics 26, doi:10.1029/2006TC002048

BRADDLEY, D.C., KIDD, W.S.F. 1991. Flexural extension of the upper continental crust in collisional foredeeps. Geological Society of America Bulletin 103, 1416-1438.

BRIX, F., SCHULTZ, O. 1993. Erdöl und Erdgas in Österreich. Naturhistorisches Museum Wien, Wien, 714 pp.

BROWN, D., ÁLVAREZ-MARRÓN, J., SCHIMMEL, M., WU, Y.M., CAMANNI, G. 2012. The structure and kinematics of the central Taiwan mountain belt derived from geological and seismicity data. Tectonics 31 TC5013, doi:10.1029/2012TC003156.

BRÜCKL, E., BEHM, M., DECKER, K., GRAD, M., GUTERCH, A., KELLER, G.R., THYBO, H. 2010. Crustal structure and active tectonics in the Eastern Alps. Tectonics 29, TC2011, doi:10.1029/2009TC002491.

BRÜCKL, E., BLEIBINHAUS, F., GOSAR, A., GRAD, M., GUTERCH, A., HRUBCOVA, P., KELLER, G.R., MAJDAŃSKI, M., ŠUMANOVAC, F., TIIRA, T., YLINIEMI, J., HEGDŰS, E., THYBO, H. 2007. Crustal structure due to collisional and escape tectonics in the Eastern Alps region based on profiles Alp01 and Alp02 from the ALP 2002 seismic experiment. Journal of Geophysical Research 112, B06308, doi:10.1029/2006JB004687.

BRUN, J.P., NALPAS, T., 1996. Graben inversion in nature and experiments. Tectonics 15, 677-687.

BUCHANAN, P.G., MCCLAY, K.R. 1991. Sandbox experiments of inverted listric and planar fault systems. Tectonophysics 188, 97-115.

BUCHANAN, P.G., MCCLAY, K.R. 1992. Experiments on basin inversion above reactivated domino faults. Marine and Petroleum Geology 9, 486-500.

BUDAY, T., CICHA, J. 1968. The Vienna Basin. In: Regional Geology of Czechoslovakia, Part II, The West Carpathians. Geological Survey of Czechoslovakia in Akademia, Praha. 721pp

BUITER, S., PFIFFNER, O.A., BEAUMONT, C. 2009. Inversion of extensional sedimentary basins: A numerical evaluation of the localization of shortening. Earth and Planetary Science Letters 288, 492-504.

BUROV, E.B., DIAMENT, M. 1995. The effective elastic thickness (T_e) of continental lithosphere: What does it really mean? Journal of Geophysical Research 100, 3905-3927.

BUTLER, R.W.H. 1989. The influence of pre-existing basin structure on thrust system evolution in the Western Alps. In Inversion Tectonics (Eds. M. A. Cooper & G. D. Williams), Geological Society, London, Special Publication no. 44, pp. 105–122.

BUTLER, R.W.H., MAZZOLI, S. 2006. Styles of continental contraction: A review and introduction. In: Styles of continental contraction (Eds. S. Mazzoli & R.W.H. Butler). Geological Society of America, Boulder, Special Paper 414, pp. 1-10.

CARMINATI, E., DOGLIONI, C. 2012. Alps vs. Apennines. The paradigm of a tectonically asymmetric Earth. Earth-Science Reviews 112, 67-96.

CARMINATI, E., FABBI, S., SANTANTONIO, M. 2015. Slab bending, syn-subduction normal faulting, and out-of-sequence thrusting in the Central Apennines. Tectonics 33, 530-551, doi:10.1002/2d13TC003386.

CAROLA, E., TAVANI, S., FERRER, O., GRANADO, P., QUINTÀ, A., BUTILLÉ, M., MUÑOZ, J.A. 2013. Along-strike extrusion at the transtion between thin- and thick-skinned domains in the Pyrenean Orogen (northern Spain). In: Thick-skinned Dominated Orogens: From Initial Inversion to Full Accretion (Eds. M. Nemčok, A. Mora, J.W. Cosgrove). Geological Society, London, Special Publication no. 377, pp. 119-140.

CARRERA, N., MUÑOZ, J.A. 2013. Thick-skinned tectonic style resulting from the inversion of previous structures in the southern Cordillera Oriental (NW Argentine Andes). In: Thick-skinned Dominated Orogens: From Initial Inversion to Full Accretion (Eds. Nemčok, M., Mora, A., Cosgrove, J.W.). Geological Society, London, Special Publication no. 377, pp. 119-140.

CARTWRIGTH, J.A., MANSFIELD, C., TRUDGILL, B. 1996. The growth of normal faults by segment linkage. In: Modern Developments in Structural Interpretation, Validation and Modelling (Eds. P.G. Buchanan & D.A. Nieuwland). Geological Society, London, Special Publication no. 99, pp.163-177.

CASTELLUCCIO, A., ANDREUCCI, B., ZATTIN, M., KETCHMAN, R.A., JANKOWSKI, L., MAZZOLI, S., SZANIAWSKI, R. 2015. Coupling sequential restoration of balanced cross sections and low-temperature thermochronometry: The case study of the Western Carphatians. Lithosphere 7, 367-378.

CAVAZZA, W., ROURE, F., SPAKMAN, W., STAMPLFLI, G.M., ZIEGLER, P.A. (EDS.) 2004. The TRANSMED Atlas - The Mediterranean Region from Crust to Mantle. Springer-Verlag, Berlin-Heidelberg.

CHANNEL, J., KOZUR, H. 1997. How many oceans? Meliata, Vardar, and Pindos oceans in Mesozoic Alpine paleogeography. Geology 25, 183–186.

CHAPPLE, W.M. 1978. Mechanics of Thin-Skinned Fold-and-Thrust Belts: Geological Society of America Bulletin 89, 1189–1198.

CHILDS, C., WATTERSON, J., WALSH, J.J. 1995. Fault overlap zones within developing normal fault systems. Journal of Geological Society of London 152, 535-549.

CHUANG, R.Y., JOHNSON, K.M, WU, Y.-M., CHING, K., KUO, L-C. 2013. A mid-crustal ramp-fault structure beneath the Taiwan tectonic wedge illuminated by the 2013 Nantou earthquake series. Geophysical Research Letters 40, 5080-5084.

CLERC, C., LAGABRIELLE, Y. 2014. Thermal control on the models of crustal thinning leading to mantle exhumation. Insights from the Cretaceous Pyrenean hot paleomargins. Tectonics 33 (7), 1340-1359. doi:10.1002/2013TC003471.

CLOETINGH, S., BADA, F., MATENCO, L., LANKREIJER, A., HORVÁRTH, F., DINU, C. 2006. Modes of basin (de)formation, lithospheric strength and vertical motions in the Pannonian-Carpathian system: inferences from thermos-mechanical modelling. In: European Lithosphere Dynamics (Eds. D.G. Gee & R.A. Stephenson). Geological Society, London, Memoirs no. 32, pp. 207-221.

CLOETINGH, S., BUROV, E., MATENCO, L., TOUSSAINT, G., BERTOTTI, G., ANDRIESSEN, P.A.M., WORTEL, M.J.R., SPAKMAN, W. 2004. Thermo-mechanical controls on the mode of continental collision in the SE Carpathians (Romania). Earth and Planetary Science Letters 218, 57-76.

CLOETINGH, S., BUROV, E.B. 1996. Thermomechanical structure of European continental lithosphere: constraints from rheological profiles and EET estimates. Geophysical Journal International 124, 695-723.

COLLETINI, C., NIEMEIJER, A., VITI, C., MARONE, C. 2009. Fault zone fabric and fault weakness. Nature 462, 907-910, doi:10.1038/nature08585

COOPER, M. 2007. Structural style and hydrocarbon prospectivity in fold and thrust belts: a global view. In: Deformation of the continental crust: The legacy of Mike Coward (Eds. A.C. Ries, R.W.H. Butler & R.H. Graham). Geological Society, London, Special Publication no. 272, pp 447-472.

COOPER, M.A., WILLIAMS, G.D. 1989. Inversion Tectonics (Eds.), Geological Society, London, Special Publication no. 44, 375pp.

CORNFIELD, S., SHARP, I.R. 2000. Structural style and stratigraphic architecture of fault propagation folding in extensional settings: a seismic example from the Smørbukk area, Halten Terrace, Mid-Norway. Journal of Basin Research 12, 329-341.

CORTIANA, G., DAL PIAZ, G.V., DEL MORO, A., HUNZIKER, J.C., MARTIN, S. 1998. 40Ar-39Ar and Rb-Sr dating of the Pillonet klippe and Sesia-Lanzo basal slice in the Ayas valley and evolution of the Austroalpine-Piedmont nappe stack. Mem. Sci. Geol. 50, 177–194.

COSGROVE, J.W., AMEEN, M.S. 2000. A comparison of the geometry, spatial organization and fracture patterns associated with forced folds and buckle folds. In: Forced folds and fractures (Eds. J.W. Cosgrove & M.S. Ameen). Geological Society, London, Special Publication no. 169, pp 7-21.

COUBAL, M. 1990. Compression along faults: example from the Bohemian Cretaceous Basin. Mineralia Slovaca 22, 139-144.

COUZENS-SCHULTZ, B.A., VENDEVILLE, B.C., WILTSCHKO, D.V., 2003. Duplex style and triangle zone formation: insights from sandbox analogue physical modelling. Journal of Structural Geology 25, 1623-1644.

COWARD, M.P.A., DIETRICH, D. 1989. Alpine Tectonics – an overview. In: Alpine Tectonics (Eds. M.P.A. Coward, D. Dietrich, & R.G. Park). Geological Society, London, Special Publication no.45, pp. 1-99.

COWARD, M.P.A., GILLCRIST, R., TRUDGILL, B. 1991. Extensional structures and their tectonic inversion in the Western Alps. In: The Geometry of Normal Faults (Eds. A.M. Roberts, G. Yielding, B. Freeman). Geological Society, London, Special Publication no. 56, pp. 93-112.

COX, S.F., KNACKSEDT, M.A., BRAUN, J. 2001. Principles of Structural Control on Permeability and Fluid Flow in Hydrothermal Systems. In: Structural Controls on Ore Genesis (Eds. J.P. Richards & R.M. Tosdal). Society of Economic Geologists Inc., Littleton, USA. Reviews in Economic Geology, Reviews no. 14, pp. 1-22

CSONTOS, L. 1995. Tertiary tectonic evolution of the Intra-Carpathian area: a review. Acta Vulcanologica 7, 1–13.

CSONTOS, L., NAGYMAROSI, A., HORVÁRTH, F., KOVÁČ, M. 1992. Tertiary evolution of the Intra-Carpathian area: a model. Tectonophysics 208, 221–241.

CSONTOS, L., VÖRÖS, A. 2004. Mesozoic plate tectonic reconstruction of the Carpathian region. Paleogeography Paleoclimatology Paleoecology 210, 1–56.

D'ADDA, P., LONGONI, R., MAGISTRONI, C., MEDA, M., RIGHETTI, F., CAVOZZI, C., NESTOLA, Y., STORTI, F. 2017. Extensional reactivation of a deep transpressional architecture: insights from sandbox analogue modelling applied to the Val d'Agri basin (Southern Apennines, Italy). Interpretation 5 (1), SD55-SD66. doi:10.1190/INT-2016-0078.1

DAL PIAZ, G.V. 2001. History of tectonic interpretations of the Alps. Journal of Geodynamics 32, 99-114

DAL PIAZ, G.V. 1999. The Austroalpine-Piedmont nappe stack and the puzzle of western Alpine Tethys. Third Workshop on Alpine Geological Studies, Biella-Oropa 1997 (Eds. GOSSO, G. et al.). Mem. Sci. Geol. It. 51, 155–176.

DAL PIAZ, G.V., CORTIANA, G., DEL MORO, A., MARTIN, S., PENNACCHIONI, G., TARTAROTTI, P. 2001. Tertiary age and paleostructural inferences of the eclogitic imprint in the Austroalpine outliners and Zermatt-Saas ophiolite, Western Alps. International Journal of Earth Sciences 90, 668-684.

DAL PIAZ, G.V., HUNZIKER, J.C., MARTINOTTI, G., 1972. La Zona Sesia-Lanzo e l'evoluzione tettonico-metamorfica delle Alpi nordoccidentali interne. Mem. Soc. Geol. Ital. 11, 433–466.

DANIŠÌK, M., KOHÚT, M., BROSKA, I., FRISCH, W. 2010. Thermal evolution of the Malá Fatra Mountains (Central Western Carpathians): insights from zircon and apatite fission track thermochronology. Geologica Carpathica 61, 19-27.

DAVIS, D.M., ENGELDER, T. 1985. The role of salt in fold-and-thrust belts. Tectonophysics 119, 67-88.

DAVY, P., COBBOLD, P.R. 1991. Experiments of shortening of a 4-layer model of the continental lithosphere. Tectonophysics 188, 1-25.

DE GRACIANSKY, P.C., DARDEU, G., LEMOINE, M., TRICART, P. 1989. The inverted margin of the French Alps and foreland inversion. In: Inversion Tectonics (Eds. M.A. Cooper & G.D. Williams). Geological Society, London, Special Publications no. 44, 87-104.

DE GRACIANSKY, P.C., ROBERTS, D.G., TRICART, P. 2011. The Western Alps, from Rift to Passive Margin to Orogenic Belt (Ed. J.F. Jr. Shroder) Development in Earth Surface Processes 14, Amsterdam, 432pp.

DECELLES, P., GILES, K.A. 1996. Foreland basin systems. Basin Research 8, 105-123.

DECKER, K. 1990. Plate tectonics and pelagic facies: Late Jurassic to Lower Cretaceous deep-sea sediments of the Ybbsitz ophiolite unit (Eastern Alps, Austria). Sedimentary Geology 67, 85-99.

DECKER, K., FAUPL, P., MÜLLER, A. 1987. Synorogenic sedimentation on the Northern Calcareous Alps during the Lower Cretaceous. In: Geodynamics of the Eastern Alps (Eds. H.W. Flügel & P. Faupl). Vienna, 126-141.

DECKER, K., MESCHEDE, M., RING, U. 1993. Fault slip analysis along the northern margin of the Eastern Alps (Molasse, Helvetic Nappes, North- and South-Penninic flysch, and the Northern Calcareous Alps). Tectonophysics 223, 291-312.

DECKER, K., PERESSON, H. 1996. Tertiary kinematics in the Alpine-Carpathian-Pannonian system: links between thrusting, transform faulting and crustal extension. In: Oil and Gas in Alpidic Thrustbelts and Basins of Central and Eastern Europe (Eds. G. Wessely & W. Liebl). Geological Society, London, EAGE Special Publication no. 5, pp 69-77.

DECKER, K., PERESSON, H., HINSCH, R. 2005. Active tectonics and Quaternary basin formation along the Vienna Basin Transform fault. Quaternary Science Reviews 24, 307-322.

DEL MORO, A., PARDINI, G.C., QUERICIOLI, C., VILLA, I.M., CALLEGARI, E. 1983. Rb/Sr and K/Ar chronology of Adamello granitoids, Southern Alps. Mem. Sci. Geol. It. 26, 285-300.

DEL VENTISETTE, C., MONTANARI, D., SANI, F., BONINI, M., 2006. Basin inversion and fault reactivation in laboratory experiments. Journal of Structural Geology 28, 2067-2083.

DELL'ERTOLE, D., SCHELLART, W.P., 2013. The development of sheat folds in viscously stratified materials in simple shear conditions: an analogue approach. Journal of Structural Geology 56, 29-141.

DELLMOUR, R., HARZHAUSER, M. 2012. The Iváň Canyon, a large Miocene canyon in the Alpine-Carpathian Foredeep. Marine and Petroleum Geology 38, 83–94.

DERCOURT, J., RICOU, L.E., VRIELYNCK, B. (EDS.) 1993. Atlas Tethys Palaeoenvironmental Maps. Gauthier-Villars, Paris, 307 pp.

DESEGAULX, P., KOOI, H., CLOETINGH, S. 1991. Consequences of foreland basin development on thinned continental lithosphere: application to the Aquitaine basin (SW France). Earth and Planetary Science Letters 106, 116-132.

DESTRO, N. 1995. Release fault: a variety of cross fault in liked extensional fault systems in the Sergipe-Alagoas basin, north-eastern Brazil. Journal of Structural Geology 17, 615-629.

DEWEY, J.F. 1988. Extensional collapse of orogens. Tectonics 7 (6), 1123-1139.

DEWEY, J.F., BIRD, J.M. 1970. Mountain belts and the new global tectonics. Journal of Geophysical Research 75, 2625-2647.

DEWEY, J.F., HELMAN, M.L., TURCO, E., HUTTON, D.W.H., KNOTT, S.D. 1989. Kinematics of the Western Mediterranean. In: Alpine Tectonics (Eds. M.P.A Coward, D. Dietrich & R.G. Park). Geological Society, London, Special Publication no. 45, pp. 265-283.

DEWEY, J.F., PITMAN, W.C., RYAN, W.B.F., BONNIN, J. 1973. Plate tectonics and the evolution of the Alpine system. Geological Society American Bulletin 84, 3137-3180.

DI DOMENICA, A., BONINI, L., CALAMITA, F., TOSCANI, G., GALUPPO, C., SENO, S., 2014. Analogue modelling of positive inversion tectonics along differently oriented pre-thrusting normal faults: An application to the Central-Northern Apennines of Italy. Geological Society America Bulletin, doi:10.1130/B31001.1

DOOLEY, T.P., JACKSON, M.P.A., HUDEC, M.R. 2009. Inflation and deflation of deeply buried salt stocks during lateral shortening. Journal of Structural Geology 31, 582-600.

DUBOIS, A., ODONNE, F., MASSONNAT, G., LEBOURG, T., FABRE, R., 2002. Analogue modelling of fault reactivation: tectonic inversion and oblique remobilization of grabens. Journal of Structural Geology, 24, 1741–1752.

DUMONT, T., CHAMPAGNAC, J.D., CROUZET, C., ROCHAT, P. 2008. Multistage shortening in the Dauphiné Zone (French Alps): the record of Alpine collision and implications for pre-Alpine restoration. Swiss Journal of Geoscience 101, doi:10.1007/s00015-008-1280-2.

DUNKL, I., FRISCH, W. 2002. Thermochronologic constraints on the Late Cenozoic exhumation along the Alpine and West Carpathian margins of the Pannonian basin. EGU Stephan Mueller Special Publication Series 3, 1–13.

EGGER, H. 1990. Zur paläogeographischen Stellung de Rhenodanubischen Flysches (Neokom-Eozän) der Ostalpen. Jahrb Geol B-A 133, 147-155.

EGGER, H. 1992. Zur Geodynamik und Palägeographie des Rhenodanubischen Flysches (Neokom-Eozän) del Ostalpen. Z Dtsch Geol Ges 143, 51-65.

EISENSTADT, G., SIMS, D. 2005. Evaluating sand and clay models: do rheological differences matter? Journal of Structural Geology 27, 1399-1412.

EISENSTADT, G., WITHJACK, M.O. 1995. Estimating inversion: results from clay models. In: Basin inversion (Eds. J.G. Buchanan & P.G. Buchanan). Geological Society, London, Special Publication no. 88, pp. 119–136.

EL HARFI, A., GUIRAUD, M., LANG, J. 2006. Deep-rooted "thick skinned" model for the High Atlas Mountains (Morocco). Implications for the structural inheritance of the southern Tethys passive margin. Journal of Structural Geology 28, 1958-1976.

EMBEY-ISZTIN, A., DOWNES, H., JAMES, D.E., UPTON, B.G.J., DOBOSI, G., INGRAM, G.A., HARMON, R.S., SCHARBERT, H.G. 1993. The petrogenesis of Pliocene alkaline volcanic rocks from the Pannonian Basin, Eastern Central Europe. Journal of Petrology 34, 317–343.

ERDŐS, Z., HUISMANS, R.S., VAN DER BEEK, P., THIEULOT, C. 2014. Extensional inheritance and surface processes as controlling factors of mountain belt structure. Journal of Geophysical Research 119, 9042-9061, doi: 10.1002/2014JB011408.

ETHERIDGE, M.A. 1986. On the reactivation of extensional fault systems. Philosophical Transactions of the Royal Society A. Mathematical, Physical and Engineering Sciences 317, 179-194 doi:10.1098/rsta.1986.0031.

FARZIPOUR-SAEIN, A., NILFOUROUSHAN, F., KOYI, H. 2013. The effect of basement step/topography on the geometry of the Zagros fold and thrust belt (SW Iran): an analogue modelling approach. International Journal of Earth Sciences 102, 2117-2135.

FAULDS, J.E., VARGA, R.J., 1998. The role of accommodation zones and transfer zones in the regional segmentation of extended terranes. In: Accommodation Zones and Transfer Zones: The Regional Segmentation of the Basin and Range Province (Eds. J.E. Faulds & J.H. Stewart). Geological Society of America, Boulder, Special Paper no. 323, pp. 1-46.

FAUPL, P., WAGREICH, M. 1996. Basin analysis of the Gosau Group of the Northern Calcareous Alps (Turonian-Eocene, Eastern Alps.). In: Oil and Gas in Alpidic Thrustbelts and Basins of Central and Eastern Europe (Eds. G. Wessely & W. Liebl). Geological Society, London, EAGE Special Publication no. 5, pp.127-135.

FAUPL, P., WAGREICH, M. 2000. Late Jurassic to Eocene paleogeography and geodynamic evolution of the Eastern Alps. Mitteilungen der Österreich Geologischen Gesellschafft 92, 79-94.

FODOR, L. 1995. From transpression to transtesion: Oligocene-Miocene structural evolution of the Vienna Basin and the East-Alpine-Western Carpathian junction. Tectonophysics 242, 151-182.

FODOR, L., CSONTOS, L., BADA, G., GYÖRFI, I., BENKOVICS, L. 1999. Tertiary tectonic evolution of the Pannonian Basin system and neighbouring orogens: a new synthesis of paleostress data. In: The Mediterranean Basins: Tertiary extension within the Alpine orogen (Eds. B. Durand, L. Jolivet, F. Horváth & M. Séranne). Geological Society, London, Special Publication no. 156, 295-334.

FOSSEN, H. 1992. The role of extensional tectonics in the Caledonides of south Norway. Journal of Structural Geology 14 (8/9), 1033-1046.

FOSSEN, H. 2000. Extensional tectonics in the Caledonides: synorogenic or postorogenic. Tectonics 19 (2), 213-224. doi:10.1029/1999TC900066.

FOSSEN, H., 2010. Deformation bands formed during soft-sediment deformation: Observations from SE Utah. Marine and Petroleum Geology 27, 215-222.

FOSSEN, H., FAZLI KHANI, H., FALEIDE, J.I., KSIENZYK, A. K., DUNLAP, W.J. 2016. Post-Caledonian extension in the West Norway-northern North Sea region: the role of structural inheritance. In: The Geometry and Growth of Normal Faults (Eds. C. Childs, R.E. Holdsworth, C.A.L. Jackson, T. Manzocchi, J.J. Walsh & G. Yieldin). Geological Society, London, Special Publications no. 439, doi:10.1144/SP439.6.

FRANK, W. 1987. Evolution of the Austroalpine Elements in the Cretaceous. In: Geodynamics of the Eastern Alps (Eds. Flügel, H.W., Faupl, P.). Deutike, Wien, 379-406

FRISCH, W. 1979. Tectonic progradation and plate tectonic evolution of the Alps. Tectonophysics 60, 121-139.

FRISCH, W., KUHLEMANN, J., DUNKL, I., BRÜGL, A. 1998. Palispastic reconstruction and topographic evolution of the Eastern Alps during the late Tertiary tectonic extrusion. Tectonophysics 297, 1-15.

FROITZHEIM, N. 2001. Origin of the Monte Rosa nappe in the Pennine Alps – A new working hypothesis. Geological Society of America Bulletin 113, 604-614.

FROITZHEIM, N., MANATSCHAL, G. 1996. Kinematics of Jurassic rifting, mantle exhumation, and passive-margin formation in the Austroalpine and Penninic nappes (eastern Switzerland). Geological Society of America Bulletin 108. 1120-1133.

FROITZHEIM, N., PLAŠIENKA, D., SCHUSTER, R. 2008. Alpine tectonics of the Alps and Western Carpathians. In: The Geology of Central Europe, vol. 2 Mesozoic and Cenozoic (Ed. T. McCann). Geological Society, London, pp. 1141-1232.

FROITZHEIM, N., SCHMID, S.M., FREY, M. 1996. Mesozoic paleogeography and the timing of eclogite-facies metamorphism in the Alps: A working hypothesis. Eclogae geologicae Helvetiae 89, 81-110.

FUCHS, R., WESSELY, G. 1977. Die Oberkreide des Molasseuntergrundes im nördlichen Niederösterreich. Jahrbuch der Geologischen Bundesanstalt 120, 426-436.

GARCÍA-CASTELLANOS, D., CLOETINGH, S. 2012. Modelling the interaction between lithospheric and surface processes in foreland basins. In: Tectonics of Sedimentary Basins: Recent Advances (Eds. C. Busby & A. Azor). 1st Ed. Blackwell Publishing Ltd., pp. 152-181.

GARCÍA-CASTELLANOS, D., FERNÀNDEZ, M., TORNÉ, M. 1997. Numerical modelling of foreland basin formation: a program relating thrusting, flexure, sediment geometry and lithosphere rheology. Computers and Geosciences 23, 993-1003.

GAWTHORPE, R.L., HURST, J.M., 1993. Transfer zones in extensional basins: their structural style and influence on drainage development and stratigraphy. Journal of the Geological Society, 150(6), 1137-1152.

GENSER, J., CLOETINGH, S., NEUBAUER, F. 2007. Late orogenic rebound and oblique Alpine convergence: new constraints from subsidence analysis of the Austrian Molasse basin. Global and Planetary Change 58, 214–233

GENSER, J., NEUBAUER, F. 1989. Low angle normal faults at the eastern margin of the Tauern window (Eastern Alps). Mitteilungen der Österreich Geologischen Gesellschafft 81, 233-243.

GEOFYZIKA, 1999. Unified processing and visualization of gravity data in the Vienna Basin and surrounding petroliferous areas. OMV Internal report, unpublished, 14 pp.

GIBBS, A.D. 1984. Structural evolution of extensional basin margins. Journal Geological Society of London 141, 609-620.

GILLCRIST, R., COWARD, M.P.A., MUGNIER, J.L., 1987. Structural inversion and its controls: examples from the Alpine foreland and the French Alps. Geodinamica Acta 1, 5-34.

GMACH, H. 1999. Thermische Reife der Flyschzone im Bereich des Wienerwaldes und der Flyschanteile nödlich der Donau und deren Einfluβ auf die Kohlenwasserstoffgenese am Rand des Wieners Beckens. Diploma Thesis, Leoben.

GOLONKA, J., GAHAGAN, L., KROBICKI, M., MARKO, F., OSZCZPKO, N., ŚLĄCZKA, A. 2006. Plate tectonic evolution and paleogeography of the circum-Carpathian region. In: The Carpathians and their foreland: Geology and hydrocarbon resources (Eds. J. Golonka & F.J. Picha). AAPG Memoir 84, Tulsa, pp. 11-46.

GOLONKA, J., PICHA, F.J. 2006. Introduction. In: The Carpathians and their foreland: Geology and hydrocarbon resources (Eds. J. Golonka & F.J. Picha) AAPG Memoir 84. Tulsa, pp. 1-9.

GOOFEY, G.P., CRAIG, J., NEEDHAM, T., SCOTT, R. 2010. Fold-thrust belts: overlooked provinces or justifiably avoided. In: Hydrocarbons in constractional belts (Eds. G.P. Goofey, J. Craig, T. Needham, & R. Scott). Geological Society, London, Special Publication no. 348, pp 1-6.

GRANADO, P., FERRER, O., MUÑOZ, J.A., THÖNY, W., STRAUSS, P. 2017. Basin inversion in tectonic wedges: a comparative approach from analogue modelling and the Alpine-Carpathian fold-and-thrust belt. Tectonophysics, doi: 10.1016/j.tecto.2017.02.022.

GRANADO, P., THÖNY, W., CARRERA, N., GRATZER, O., STRAUSS, P., MUÑOZ, J.A. 2016. Basement-involved reactivation in fold-and-thrust belts: the Alpine-Carpathian Junction (Austria). Geological Magazine 153 (5-6), 1110-1135, doi: 10.1017/S0016756816000066.

GRANADO, P., THÖNY, W., CARRERA, N., MUÑOZ, J.A., GRATZER, O., STRAUSS, P. 2015. A new structural model for the Europe-derived Jurassic Para-authochthonous of Lower Austria. AAPG European Regional Conference and Exhibition. Tethys-Atlantic interaction along the European-Iberian-African plate boundaries. 18-19 May, 2015, Lisbon.

GRAND, T. 1988. Mesozoic extensional inherited structures on the European margin of the Ligurian Tethys. The example of the Bourg d'Oisans half-graben, western Alps. Bulletin de la Société Géologique de France 4, 613-621.

GRAßL, H., NEUBAUER, F., MILLAHN, K., WEBER, F. 2004. Seismic image of the deep crust at the eastern margin of the Alps (Austria): indications for crustal extension in a convergent orogen. Tectonophysics 380, 105–122.

GRAVELEAU, F., MALAVIEILLE, J., DOMINGUEZ, S. 2012. Experimental modelling of orogenic wedges: a review. Tectonophysics 538-540, 1-66.

GRUBER, P., FAUPL, P., KOLLER, F. 1992. Zur Kenntnis basischer Vulkanitgerölle aus Gosaukonglomeraten der östliche Kalkalpen – ein Vergleich mit Vulkaniten aus dem Hauselgebirge. Mitteilungen der Österreich Geologischen Gesellschafft 84, 77-100.

GRÜN, W. 1984. Die Erschliessung von Lagerstätten im Untergrund der alpin-karpatischen Stirnzone Niederösterreichs. Erdöl-Erdgas, 100 (9), 292-295.

GUEYDAN, F., LEROY, Y.M., JOLIVET, L., AGARD, P. 2003. Analysis of continental midcrustal strain localization induced by reaction softening and microfracturing. Journal of Geophysical Research 108 (B2), 2064, doi:10.1029/2001JB000611

GUIRAUD, R. 1998. Mesozoic rifting and basin inversion along the northern African Tethyan margin: an overview. In: Petroleum Geology of North Africa (Eds. D.S. MacGregor, R.T.J. Moody & D.D.Clark-Lowes). Geological Society, London, Special Publications no. 132, 217-229.

GUTERCH, A., GRAD, M., KELLER, G.R., POSGAY, K., VOZAR, J., ŠPIČÁK, A., BRUECKL, R., HAJNAL, Z., THYBO, H., SELVI, O. AND THE CELEBRATION 2000 EXPERIMENT TEAM. 2003. CELEBRATION 2000 seismic experiment. Stud. Geophys. Geod. 47, 659–669, doi:10.1023/A:1024728005301.

HAAS, J., PERO, S. 2004. Mesozoic evolution of the Tisza Mega-unit. International Journal of Earth Sciences 93, 297–313.

HAAS, J. 2001. Geology of Hungary. Eötvös University Press, Budapest, 317 pp.

HALL, R., MORLEY, C.K. 2004. Sundaland Basins. In: Continent-Ocean Interactions within East Asian Marginal Seas. (Ed. P. Clift et al.) Geophysical Monographs Series 149. AGU, Washington, D.C., 55-85.

HAMILTON, W., WAGNER, L., WESSELY, G. 2000. Oil and Gas in Austria. Mitteilungen der Österreich Geologischen Gesellschafft 92, 235-262.

HANDY, M.R., SCHMID, S.M., BOUSQUET, R., KISSLING, E., BERNOULLI, D. 2010. Reconciling plate-tectonic reconstructions of Alpine Tethys with the geological-geophysical record of spreading and subduction in the Alps. Earth Sciences Reviews 120, 121-158.

HANDY, M.R., USTASZEWSKI, K., KISSLING, E. 2015. Reconstructing the Alps-Carpathians-Dinarides as a key to understanding switches in subduction polarity, slab gaps and surface motion. International Journal of Earth Sciences 104 (1), doi: 10.1007/s00531-014-1060-3.

HARZHAUSER, M., BOEHME, M., MANDIC, O., HOFMANN, CH-CH. 2002. The Karpatian (Late Burdigalian) of the Korneuburg Basin: A palaeoecological and biostratigraphical synthesis. Beitraege zur Palaeontologie 27, 441-456.

HARZHAUSER, M., DAXNER-HÖCK, G., PILLNER, W.E. 2004. An integrated stratigraphy of the Pannonian (late Miocene) in the Vienna Basin. Austrian Journal of Earth Sciences (formerly the Mitt. Österr. Geol. Ges.), 95/96, 6-19.

HARZHAUSER, M., WESSELY, G. 2003. The Karpatian of the Korneuburg Basin (Lower Austria). In: The Karpatian - a Lower Miocene Stage of the Central Paratethys (Eds. R. Brzobohatý, I. Cicha, M. Kováč, F. Rögl). Masarykova Univerzita, Brno, Czech Respublic, pp107-109.

HÄUSLER, H. 1987. The northern AustroAlpine margin during the Jurassic: breccias from the Radstädter Tauern and the Tarntaler Berge. In: Geodynamics of the Eastern Alps (Eds. H.W. Flügel & P. Faupl). Deutike, Wien, pp.103-111.

HAYWARD, A.B., GRAHAM, R.H. 1989. Some geometrical characteristics of inversion. In: Inversion Tectonics (Eds. M.A. Cooper & G.D. Williams). Geological Society, London, Special Publication no. 44, pp. 201-219.

HEIM, A. 1921. Geologie der Schweiz. Band I Molasseland und Juragebirge. Tauchniz, Leipzig.

HINSCH, R., DECKER, K. 2011. Seismic slip rates, potential subsurface rupture areas and seismic potential of the Vienna Basin Transfer Fault. International Journal of Earth Sciences 100, 1925-1935.

HINSCH, R., DECKER, K., PERESSON, H. 2005b. 3-D seismic interpretation and structural modelling in the Vienna Basin: implications for Miocene to recent kinematics. Austrian Journal of Earth Sciences 97, 38–50.

HINSCH, R., DECKER, K., WAGREICH, M., 2005a. 3-D mapping of segmented active faults in the southern Vienna Basin. Quaternary Science Reviews 24, 321-336.

HOLDSWORTH, R.E. 2004. Weak faults – rotten cores. Science 303, 181-182.

HOLDSWORTH, R.E., STEWART, M., IMBER, J., STRACHAN, R.A. 2001. The structure and rheological evolution of reactivated continental fault zones: a review and case study. In: Continental Reactivation and Reworking (Eds. J.A. Miller, R.E. Holdworth, I.S. Buick & M. Hand). Geological Society, London, Special Publication no. 184, pp. 115-137.

HOLL, J.E., ANASTASIO, D.J. 1995. Cleavage development within a foreland fold and thrust belt, southern Pyrenees, Spain. Journal of Structural Geology 17, 357–369.

HÖLZEL, M., DECKER, K., ZÁMOLYI, A., STRAUSS, P., WAGREICH, M. 2010. Lower Miocene structural evolution of the central Vienna Basin (Austria). Marine and Petroleum Geology 27, 666-681.

HORVÁRTH, F., BADA, G., SZAFIÁN, P., TARI, G., ÁDÁM, A., CLOETINGH, S. 2006. Formation and deformation of the Pannonian Basin: constraints from observational data. In: European Lithosphere Dynamics (Eds. D.G. Gee & R.A. Stephenson). Geological Society, London, Memoir 32, pp- 191-206.

HORVÁRTH, F., CLOETINGH, S. 1996. Stress-induced late-stage subsidence anomalies in the Pannonian Basin. Tectonophysics, 266, 287–300.

HORVÁTH, F. 1993. Towards a mechanical model for the formation of the Pannonian Basin. Tectonophysics 226, 333-357.

HORVÁTH, F. 1995. Phases of compression during the evolution of the Pannonian Basin and its bearing on hydrocarbon exploration. Marine and Petroleum Geology, 12, 837–844.

HUBBERT, M.K. 1951. Mechanical basis for certain geological structures. Geological Society America Bulletin 62, 355-372.

HUISMANS, R.S., PODLADCHIKOV, Y.Y, CLOETINGH, S. 2001. Dynamic modelling of the transition from passive to active rifting, application to the Pannonian Basin. Tectonics 20, 1021-1039, doi:10.1029/2001TC900010.

HUYGHE, P., MUGNIER, J.L. 1995. A comparison of inverted basins of the Southern North Sea and inverted structures of the external Alps. In: Basin inversion (Eds. J.G. Buchanan & P.G. Buchanan). Geological Society, London, Special Publication no. 88, pp. 339-354.

JACKSON, C.A.L., GAWTHORPE, R.L., SHARP, I.R. 2006. Style and sequence of deformation during extensional fault-propagation folding: examples from the Hammam Faraun and El-Qaa fault blocks, Suez Rift, Egypt. Journal of Structural Geology 28, 519-535.

JAEGER, G.D., COOK, N.G.W. 1979. Fundamentals of rock mechanics. Chapman & Hill Ltd. London, 515pp.

JAMMES, S., HUISMANS, R.S. 2012. Structural styles of mountain building: controls of lithospheric rheologic stratification and extensional inheritance. Journal of Geophysical Research 117, B10403, doi:10.1029/2012JB009376.

JANOSCHEK, W.R., MALZER, O., ZIMMER, W. 1996. Hydrocarbons in Austria: past, present and future. In: Oil and Gas in Alpidic Thrustbelts and Basins of Central and Eastern Europe (Eds. G. Wessely & W. Liebl). Geological Society, London, EAGE Special Publication 5, pp. 43–63.

JANOSCHEK, W.R., MATURA, A. 1980. Outline of the geology of Austria and selected excursions. Abh Geol. B.-A (26 C.G.I.) 34. Wien, 325pp.

JIŘIČEK, R., TOMEK, C. 1981. Sedimentary and structural evolution of the Vienna Basin. Earth evolution sciences 1, (3-4), 195-204.

JORDAN, T.E. 1981. Thrust loads and foreland basin evolution, Cretaceous, Western United States. American Association Petroleum Geologists Bulletin 65 (12), 2506-2520.

KAPOUNEK, J., KRÖLL, A., PAPP, A., TURNOVSKY, K. 1965. Die Verbreitung von Oligozän, Unter- und Mittelmiozän in Niederösterreich. Erdöl-Erdgas-Zeitschrift 81, 109-116.

KAPOUNEK, J., KRÖLL, A., PAPP, A., TURNOVSKY, K. 1967. Der Mesozoische Sedimentanteil des Festlandsockels der Böhemischen Masse. Jb. Geol. B.-A., 110, 73-91.

KARNER, G.D., WATTS, A.B. 1983. Gravity anomalies and flexure of the lithosphere at mountain ranges. Journal of Geophysical Research 88 B12, 10449-10477.

KHALIL, S.M., MCCLAY, K.R. 2002. Extensional fault-related folding, northwestern Red Sea, Egypt. Journal of Structural Geology 24, 743-762.

KISSLING, R. 1993. Deep structure of the Alps – What do we really know?. Physics of the Earth and Planetary Interiors 79, 87-112.

KLEIN, V., MÜLLER, V., VALECKA, J. 1979. Lithofazielle und paläogeographische Entwicklung des Böhmischen Kreide-beckens. In: Aspekte der Kreide Europas (Ed. Wiedmann, J.). IUGS Ser. A. 6, 435-446.

KLOPPENBURG, A., GROCOTT, J, HUTCHINSON, D. 2010. Structural setting and syn-plutonic fault kinematics of a Cordilleran Cu-Au-Mo porphyry mineralisation system, Bingham Mining Distric, Utah. Economic Geology 105 (4), 743-761.

KOLLER, F. 1985. Petrologie und Geochimie der Ophiolite des Penninukums am Apenostrand. Jahrbuch der Geologischen Bundes-Anstalt 128, 83-1510.

KOOPMAN, A., SPEKSNIJDER, A., HORSFIELD, W.T. 1987. Sandbox models of inversion tectonics. Tectonophysics 137, 379-388.

KOVÁČ, M., BÁRATH, I., NAGYMAROSY, A. 1997. The Miocene collapse of the Alpine-Carpathian-Pannonian junction: an overview. Acta Geologica Hungarica 40, 241-264.

KOYI, H.A., SANS, M., TEIXELL, A., COTTON, J., ZEYEN, H. 2004. The significance of penetrative strain in the restoration of shortened layers—Insights from sand models and the Spanish Pyrenees. In: Thrust tectonics and hydrocarbon systems (Ed. K.R. McClay). AAPG Memoir 82, pp. 207-222.

KOZLOWSKI, E., MANCEDA, R., RAMOS, V. 1993. Estructura. In: 12 Congreso Geológico Argentino Congreso de Exploración de Hidrocarburos. Buenos Aires, pp. 235– 256.

KOZUR, H., MOSTLER, H. 1992. Erster paläontologischer Nachweis von Meliaticum und Süd-Rudabanyaicum in den Nördlichen Kalkalpen (Österreich) und ihre Beziehungen zu den Abfolgen in den Westkarpaten. Geologisch-Paläontologische Mitteilungen Innsbruck 18, 87-129.

KRÖLL, A. 1980. Das Wiener Becken. In: Erdöl und Erdgas in Österreich (Ed. Bachmayer, F.). Naturhistorisches Museum Wien, Wien. 147-179.

KRÖLL, A., WESSELY, G. 2001. Geologische Karte de Molassebasis. In Geologische Themenkarten der Republik Österreich, 1:200.000. Molassezone Niederösterreich und angrenzende Gebiete, 4 Themenkarten mit Erläut. Wien (Geol. B.-A).

KRONER, U., MANSY, J.L., MAZUR, S., ALEKSANDROWSKI, P., HANN, H.P., HUCKRIEDE, H. 2008. Variscan tectonics. In: The Geology of Central Europe: Vol. 1 Precambrian and Paleozoic (Ed.Mc T.Cann). Geological Society, London, pp. 665-712.

KURZ, W., FRITZ, H., PILLER, W.E., NEUBAUER, F., GENSER, J. 2001. Overview of the Paleogene of the Eastern Alps. In: Paleogene of the Eastern Alps (Eds. Piller, W.E., Rasser, M.) Schriftenreihe der Erdwissenschaftlichen Komissionen – Österreichische Akademie der Wissenschafen 14, 11-56.

LACOMBE, O., BELLAHSEN, N. 2016. Thick-skinned tectonics and basement-involved fold-thrust-belts: insights from selected Cenozoic orogens. In: Tectonic evolution and mechanics of basement-involved fold-and-thrust belts (Eds. O. Lacombe, J.Ruh, D. Brown, F. Nilfouroushan). Geological Magazine 153 (5-6), 763-810. doi:10.1017/S0016756816000078.

LACOMBE, O., MOUTHEREAU, F. 2002. Basement-involved shortening and deep detachment tectonics in foreland of orogens: Insigths from recent collision belts (Taiwan, Western Alps, Pyrenees). Tectonics 21(4), doi: 10.1029/2001TC901018.

LACOMBE, O., MOUTHEREAU, F., ANGELIER, J. 2003. Frontal belt curvature and oblique ramp development at an obliquely collided irregular margin: Geometry and kinematics of the NW Taiwan fold-thrust belt. Tectonics 22 (3) doi: 10.1029/2002TC001436.

LACOMBE, O., RUH, J., BROWN, D., NILFOUROUSHAN, F. 2016. Introduction: tectonic evolution and mechanics of basement-involved fold-and-thrust belts. Geological Magazine 153 (5-6), 759-762.

LADWEIN, W. 1976. Sedimentologische Untersuchungen an Karbonatgestein des autochthonen Upper Jurassic in Niederösterreich (Raum Altenmarkt-Staaz). Diss. Philos. Fak. Univ. Innsbruck.

LADWEIN, W. 1988. Organic geochemistry of Vienna Basin: model for hydrocarbon generation in overthrust belts. American Association Petroleum Geologists Bulletin 72, 586-599.

LAFOSSE, M., BOTOUX, A., BELLAHSEN, N., LE POURHIET, L. 2016. Role of tectonic burial and temperature on the inversion of inherited extensional basins during collision. Geological Magazine 153 (5/6), 811-826.

LANKREIJER, A., BIELIK, M., CLOETINGH, S., MAJCIN, D. 1999. Rheology predictions across the western Carpathians, Bohemian massif, and the Pannonian basin: implications for tectonic scenarios. Tectonics 18 (6), 1139-1153.

LANKREIJER, A., KOVÁČ, M., CLOETINGH, S., PITOŇAK, P., HLÔŠKA, M., BIERMANN, C. 1995. Quantitative subsidence analysis and forward modelling of the Vienna and Danube basins: thin-skinned vs. thick-skinned extension. Tectonophysics 252, 433-451.

LANZA, R. 1982. Models for the interpretation of the magnetic anomaly of the Ivrea body. Geologie Alpine 58, 85-94.

LASKAREV, V.N. 1924. Sur les equivalentes du Sarmatien supérieur en Serbie. Recueil de traveaux ofert a M. Jovan Cvijic par ses amis et collaborateurs, 73–85.

LAUBSCHER, H.P. 1969. Mountain building. Tectonophysics 7, 551–563.

LAUBSCHER, H.P. 1971. The large-scale kinematics of the Western Alps and the Northern Apennines and its palinspastic implications. American Journal of Science 271, 193–226.

LEE, E.Y., WAGREICH, M. 2016. Polyphase tectonic subsidence evolution of the Vienna Basin inferred from quantitative subsidence analysis of the northern and central parts. International Journal of Earth Sciences, doi: 10.1007/s00531-016-1329-9

LEGRAIN, N., DIXON, J., STÜWE, K., VON BLANCKENBURG, F., KUBIK, P. 2015. Post-Miocene landscape rejuvenation at the eastern end of the Alps. Lithosphere 7, 3-13.

LENHARDT, W.A., ŠVANKARA, J., MELAICHAR, P., PAZDÍRKOVÁ, J., HAVÍŘ, J., SÝKOROVÁ, Z. 2007. Seismic activity of the Alpine-Carpathian-Bohemian massif region with regard to geological and potential field data. Geologica Carpathica 58, 397-412.

LETOUZEY, J., WERNER, P., MARTY, A. 1990. Fault reactivation and structural inversion. Backarc and intraplate compressive deformations. Example of the eastern Sunda shelf (Indonesia). Tectonophysics 183, 341-362.

LINZER, H.-G. 1996. Kinematics of retreating subduction along the Carpathian arc, Romania. Geology 24, 167-170.

LINZER, H.-G., DECKER, K., PERESSON, H., DELLMOUR, R., FRISCH, W. 2002. Balancing lateral orogenic float of the Eastern Alps. Tectonophysics 354, 211-237.

LINZER, H.-G., MOSER, F., NEMES, F., RATSCHBACHER, L., SPERNER, B. 1997. Build-up and dismembering of a classical fold-thrust belt: from non-cylindrical staking to lateral extrusion in the eastern Northern Calcareous Alps. Tectonophysics 272, 97-124.

LINZER, H.-G., RATSCHBACHER, L., FRISCH, W. 1995. Transpressional collision structures in the upper crust: the fold-thrust belt of the Northern Calcareous Alps. Tectonophysics 242, 41-61.

LIPPITSCH, R., KISSLING, E., ANSORGE, J. 2003. Upper mantle structure beneath the Alpine orogen from high-resolution teleseismic tomography. Journal of Geophysical Research 108, 2376, doi:10.1029/2002JB002016, B8.

LOHRMANN, J., KUKOWSKI, N., ADAM, J., ONCKEN, O. 2003. The impact of analogue material properties on the geometry, kinematics and dynamics of convergent sand wedges. Journal of Structural Geology 25, 1691-1711.

LOWELL, J.D. 1995. Mechanics of basin inversion from worldwide examples. In: Basin Inversion (Eds. J.G. Buchanan & P.G. Buchanan). Geological Society, London, Special Publication no. 88, pp. 39-57.

MACEDO, J., MARSHAK, S. 1999. Controls on the geometry of fold-thrust salients. Geological Society of America Bulletin 111, 1808-1822.

MACGREGOR, D.S. 1995. Hydrocarbon habitat and classification of inverted rift basins. In: Basin Inversion (Eds. J.G. Buchanan & P.G. Buchanan). Geological Society, London, Special Publication no. 88, pp. 83-93.

MAGNI, V., FACCENA, C., VAN HUNEN, J., FUNICELLO, F. 2013. Delamination vs. break off: the fate of continent collision. Geophisical Research Letters 40, 285-289.

MALAVIEILLE, J. 2010. Impact of erosion, sedimentation, and structural heritage on the structure and kinematics of orogenic wedges: analogue models and case studies. GSA Today 20 (1) doi: 10.1130/GSATG48A.1

MALUSÀ, M.C., FACCENA, C., GARZANTI, E., POLINO, R. 2011. Divergence in subduction zones and exhumation of high pressure rocks (Eocene Western Alps). Earth and Planetary Science Letters 310, 21-32.

MALZ, A., KLEY, J. 2012. The Finne fault zone (central Germany): structural analysis of a partially inverted extensional fault zone by balanced cross-section. International Journal of Earth Sciences 101 (8), 2167-2182.

MANATSCHAL, G., NIEVERGELT, P. 1997. A continent-ocean transition recorded in the Err and Platta nappes (Eastern Switzerland). Eclogae Geol. Helv. 90, 3–27.

MANCKTELOW, N.S., STÖCKLI, D., FÜGENSCHUH, B., SEWARD, D. 1995. Tertiary kinematics of the southwest Tauern Window region. Terra Abstract 7, 123.

MANDIC, O. 2004. Foraminiferal paleocology of a subarine swell – the Lower Badenian (middle Miocene) of the Mailberg Formation at the Buchberg in the Eastern Alpine Foredeep: initial report. Ann. Naturhist. Mus. Wien 105, 161-174.

MANDL, G.W. 2000. The alpine sector of the Tethyan shelf. Examples of Triassic to Jurassic sedimentation and deformation from the Northern Calcareous Alps. Aspects of Geology in Austria. Mitteilungen der Österreich Geologischen Gesellschafft 92, 61-77.

MARRONI, M., MOLLI, G., OTTIA, G., PANDOLFI, L., TRIBUZIO, R. 2002. The External Ligurian Units (Northern Apennine, Italy): From rifting to convergence of a fossil ocean-continent transition zone. Ofioliti 27, 119–132.

MARSHAK, S. 2004. Salients, recesses, arcs, oroclines, and syntaxes: a review of ideas concerning the formation of map-view curves in fold-thrust belts. In: Thrust tectonics and hydrocarbon systems (Ed. K.R. McClay). AAPG Memoir 82, American Association of Petroleum Geologists. Tulsa, pp. 131-156.

MARTÍNEZ, A., VERGÉS, J., CLAVELL, E., KENNEDY, J. 1989. Stratigraphic framework of the thrust geometry and structural inversion in the southeastern Pyrenees: La Garrotxa area. Geodinamica Acta 3 (3), 185-194.

MÁRTON, E., GRABOWSKI, J., PLAŠIENKA, D., TÚNYI, I., KROBICKI, M., HAAS, J., PETHE, M. 2013. New paleomagnetic results from the Upper Cretaceous red marls of the Pieniny klippen Belt, Western Carpathians: Evidence for general CCW rotation and implications for the origin of the structural arc formation. Tectonophysics 592, 1-13.

MÁRTON, E., KUHLEMANN, J., FRISCH, W., DUNKL, I. 2000. Miocene rotations in the Eastern Alps – palaeomagnetic results from intramontane basin sediments. Tectonophysics 323, 163-182.

MATENCO, L., RADIVOJEVIC, D. 2012. On the formation and evolution of the Pannonian Basin: Constraints derived from the structure of the junction are between the Carpathians and Dinarides. Tectonics 31 TC6007, doi:10.1029/2012TC003206.

MAURIN, J.C., NIVIERE, B. 2000. Extensional forced folding and decollement of the pre-rift series along the Rhine graben and their influence on the geometry of the syn-rift sequences. In: Forced folds and fractures (Eds. J.W. Cosgrove & M.S. Ameen) Geological Society, London, Special Publication no. 169, pp. 73-86.

MAZZOLI, S., JANKOWSKI, L., SZANIAWSKI, R., ZATTIN M. 2010. Low-T thermochronometric evidence for post-thrusting (< 11 Ma) exhumation in the Western Outer Carpathians, Poland. Comptes Rendus - Geoscience 342, 162-169.

MCCLAY, K.R. 1989. Analogue models of inversion tectonics. In: Inversion Tectonics (Eds. M.A. Cooper & G.D. Williams). Geological Society, London, Special Publication no. 44, pp. 41-62.

MCCLAY, K.R. 1995. The geometries and kinematics of inverted fault systems: a review of analogue model studies. In: Basin inversion (Eds. J.G. Buchanan & P.G. Buchanan). Geological Society, London, Special Publication 88, pp. 97-118.

MCCLAY, K.R. 1996. Recent advances in analogue modelling: uses in section interpretation and validation. In: Modern developments in structural interpretation, validation and modelling (Eds. P.G. Buchanan & D.A. Nieuwland). Geological Society, London, Special Publications no 99, pp. 201-225.

MCCLAY, K.R., DOOLEY, T., WHITEHOUSE, P., FULLARTON, L., CHANTRAPRASERT, S. 2004. 3d analogue models of rift systems: templates for 3d seismic interpretation. In: 3d Seismic Technology (Eds. R.J. Davies, S.A. Stewart, M. Lappin & J.R. Underhill). Application to the Exploration of Sedimentary Basins. Geological Society, London, Memoirs 29, pp. 101-115.

MCCLAY, K.R., INSLEY, M.W., ANDERTON, R. 1989. Inversion in the Kechika Trough, Northeastern British Columbia, Canada. In: Inversion Tectonics (Eds. M.A. Cooper & G.D. Williams).Geological Society, London, Special Publication no. 44, pp.235-258.

MCKENZIE, D. 1978. Some remarks on the development of sedimentary basins. Earth and Planetary Science Letters 40 (1), 25-32.

MENCOS, J., CARRERA, N., MUÑOZ, J.A. 2015. Influence of rift basin geometry on the subsequent post-rift sedimentation and basin inversion: the Organyà Basin and the Bóixols thrust sheet (south Central Pyrenees). Tectonics 34, 1452-1474. doi:10.1002/2014TC003692.

MITRA, G. 1994. Strain variation in thrust sheets across the Sevier fold-and-thrust belt (Idaho-Utah-Wyoming): implications for section restoration and wedge taper evolution: Journal of Structural Geology 6, p.51–61.

MOLNAR, P., TAPPONNIER, P. 1975. Cenozoic tectonics of Asia: effects on a continental collision. Science 189, 419-426.

MORLEY, C.K. 1993. Discussion of origins of hinterland basins to the Rif-Betic Cordillera and Carpathians. Tectonophysics 226, 359-376.

MORLEY, C.K., NELSON, R.A., PATTON, T.L., MUNN, S.G. 1990. Transfer zones in the East African rift system and their relevance to hydrocarbon exploration in rifts. AAPG Bulletin, 74(8), 1234-1253.

MORLEY, C.K. 2010. Stress re-orientation along zones of weak fabrics in rifts: An explanation for pure extension in 'oblique' rift segments? Earth and Planetary Science Letters 297, 667–673, doi:10.1016/j.epsl.2010.07.022.

MOUTHEREAU, F., DEFFONTAINES, B., LACOMBE, O., ANGELIER, J. 2002. Variations along the strike of the Taiwan thrust belt: basement control on structural style, wedge geometry, and kinematics. In: Geology and Geophysics of an arc-continent collision, Taiwan, Republic of China (Eds. T.B Byrne & C.S. Liu). Geological Society of America, Special Paper 358, Boulder, USA, pp. 35-58

MOUTHEREAU, F., WATTS, A.B., BUROV, E. 2013. Structure of orogenic belts controlled by lithospheric age. Nature Geoscience 6, 785-789.

MUGNIER, J.L., BABY, P., COLLETTA, B., VINOUR, P., BALE, P., LETURMY, P. 1997. Thrust geometry controlled by erosion and sedimentation: a view from analogue models. Geology 25, 427-430.

MUÑOZ, J.A. 2002. Alpine Tectonics I: the alpine system north of the Betic Cordillera tectonic setting: the Pyrenees. In: The Geology of Spain (Eds. W. Gibbons & T. Moreno). Geological Society, London, pp. 370-385.

MUÑOZ, J.A., BEAMUD, E., FERNÁNDEZ, O., ARBUÉS, P., DINARÈS-TURREL, J., POBLET, J. 2013. The Ainsa Fold and Thrust oblique zone of the central Pyrenees: kinematics of a curved contractional system from paleomagnetic and structural data. Tectonics 32, 1142–1175, doi:10.1002/tect.20070.

NACHTMANN, W., WAGNER, L. 1987. Mesozoic and early Tertiary evolution of the Alpine foreland in Upper Austria and Salzburg, Austria. Tectonophysics 137, 61-76.

NEMČOK, M., MORA, A., COSGROVE, J.W. 2013 (EDS). Thick-skinned dominated orogens: from initial inversion to full accretion. Geological Society, London, Special Publication 377, 482pp.

NEMČOK, M., POSPISIL, L., LEXA, J., DONELICK, R.A. 1998. Tertiary subduction and slab break-off model of the Carpathian-Pannonian region. Tectonophysics 295, 307–340.

NEUBAUER, F., GENSER, J., HANDLER, R. 2000. The Eastern Alps: results of a two-stage collision process. Mitteilungen der Österreichischen Geologischen Gesellschaft 92, 117–134.

NEUBAUER, F., HANDLER, R. 2000. Variscan orogeny in the Eastern Alps and Bohemian massif: how do these units correlate. Mitteilungen der Österreichischen Geologischen Gesellschaft 92, 35–59.

NILFOUROUSHAN, F., KOYI, H.A. 2007. Displacement fields and fininte strains in a sandbox model simulating a fold-thrust-belt. Geophysical Journal International 169, 1341-1355.

NILFOUROUSHAN, F., PYSKLYWEC, R., CRUDEN, A., KOYI, H. 2013. Thermal-mechanical modelling of salt-based mountain belts with pre-existing basement faults: Application to the Zagros fold and thrust belt, southwest Iran. Tectonics 32, 1212-1226.

OMV INTERNAL REPORT 2013. Geological work program, exploration well Höflein5b (HOE 5b), Molasse Basin, Austria. Unpublished proprietary report, 21pp.

PANAYOTOPOULOS., Y., HIRATA, N., HASHIMA, A., IWASAKI, T., SAKAI, S., SATO, H. 2016. Seismological evidence of an active footwall shortcut thrust in the Northern Itoigawa-Shizuoka Tectonic Line derived by the aftershock sequence of the 2014 M6.7 Northern Nagano earthquake. Tectonophysics 679, 15-28.

PANIEN, M., SCHREUS, G., PFIFFNER, A.O. 2005. Sandbox experiments on basin inversion: testing the influence of basin orientation and basin fill. Journal of Structural Geology 27, 433-445.

PAPP, A., KROBOT, W., HLADECEK, K. 1973. Zur Gliederung des Neogens im Zentralen Wiener Becken. Mitteilungen der Gesellschaft der Geologie und Bergbaustudenten in Österreich 22, 191-199.

PEACOCK, D.C.P., SANDERSON, D.J. 1991. Displacements, segment linkage and relay ramps in normal fault zones. Journal of Structural Geology 13, 721-733.

PEACOCK, D.C.P., TAVARNELLI, E., ANDERSON, M.W. 2016. Interplay between stress permutations and overpressure to cause strike-slip faulting during tectonic inversion. Terra Nova, doi:10.1111/ter.12249.

PERESSON, H., DECKER, K. 1997. Far-field effects of late Miocene subduction in the Eastern Carpathians: E-W compression and inversion of structures in the Alpine-Carpathian-Pannonian region. Tectonics 16, 38-56.

PERRIN, C., CLEMENZI, L., MALAVIEILLE, J., MOLLI, G., TABOADA, A., DOMINGUEZ, S. 2013. Impact of erosion and décollements on large-scale faulting and folding in orogenic wedges: analogue models and case studies. Journal of the Geological Society 170, 893-904.

PFIFFNER, O.A., ERARD, P.F., STAUBLE, M. 1997. Two cross sections trough the Swiss Molasse Basin. In: Deep Structure of the Swiss Alps: Results of NRP 20 (Eds. O.A. Pfiffner, P. Lehner, P. Heitzmann, St. Mueller & A. Steck). Basel, 64-71.

PFIFFNER, O.A. 2016. Basement-involved thin-skinned and thick-skinned tectonics in the Alps. Geological Magazine 153 (5-6), 1085-1109, doi:10.1017/S0016756815001090.

PHILIPPON, M., WILLINGSHOFER, E., SOKOUTIS, D., CORTI, G., SANI, F., BONINI, M., CLOETINGH, S. 2015. Slip re-orientation in oblique rifts. Geology 43, 147-150.

PICHA, F.J., ZDENĚK, S., KREJČÍ, O. 2006. Geology and hydrocarbon resources of the Outer Western Carpathians and their foreland, Czech Republic. In: The Carpathians and their foreland: Geology and hydrocarbon resources (Eds. J. Golonka & F.J. Picha). AAPG Memoir 84, Tulsa, pp. 49-175.

PILLER, W.E., HARZHAUSER, M., MANDIC, O. 2007. Miocene Central Paratethys stratigraphy – current status and future directions. Stratigraphy 4, 151-168.

PLAŠIENKA, D., GRECULA, P, PUTIŠ, M., HOVORKA, D., KOVAĆ, M. 1997a. Evolution and structure of the Western Carpathians: an overview. In: Geological Evolution of the Western Carpathians (Eds P. Grecula, D. Hovorka & M. Putiš). Mineralia Slovaca Monograph, Bratislava, pp. 1–24.

PLAŠIENKA, D., PUTIŠ, M., KOVAĆ, M., ŠEFARA, J., HRUŠECKÝ, I. 1997b. Zones of Alpidic subduction and crustal underthrusting in the Western Carpathians. In: In: Geological Evolution of the Western Carpathians (Eds P. Grecula, D. Hovorka & M. Putiš). Mineralia Slovaca Monograph, Bratislava, pp. 35–42.

PLATT, J.P. 1986. Dynamics of orogenic wedges and the uplift of high-pressure metamorphic rocks. Geological Society of America Bulletin 96, 1037–53.

PLEUGER, J., ROLLER, S., WALTER, J.M., JANSEN, E., FROITZHEIM, N. 2007. Structural evolution of the contact between two Penninic nappes (Zermatt-Saas zone and Combin zone, Western Alps) and implications for the exhumation mechanism and palaeogeography. International Journal of Earth Science 96, 229-252.

PUJADAS, J., CASAS, J.A., MUÑOZ, J.A., SÀBAT, F. 1989. Thrust tectonics and paleogene syntectonic sedimentation in the Empordà area, Southeastern Pyrenees. Geodinamica Acta 3 (3), 195-206.

QORBANI, E., BIANCHI, I., BOKELMANN, G. 2014. Slab detachment under the Eastern Alps seen by seismic anisotropy. Earth and Planetary Science Letters 409, 96-108.

RAMSAY, J.G. 1967. Folding and Fracturing of Rocks. McGraw-Hill, New York. 568pp.

RATSCHBACHER, L., FRISCH, W., LINZER, H.G., MERLE, O. 1991b. Lateral extrusion in the Eastern Alps, part 2. Structural analysis. Tectonics 10 (2), 257-271.

RATSCHBACHER, L., MERLE, O., DAVY, P., COOBOLD, P. 1990a. Lateral extrusion in the Eastern Alps, part 1: Boundary conditions and experiments scaled for gravity. Tectonics 10 (2) 245-256.

REBAÏ, S., PHILIP, H., TABOADA, A. 1992. Modern tectonic stress field in the Mediterranean region: evidence for variation in stress directions at different scales. Geophysical Journal International 110, 106-140.

REINECKER, J., LENHARDT, W.A. 1999. Present-day stress field and deformation in eastern Austria. International Journal of Earth Sciences 88, 532-550.

ROCA, E., BESSEREAU, G., JAWOR, E., KOTARBA, M., ROURE, F. 1995. Pre-Neogene evolution of the Westem Carpathians: constraints from the Bochnia-Tatra Mountains section (Polish Western Carpathians). Tectonics 14 (4), 855-873.

ROEDER, D. 2010. Fold-thrust belts at Peak Oil. In: Hydrocarbons in constractional belts (Eds. G.P. Goofey, J. Craig, T. Needham & R. Scott). Geological Society, London, Special Publication no. 348, pp 7-31.

RÖGL, F., PEZZAFERRI, S., CORIC, S. 2002. Micropaleontology and biostratigraphy of the Karpatian-Badenian transition (Early-Middle Miocene boundary) in Austria (Central Paratethys). Courier Forschungsinstitut Senckenberg 237, 47-67.

RÖGL, F., STEININGER, F.F. 1983. Vom Zerfall der Tethys zu Mediterran und Paratethys. Die neogene Paläogeographie und Palinspastik des zirkum-mediterranen Raumes. Annalen des Naturhistorischen Museums, Wien, 85/A: 135-163.

ROSENBAUM, G., LISTER, G.S. 2005. The Western Alps from the Jurassic to Oligocene: spatiotemporal constraints and evolutionary reconstructions. Earth Science Reviews 69, 281–306.

ROSENBAUM, G., LISTER, G.S., DUBOZ, C. 2002. Relative motions of Africa, Iberia and Europe during Alpine orogeny. Tectonophysics 359, 117–129.

ROURE, F., BERGERAT, F., DAMOTTE, B., MUGNIER, J.L., POLINO, R. (EDS.) 1996. The ECORS-CROP Alpine Seismic Traverse. Bulleting Société Géologique de France 170, 1-113.

ROURE, F., COLLETTA, B., 1996. Cenozoic inversion structures in the foreland of the Pyrenees and Alps. In: Peri-Tethys Memoir 2: Structure and Prospects of the Alpine Basins and Forelands (Eds. P.A. Ziegler & F. Horvath). Mémoires Muséum National d'Histoire Naturelle 170, Paris, pp. 173-209.

ROURE, F., ROCA, E., SASSI, W. 1993. The Neogene evolution of the outer Carpathian flysch units (Poland, Ukraine and Romania): kinematics of a foreland/fold-and-thrust belt system. Sedimentary Geology 86, 177-201.

ROYDEN, L.H. 1985. The Vienna Basin: a thin-skinned pull-apart basin. In: Strike Slip Deformation, Basin Formation and Sedimentation (Eds. K. Biddle & K. Kristie-Blick). Society of Economic Paleontologists and Mineralogists, Special Publication no. 37, Tulsa, pp. 319–338.

ROYDEN, L.H., DÖVÉNYI, P. 1988. Variations in extensional styles at depth across the Pannonian Basin system. In: The Pannonian Basin, a study of basin evolution (Eds. L.H. Royden & F. Horvárth) The American Association of Petroleum Geologists, Memoir 45, Tulsa, 235-255.

RUH, J.B., KAUS, B.J.P., BURG, J.P. 2012. Numerical investigation of deformation mechanics in fold-and-thrust belts: Influence of rheology of single and multiple décollements. Tectonics 31 TC3005, doi:10.1029/2011TC003047.

RUTTER, E.H., HOLDSWORTH, R.E., KNIPE, R.J. 2001. The nature and tectonic significance of fault-zone weakening: an introduction. In: The nature and tectonic significance of fault-zone weakening (Eds. R.E. Holdsworth, R.A. Strachan, J.F. Magloughlin & R.J. Knipe). Geological Society, London, Special Publication no. 186, pp. 1-11.

RUTTER, E.H. 1986. On the nomenclature of mode of failure transitions in rocks. Tectonophysics 122, 381-387.

SACHSENHOFER, R.F., BECHTEL, A., KUFFNER, T., RAINER, R., GRATZER, R., SAUER, R. SPERL, H. 2006. Depositional environment and source potential of Jurassic coal-bearing sediments (Gresten Formation, Höflein gas/condensate field, Austria). Petroleum Geoscience 12, 99-114.

SACHSENHOFER, R.F., KOGLER, A., POLESNY, H., STRAUSS, P., WAGREICH, M. 2000. The Neogene Fohnsdorf Basin: Basin formation and basin inversion during the lateral extrusion in the Eastern Alps (Austria). International Journal of Earth Sciences 89, 415–430.

SALAS, R., GUIMERÀ, J., MAS, R., MARTÍN-CLOSAS, C., MELÉNDEZ, A., ALONSO, A. 2001. Evolution of the Mesozoic Central Iberian System and its Cainozoic inversion (Iberian Chain). In: Peri-Tethys Memoir 6: Peri-Tethyan Rift/Wrench Basins and Passive Margins. (Eds. P.A. Ziegler, W. Cavazza, A.H.F. Robertson & S. Crasquin-Soleau). Mém. Mus. natn. Hist. nat. 186, Paris pp. 145-185.

SĂNDULESCU, M. 1994. Overview on Romanian Geology 2. Alcapa Congress Field Guidebook. Romanian Journal of Tectonics and Regional Geology 75 Suppl. 2, 3–15.

SANTOLARIA, P., VENDEVILLE, B.C., GRAVELEAU, F., SOTO, R., CASAS-SAINZ, A. 2015. Double evaporitic décollements: Influence on pinch-out overlapping in experimental thrust wedges. Journal of Structural Geology 76, 35-51.

SASSI, W., COLLETTA, B., BALÉ, P., PAQUEREAU, T., 1993. Modelling of structural complexity in sedimentary basins: the role of pre-existing faults in thrust tectonics. Tectonophysics 226, 97-112.

SAUER, R., SEIFERT, P., WESSELY, G. 1992. Guidebook to excursions in the Vienna Basin and the adjacent Alpine-Carpathian thrust belt in Austria. Mitteilungen der Österreichischen Geologischen Gesellschaft 85, 1-264.

SCHCLUNEGGER, F., KISSLING, E. 2015. Slab rollback orogeny in the Alps and evolution of the Swiss Molasse Basin. Nature Communications 6, 1-10, doi:10.1038/ncomms9605.

SCHELLART, W.P. 2000. Shear test results for cohesion and friction coefficients for different granular materials: scaling implications for their usage in analogue modelling. Tectonophysics 324, 1-16.

SCHELLART, W.P., STRAK, V. 2016. A review of analogue modelling of geodynamic processes: Approaches, scaling, materials and quantification, with an application to subduction experiments. Journal of Geodynamics 100, 7-32.

SCHMID, S.M., FÜGENSHCHUH, B., KISSLING, E., SCHUSTER, R. 2004. Tectonic map and overall architecture of the Alpine orogen. Eclogae Geologicae Helvetiae 97, 93-117.

SCHMID, S.M., AEBLI, H.R., HELLER, F., ZINGG, A. 1989. The role of the Periadriatic Line in the tectonic evolution of the Alps. In: Alpine Tectonics (Eds. M.P.A. Coward, D. Dietrich & R.G. Park). Geological Society, London, Special Publication no. 45, pp. 153-171.

SCHMID, S.M., BERNOULLI, D., FÜGENSCHUH, B., MATENCO, L., SCHEFER, S., SCHUSTER, R., TISCHLER, M., UZTASZEWSKI, K. 2008. The Alpine-Carpathian-Dinaridic orogenic system: correlation and evolution of tectonic units. Swiss Journal of Geoscience 101, 139-183, doi:10.1007/s00015-008-1247-3.

SCHMID, S.M., KISSLING, E. 2000. The arc of the western Alps in the light of geophysical data on deep crustal structure. Tectonics 19 (1), 62–85.

SCHMID, S.M., PFIFFNER, O.A., FROITZHEIM, N. SCHÖNBORN, G., KISSLING, E. 1996. Geophysical-geological transect and tectonic evolution of the Swiss-Italian Alps. Tectonics 15, 1036-1064.

SCHMID, S.M., RÜCK, P., SCHREURS, G. 1990. The significance of the Schams nappes for the reconstruction of the paleotectonic and orogenic evolution of the Penninic Zone along the NPF-20 East traverse (Grisons, eastern Switzerland). Mémoires de la Société Géologique de France 156, 263-287.

SCHNABEL, G. W. 1992. New data on the Flysch Zone of the Eastern Alps in the Austrian sector and new aspects concerning the transition to the Flysch Zone of the Carpathians. Cretaceous Research 13, 405-419.

SCHNEIDER, S., HARZHAUSER, M., KROH, A., LUKENEDER, A., ZUSCHIN, M. 2013. Ernstbrunn Limestone and Klentnice beds (Kimmeridgian-Berriasian; Waschberg-Ždánice Unit; NE Austria and SE Czech Republic): state of the art and bibliography. Bulletin of Geosciences 88, 105-130, doi:10.3140/bull.geosci.1360.

SCHOLZ, C.H. 1988. The brittle-plastic transition and the depth of seismic faulting. Geologische Rundschau 77 (1), 319-328.

SCHREURS, G., BUITER, S.J.H., BOUTELIER, D., CORTI, G., COSTA, E., CRUDEN, A.R., DANIEL, J.-M., HOTH, S., KOYI, H.A., KUKOWSKI, N., LOHRMANN, J., RAVAGLIA, A., SCHLISCHE, R.W., WITHJACK, M.O., YAMADA, Y., CAVOZZI, C., DELVENTISETTE, C., ELDER BRADY, J.A., HOFFMANN-ROTHE, A., MENGUS, J.-M., MONTANARI, D., NILFOROUSHAN, F. 2006. Analogue benchmarks of shortening and extension experiments. In: Analogue and Numerical Modelling of Crustal-scale Processes (Eds. S.J.H. Buiter & G. Schreurs,). Geological Society, London, Special Publication, no. 253, pp. 1-27.

SCHRÖDER, B. 1987. Inversion tectonics along the western margin of the Bohemian massif. Tectonophysics 137, 93-100.

SCHUSTER, R. 2004. The Austroalpine crystalline units in the Eastern Alps. Abstract Volume PANGEO 2004. Berichte des Intituts für Erdwissenschaften der Karl-Franzens-Üniversität Graz 9, 30-36.

SCISCIANI, V. 2009. Styles of positive inversion tectonics in the Central Apennines and in the Adriatic foreland: Implications for the evolution of the Apennine chain (Italy). Journal of Structural Geology 31, 1276-1294.

SEGHEDI, I., DOWNES, H., VASELLI, O., SZAKÁCS, A., BALOGH, K., PÉCSKAY, Z. 2004. Post-collisional Tertiary-Quaternary mafic alkali magmatism in the Carpathian-Pannonian region: a review. Tectonophysics 393, 43-62.

SEIFERT, P. 1992. Palinspastic reconstruction of the easternmost Alps between upper Eocene and Miocene. Geologica Carpathica 43, 327–331.

SELVERSTONE, J. 1988. Evidence for east-west crustal extension in the Eastern Alps: implications for the unroofing history of the Tauern Window. Tectonics 7, 87-105.

SHINER, P., BECCACINI, A., MAZZOLI, S. 2004. Thin-skinned versus thick-skinned structural models for Apulian carbonate reservoirs: constraints from the Val d'Agri Fields, S. Apennines, Italy. Marine and Petroleum Geology 21, 805-827.

SIBSON, R.H. 1985. A note of fault reactivation. Journal of Structural Geology 7, 751–754.

SIBSON, R.H. 1990. Rupture nucleation on unfavourably oriented faults. Bulletin of the Seismological Society of America 80, 1580–1604.

SIBSON, R.H. 2001. Seismogenic framework for hydrothermal transport and ore deposition. In: Structural Controls on Ore Genesis (Eds. J. P. Richards & R.M. Tosdal). Society of Economic Geologists, Littleton, USA. Reviews in Economic Geology, Reviews no. 14, pp. 25-47.

SIBSON, R.H. 1983. Continental fault structure and the shallow earthquake source. Journal of the Geological Society of London 140, 741-767.

SIBSON, R.H. 2007. An episode of fault-valve behavior during compressional inversion? – the 2004 MJ6.8 Mid-Niigata Prefecture, Japan, earthquake sequence. Earth and Planetary Science Letters 257, 188-199.

SINCLAIR, H.D. 1997. Tectonostratigraphic model for underfilled peripheral foreland basins: An Alpine perspective. Geological Society America Bulletin 109 (3), 324-346.

SMIT, J.H. W., BRUN, J.P., SOKOUTIS, D., 2003. Deformation of brittle-ductile thrust wedges in experiments and nature. Journal of Geophysical Research 108, doi:10.1029/2002JB002190.

SMITH, A.G. 1971. Alpine deformation and oceanic areas of the Tethys, Mediterranean and Atlantic. Geological Society of America Bulletin 82, 2039–2070.

SOTO, R., STORTI, F., CASAS-SAINZ, A. 2006. Impact of backstop thickness lateral variations on the tectonic architecture of orogens: Insights from sandbox analogue modelling and application to the Pyrenees. Tectonics 25, TC2005, doi:10.1029/2004TC001693.

ŠPIČÁKOVÁ, L., ULIČNÝ, D., KOULDLKOVÁ, G. 2000. Tectonosedimentary evolution of the Cheb Basin (NW Bohemia, Czech Republic) between Late Oligocene and Pliocene: A preliminary note. Studia Geophysica et Geodetica 44, 556-580.

STAMPFLI, G.D. 1993. Le Briançonnais, terrain exotique dans les Alpes? Eclogae geolicae Helvetiae 86 (1), 1-45.

STAMPFLI, G.M., BOREL, G.D. 2002. A plate tectonic model for the Paleozoic and Mesozoic constrained by dynamic plate boundaries and restored synthetic oceanic isochrons. Earth and Planetary Science Letters 196, 17-33.

STAMPFLI, G.M., BOREL, G.D. 2004. The TRANSMED transects in space and time: constraints on the Paleotectonic evolution of the Mediterranean Domain. In: The TRANSMED Atlas - The Mediterranean Region from Crust to Mantle (Eds. W. Cavazza, F. Roure, W. Spakman, G.M. Stamplfli, P.A. Ziegler). Springer-Verlag, Berlin-Heidelberg, pp. 53-80.

STEARNS, D.W. 1978. Faulting and forced folding in the Rocky Mountain foreland. Geological Society of America Memoir 151, 1-38.

STIPP, M., FÜGENSCHUH, B., GROMET, L.P., STÜNIZT, H., SCHMID, S.M. 2004. Contemporaneous plutonism and strike-slip faulting: A case study from the Tonale fault zone north of the Adamello pluton (Italian Alps). Tectonics 23, TC3004, doi:10.1029/2003TC001515.

STORTI, F., MCCLAY, K., 1995. Influence of syntectonic sedimentation on thrust wedges in analogue models. Geology 23 (11) 999-1002.

STORTI, F., SOTO, R., ROSSETTI, F., CASAS-SAINZ, A. 2007. Evolution of experimental thrust wedges accreted from along-strike tapered silicone-floored multilayers. Journal of the Geological Society, London, 164, 73-85.

STRAUSS, P., HARZHAUSER, M., HINSCH, R., WAGREICH, M. 2006. Sequence stratigraphy in a classic pull-apart basin (Neogene, Vienna Basin). A 3D seismic based integrated approach. Geologica Carpathica 57, 185-197.

STRAUSS, P., WAGREICH, M., DECKER, K., SACHSENHOFER, R. F. 2001. Tectonics and sedimentation in the Fohnsdorf-Seckau Basin (Miocene, Austria): from a pull-apart basin to a half-graben. International Journal of Earth Sciences 90, 549–559.

SUESS, E. 1875. Die Entstehung der Alpen. Braunmüller, Wien. 168pp.

SZANIAWSKI, R., MAZZOLI, S., JANKOWSKI, L., ZATTIN, M. 2013. No large-magnitude tectonic rotations of the Subsilesian Unit of the Outer Western Carpathians: Evidence from primary magnetization recorded in hematite-bearing Węglówka Marls. Journal of Geodynamics 71, 14-24.

TARI, G. 2005. The divergent continental margins of the Jurassic proto-Pannonian Basin: implications for the petroleum systems of the Vienna Basin and Moesian Platform. 25th Annual Bob. F. Perkins Research Conference: Petroleum Systems of Divergent Continental Margin Basins. Society of the Sedimentary Geology, Gulf Coast Section, 955-986.

TARI, G., HORVÁRTH, F., RUMPLER, J. 1992. Styles of extension in the Pannonian Basin. Tectonophysics 208, 203-219.

TASSONE, A., ROCA, E., MUÑOZ, J.A., CABRERA, L., CANALS, M. 1994. Evolución del sector septentrional del margen continental catalán durante el Cenozoico. Acta Geologica Hispanica 29, 3-37.

TAVANI, S., STORTI, S., LACOMBE, O., CORRADETTI, A., MUÑOZ, J.A., MAZZOLI, S. 2015. A review of deformation pattern templates in foreland basin systems and fold-and-thrust belts: Implications for the state of stress in the frontal regions of thrust wedges. Earth-Science Reviews 141, 82-104, doi:10.1016/j.earscirev.2014.11.013.

TAVANI, S., ARBUÉS, P., SNIDERO, M., CARRERA, N., MUÑOZ, J.A. 2011. Open Plot Project: an open-source toolkit for 3-D structural data analysis. Solid Earth 2, 53-63.

TAVANI, S., GRANADO, P. 2015. Along-strike evolution of folding, stretching and breaching of supra-salt strata in the Plataforma Burgalesa extensional forced fold system (northern Spain). Basin Research 27, 573-585.

THOMAS, D.W., COWARD, M.P.A. 1995. Late Jurassic-Lower Cretaceous inversion of the northern East Shetland Basin, northern North Sea. In: Basin Inversion (Eds. J.G. Buchanan & P.G. Buchanan). Geological Society, London, Special Publication no. 88, pp. 275-306.

THÖNY, W., ORTNER, H., SCHOLGER, R. 2006. Paleomagnetic evidence for large en-bloc rotations in the Eastern Alps during Neogene orogeny. Tectonophysics 414, 169–189.

TOLLMANN, A. 1959. Der Deckenbau der Ostalpen auf Grund der Neuuntersuchung des zentralpin Mesozoikums. Mitteilungen der Österreich Geologischen Bergbaustud 10, 1-62.

TOLLMANN, A. 1977. Geologie von Österreich, 1. Die Zentralalpen. XVI+766 S. Wien.

TOLLMANN, A. 1985. Geologie von Österreich, 2. Auβer-zentralpiner Anteil. Wien (Franz Deuticke).

TOLLMANN, A. 1986. Geologie von Österreich, 3. Gesamtübersicht. Wien (Franz Deuticke).

TOMEK, Č., HALL, J. 1993. Subducted continental margin imaged in the Carpathians of Czechoslovakia. Geology 21, 535-538.

TRANSALP WORKING GROUP. 2002. First deep seismic reflection images of the Eastern Alps reveal giant crustal wedges and transcrustal ramps. Geophysical Research Letters 29 doi:10.1029/2001GL014911.

TRAUTWEIN, B. 2000. Detritus provenance and thermal history of the Rhenodanubian flysch zone: mosaic stones for the reconstruction of the geodynamic evolution of the Eastern Alps. Tübinger Geowiss Arb A59, 1-68

TRAUTWEIN, B., DUNKL, I., FRISCH, W. 2001. Accretionary history of the Rhenodanubian flysch zone in the Eastern Alps – evidence from apatite fission-track geochronology. International Journal of Earth Sciences 90, 703-713

TRÜMPY, R. 2001. Why plate tectonics was not invented in the Alps. International Journal of Earth Sciences 90, 477-483.

TURCOTTE, D.L., SCHUBERT, G. 1982. Geodynamics. Wiley, New York.

TURNER, J.P., WILLIAMS, G.A. 2004. Sedimentary basin inversion and intra-plate shortening. Earth-Science Reviews 65, 277–304.

TWISS, R.J., MOORES, E.M. 1992. Structural Geology. Freeman, San Francisco.

ULIANA, M.A., ARTEAGA, M.E., LEGARRETA, L., CERDAN, L., PERONI, G.H. 1995. Inversion structures and hydrocarbon occurrence in Argentina. In: Basin inversion (Eds. J.G. Buchanan & P.G. Buchanan). Geological Society, London, Special Publication no. 88, pp. 211-234.

USTASZEWSKI, K., SCHMID, S., FÜGENSCHUH, B., TISCHLER, M., KISSLING, E., SPAKMAN, W. 2008. A map-view restoration of the Alpine-Carpathian-Dinaridic system for the early Miocene. Swiss Journal of Geosciences 101, 273-294.

VERNANT, PH., NILFOROUSHAN, F., HATZFELD, D., ABBASI, M.R., VIGNY, C., MASSON, F., NANKALI, H., MARTINOD, J., ASHTIANI, A., BAYER, R., TAVAKOLI, F., CHÉRY, J. 2004. Present-day crustal deformation and plate kinematics in the Middle East constrained by GPS measurements in Iran and northern Oman. Geophysical Journal International 157, 381-398.

VIALLY, R., LETOUZEY, J., BENARD, F., HADDADI, N., DESFORGES, G., ASKRI, H., BOUDJEMA, A. 1994. Basin inversion along the North African Margin: the Saharan Atlas (Algeria). In: Peri-Tethyan Platforms (Ed. F. Roure). Editions Technip, Paris, pp. 79-120.

VON BLANCKENBURG, F., DAVIES, J.H. 1995. Slab breakoff: A model for syncollisional magmatism and tectonics in the Alps. Tectonics 14, 120–131.

WAGNER, L.R. 1996. Stratigraphy and hydrocarbons in the Upper Austrian Molasse Foredeep (active margin). In: Oil and Gas in Alpidic Thrustbelts and Basins of Central and Eastern Europe (Eds. G. Wessely & W. Liebl). Geological Society, London, EAGE Special Publication no. 5, pp. 217–235.

WAGNER, L.R. 1998. Tectono-stratigraphy in the Molasse Foredeep of Salzburg, Upper and Lower Austria. In: Cenozoic Foreland Basins of Western Europe (Eds. A. Mascle, C. Puigdefàbregas, H.P. Luterbacher & M. Fernàndez). Geological Society, London, Special Publication 134, pp. 339–369.

WAGREICH, M. 1993. Subcrustal tectonic erosion in orogenic belts. A model for the Upper Cretaceous subsidence of the Northern Calcareous Alps (Austria). Geology, 21: 941–944.

WAGREICH, M. 2001. A 400-km-long piggyback basin (Upper Aptian-Lower Cenomanian) in the Eastern Alps. Terra Nova 13, 401-406.

WATTS, A.B., BUROV, E.B. 2003. Lithospheric strength and its relationships to the elastic and seismogenic layer thickness. Earth and Planetary Science Letters 213, 113-131.

WEIJERMARS, R., JACKSON, M.P.A., VENDEVILLE, B.C. 1993. Rheological and tectonic modelling of salt provinces. Tectonophysics 217, 143-174.

WEIJERMARS, R., SCHMELING, H. 1986. Scaling of Newtonian and non-Newtonian fluid dynamics without inertia for qualitative modelling of rock flow due to gravity. Physics of the Earth and Planetary Interiors 43, 316-330.

WERNICKE, B., BURCHFIELD, B.C. 1982. Models of extensional tectonics. Inaugural meeting of the Canadian Tectonics Group 4, 105-115.

WESSELY, G. 1987. Mesozoic and Tertiary evolution of the Alpine-Carpathian foreland in eastern Austria. Tectonophysics 137, 45-49.

WESSELY, G. 1988. Structure and development of the Vienna Basin in Austria. In: The Pannonian Basin: a Study of Basin Evolution (Eds. L.H. Royden & F. Horvárth). Memoir 45, America Association of Petroleum Geologists, Tulsa, pp. 333-346.

WESSELY, G. 1992. The Calcareous Alps below the Vienna Basin in Austria and their structural and facial development in the Alpine-Carpathian border zone. Geological Carpathica 43 (6), 347-353.

WESSELY, G. 2006. Geologie der Österreichischen Bundesländer. Geologische Bundesanstalt, Wien, 416 pp.

WESSELY, G., LIEBL, W. 1996 (EDS). Oil and Gas in Alpidic Thrustbelts and Basins of Central and Eastern Europe (Geological Society, London, EAGE Special Publication no. 5., 456pp.

WHITE, N.J., JACKSON, J.A., MCKENZIE, D.P. 1986. The relationship between the geometry of normal faults and that of the sedimentary layers in their hanging walls. Journal of Structural Geology 8, 897-909.

WIBBERLEY, C.A.J. 2005. Initiation of basement thrust detachments by fault-zone reaction weakening. In: High Strain Zones: Structure and Physical Properties. (Eds. D. Bruhn & L. Burlini). Geological Society, London, Special Publication no. 245, pp. 347–372.

WIBBERLEY, C.A.J., KURZ, W., IMBER, J., HOLDSWORTH, R.E., COLLETINI, C. 2008 (EDS.). The internal structure of fault zones: Implications for Mechanical and Fluid-flow Properties. Geological Society, London, Special Publication no. 299, pp.5-33.

WILLEMSE, E.J.M., POLLARD, D.D., AYDIN, A. 1996. Three-dimensional analysis of slip distributions on normal fault arrays with consequences for fault scaling. Journal of Structural Geology 18, 295-309.

WILLIAMS, G.D., POWELL, C.M., COOPER, M.A. 1989. Geometry and kinematics of inversion tectonics. In: Inversion Tectonics (Eds. M.A. Cooper & G.D. Williams). Geological Society, London, Special Publication no. 44, pp. 3-15.

WITHJACK, M.O., OLSON, J., PETERSON, E. 1990. Experimental models of extensional forced folds. American Association of Petroleum Geologists Bulletin 74, 1038-1054.

WITHJACK, M.O., SCHLISCHE, R.W. 2006. Geometric and experimental models of extensional fault-bend folds. In: Analogue and Numerical of Crustal-Scale Processes (Eds. S.J.H. Buiter & G. Schreurs). Geological Society, London, Special Publication no. 253, pp. 285-305.

WÖLFLER, A., KURZ, W., FRIZT, H., STÜWE, K. 2011. Lateral extrusion in the Eastern Alps revisited: refining the model by thermochronological, sedimentary, and seismic data. Tectonics 30, TC4006, doi:10.1029/2010TC002782.

WOODWARD, N.B., GREY, D.R., SPEARS, D.B. 1986. Including strain data in balanced cross-sections. Journal of Structural Geology 8, 313–324.

XIAO, H., SUPPE, J. 1992. Origin of rollover. American Association of Petroleum Geologists Bulletin 76, 509-529.

YAMADA, Y., MCCLAY, K.R. 2004. 3-D Analogue modelling of inversion thrust structures. In: Thrust tectonics and hydrocarbon systems (Ed. K.R. McClay). America Association of Petroleum Geologists, Tulsa, Memoir 82, pp. 276– 301.

ZATTIN, M., ANDREUCCI, B., JANKOWSKI, L., MAZZOLI, S., SZANIAWSKI, R. 2011. Neogene exhumation in the Outer Western Carpathians. Terra Nova 23, 283-291.

ZIEGLER, P.A. 1987. Compressional intraplate deformation in the Alpine foreland – an introduction. Tectonophysics 137 (1-4), 1-5.

ZIEGLER, P.A., BERTOTTI, G.V., CLOETINGH, S. 2002. Dynamic processes controlling foreland development. The role of mechanical decoupling of orogenic wedges and forelands. European Geosciences Union, Stephan Mueller Special Publications v.1, 17-56.

ZIEGLER, P.A., CLOETINGH, S., GUIRAUD, R., STAMPFLI, G. 2001. Peri-Tethyan platforms: constraints on dynamics of rifting and basin inversion. In: Peri-Tethys Memoir 6: Peri-Tethyan rift/wrench basins and passive margins (Eds. P.A. Ziegler, W. Cavazza, A.H.F. Robertson & S. Crasquin-Soleau). Mém. Mus. natn. Hist. nat., Paris, no. 186, pp. 9-49.

ZIEGLER, P.A., CLOETINGH, S., VAN WEES, J.D. 1995. Dynamics of intra-plate compressional deformation: the Alpine foreland and other examples. Tectonophysics 252, 7-59.

ZIEGLER, P.A., VAN WEES, J.D., CLOETINGH, S. 1998. Mechanical controls on collision-related compressional intraplate deformation. Tectonophysics 300, 103-129.

ZIMMER, W., WESSELY, G. 1996. Exploration results in thrust and sub-thrust complexes in the Alps and below the Vienna Basin in Austria. In: Oil and Gas in Alpidic Thrustbelts and Basins of Central and Eastern Europe (Eds. G. Wessely & W. Liebl). Geological Society, London, EAGE Special Publication no. 5, pp. 81-107.

ZOBACK, M.D. 2010. Reservoir Geomechanics. Cambridge University Press, Cambridge, UK. 449 pp.

ZULAUF, G. 1993. Brittle deformation events at the western border of the Bohemian massif (Germany). Geologische Rundschau 82 (3), 489-504.

APPENDIX

Basement-involved reactivation in fold-and-thrust belts: the Alpine-Carpathian Junction (Austria)

Geol. Mag. **153** (*5/6*), *2016, pp. 1110–1135.* © *Cambridge University Press 2016*
doi:10.1017/S0016756816000066

Basement-involved reactivation in foreland fold-and-thrust belts: the Alpine–Carpathian Junction (Austria)

P. GRANADO*†, W. THÖNY‡, N. CARRERA*, O. GRATZER‡, P. STRAUSS‡ & J. A. MUÑOZ*

*Institut de Recerca Geomodels, Departament de Geodinàmica i Geofísica, Facultat de Geologia, Universitat de Barcelona, Martí i Franquès s/n, 08028 Barcelona, Spain
‡OMV AUSTRIA Exploration and Production GmbH, Trabrennstraße 6–8. 1020 Vienna, Austria

(*Received* 21 October 2015; *accepted* 7 January 2016; *first published online* 23 February 2016)

Abstract – The late Eocene – early Miocene Alpine–Carpathian fold-and-thrust belt (FTB) lies in the transition between the Eastern Alps and the Western Carpathians, SE of the Bohemian crystalline massif. Our study shows the involvement of crystalline basement from the former European Jurassic continental margin in two distinct events. A first extensional event coeval with Eggerian–Karpatian (*c.* 28–16 Ma) thin-skinned thrusting reactivated the rift basement fault array and resulted from the large degree of lower plate bending promoted by high lateral gradients of lithospheric strength and slab pull forces. Slab break-off during the final stages of collision around Karpatian times (*c.* 17–16 Ma) promoted large-wavelength uplift and an excessive topographic load. This load was reduced by broadening the orogenic wedge through the reactivation of the lower-plate deep detachment beneath and ahead of the thin-skinned thrust front (with the accompanying positive inversion of the basement fault array) and ultimately, by the collapse of the hinterland summits, enhanced by transtensional faulting. Although this work specifically deals with the involvement of the basement in the Alpine–Carpathian Junction, the main conclusions are of general interest to the understanding of orogenic systems.

Keywords: Alpine–Carpathian Junction, thin-skinned, thick-skinned, basin inversion, slab break-off.

1. Introduction

There is a growing body of literature recognizing that the commonly used transition from thick-skinned dominated regions in the orogenic hinterlands to purely thin-skinned dominated regions in adjacent forelands does not reflect the heterogeneous degree of crustal coupling observed in fold-and-thrust belts (FTB) worldwide (e.g. Cooper, 2007; Goofey *et al.* 2010). Compelling evidence for mixed modes of deformation taking place at different places and times for one single FTB have been undoubtedly recognized (e.g. Salas *et al.* 2001; Lacombe & Mouthereau, 2002; Mouthereau *et al.* 2002; Lacombe, Mouthereau & Angelier, 2003; Butler & Mazzoli, 2006; Butler, Tavarnelli & Grasso, 2006). The fundamental factors controlling the degree of crustal coupling within FTB are: (1) the presence and distribution of efficient decollement levels (e.g. Davis & Engelder, 1985; Macedo & Marshak, 1999; Carola *et al.* 2013; Farzipour-Saein, Nilfouroushan & Koyi, 2013; Muñoz *et al.* 2013); (2) the inheritance of rift-related structures and amount of convergence (e.g. Desegaulx, Kooi & Cloetingh, 1991; Macedo & Marshak, 1999; Marshak, 2004; Butler, Tavarnelli & Grasso, 2006; Brown *et al.* 2012); (3) the orientation and magnitude of the stress field as well as the strain rate (e.g. Rebaï, Philip & Taboada, 1992; Ziegler, Cloetingh & van Wees, 1995; Vernant *et al.* 2004; Zoback, 2010); and (4) the integrated lithospheric strength profile as well as its evolution through time (e.g. Burov & Diament, 1995; Ziegler, Cloetingh & van Wees, 1995; Cloetingh & Burov, 1996; Ziegler, van Wees & Cloetingh, 1998; Ziegler *et al.* 2001; Watts & Burov, 2003; Holdsworth, 2004; Butler, Tavarnelli & Grasso, 2006; Mouthereau, Watts & Burov, 2013).

In addition to this, widespread extension is a recognized process taking place during orogenic shortening as a result of several mechanisms such as unroofing of the orogenic wedge and lateral escape of crustal blocks (e.g. Molnar & Tapponnier, 1975; Platt, 1986; Dewey, 1988; Ratschbacher *et al.* 1991; Fossen, 2000). Extension and creation of accommodation space in the lower plate of orogenic wedges (i.e. in the foreland basin) has also been recognized in relation to the flexural isostatic subsidence in response to the growing weight of the orogenic wedge and the slab pull and slab retreat forces derived from the sinking lower plate (e.g. Bradley & Kidd, 1991; DeCelles & Gilles, 1996; Andeweg & Cloetingh, 1998; García-Castellanos & Cloetingh, 2012; Schlunegger & Kissling, 2015). Such complex evolution of orogenic systems and associated FTB has also been demonstrated by numerical (e.g. García-Castellanos, Fernàndez & Torné, 1997; Andeweg & Cloetingh, 1998; Beaumont *et al.* 2000; Jammes & Huismans, 2012; Ruh, Kaus & Burg, 2012; Nilfouroushan *et al.* 2013; Erdős *et al.* 2014) and analogue

†Author for correspondence: pablomartinez_granado@ub.edu

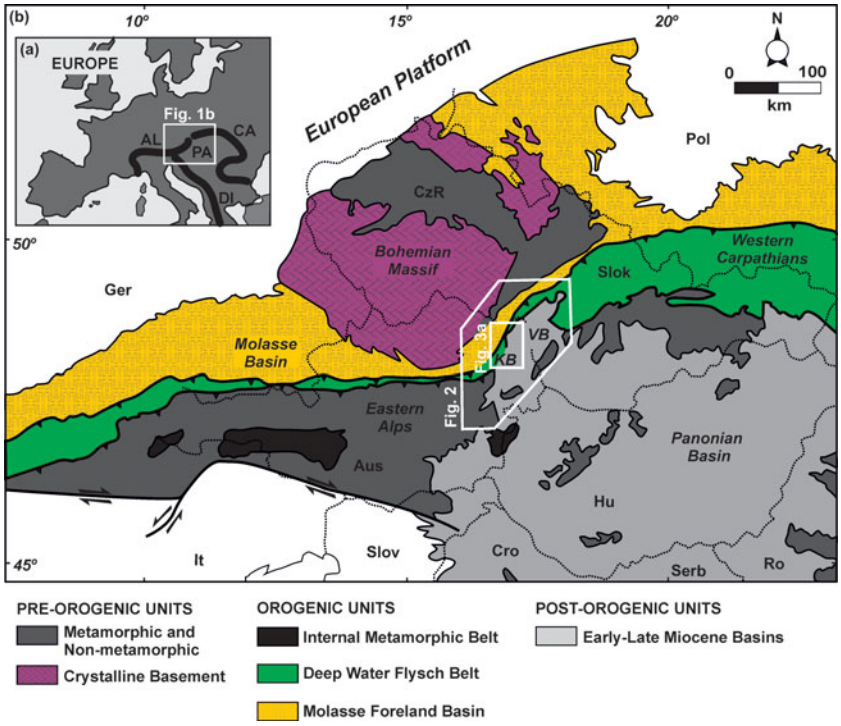

Figure 1. (Colour online) (a) Geological setting of the studied area. AL – Alps; CA – Carpathians; PA – Pannonian Basin; DI – Dinarides. (b) The Alpine–Carpathian Junction is located in the transition from the Eastern Alps to the Western Carpathians within the boundaries of Austria, Slovakia and the Czech Republic. Inset shows the location of Figures 2 and 3a. Aus – Austria; Cro – Croatia; CzR – Czech Republic; Ger – Germany; Hu – Hungary; Pol – Poland; Ro – Romania; Slok – Slovakia; Slov – Slovenia; Serb – Serbia; VB – Vienna Basin; KB – Korneuburg Basin. Modified from Tari (2005).

modelling studies (e.g. Mugnier *et al.* 1997; Nilfouroushan & Koyi, 2007; Malavieille, 2010; Graveleau, Malavieille & Dominguez, 2012; Perrin *et al.* 2013).

In this work, we provide evidence for the involvement of crystalline basement by basement fault reactivation (in extension and shortening modes) beneath and ahead of the external parts of Alpine–Carpathian thin-skinned FTB. Evidence arises from the interpretation of seismic datasets, cross-section construction and calculated fault-displacement profiles. These were integrated with existing gravity data (Geofyzika, unpub. report, 1999; Lenhardt *et al.* 2007), recent and historic earthquake distributions (Reinecker & Lenhardt, 1999; Lenhardt *et al.* 2007), lithospheric rheology (Andeweg & Cloetingh, 1998; Lankreijer *et al.* 1999) and thermochronological studies (Mazzoli *et al.* 2010; Andreucci *et al.* 2013, 2015; Castelluccio *et al.* 2015).

2. Geological setting

The Alpine–Carpathian FTB is located in the transition between the Eastern Alps and the Western Carpathians, between the Vienna Basin to the SE and the Bohemian massif to the NW (Fig. 1). A simplified geological evolution of the studied area is summarized in a tectono-chronostratigraphic chart (Fig. 2), whereas the main structural elements and regional structure are illustrated in Figure 3. The reader should refer to Figure 2 for the correlation of the Mediterranean and Central Paratethys Miocene stages. The basement of the Alpine–Carpathian FTB presents a general tilting towards the south (Wessely, 1987, 1988) which relates to the subduction of the European lower plate and the associated orogenic flexure of the foreland region (Turcotte & Schubert, 1982). The basement is elongated towards the south in the so-called Bohemian Spur extending as much as 50 km beneath the FTB, as confirmed by seismic data (Grassl *et al.* 2004; this study), gravity data (Geofyzika, unpub. report, 1999; Fig. 4) and the many hydrocarbon exploration wells reaching the crystalline substrate (Wessely, 2006). The Bohemian spur is delineated and dissected by NE–SW- and NW–SE-striking basement faults and, to a minor extent, by N–S- and E–W-oriented fault systems (Wessely, 1987; Wagner, 1996, 1998). Gravity data (Geofyzika, unpub. report, 1999) confirms the regional structural trends derived from these previous studies as well as the location and distribution of the major basin depocentres (Fig. 4). The oldest rocks unconformably overlying the crystalline basement are represented by Carboniferous–Permian units related to the latest Variscan cycle (Kroner *et al.* 2008). The Lower Austria Mesozoic Basin (hereafter referred to as the LAMB) locates to the east of the Bohemian Spur. The LAMB was formed during the Jurassic–Cretaceous development of the Alpine Tethys (Wessely, 1987; Zimmer & Wessely, 1996; Wagner, 1998; Ziegler *et al.* 2001; Schmid *et al.* 2004; Handy *et al.* 2010; Handy, Ustaszewski & Kissling, 2015). The basin

https://doi.org/10.1017/S0016756816000066

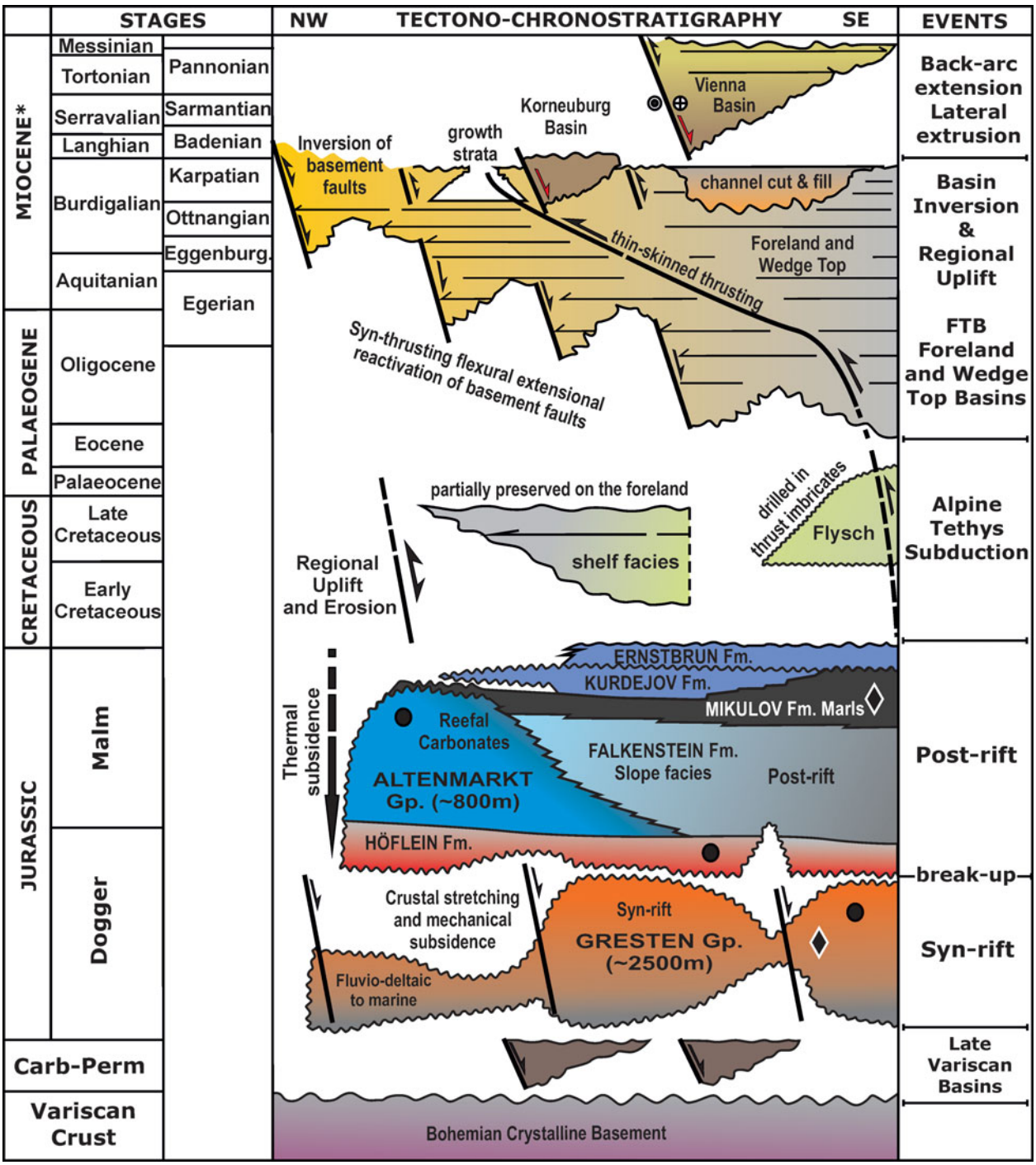

Figure 2. (Colour online) Simplified tectono-chronostratigraphic chart of the Alpine–Carpathian Junction. Central Paratethys stages (as defined by Piller, Harzhauser & Mandic, 2007) and corresponding Mediterranean equivalents are included for reference.

defines a large concave-to-the-SE segment belonging to the European Jurassic continental margin (Fig. 3). The LAMB sedimentary infill consists of pre-rift, syn-rift and post-rift megasequences (Fig. 2). The Middle Jurassic pre-rift to syn-rift megasequence consists of a continental to fluvio-deltaic transgressive sequence represented by the Gresten Group. This unit hosts both reservoir and source-rock intervals (Sachsenhofer *et al.* 2006). The post-rift megasequence is represented by the onset of a carbonate platform to slope system which commences with the Middle Jurassic Höflein Formation (e.g. Sauer, Seifert & Wessely, 1992). The Höflein Formation is made up of silicified cherty and sandy dolostones and constitutes the most important reservoir in the Alpine–Carpathian sub-thrust region (e.g. Sauer, Seifert & Wessely, 1992; Zimmer & Wessely, 1996; Sachsenhofer *et al.* 2006). The remaining part of the post-rift megasequence is constituted by Upper Jurassic reef build-ups and slope to deeper-water facies as represented by the Mikulov, Ernsbrunn and Kurdejov formations. The Mikulov marls represent the most important source rock of the Alpine–

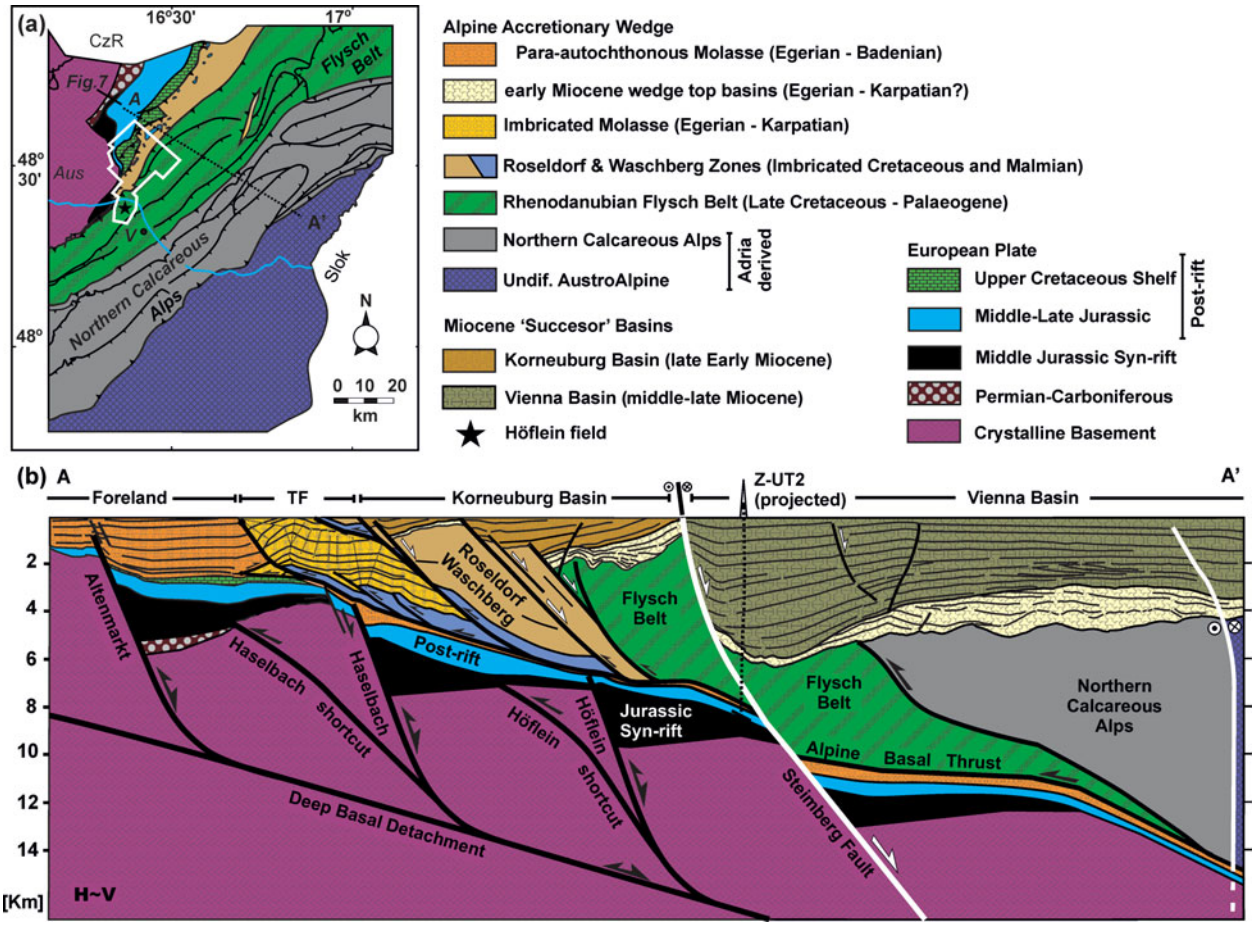

Figure 3. (Colour online) (a) Neogene subcrop map of the Alpine–Carpathian Junction in Lower Austria with the location of the 3D seismic data. (b) Regional cross-section where the Para-autochthonous foreland and lower plate, the Alpine–Carpathian FTB and the overlying Miocene 'successor' basins are illustrated. Modified from Zimmer & Wessely (1996), Wessely (2006), Roeder (2010) and Beidinger & Decker (2014). Aus – Austria; Slok – Slovakia; CzR – Czech Republic; TF – thrust front.

Carpathian Junction (Sauer, Seifert & Wessely, 1992). The remaining part of the post-rift is constituted by an unevenly distributed Late Cretaceous shelf unconformably overlying the Jurassic units (Wessely, 1987, 2006).

The Alpine–Carpathian FTB developed from the late Eocene – early Miocene N- to NW-directed shortening and overthrusting of the Alpine Tethys continental margin successions on the previously rifted European Platform (e.g. Fodor, 1995; Decker & Peresson, 1996; Frisch *et al.* 1998; Ziegler *et al.* 2001; Schmid *et al.* 2004; Ustaszewski *et al.* 2008; Handy *et al.* 2010; Beidinger & Decker, 2014; Handy, Ustaszewski & Kissling, 2015). This thin-skinned shortening was preceded by an earlier phase of shortening in Cretaceous times responsible for thick-skinned deformation and uplift on the Alpine Foreland (e.g. Nachtmann & Wagner, 1987; Schröder, 1987). This early thick-skinned deformation is probably responsible for the partial erosion and uneven distribution of the Cretaceous cover as reported by Wessely (1987). From SE to NW, the Alpine–Carpathian thin-skinned orogenic wedge is represented by the Austroalpine (including the Northern Calcareous Alps), the Rhenodanubian Flysch, the Waschberg, Roseldorf and Imbricated Molasse zones and the Para-autochthonous Molasse (Fig. 3). Thin-skinned thrusting followed a general forwards breaking sequence characterized by strong transpressional and transtensional deformation (e.g. Wessely, 1987; Decker, Meschede & Ring, 1993; Fodor, 1995; Linzer, Ratschbacher & Frisch, 1995; Decker & Peresson, 1996; Linzer *et al.* 1997, 2002; Peresson & Decker, 1997; Hölzel *et al.* 2010; Beidinger & Decker, 2014). The characteristic structural styles are represented by imbricate thrust systems and related folds detached along the Alpine basal thrust which soles within the Mikulov Formation and the Para-autochthonous Molasse foreland sediments. Notoriously, the foreland basin is narrowest in front of the Bohemian Spur (*c.* 9 km), widening out up to 10 times to the west and to the east (Fig. 1). Large incisions and canyons in the Alpine–Carpathian foreland (e.g. Dellmour & Harzhauser, 2012) provide evidence for a regional long-wavelength uplift in latest early Miocene time (i.e. Karpatian), such as that reported for the Upper Austria Molasse (Andeweg & Cloetingh, 1998). More recently, thermochronological studies to the ENE of the studied area in the Central Western Carpathians (e.g. Danišik *et al.* 2010; Anczkiewicz, Środoń & Zattin, 2013; Andreucci *et al.* 2013; Castelluccio *et al.* 2015) also support large Miocene exhumation events related

https://doi.org/10.1017/S0016756816000066

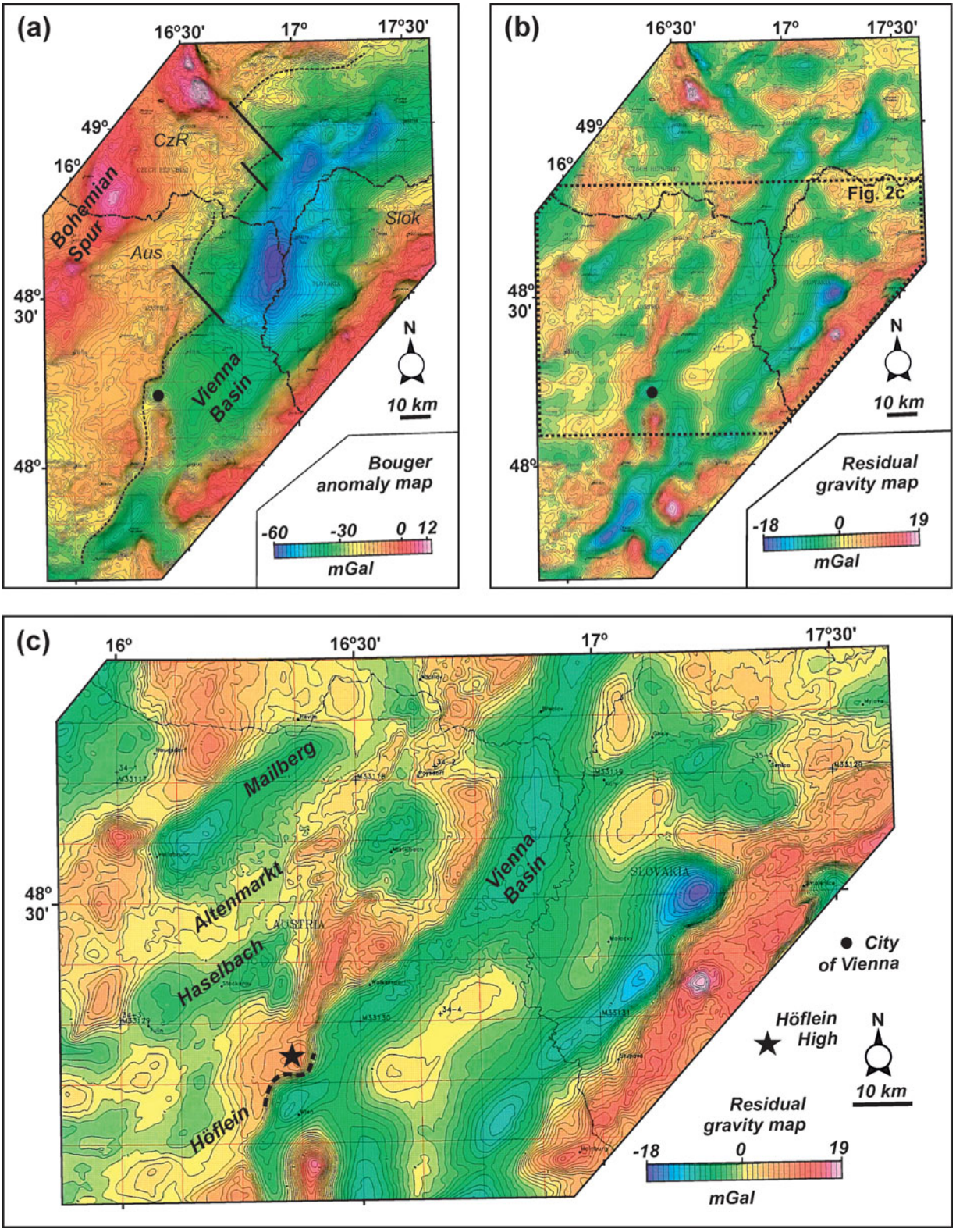

Figure 4. (Colour online) Gravity maps of the Alpine–Carpathian Junction of Austria, Slovakia and Czech Republic. (a) The Bouger anomaly map shows the trend of the Bohemian crystalline massif (higher gravity readings) and the NE–SW-striking Vienna Basin (low gravity readings). (b) The residual gravity map illustrates several NE–SW gravity lows associated with the structural trends of the half-graben basins in the foreland and sub-thrust region as well as the Vienna Basin. (c) Inset of residual gravity map in (b), illustrating the gravity lows associated with the Mailberg, Altenmarkt, Haselbach and Höflein half-grabens in more detail. The E–W-striking Höflein high is shown as a prominent high related to the significant change in the basement structural trend. Data from Geofyzika (unpub. report, 1999) and provided by OMV Exploration and Production GmbH.

https://doi.org/10.1017/S0016756816000066

to thrusting, erosion and post-thrusting extension (e.g. Mazzoli *et al.* 2010; Zattin *et al.* 2011).

On top of the Flysch Zone and the more internal parts of the Alpine–Carpathian FTB, the latest early Miocene – late Miocene 'successor' basins (i.e. Korneuburg, Vienna and subsidiary basins; Figs 2, 3) were developed. These basins are characterized by up to 6000 m thick Miocene depocentres associated with strike-slip pull-apart basins and related fault systems (e.g. Royden, 1985; Wessely, 1987, 1988; Fodor, 1995; Strauss *et al.* 2001, 2006; Hinsch, Decker & Peresson, 2005; Arzmüller *et al*. 2006; Hölzel *et al.* 2010). The origin of these basins has been traditionally ascribed to the lateral extrusion of the Alpine edifice encompassing the extensional collapse of an orogenically thickened and gravitationally unstable crust, as well as the tectonic escape driven by the retreat of the eastern Carpathian subduction zone (e.g. Ratschbacher *et al.* 1991; Decker & Peresson, 1996; Linzer, 1996; Frisch *et al.* 1998; Wölfler *et al.* 2011). In this sense, the Steinberg and Mur-Mürz fault systems of the Vienna Basin most probably played a significant role on the Alpine lateral extrusion and the late dismantling of the orogenic edifice. It has also been suggested that the lateral extrusion and the end of the eastern Carpathian subduction is responsible for the late Miocene – Pliocene gentle inversion of some of these 'successor' basins (e.g. Ratschbacher *et al.* 1991; Decker & Peresson, 1996; Sachsenhofer *et al.* 2000; Strauss *et al.* 2001; Genser, Cloetingh & Neubauer, 2007).

In addition, a significant amount of work has been dedicated to constraining the Cenozoic kinematics in the Eastern Alps (e.g. Thöny *et al.* 2006), the Alpine–Carpathian Junction and the Western Carpathians through palaeomagnetic studies (e.g. Márton *et al.* 2003, 2013). Their research concluded that significant Miocene anticlockwise vertical axis rotations took place, and that the present shape of the Alpine–Carpathian arc is partly due to a certain amount of oroclinal bending. However, more recent works (e.g. Szaniawski *et al.* 2013) report an inconsistency in their results compared to those from previous works. These authors indicate palaeomagnetic declinations similar to those expected for stable parts of the European Platform, implying limited amounts of vertical axis rotations in the Western Carpathians. This debate shows the geological complexity of the studied area and deserves further consideration; however, it is considered to be outwith the scope of this manuscript.

3. Dataset and methodologies

For our study we have mostly used three-dimensional (3D) and 2D seismic data. The 3D volume is a post-stack depth-migrated merge covering *c.* 550 km^2 with a maximum recorded depth of 7 km. Spacing of the NE–SW-trending Inlines is 15 m, whereas for the NW–SE-trending cross-lines it is 30 m. The quality of the 3D seismic data is generally good but decreases in structurally complicated areas. In addition, seismic velocity inversions associated with the post-rift carbonate units also produce local reduced resolution. The studied area is also covered by a dense network of 2D time-migrated seismic profiles which cover the foreland deformation front without 3D coverage. Several tens of wells containing a downhole suite of gamma ray, sonic, resistivity, spontaneous potential surveys, checkshot logs and biostratigraphically constrained formation tops were tied to the seismic data. Gravity anomaly maps were used to illuminate the shape of the Bohemian crystalline basement, the border of the LAMB as well as the extent and strike of the Jurassic half-graben basins, and the overlying 'successor' Miocene basins. All data were integrated to identify and constrain the regional structure with an emphasis on the LAMB and its basement fault array. Key megasequence boundaries were defined based on well intersections, the regional unconformities observed, their internal architecture and seismic reflectors' geometries, their seismic facies and the relationships of all these features to the major structures of the basin.

4. Seismic interpretation and structural analysis

Regional well-tied surfaces for the top of the crystalline basement and the base of the post-rift megasequence were generated from the 3D data volume (Fig. 5). The basement fault array of the LAMB is relatively well imaged in the seismic data from the foreland in the NW to the hinterland in the SE. In the studied area, the LAMB is constituted by a series of basement-involved faults that from NW to SE are referred to here as: Mailberg, Altenmarkt, Haselbach, Höflein, Kronberg and Kasernberg faults (Fig. 5). The Mailberg fault is imaged by a series of NW–SE-striking 2D time-migrated profiles in the foreland region, whereas the remaining basement faults are imaged by the 3D depth-migrated seismic cube. Fault surfaces were generated for these faults and their average orientations extracted from the 3D model (Fig. 5c, d).

4.a. The LAMB basement fault array

The LAMB basement fault array is constituted by steeply to moderately SE-dipping extensional faults, whereas minor antithetic faults are steeply to moderately NW-dipping (Fig. 5). These basement-involved faults are arranged in segments with slightly different orientations, striking from NNE–SSW to E–W and NW–SE, but overall configuring a general NE–SW trend (Fig. 5c). Major faults display lengths in excess of 10 km along-strike. In the studied area, the general trend of the basement fault array is roughly parallel to the strike of the overlying thin-skinned thrust front (Fig. 3). One NW–SE-striking basement fault (i.e. trending approximately perpendicular to the general basement fault array) was interpreted from the 3D seismic data (Fig. 5). According to the Bouguer anomaly map, this fault set could correspond to transfer systems segmenting the regional basement fault trend

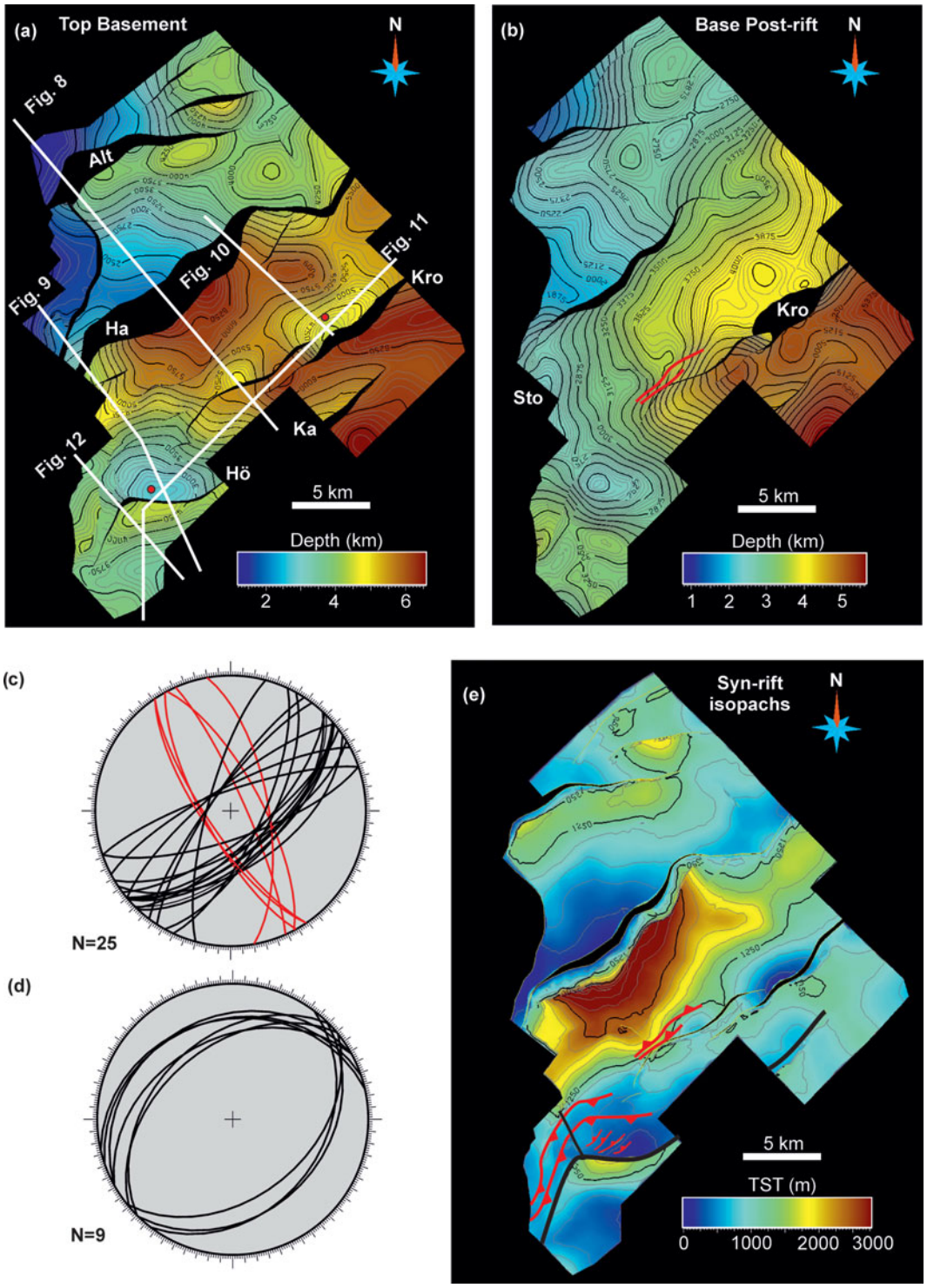

Figure 5. (Colour online) Depth structure maps. (a) Top of crystalline basement. (b) Base of the post-rift megasequence (i.e. Höflein Formation). (c) Stereographic projection showing the orientation of the interpreted fault systems, with great circles representing faults. Note the predominant NE–SW-striking steeply dipping sets (in black) corresponding to the large Jurassic rift faults. The NW–SE-striking set (in red) corresponds to the less-abundant release and transfer faults. (d) Stereographic projection showing the predominant NE–SW strike of the inversion-related fault system. All stereographic plots are equal-area, lower-hemisphere projections. (e) Syn-rift isopach map (i.e. true stratigraphic thickness). The largest syn-rift depocentre is related to the Haselbach fault, whereas the thickest syn-rift in the Höflein half-graben is related to its E–W-striking segment. Alt – Altenmarkt fault; Ha – Haselbach fault; Hö – Höflein fault; Kro – Kronberg fault; Ka – Kasernberg fault; Sto – Stockerau anticline. Red dots in (a) indicate the position of the Höflein and Kronberg basement highs. Stereoplots generated with OpenPlot software (Tavani *et al.* 2011).

https://doi.org/10.1017/S0016756816000066

(Fig. 4a). Other NW–SE-striking faults in the order of tens to hundreds of metres long (i.e. up to two orders of magnitude smaller than the major faults) are localized within the basement and pre-rift to early syn-rift infill. Characteristically, these small faults display lower throw values than the master faults and are here interpreted as release faults (*sensu* Destro, 1995). This type of fault accommodates the along-strike stretching of the hanging-wall layers during regional extension and accounts for the NW–SE-striking fault sets shown in the fault strike diagram (Fig. 5c).

As no fault plane reflections are shown by the seismic data, the shape of the basement faults has been resolved from the location of the reflector's cut-offs and by the geometry of the corresponding hanging-wall layers (e.g. White, Jackson & McKenzie, 1986; Xiao & Suppe, 1992; Withjack & Schlische, 2006). The hanging-wall layers of the major basement-involved faults display either a straight panel dipping into the fault or slightly kinked panels indicating that the underlying extensional faults display a planar to slightly kinked geometry. The average spacing of the basement-involved faults is *c.* 10 km measured normal to the strike of the structures. According to this, the general structure of the LAMB corresponds to a series of tilted fault blocks and associated half-graben basins that belong to the former Alpine Tethys Jurassic continental margin. The basal detachment of these faults should be located at around 12 km depth, close to the base of the seismogenic crust (Sibson, 1983; Twiss & Moores, 1992).

4.b. Assessment of basement fault reactivation

The evolution of the LAMB basement fault array was studied by documenting the observed structural styles and the relative timing of cross-cutting relationships. In addition, a quantitative approach was taken by computing fault-displacement profiles (i.e. fault length v. throw values). Fault displacement profiles were calculated for the top basement and the base of the post-rift megasequence given their fundamental role in constraining the magnitude of fault reactivation (e.g. Williams, Powell & Cooper, 1989; Turner & Williams, 2004). This is based on the assumption that during the post-rift, subsidence is mostly controlled by the thermal re-equilibration of the lithosphere as opposed to the syn-rift subsidence which is fundamentally fault controlled (e.g. McKenzie, 1978; Allen & Allen, 2005). Large offsets affecting the post-rift megasequence are therefore indicative of post-rift fault reactivation. Fault-displacement profiles illustrate the along-strike variation of throw but can also indicate which faults (or fault segments) underwent extensional reactivation and inversion (e.g. Thomas & Coward, 1995; Willemse, Pollard & Aydin, 1996). The obtained throw values for each fault should be taken as representative values of the minimum vertical offset, as additional faults and folds of sub-seismic entity might have contributed to the total offset.

The observed displacement along the basement-involved faults of the LAMB decreases upwards by developing fault-propagation folds or forced folds (e.g. Stearns, 1978; Withjack, Olson & Peterson, 1990; Cornfield & Sharp, 2000; Cosgrove & Ameen, 2000; Maurin and Niviere, 2000; Khalil & McClay, 2002; Jackson, Gawthorpe & Sharp, 2006; Tavani & Granado, 2015). These folds also affect the post-rift megasequence, the foreland sediments of the Molasse Basin and, locally, the overlying thin-skinned thrust system. For the major faults, the top of the crystalline basement displays fault-parallel hanging-wall synclines (Fig. 5a) which trend parallel to slightly oblique to the orientation of the immediate fault segment. The Altenmarkt fault displays two of these synclines separated by a fault perpendicular ridge (Fig. 5a). Calculated fault displacement profiles (Fig. 6) indicate displacement maxima slightly shifted sideways from the central position of the faults. These observations suggest that the extensional faults grew to a certain point by the lateral linkage of isolated fault segments (Peacock & Sanderson, 1991; Cartwright, Mansfield & Trudgill, 1996; Willemse, Pollard & Aydin, 1996).

Syn-rift sediment distribution was calculated and represented as a True Stratigraphic Thickness map (Fig. 5e). The calculated map indicates several syn-rift depocentres juxtaposed to the major basement faults as well as stratigraphic thickness lows associated with the uplifted footwalls of the basement faults. The largest syn-rift depocentre is associated with the Haselbach fault, where the syn-rift reaches up to 2770 m in thickness. Broadly speaking, the LAMB is characterized by a well-preserved extensional architecture, mostly inherited from the Jurassic rifting episode. In the following, evidence for the reactivation of the basement fault array following the sedimentation of the syn-rift megasequence from cross-sections, generated surfaces and fault displacement profiles, is provided. In the cross-sections, geometrical characteristics typical of extensional faulting but also typical of positive inversion of the extensional fault array are shown.

4.b.1. The Mailberg fault

The Mailberg fault is located in the foreland region ahead of the thin-skinned thrust front. This fault runs along-strike for as much as 30 km. It is only covered by 2D time-migrated profiles, but its associated hanging-wall depocentre is well shown as a NE–SW-striking gravity low (Fig. b, c). In the central segment of the Mailberg fault, the top of the crystalline basement is folded into an open hanging-wall syncline. The top of the basement has been downthrown in excess of 2 s two-way time, although thickness difference of the Jurassic syn-rift sequence between the footwall and the hanging wall is less than 1 s (Figs 6a, 7). Well and seismic data show that the post-rift megasequence in the hanging wall displays net extensional displacements along most of the length of the fault. In addition, well data indicate that to the SW the post-rift is not present

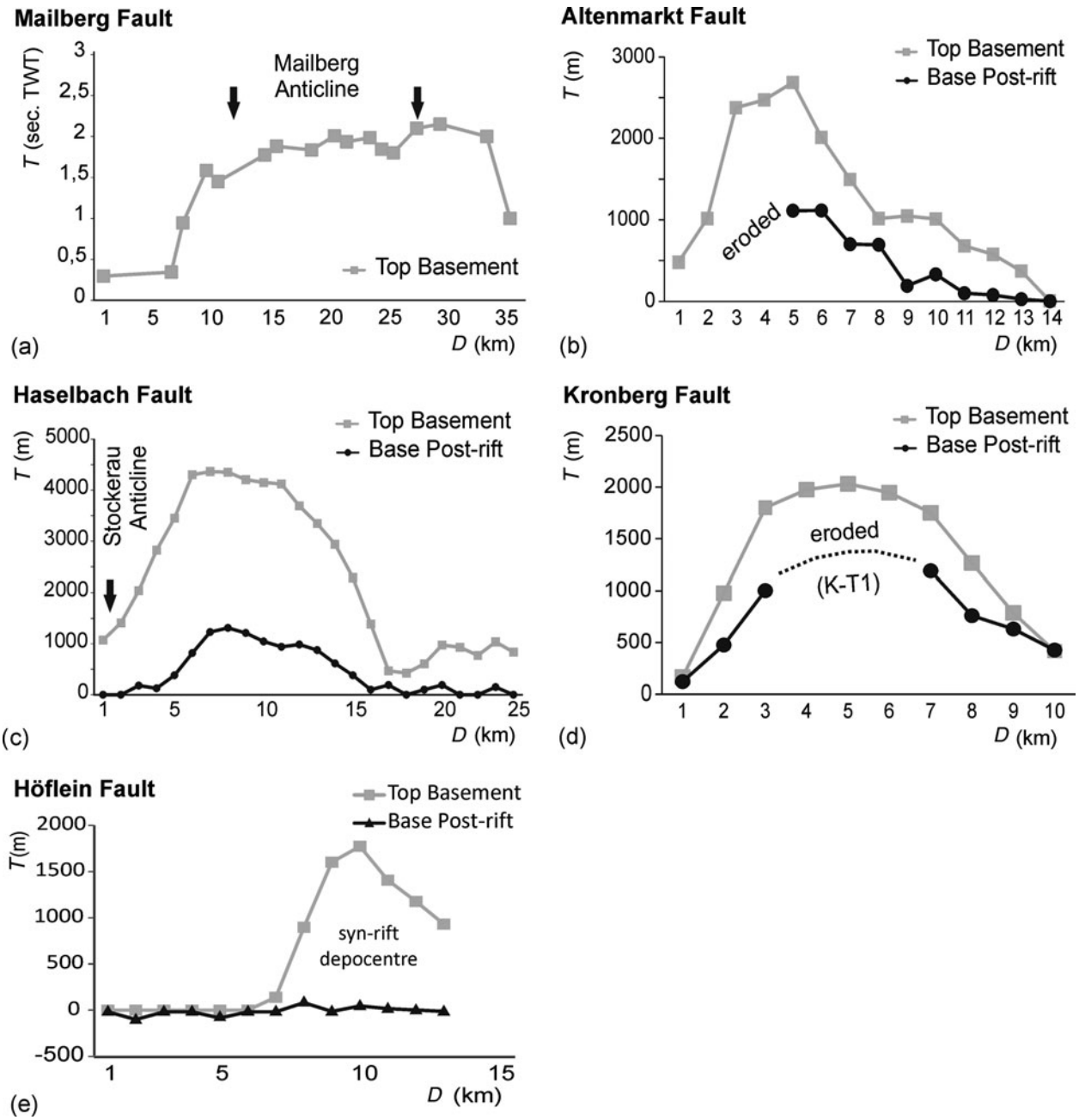

Figure 6. Fault displacement profiles for the studied basement faults. *D* is the length of the extensional fault measured along-strike and *T* (throw) is vertical offset. Note all throw values are in metres, except for the Mailberg fault which is reported as two-way time. Note the extensional offset in excess of 1000 m for the base of the post-rift, providing evidence for the early Miocene extensional reactivation event. The observed erosion of the basal post-rift section (see (b) and (d) plots) is also spatially coincident with the location of maximum throw values. The Höflein fault displays either no extensional offset for the post-rift section or minor reverse offset, indicating the partial positive inversion of the fault.

in the footwall; it has therefore been eroded or non-deposited. On the other hand, the Eggerian–Karpatian (i.e. late Oligocene – late early Miocene) foreland sediments are significantly thicker in the hanging wall than in the footwall. These foreland sediments downlap onto the hanging-wall post-rift megasequence to the SE and onlap and overlap the faulted post-rift units above the basement fault. Extensional displacement along this fault generated a breached forced fold affecting the post-rift and overlying foreland units. Moreover, the uppermost units immediately above the Mailberg fault are Karpatian–Badenian in age (i.e. latest early – earliest middle Miocene; Fig. 2). These units are folded into an open but slightly asymmetric anticline (referred to as the Mailberg Anticline) which lies above the regional elevation and displays a larger gently dipping back-limb and a shorter more steeply dipping forelimb (Fig. 7). In addition to this, a Badenian-age (i.e. early middle Miocene) coralline-algal reef was developed onto this anticline, surrounded by and interfingering with deeper-water siliciclastic-dominated facies (Mandic, 2004).

https://doi.org/10.1017/S0016756816000066

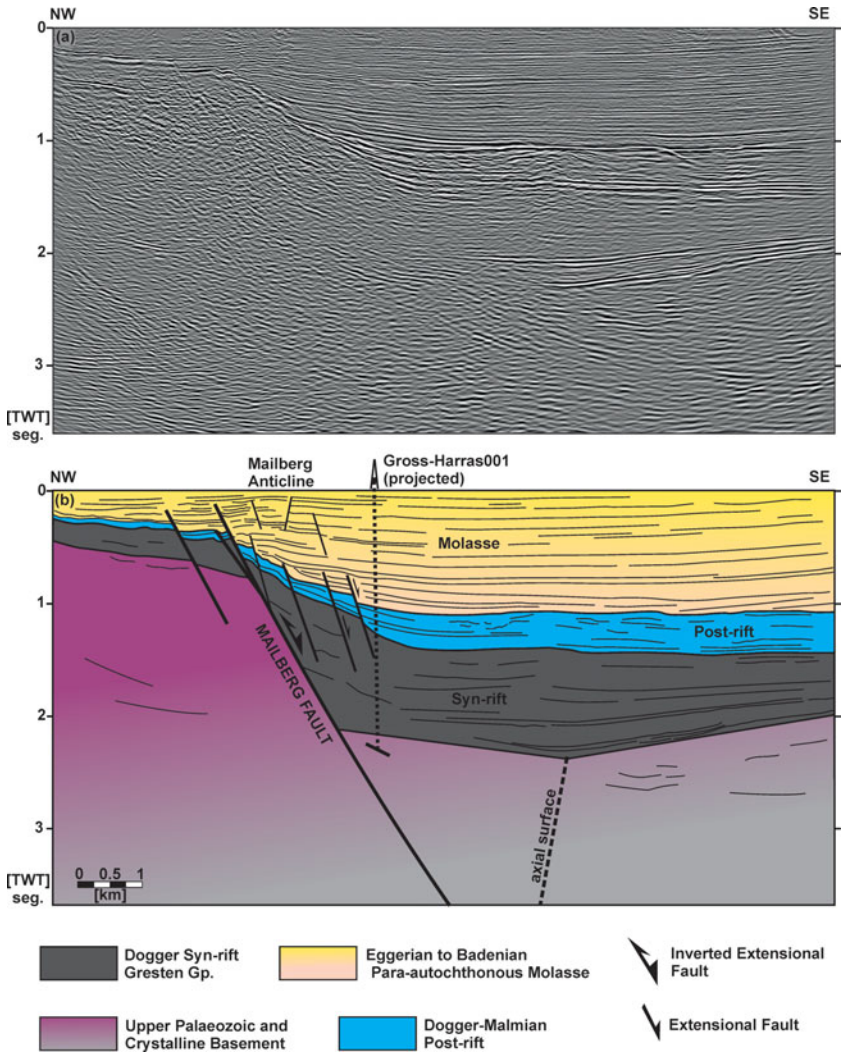

Figure 7. (Colour online) (a) NW–SE-striking time-migrated profile. (b) Geoseismic interpretation showing the Mailberg half-graben in the foreland region ahead of the thin-skinned thrust front. Note the extensional offset shown by the top of the basement and the post-rift megasequence. Note the thicker sections of syn-rift and Molasse basin strata in the hanging wall than in the footwall, and the erosion of the upper section of the post-rift megasequence in the elevated footwall. The Mailberg Anticline developed above the extensional fault shows a larger back-limb and a shorter forelimb. These features are indicative of thick-skinned positive inversion following an early Miocene extensional reactivation of the Jurassic Mailberg fault. See Figure 3 for location of the profile.

The calculated fault displacement profile for the top basement in the Mailberg fault displays two displacement minima at both ends of the fault, whereas the central portions of the fault display a rather uniform throw (Fig. 6a). Such a displacement profile is not in agreement with the commonly observed displacement profiles of extensional faults, where the displacement maximum is commonly located near the centre of the faults (e.g. Peacock & Sanderson, 1991; Cartwright, Mansfield & Trudgill, 1996; Willemse, Pollard & Aydin, 1996). In this case, the central portion of the Mailberg fault is spatially coincident with the above-mentioned Mailberg Anticline. Based on the evidence provided, we interpreted that the Mailberg fault underwent two episodes of reactivation. The first was in extension during Eggerian–Karpatian time (i.e. late Oligocene – late Early Miocene), as shown by the extensional displacement of the post-rift units and thickness differences observed across the fault for the lower Miocene sequences. This first extensional reactivation is therefore synchronous with the thin-skinned thrusting. It was followed by a later episode of shortening in Badenian times (i.e. earliest middle Miocene), responsible for the development of the Mailberg Anticline and the partial removal of the extensional displacement.

4.b.2. The Altenmarkt fault

The Altenmarkt fault is located just ahead of the thin-skinned thrust front of the Alpine–Carpathian Junction (Fig. 8). This fault runs along-strike for at least 15 km, dying out towards the NE where it is relayed by a system of two smaller SE-dipping rift faults; towards the SW, it continues out of the 3D cube (Fig. 5). This is also supported by the calculated fault displacement profiles for the top of the basement and the base of the post-rift megasequence (Fig. 6b). This plot indicates that the fault is in net extensional displacement and that the

https://doi.org/10.1017/S0016756816000066

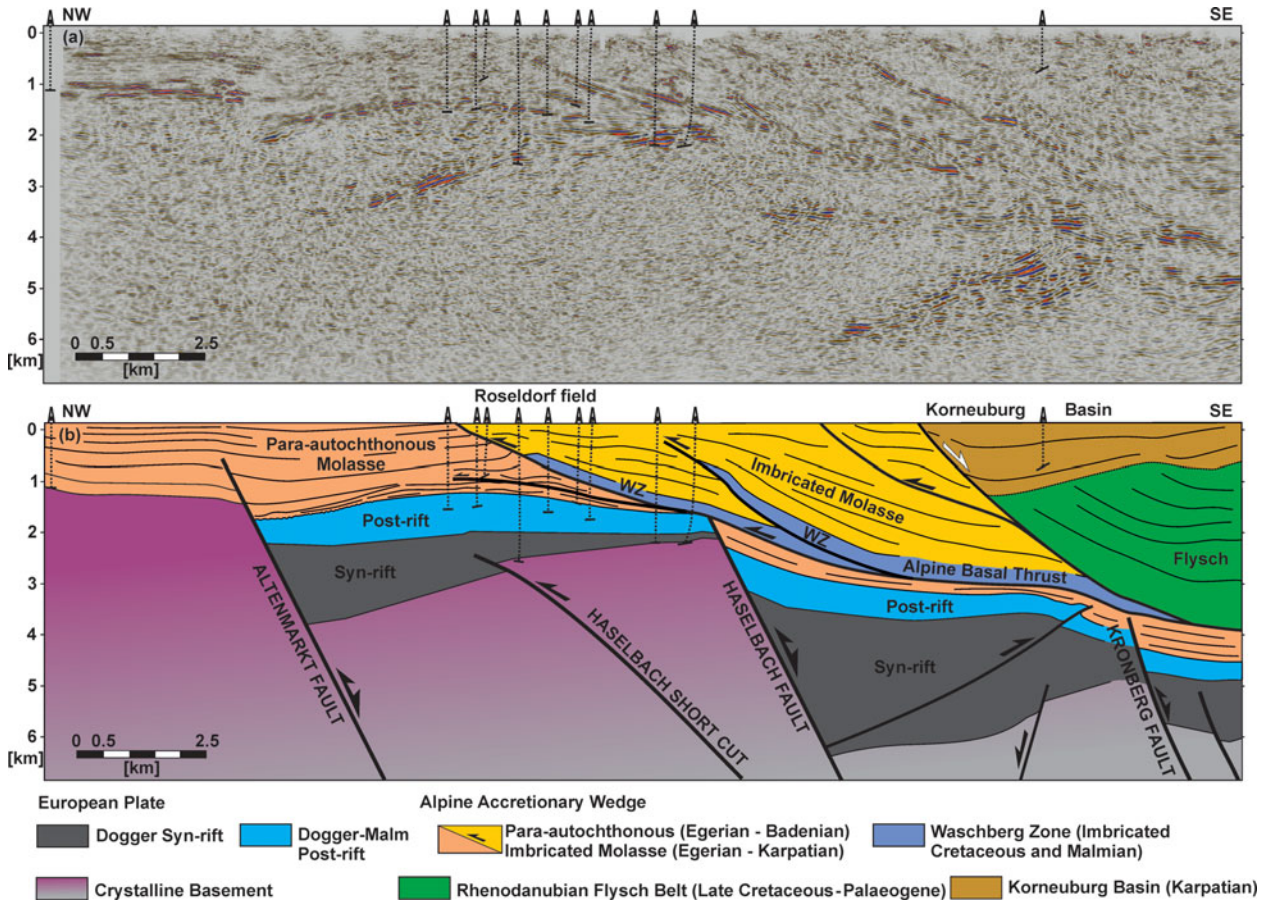

Figure 8. (Colour online) (a) NW–SE-striking depth-migrated seismic profile. (b) Geoseismic interpretation. The Altenmarkt fault locates ahead of the thin-skinned thrust front where the Roseldorf hydrocarbon field is located. Note extensional offset shown by the post-rift megasequence and the Para-autochthonous Molasse growth strata wedges indicative of Eggerian–Ottnangian (i.e. late Oligocene – early Miocene) extensional reactivation of the Altenmarkt and Haselbach faults. Positive inversion of the basement fault array is shown by open folding of the Altenmarkt hanging-wall strata, and the formation of a basement involved a shortcut fault and a backthrust emerging from the Haselbach fault. Gentle folding of the cover strata and thrust sheets above these inversion-related faults indicate that extensional reactivation of the basement fault array was followed by its positive inversion. See Figure 5 for location of the profile. WZ – Waschberg Zone.

displacement maximum is strongly shifted towards the SW. The Altenmarkt fault comprises several segments of differing orientation ranging from NNE- to NE–SW- to E–W-striking. In addition, the fault is connected to a roughly NW–SE-striking fault that could be a transfer zone.

Seismic interpretation and well data indicate that the post-rift megasequence is missing to the west and SW on the footwall of the Altenmarkt fault, where Eggerian (i.e. late Oligocene – early Miocene) strata are unconformably overlying the top of the crystalline basement. The base of the post-rift megasequence is also considerably downthrown in the hanging wall of the fault. Seismic and fault displacement profiles show that the missing post-rift megasequence is spatially coincident with the fault segment that displays the largest throw values. In addition, the Eggerian – Karpatian (i.e. late Oligocene – late early Miocene) sequence is significantly thicker in the hanging wall than in the footwall, indicating that the extensional reactivation of the Altenmarkt fault during that time. Seismic evidence also suggests partial erosion of the post-rift section in the immediate hanging wall below these sediments. Extensional displacement along this fault decreases upwards by developing an extensional fault-propagation fold (Fig. 8).

The top of the crystalline basement in the hanging wall of the Altenmarkt fault is divided into two panels which are slightly separated by a low-angle offset (Fig. 8). The NW panel dips toward the fault more steeply than the SE panel. The units above this basement kink (i.e. syn-rift and post-rift megasequences and overlying Molasse basin sediments) are folded into a broad open anticline, above which the Roseldorf hydrocarbon field is located. This anticline and the low-angle offset affecting the top of the basement are interpreted to be related to a NW-directed basement-involved thrust fault (Figs 5e, 8). This thrust is interpreted as a footwall shortcut thrust (Badley, Price & Backshall, 1989; Hayward & Graham, 1989) emanating from and kinematically linked to the steeply dipping Haselbach fault.

4.b.3. The Haselbach fault

The Haselbach fault is located in the middle of the 3D cube and runs in excess of 20 km along-strike below the thin-skinned thrust front. The Haselbach fault displays the largest observed throw values of the basement fault array, exceeding 4000 m for the top of the crystalline basement (Fig. 6c). In the section corresponding to the displacement maximum of the fault, the top of the crystalline basement dips towards the NW (i.e. towards the Haselbach fault), where extension is related to one large basement fault (Fig. 8). Towards the NE, seismic and well data indicate that the top of the basement is folded into a hanging-wall syncline; to the SW, the top of the basement displays a down-to-the-SE terraced geometry. Such terraced geometry is in agreement with the existence of several planar extensional faults (Fig. 9). The observed lateral variation in the geometry of the basement top of the hanging wall suggests a slightly kinked geometry for the Haselbach fault at depth, with the hanging-wall syncline developed for those layers with less extensional displacement and still above the fault kink (Xiao & Suppe, 1992). The kink in the fault is not observed in the seismic data and should be located at greater depth. In addition, the base of the post-rift megasequence in the hanging wall is downthrown in excess of 1000 m (Figs 6c, 8, 9). Such extensional offset is also accompanied by a thick Eggerian–Ottnangian (i.e. late Oligocene – early Miocene) sedimentary wedge. Well and seismic data also indicate that the sedimentation of this sedimentary wedge is responsible for the partial erosion of the underlying post-rift section.

In cross-section, the base of the post-rift megasequence on the hanging wall of the Haselbach fault displays a subhorizontal attitude (Figs 8, 9). On map view (Fig. 5b), the base of the post-rift megasequence dips towards the NE (i.e. towards the Haselbach half-graben depocentre), indicating that its regional attitude relates to the inherited extensional architecture of the LAMB. To the SW, the post-rift section above the Haselbach fault is folded into an open anticline (Fig. 9). This anticline (referred to as the Stockerau Anticline) affects the autochthonous foreland units and the overlying imbricated foreland strata. To the east, the hanging-wall section is folded into an anticline with a large shallowly NW-dipping limb and a shorter SE-dipping limb (Figs 5e, 8). This anticline gently folds the overlying strata and structural units above the hanging wall. This structure is interpreted as related to a SE-directed backthrust nucleated from the Haselbach fault along the basal pre-rift to syn-rift section. According to the geometries described, the steeply dipping Haselbach fault seems to have acted as a buttress upon shortening (e.g. Butler, 1989), promoting the development of the basement-involved shortcut and hanging-wall backthrust.

4.b.4. The Kronberg high and related extensional fault

The Kronberg high locates to the eastern part of the 3D model (Fig. 5). This basement high strikes NE–SW and corresponds to the elevated footwall of the NE–SW-striking Kronberg extensional fault (Figs 10, 11). The Kronberg fault runs along-strike for about 10 km and is relayed to the SW by another extensional fault (Fig. 5). The calculated fault displacement profile shows a displacement maxima located within the central part of the fault. At this position, extensional offsets for the top of the crystalline basement are in excess of 2 km. The Kronberg high locates in the immediate footwall of the displacement maxima of this fault (Figs 5, 6d).

The high was drilled by the Kronberg T1 well, targeting the sub-thrust post-rift and syn-rift reservoir sections (Zimmer & Wessely, 1996). The well drilled down to 4714 m through the imbricated units of the Flysch and Waschberg zones, and found Eggerian (i.e. late Oligocene – early Miocene) Molasse sediments on top of the syn-rift megasequence; the post-rift carbonate section (i.e. the reservoirs) were missed (Fig. 10). Fault displacement profiles calculated for the preserved base of the post-rift megasequence away from the footwall high indicate extensional offsets in excess of 1000 m (Fig. 6d). The fault displacement profile for the base of the post-rift displays a similar displacement distribution to that shown by the top of the crystalline basement. In addition to this, the Kronberg fault hanging wall displays a Molasse sedimentary wedge above the syn-rift and post-rift megasequences thicker than that drilled by the Kronberg T1 well. These observations suggest that the basal section of the post-rift megasequence on the Kronberg high was eroded by the footwall uplift related to the Eggerian–Ottnangian (i.e. late Oligocene – early Miocene) extensional reactivation of the Kronberg fault.

4.b.5. The Höflein high and related fault system

The Höflein high is located at the southern corner of the 3D model, about 10 km NNW of the city of Vienna (Figs 3, 5) and beneath the Flysch Zone imbricates (Figs 9, 11, 12). Available well and seismic data indicate that the master basement fault extends for as much as 12 km along-strike and displays two important changes in strike: from NNE- to E–W to NE–SW-striking (Fig. 5). These fault segments are steeply dipping and display a slightly concave-upwards geometry. The Höflein high corresponds to the elevated footwall of the E–W-striking fault segment (Fig. 5); in addition, the hanging wall of this fault segment displays the thickest syn-rift depocentre of the Höflein half-graben (Fig. 5e).

At this position, the footwall of the Höflein fault hosts the most important gas and condensate field in the sub-thrust region of Lower Austria (Janoscheck, Malzer & Zimmer, 1996; Zimmer & Wessely, 1996; Sachsenhofer *et al*. 2006). This hydrocarbon field produces from the (Para)-autochthonous post-rift carbonates and the syn-rift siliciclastic section in a footwall four-way-dip closure (Figs 5, 13). The E–W orientation of the footwall basement high significantly departs

https://doi.org/10.1017/S0016756816000066

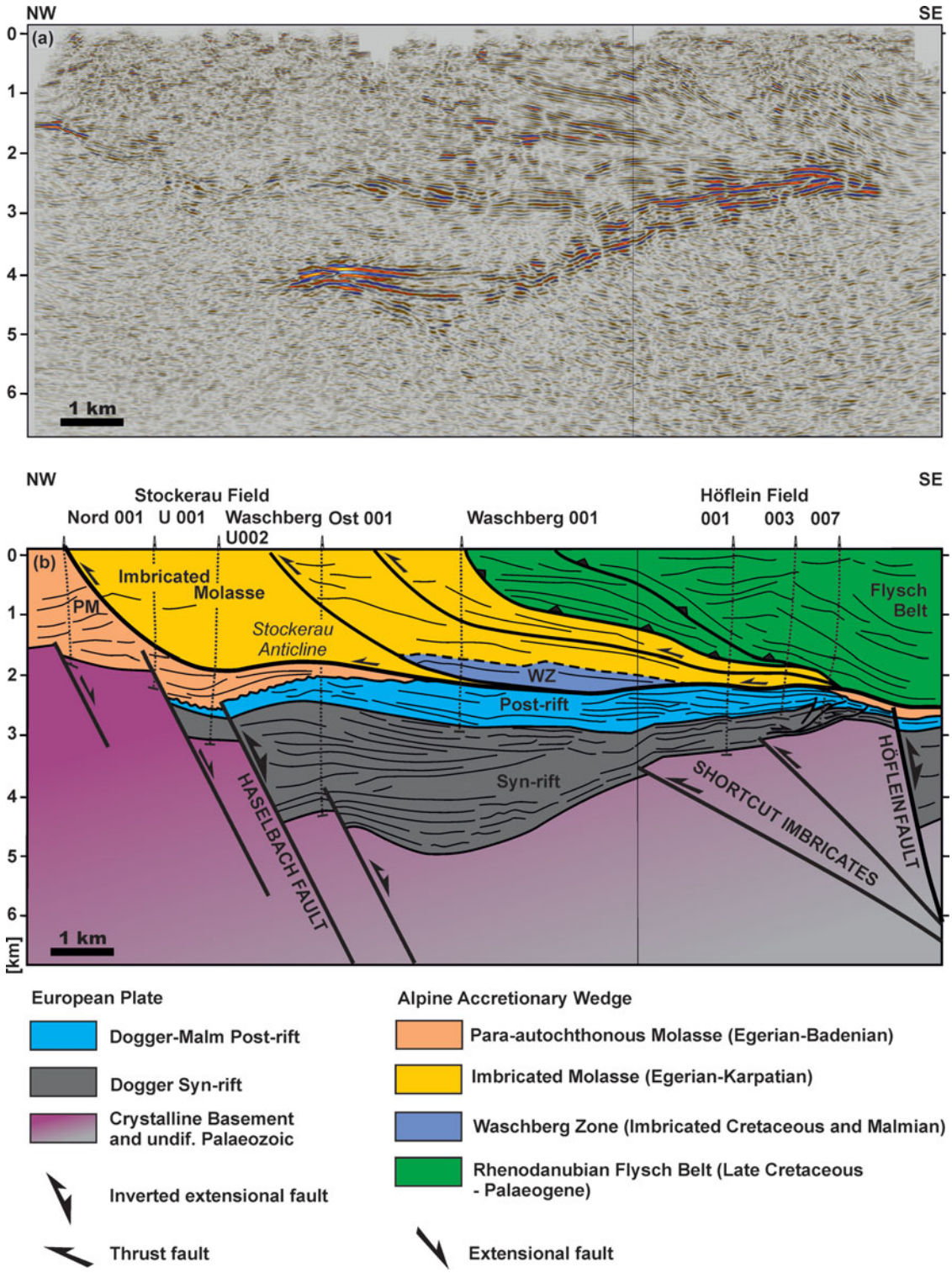

Figure 9. (Colour online) (a) NW–SE-striking depth-migrated seismic profile through the Stockerau and Höflein fields. (b) Geoseismic interpretation. Note the energetic reflections given by the pre-rift units near the top of the crystalline basement and those above corresponding to the post-rift carbonates. The Eggerian–Ottnangian (i.e. late Oligocene – early Miocene) wedges above the Haselbach and Höflein faults indicate the timing of extensional reactivation of the basement fault array. Positive inversion followed as indicated by the development of the Stockerau Anticline, the elevated Höflein footwall and the associated folding of the overlying thrust sheets. See Figure 5 for location of the profile. WZ – Waschberg Zone; PM – Para-autochthonous Molasse.

from the regional NE–SW-striking basement fault array trend. The Höflein high is slightly offset by a NW–SE-striking extensional fault, with its downthrown block located to the SW. The Höflein extensional fault could be correlated to the NE with the Kasernberg fault, but the lack of 3D seismic data avoided this correlation (Fig. 5). At the footwall high, the crystalline basement is located at *c.* 2500 m below mean sea level. This is about 2000 m above the top of the crystalline basement drilled by the Kronberg T1 well (Fig. 11). As

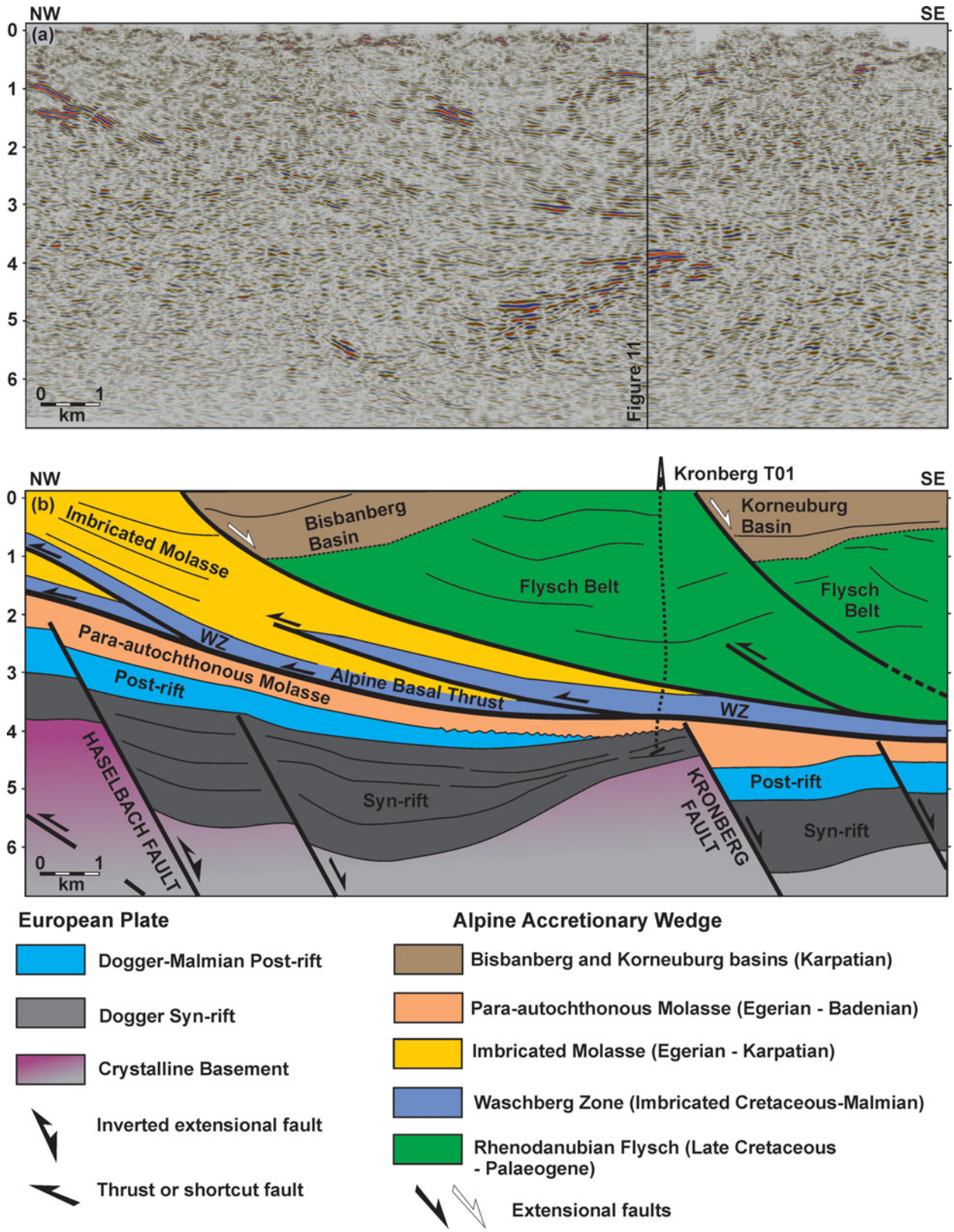

Figure 10. (Colour online) (a) NW–SE-striking depth-migrated seismic profile along the Kronberg high. (b) Geoseismic interpretation. Kronberg T01 well drilled Eggerian–Ottnangian (i.e. late Oligocene – early Miocene) sediments unconformably overlying the basal syn-rift section. Note the missing post-rift onto the Kronberg fault footwall. The Waschberg Zone and basal Alpine thrust consist of imbricated Cretaceous and Malmian units scrapped off from the underlying autochthonous units. WZ – Waschberg Zone.

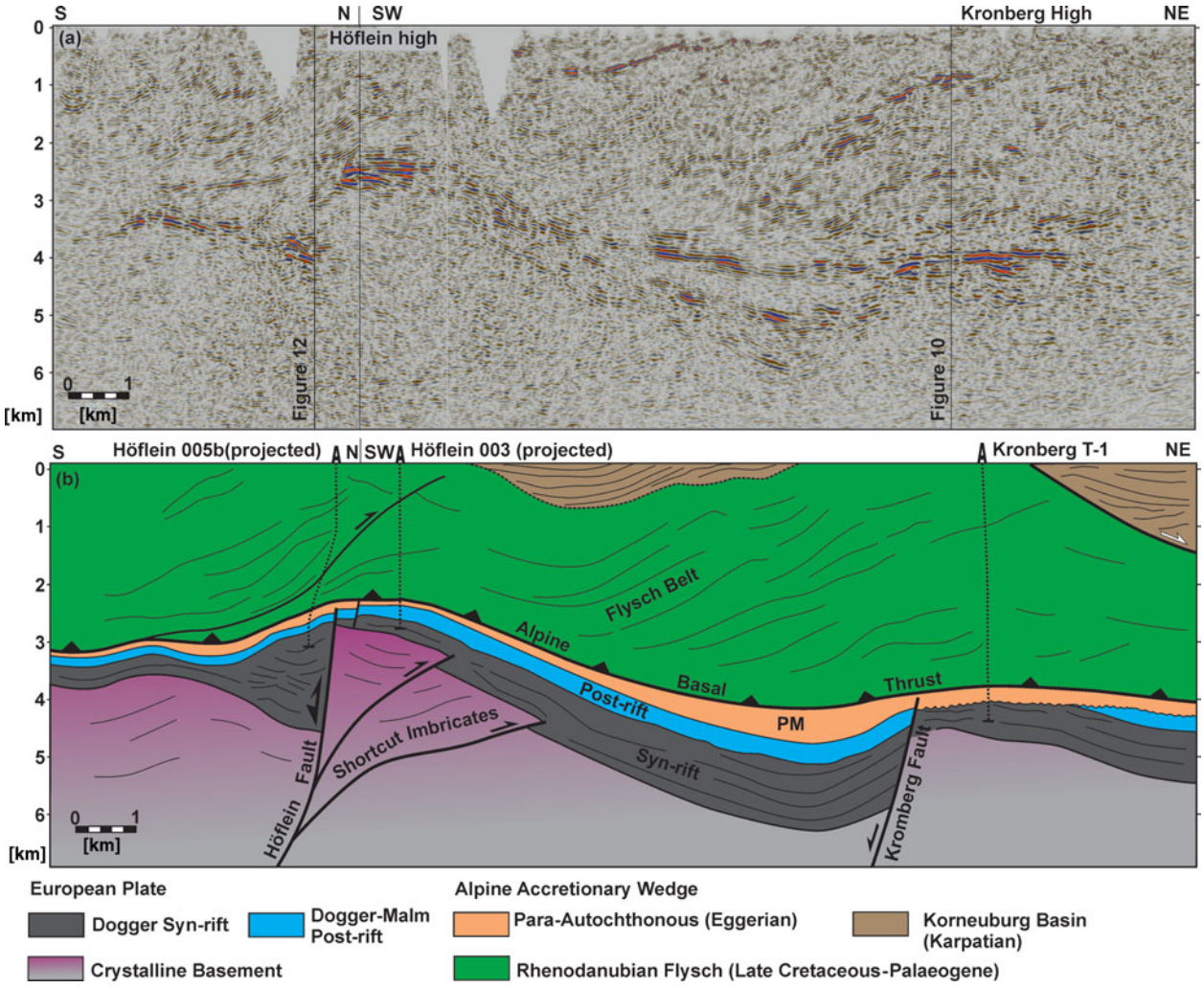

Figure 11. (Colour online) (a) Composite depth-migrated section from the Höflein field to the SW and the Kronberg high to the NE. (b) Geoseismic interpretation. Energetic reflectors on the Höflein high correspond to the post-rift carbonates and underlying syn- and pre-rift siliciclastics. On the Kronberg high the high-energy reflections correspond to the Autochthonous Molasse unconformably overlying the syn-rift units; post-rift carbonates are missing. Seismic and well data show the substantially higher elevation of the basement in the Höflein high than in the Kronberg high, as well as the folding of the overlying imbricates of the Flysch Zone. The basal thrust zone is constituted by imbricated Malmian, Cretaceous and Eggerian (i.e. late Oligocene) sediments. Dipping reflections within the Rhenodanubian Flysch indicate a transport direction oblique to the seismic profile. See Figure 5 for location of the profile. PM – Para-autochthonous Molasse.

previously stated, the whole post-rift section is preserved at Höflein high, but not at Kronberg high (Fig. 11). Regarding the hanging wall, the basement top is folded into a plunging NE–SW-striking syncline and anticline pair (i.e. slightly oblique to the trend of the Höflein fault).

In order to illustrate the geometry of the Höflein high and related fault systems, two NW–SE-striking cross-sections (Figs 9, 12) and a composite NE–SW-striking cross-section (Fig. 11) were made (see Fig. 5a for location). The first of these cross-sections goes from the Stockerau field to the NW to the Höflein field to the SE, and shows the elevated footwall of the Höflein extensional fault (Fig. 9). At this position, the Höflein high is characterized by the prominent footwall reflections of the post-rift carbonates. To the SE, these reflections disappear and locate on the Höflein's downthrown hanging wall. On the footwall, the post-rift carbonates are offset and imbricated several times by a series of NE–SW-striking small-displacement backthrusts (Figs 5, 9). The top of the crystalline basement is folded into two panels which relate to two roughly NE–SW-striking basement-involved reverse faults emerging from the Höflein extensional fault (Figs 5, 9b). Displacement and folding associated with these reverse faults are, at least partially, responsible for the high elevation of the Höflein high.

Further to the SW, a section across the Höflein fault away from the elevated footwall displays a thick package of subhorizontal reflections at 3.5 km depth which are unconformably overlain by SE-dipping reflections (Fig. 12). Similarly, these relationships are shown in a roughly perpendicular section (Fig. 11). Well data from the recently drilled well Höflein5b (OMV, unpub. report, 2013) indicate that these thick subhorizontal reflections belong to the syn-rift Gresten Group, whereas

https://doi.org/10.1017/S0016756816000066

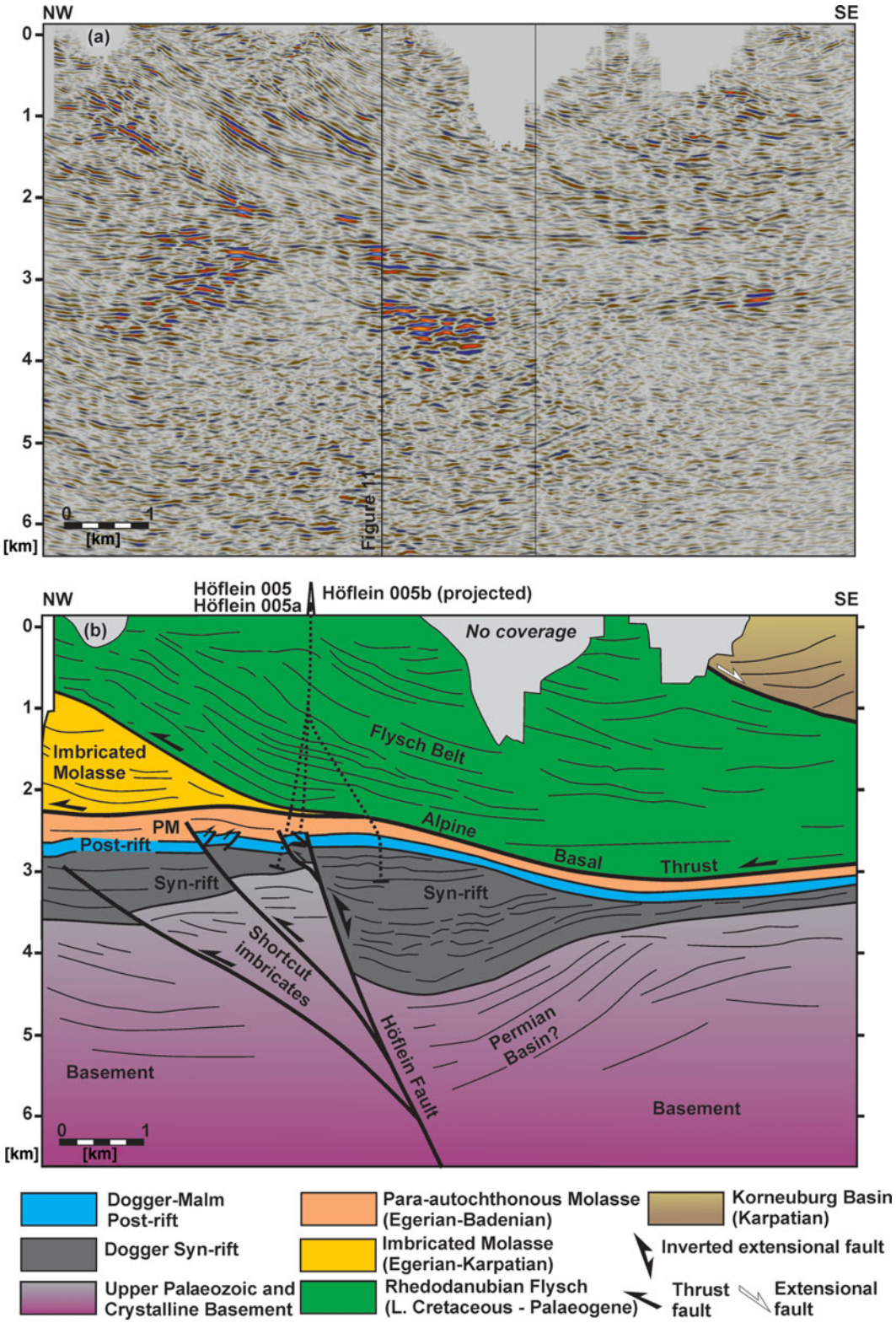

Figure 12. (Colour online) (a) NW–SE-striking depth-migrated seismic profile SW of the elevated Höflein footwall. (b) The geoseismic interpretation shows a reactivated extensional fault with two associated basement-involved shortcut faults interpreted as harpoon or arrowhead structure. This structure is responsible for the imbrication of the basement and the syn-rift section and the folding of the overlying cover and thrust sheets. Small displacement thrusts and backthrusts repeat the carbonate reservoir section.

the dipping reflections immediately above belong to the post-rift reservoir section. Significantly thicker Eggenburgian–Ottnangian (i.e. early Miocene) strata in the hanging wall than in the footwall were found. At this position, the post-rift carbonates lie slightly above the regional elevation (Fig. 6e). Well data also indicate a tectonic repetition of the Höflein Formation in the footwall of the Höflein extensional fault (Fig. 12b). In addition to this, regional elevation also indicates the local repetitions of the syn-rift footwall section to the

https://doi.org/10.1017/S0016756816000066

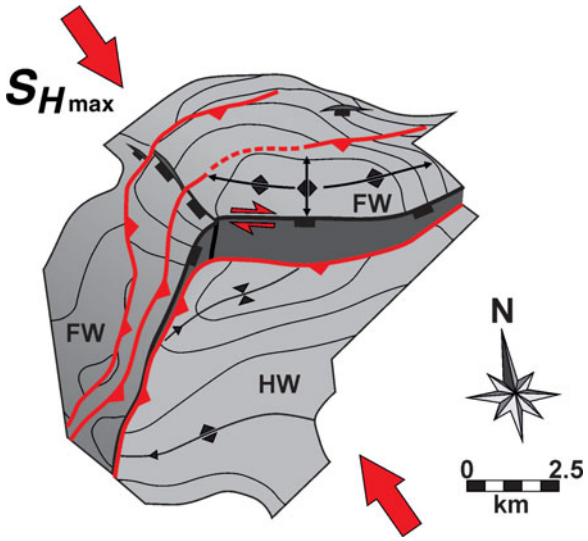

Figure 13. (Colour online) Conceptual 3D model of the Höflein high based on the interpretation of 3D seismic. The surface represents the top of the crystalline basement. Extensional faults are depicted in black, whereas inversion-related thrust faults and reactivated faults are shown in red. The favoured interpretation is a complex harpoon structure related to the mild right-lateral transpressive inversion of a non-rectilinear steeply dipping extensional fault (i.e. Höflein fault) and the associated formation of basement-involved footwall shortcuts. HW – hanging wall; FW – footwall.

NW (Fig. 12). Above the folded post-rift carbonates, the reflections belonging to the Flysch Zone imbricates and the Basal Alpine Thrust are folded into an open anticline (Fig. 12). These cross-cutting relationships provide strong time constraints on the structural evolution of the Höflein field in particular, but also for the studied area.

Fault displacement profiles were calculated for the top of the crystalline basement and the base of the post-rift megasequence (Fig. 6e). The Höflein extensional fault shows a dramatic change in the along-strike throw distribution, as also reflected in the syn-rift isopach map (Fig. 5e). This sharp change in throw and syn-rift sediment thickness is coincident with the change in the strike of the extensional fault from the E–W-striking segment to the NNE–SSW-striking segment. Based on the constructed sections and the 3D structural model, the Höflein field is interpreted as a complex harpoon structure (Badley, Price & Backshall, 1989; Hayward & Graham, 1989; Buchanan & McClay, 1991) consisting of a mildly inverted extensional fault with two basement-involved footwall shortcut faults, and a series of small-displacement thrust and backthrusts which are responsible for the locally observed repetitions of the reservoir carbonate section. According to the geometries described it is suggested that the Höflein extensional fault acted as a buttress upon shortening, promoting the development of the basement-involved shortcut faults and the secondary backthrusts.

5. Discussion and concluding remarks

5.a. Summary of observations: stress-fields and timing constraints

In our work we document several reactivation episodes of the Lower Austria basement fault array in both extensional and shortening modes. The LAMB basement fault array is represented by thick Doggerian wedges related to the rifting and opening of the Alpine Tethys, but some of these basement-involved faults can be as old as of late Palaeozoic age as suggested by borehole data (Wessely, 2006). The LAMB basement-involved faults underwent a first episode of extensional reactivation as shown by the large extensional offsets of the post-rift megasequence and thick (i.e. in excess of 1000 m thick) Eggerian–Karpatian (i.e. late Oligocene – late early Miocene) extensional growth wedges. Biostratigraphically constrained well tops and seismic evidence indicate that the extensional reactivation of the basement faults was synchronous with the development of the thin-skinned FTB and its flexural foreland basin. Broadly speaking, the growth wedges young towards the NW, from Eggerian–Karpatian (i.e. late Oligocene – late early Miocene) age. This provides evidence for the forwards migration of the basement fault array extensional reactivation as the thin-skinned orogenic wedge overrode the subducting European lower plate.

Afterwards, selective mild positive tectonic inversion of the basement fault array took place. This positive inversion event is represented by the mild reactivation upon shortening of several basement-involved faults or fault segments, and the associated folding of the cover. The positive inversion is also shown by a suite of new structures including basement-involved footwall shortcut thrusts (i.e. Haselbach shortcut and Höflein shortcuts) and second-order thrusts (Haselbach backthrust and Höflein backthrusts). The NE–SW orientation of the inversion-related faults is parallel to that of the basement fault array (Fig. 5c, d, e) and suggests roughly coaxial (at least locally) stress fields for the Jurassic rifting and the late Alpine shortening (i.e. NW-directed). In this sense, and in the absence of large fluid overpressures (e.g. Sibson, 1983, 1985, 1990), the generation of new moderately dipping reverse faults is mechanically favoured rather than reactivating the steeply dipping pre-existing basement faults. Moreover, the formation of the footwall shortcuts would have been facilitated by the kinked nature of the basement faults (i.e. Haselbach fault).

The Höflein high is the most important hydrocarbon field in the sub-thrust region of Lower Austria and previous works interpreted its origin as related to purely extensional tectonics (Zimmer & Wessely, 1996). In this work, we propose an alternative interpretation based on a re-interpretation of data where the Höflein high is a complex harpoon structure associated with the inversion of a non-rectilinear extensional fault system (Figs 5, 13). As shown by 3D seismic, well and gravity data, the Höflein high is located nearby the margin of the LAMB, in close proximity to the rigid

Bohemian crystalline massif (Figs 3, 4c) and the Vienna Basin boundary. This fact also suggests that the Bohemian crystalline massif behaved as a rigid buttress promoting the mild inversion of the extensional fault system and the formation of footwall shortcut structures and backthrusts. Whether the positive inversion of the basement fault array was associated with the late stages of the Miocene NW-directed Alpine–Carpathian shortening or the east-directed lateral extrusion is arguable. Present-day seismicity shows the absence of thrust-faulting earthquakes and points to oblique transpressional kinematics (Reinecker & Lenhardt, 1999).

These authors also discuss stress orientation data from borehole breakouts in the Höflein field, indicating large dispersion in the orientation of the principal horizontal compressive stress (i.e. SH_{max} or σ_1), from NNE–SSW- to NW–SW- to NE–SW striking. This is most probably related to two fundamental factors: (1) these borehole break-outs relate to the present-day stress field, which does not need to be the same as the prevailing Miocene stress field; and (2) stress deviations between the local orientation of the SH_{max} and the average regional stress orientation (Rebaï, Philip & Taboada, 1992; Zoback, 2010). The non-rectilinear Höflein half-graben was probably preferentially reactivated than the other basement-involved faults, as the E–W-striking fault plane was not perpendicular to the prevailing subhorizontal NW-directed Alpine principal compressive stress (SH_{max} or σ_1) and not containing the intermediate principal stress (SH_{int} or σ_2), as fault reactivation is partly dependent on the magnitude of σ_2 (Jaeger & Cook, 1979; Zoback, 2010). A NW-directed shortening would have reactivated the E–W-striking segment of the Höflein extensional fault in right-lateral transpressive kinematics. On the other hand, if the inversion of the extensional fault system was related to the lateral E-directed extrusion, the Höflein high would correspond to a restraining bend resulting from left-lateral transpression. In this sense, the orientation, shape and transport direction of the footwall shortcuts and the backthrusts (Fig. 5d, e) fit better with the right-lateral transpressive inversion model in relation to the regional NW-directed shortening.

In the absence of syn-inversion growth strata in the sub-thrust region, relative time constraints can be inferred from the observed cross-cutting relationships. The final activity of the thin-skinned thrust system in the studied area is constrained by the latest early Miocene (i.e. Karpatian) thrust front and piggy-back basins growth strata (Decker & Peresson, 1996; Hölzel *et al.* 2010; Beidinger & Decker, 2014) which is also coincident with the initial infill of the Korneuburg, Fohnsdorf-Seckau and related pull-apart basins developed on top of the FTB (i.e. Ratschbacher *et al.* 1991; Strauss *et al.* 2001; Harzhauser *et al.* 2002; Fig. 3b). The thick-skinned inversion of the sub-thrust basement fault array (i.e. Höflein) should therefore be as old as of Karpatian (latest early Miocene) age, whereas in the foreland (i.e. Mailberg) the Badenian facies distribution (Mandic, 2004) suggests a slightly younger age of inversion (i.e. earliest middle Miocene). This is in agreement with the progressive, although very fast, forwards migration of thick-skinned basement fault reactivation.

5.b. The role of the basement in the Alpine–Carpathian FTB development

The basement of the Alpine–Carpathian FTB presents a general tilting towards the south underneath the Alpine–Carpathian edifice (Wessely, 1987). Deep exploration wells have indicated a differing nature for the crystalline basement of the LAMB and that of the Bohemian Spur. The LAMB sits on crystalline and metasedimentary basement of Moravo–Silesian affinity, whereas the Bohemian Spur is constituted by rigid crystalline basement of Moldanubikum affinity (Kröll & Wessely, 2001; Wessely, 2006). These different basement domains were assembled during the Late Palaeozoic Variscan Orogeny and their boundary corresponds to a major orogenic suture (Neubauer & Handler, 1999).

Lankreijer *et al.* (1999) defined several thermo-lithospheric domains of contrasting equivalent elastic thickness (EET) and rheology for the Bohemian and Alpine–Carpathian domains. According to these authors, the Bohemian domain is represented by extreme values of lithospheric strength and large EET, whereas the inherited Jurassic European continental margin is characterized by significantly lower values. As suggested by Reinecker & Lenhardt (1999), such differing basement nature and associated rheological contrasts controlled the development and architecture of the Upper and Lower Austria Mesozoic Basins, the subsequent development of the Alpine–Carpathian FTB and probably that of the 'successor' middle–late Miocene basins.

More recently, Beidinger & Decker (2014) have shown that the thin-skinned thrust front in the Alpine–Carpathian Junction parallels the –1000 m isoline (i.e. metres below mean sea level), and that the Bohemian Spur probably generated a buttressing effect that limited the forwards thrust propagation and led to generalized out-of-sequence thrusting. The present-day stress field and the recent earthquake distribution also indicate a strong basement control of the Bohemian massif, where the highest observed seismicity is located in its southernmost tip and displays a radial stress configuration (Reinecker & Lenhardt, 1999). The Alpine Molasse basin drastically changes in width from west to east (Andeweg & Cloethigh, 1998), forming two well-developed thrust salients with wide foreland basins in the Upper Austria and the Polish Carpathians regions. On the contrary, the Alpine–Carpathian Junction represents a recess, where the foreland basin is *c.* 9 km wide (Fig. 1). The observed lateral variation in the width of the Molasse Basin correlates with the degree of tilting of the foreland region and therefore with a lateral change in the EET (Andeweg & Cloetingh, 1998).

5.c. Possible controls on crustal coupling and geodynamic implications

Early orogenic shortening in the Alpine–Carpathian Junction was accommodated by shallow flat-dominated thin-skinned tectonics coeval with extension in the foreland plate. Late orogenic shortening was however accommodated by the reactivation of a deeper ramp-dominated thick-skinned system prograding beneath and ahead of the thin-skinned thrust front. Similar structural styles and timing relationships have recently been reported to the ENE of the studied area in the Western Carpathians (e.g. Castellucio *et al.* 2015) and in other collisional settings such as Taiwan, Western Alps, French Pyrenees (e.g. Lacombe & Mothereau, 2002) or the Andes (e.g. Carrera & Muñoz, 2013), among others (e.g. Cooper, 2007).

The reasons for a change from initial extension in the foreland to generalized crustal coupling, shortening and late widespread erosion and extension in the Alpine–Carpathian Junction must be the result of large, lithospheric-scale processes. Based on seismic and tomographic studies, Kissling (1993) and later Lippitsch, Kissling & Ansorge (2003) concluded that a lithospheric slab beneath the Western and Central Alps is present, and probably connected to some point to the European continental lithosphere. However, in the Eastern Alps a high-velocity body corresponding to a subvertical to steeply NE-dipping subducted lithosphere has been interpreted (Lippitsch, Kissling & Ansorge, 2003). More recent works have indicated that a detached European slab might still be connected to the lithosphere that is still in place in the Central Alps and might also be connected to a slab graveyard further to the east, at the depth of the upper mantle transition zone (e.g. Bianchi, Miller & Bokelmann, 2014; Qorbani, Bianchi & Bokelmann, 2014).

In either case, subduction and related bending of the lower plate seems to be – at least partially – responsible for the syn-thrusting Eggerian–Karpatian (i.e. late Oligocene – late early Miocene) extension accommodated by the reactivation of the foreland and sub-thrust basement fault array (Fig. 14a). The curvature radii and the thickness of the bending plate would have controlled the amount of extension along the outer arc of the plate (e.g. Ramsay, 1967; Turcotte & Schubert, 1982; Twiss & Moores, 1992; Fig. 14b). An important component of the observed extension could also relate to the retreat of the subducting lithospheric slab as a result of slab-pull forces, a process formerly proposed for the Carpathian arc (e.g. Decker & Peresson, 1996; Linzer, 1996) and more recently for the central region of the European Alps (e.g. Schlunegger & Kissling, 2015). The reported high lateral gradient of EET from the rigid Bohemian massif to the significantly softer Jurassic continental margin seems to be the fundamental cause of the large degree of bending needed to explain the observed extension.

This high EET gradient is also supported by the narrow foreland basin of the Alpine–Carpathian Junction (Fig. 1). A SE-dipping deep detachment is therefore needed to explain the extension accommodated by the reactivation of the basement fault array (e.g. Bradley & Kidd, 1991). A similar detachment beneath the Western–Central Alps foreland basin has also been proposed from the TRANSALP seismic profiling (TRANSALP Working Group, 2002) and field studies (e.g. Butler, 1989; Gillcrist, Coward & Mugnier, 1987). Synchronously, widespread out-of-sequence thrusting (e.g. Beidinger & Decker, 2014) in the extremely flexed region was probably a response of the prowedge to compensate the sinking of the foreland by regaining relief whereas in the platform, out-of-sequence thrusting was favoured by the buttressing effect of the rigid foreland and the foreland pinch-out of the efficient Mikulov Formation detachment. In addition, thrust loading and formation of a retrowedge seem likely given the strong shortening recorded by tight folds in the basement of the Vienna Basin as well as S-verging folds in the Northern Calcareous Alps (e.g. Grünbach syncline) west of the Vienna Basin (Wessely, 2006).

We propose that deep-seated processes affecting the European slab (Fig. 14c) during the final stages of collision are the trigger mechanisms to explain the general uplift of the area as evidenced by landscape evolution, changes in the drainage and subsidence patterns, and the observed shortening styles (e.g. Fodor, 1995; VonBlanckenburg & Davies, 1995; Neubauer, Genser & Handler, 1999; Wessely, 2006; Genser, Cloetingh & Neubauer, 2007; Qorbani, Bianchi & Bokelmann, 2014; Legrain *et al.* 2015). A large-wavelength rebound is well documented by Andeweg & Cloetingh (1998) in the Molasse Basin of western Austria, whereas in the studied area such uplift is demonstrated by the presence of Karpatian-age kilometre-scale canyon incisions (e.g. Dellmour & Harzhauser, 2012). This broad uplift is also supported by thermochronological and field studies in the Western Carpathians (e.g. Danišík *et al.* 2010; Mazzoli *et al.* 2010; Zattin *et al.* 2011; Anczkiewicz, Środoń & Zattin, 2013; Andreucci *et al.* 2013, 2015; Castelluccio *et al.* 2015). The most probable candidates for such deep-seated processes are either oceanic slab roll-back and subsequent break-off, or delamination of the tectonically thickened European lithosphere (see Magni *et al.* 2013). These processes probably started around Karpatian time (e.g. Dellmour & Harzhauser, 2012), but their effects protracted as shown by foreland subsidence analysis (e.g. Genser, Cloetingh & Neubauer, 2007) and the ages of calc-alkaline (20–11 Ma) and late alkaline magmatic series (9–1 Ma), indicating a transition from crustal contaminated magmas to asthenosphere-derived magmas generated by lithosphere extension, respectively (e.g. Embey-Isztin *et al.* 1993; Nemcok *et al.* 1998; Seghedi *et al.* 2004).

The fast rebound following the slab break-off (or delamination) most probably created an excessive topographic load along with drastic changes in the stress regime and high levels of shortening (e.g. Cloetingh *et al.* 2004; Genser, Cloetingh & Neubauer, 2007). We propose that the Alpine–Carpathian tectonic wedge

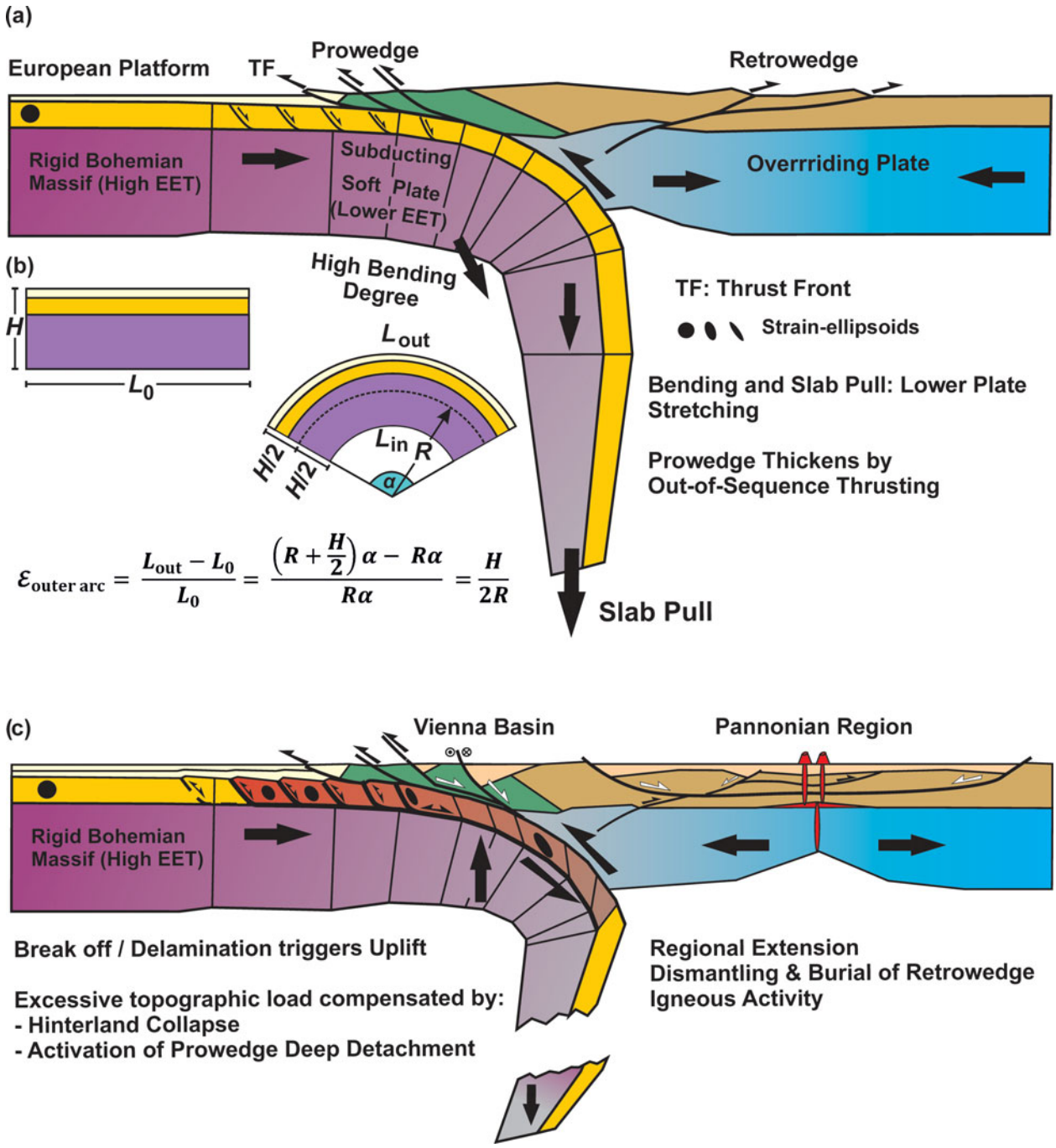

Figure 14. (Colour online) Lithospheric cross-section of the early Miocene collision represented by a subducting lower plate (left) being overridden by an upper plate (right). (a) The sharp transition from an extremely strong and rigid Bohemian massif to the softer Jurassic continental margin favours the acute bending of the lower plate, enhanced by the downward pull of the subducting slab. (b) Bending of a plate leads to the extension of the outer arc and contraction in the inner arc following the given equation. (c) Present-day lithospheric sketch. Slab break-off (or delamination of the orogenically thickened European lithosphere) triggered regional uplift (starting around Karpatian times in the studied area) and the associated excessive topographic load is compensated by basin inversion in the foreland and sub-thrust and the collapse of the hinterland summits. The retrowedge depicted in (a) has been dismantled by the middle–late Miocene regional extension and buried beneath the successor basins.

reacted by two mechanisms. (1) The reactivation of a deep detachment and the basement-involved extensional faults in the prowedge (i.e. basin inversion in the sub-thrust and in the foreland), with the subsequent broadening of the orogen. Basement shortening was most probably accommodated by a combination of distributed deformation in the crystalline basement and discrete heterogeneous simple shear along the deep detachment. (2) This was followed by the collapse of the hinterland orogenic edifice as represented by the opening of the Korneuburg, Vienna, Danube and Pannonian basins. Independently of the dominant strike-slip or oblique-slip activity of the Vienna Basin bounding faults (i.e. Steimberg and Mur-Mürz faults), these faults were key structural elements for the dismantling of the orogenic edifice. The transtensional dismantling

around the Vienna Basin might have been enhanced by the shape of the Bohemian Massif foreland buttress.

A similar evolution has recently been proposed for the Western Carpathians and the associated Sub-Trata fault and its hanging-wall Liptov Basin (e.g. Castellucio *et al.* 2015). In this sense, the 'missing' retrowedge (Fig. 14c) has been extended and buried beneath the thick sedimentary cover of the middle–late Miocene basin systems. Once the topographic load was reduced, the thrust system shut off. The collapse of the orogenic wedge was ultimately driven by subduction processes (i.e. roll back, retreat and final break-off or lithosphere delamination).

Acknowledgements. This is a contribution of the Institut de Recerca Geomodels and the Geodinàmica i Analisi de Conques research group (2014SGR467SGR) from the Agència de Gestió d'Ajuts Universitaris i de Recerca (AGAUR) and the Secretaria d'Universitats i Recerca del Departament d'Economia i Coneixement de la Generalitat de Catalunya. PG acknowledges financial support from OMV Exploration and Production GmbH (Project FBG307451). OMV Exploration and Production GmbH is also thanked for data supply and permission to publish. Andreas Beidinger, Ralph Hinsch and Herwig Peresson from OMV Exploration and Production GmbH are thanked for their comments and suggestions on the very first version of the manuscript. The final version of this paper greatly benefited from the thoughtful revisions by two anonymous reviewers. We would like to extend our appreciation to the editors for allowing us to publish in this special volume. Petrel modelling software by Schlumberger and Skua modelling software by Paradigm were used to build the 3D geological models. Move restoration software was used for cross-section construction.

References

ALLEN, P. A. & ALLEN, J. R. 2005. Basins due to flexure. In *Basin Analysis. Principles and Applications*, 2nd edn. (eds P. A. Allen & J. R. Allen), pp. 116–66. Malden, MA: Blackwell Publishing.

ANCZKIEWICZ, A. A., ŚRODOŃ, J. & ZATTIN, M. 2013. Thermal history of the Podhale Basin in the internal Western Carpathians from the perspective of apatite fission track analysis. *Geologica Carpathica* **64**, 141–51.

ANDEWEG, B. & CLOETINGH, S. 1998. Flexure and 'unflexure' of the North Alpine German-Austrian Molasse Basin: constraints from forwards tectonic modelling. In *Cenozoic Foreland Basins of Western Europe* (eds A. Mascle, C. Puigdefàbregas, H. P. Luterbacher & M. Fernàndez), pp. 403–22. Geological Society of London, Special Publication no. 134.

ANDREUCCI, B., CASTELLUCCIO, A., CORRADO, S., JANKOWSKI, L., MAZZOLI, S., SZANIAWSKI, R. & ZATTIN, M. 2015. Interplay between the thermal evolution of an orogenic wedge and its retro wedge basin: an example from the Ukrainian Carpathians. *Geological Society of America Bulletin* **127**, 410–27.

ANDREUCCI, B., CASTELLUCCIO, A., JANKOWSKI, L., MAZZOLI, S., SZANIAWSKI, R. & ZATTIN, M. 2013. Burial and exhumation history of the Polish Outer Carpathians: discriminating the role of thrusting and post-thrusting extension. *Tectonophysics* **608**, 866–83.

ARZMÜLLER, G., BUCHTA, S., RALBOVSKÝ, E. & WESSELY, G. 2006. The Vienna Basin. In *The Carpathians and their Foreland: Geology and Hydrocarbon Resources*. (eds J. Golonka & F. J. Picha), pp. 191–204. American Association of Petroleum Geologists, Memoir no. 84.

BADLEY, M. E., PRICE, J. D. & BACKSHALL, L. C. 1989. Inversion, reactivated faults and related structures: seismic examples from the southern North Sea. In *Inversion Tectonics* (eds M. A. Cooper & G. D. Williams), pp. 201–19. Geological Society of London, Special Publication no. 44.

BEAUMONT, C., MUÑOZ, J. A., HAMILTON, J. & FULLSACK, P. 2000. Factors controlling the Alpine evolution of the central Pyrenees inferred from a comparison of observations and geodynamical models. *Journal of Geophysical Research* **105**(B4), 8121–45, doi: 10.1029/1999JB900390.

BEIDINGER, A. & DECKER, K. 2014. Quantifying Early Miocene in-sequence and out-of-sequence thrusting at the Alpine-Carpathian junction. *Tectonics* **33**, 222–52.

BIANCHI, I., MILLER, M. & BOKELMANN, G. 2014. Insights on the upper mantle beneath the Eastern Alps. *Earth and Planetary Science Letters* **403**, 199–209.

BRADLEY, D. C. & KIDD, W. S. F. 1991. Flexural extension of the upper continental crust in collisional foredeeps. *Bulletinof the Geological Society of America* **103**, 1416–38.

BROWN, D., ÁLVAREZ-MARRÓN, J., SCHIMMEL, M., WU, Y. M. & CAMANNI, G. 2012. The structure and kinematics of the central Taiwan mountain belt derived from geological and seismicity data. *Tectonics* **31** TC5013, doi: 10.1029/2012TC003156.

BUCHANAN, P. G. & MCCLAY, K. R. 1991. Sandbox experiments of inverted listric and planar fault systems. *Tectonophysics* **188**, 97–115.

BUROV, E. B. & DIAMENT, M. 1995. The effective elastic thickness (T_e) of continental lithosphere: what does it really mean? *Journal of Geophysical Research* **100**, 3905–27.

BUTLER, R. W. H. 1989. The influence of pre-existing basin structure on thrust system evolution in the Western Alps. In *Inversion Tectonics* (eds M. A. Cooper & G. D. Williams), pp. 105–22. Geological Society of London, Special Publication no. 44.

BUTLER, R. W. H. & MAZZOLI, S. 2006. Styles of continental contraction: A review and introduction. In *Styles of Continental Contraction* (eds S. Mazzoli & R. W. H. Butler), pp. 1–10. Geological Society of America, Boulder, Special Paper no. 414.

BUTLER, R. W. H., TAVARNELLI, E. & GRASSO, M. 2006. Structural inheritance in mountain belts: an Alpine-Apennine perspective. *Journal of Structural Geology* **28**, 1893–908.

CAROLA, E., TAVANI, S., FERRER, O., GRANADO, P., QUINTÀ, A., BUTILLÉ, M. & MUÑOZ, J .A. 2013. Along-strike extrusion at the transtion between thin- and thick-skinned domains in the Pyrenean Orogen (northern Spain). In *Thick-skinned Dominated Orogens: From Initial Inversion to Full Accretion* (eds M. Nemčok, A. Mora & J.W. Cosgrove), pp. 119–40. Geological Society of London, Special Publication no. 377.

CARRERA, N. & MUÑOZ, J. A. 2013. Thick-skinned tectonic style resulting from the inversion of previous structures in the southern Cordillera Oriental (NW Argentine Andes). In *Thick-skinned Dominated Orogens: From Initial Inversion to Full Accretion* (eds M. Nemčok, A. Mora & J. W. Cosgrove), pp. 119–40. Geological Society of London, Special Publication no. 377.

CARTWRIGHT, J. A., MANSFIELD, C. & TRUDGILL, B. 1996. The growth of normal faults by segment linkage.

In: *Modern Developments in Structural Interpretation, Validation and Modelling* (eds P. G. Buchanan & D. A. Nieuwland), pp. 163–77. Geological Society of London, Special Publication no. 99.

CASTELLUCCIO, A., ANDREUCCI, B., ZATTIN, M., KETCHMAN, R. A., JANKOWSKI, L., MAZZOLI, S. & SZANIAWSKI, R. 2015. Coupling sequential restoration of balanced cross sections and low-temperature thermochronometry: the case study of the Western Carphatians. *Lithosphere* **7**, 367–78.

CLOETINGH, S. & BUROV, E. B. 1996. Thermomechanical structure of European continental lithosphere: constraints from rheological profiles and EET estimates. *Geophysical Journal International* **124**, 695–723.

CLOETINGH, S. A. P. L., BUROV, E., MATENCO, L., TOUSSAINT, G., BERTOTTI, G., ANDRIESSEN, P. A. M., WORTEL, M. J. R. & SPAKMAN, W. 2004. Thermo-mechanical controls on the mode of continental collision in the SE Carpathians (Romania). *Earth and Planetary Science Letters* **218**, 57–76.

COOPER, M. 2007. Structural style and hydrocarbon prospectivity in fold and thrust belts: a global view. In *Deformation of the Continental Crust: The Legacy of Mike Coward* (eds A. C. Ries, R. W. H. Butler & R. H. Graham), pp. 447–72. Geological Society of London, Special Publication no. 272.

CORNFIELD, S. & SHARP, I. R. 2000. Structural style and stratigraphic architecture of fault propagation folding in extensional settings: a sesmic example from the Smørbukk area, Halten Terrace, Mid-Norway. *Journal of Basin Research* **12**, 329–41.

COSGROVE, J. W. & AMEEN, M. S. 2000. A comparison of the geometry, spatial organization and fracture patterns associated with forced folds and buckle folds. In: *Forced Folds and Fractures* (eds J. W. Cosgrove & M. S. Ameen), pp. 7–21. Geological Society of London, Special Publication no. 169.

DANIŠìK, M., KOHÚT, M., BROSKA, I & FRISCH, W. 2010. Thermal evolution of the Malá Fatra Mountains (Central Western Carpathians): insights from zircon and apatite fission track thermochronology. *Geologica Carpathica* **61**, 19–27.

DAVIS, D. M. & ENGELDER, T. 1985. The role of salt in fold-and-thrust belts. *Tectonophysics* **119**, 67–88.

DECELLES, P. & GILLES, K. A. 1996. Foreland basin systems. *Basin Research* **8**, 105–23.

DECKER, K., MESCHEDE, M. & RING, U. 1993. Fault slip analysis along the northern margin of the Eastern Alps (Molasse, Helvetic Nappes, North- and South-Penninic flysch, and the Northern Calcareous Alps). *Tectonophysics* **223**, 291–312.

DECKER, K. & PERESSON, H. 1996. Tertiary kinematics in the Alpine-Carpathian-Panonnian system: links between thrusting, transform faulting and crustal extension. In *Oil and Gas in Alpidic Thrustbelts and Basins of Central and Eastern Europe* (eds G. Wessely & W. Liebl), pp. 69–77. Geological Society of London, EAGE Special Publication no. 5.

DELLMOUR, R. & HARZHAUSER, M. 2012. The Iváň Canyon, a large Miocene canyon in the Alpine-Carpathian Foredeep. *Marine and Petroleum Geology* **38**, 83–94.

DESEGAULX, P., KOOI, H. & CLOETINGH, S. 1991. Consequences of foreland basin development on thinned continental lithosphere: application to the Aquitaine basin (SW France). *Earth and Planetary Science Letters* **106**, 116–32.

DESTRO, N. 1995. Release fault: a variety of cross fault in liked extensional fault systems in the Sergipe-Alagoas basin, north-eastern Brazil. *Journal of Structural Geology* **17**, 615–29.

DEWEY, J. 1988. Extensional collapse of orogens. *Tectonics* **7**(6), 1123–39, doi: 10.1029/TC007i006p01123.

EMBEY-ISZTIN, A., DOWNES, H., JAMES, D. E., UPTON, B. G. J., DOBOSI, G., INGRAM, G. A., HARMON, R. S. & SCHARBERT, H. G. 1993. The petrogenesis of Pliocene alkaline volcanic rocks from the Pannonian Basin, Eastern Central Europe. *Journal of Petrology* **34**, 317–43.

ERDŐS, Z., HUISMANS, R. S., VAN DER BEEK, P. & THIEULOT, C. 2014. Extensional inheritance and surface processes as controlling factors of mountain belt structure. *Journal of Geophysical Research* **119**, 9042–61, doi: 10.1002/2014JB011408.

FARZIPOUR-SAEIN, A., NILFOUROUSHAN, F. & KOYI, H. 2013. The effect of basement step/topography on the geometry of the Zagros fold and thrust belt (SW Iran): an analogue modeling approach. *International Journal of Earth Sciences* **102**, 2117–35.

FODOR, L. 1995. From transpression to transtesion: Oligocene-Miocene structural evolution of the Vienna Basin and the East-Alpine-Western Carpathian junction. *Tectonophysics* **242**, 151–82.

FOSSEN, H. 2000. Extensional tectonics in the Caledonides: Synorogenic or postorogenic. *Tectonics* **19**, 213–24, doi: 10.1029/1999TC900066.

FRISCH, W., KUHLEMANN, J., DUNKL, I. & BRÜGL, A. 1998. Palispastic reconstruction and topographic evolution of the Eastern Alps during the late Tertiary tectonic extrusion. *Tectonophysics* **297**, 1–15.

GARCÍA-CASTELLANOS, D. & CLOETINGH, S. 2012. Modelling the interaction between lithospheric and surface processes in foreland basins. In *Tectonics of Sedimentary Basins: Recent Advances*, 1st edition (eds C. Busby & A. Azor), pp. 152–81. Chichester: Blackwell Publishing Ltd.

GARCÍA-CASTELLANOS, D., FERNÀNDEZ, M. & TORNÉ, M. 1997. Numerical modelling of foreland basin formation: a program relating thrusting, flexure, sediment geometry and lithosphere rheology. *Computers and Geosciences* **23**, 993–1003.

GENSER, J., CLOETINGH, S. & NEUBAUER, F. 2007. Late orogenic rebound and oblique Alpine convergence: new constraints from subsidence analysis of the Austrian Molasse basin. *Global and Planetary Change* **58**, 214–33.

GILLCRIST, R., COWARD, M. P. A. & MUGNIER, J. L. 1987. Structural inversion and its controls: examples from the Alpine foreland and the French Alps. *Geodinamica Acta* **1**, 5–34.

GOOFEY, G. P., CRAIG, J., NEEDHAM, T. & SCOTT, R. 2010. Fold-thrust belts: overlooked provinces or justifiably avoided. In: *Hydrocarbons in Contractional Belts* (eds G. P. Goofey, J. Craig, T. Needham & R. Scott), pp. 1–6. Geological Society of London, Special Publication no. 348.

GRASSL, H., NEUBAUER, F., MILLAHN, K. & WEBER, F. 2004. Seismic image of the deep crust at the eastern margin of the Alps (Austria): indications for crustal extension in a convergent orogen. *Tectonophysics* **380**, 105–22.

GRAVELEAU, F., MALAVIEILLE, J. & DOMINGUEZ, S. 2012. Experimental modelling of orogenic wedges: a review. *Tectonophysics* **538–540**, 1–66.

HANDY, M. R., SCHMID, S. M., BOUSQUET, R., KISSLING, E. & BERNOULLI, D. 2010. Reconciling plate-tectonic reconstructions of Alpine Tethys with the geological-geophysical record of spreading and subduction in the Alps. *Earth Sciences Reviews* **120**, 121–58.

HANDY, M. R., USTASZEWSKI, K. & KISSLING, E. 2015. Reconstructing the Alps-Carpathians-Dinarides as a key to understanding switches in subduction polarity, slab gaps and surface motion. *International Journal of Earth Sciences* **104**, 1–26.

HARZHAUSER, M., BOEHME, M., MANDIC, O. & HOFMANN, CH-CH. 2002. The Karpatian (Late Burdigalian) of the Korneuburg Basin: a palaeoecological and biostratigraphical synthesis. *Beitraege zur Palaeontologie* **27**, 441–56.

HAYWARD, A. B. & GRAHAM, R. H. 1989. Some geometrical characteristics of inversion. In *Inversion Tectonics* (eds M. A. Cooper & G. D. Williams), pp. 201–19. Geological Society of London, Special Publication no. 44.

HINSCH, R., DECKER, K. & PERESSON, H. 2005. 3-D seismic interpretation and structural modelling in the Vienna Basin: implications for Miocene to recent kinematics. *Austrian Journal of Earth Sciences* **97**, 38–50.

HOLDSWORTH, R. E. 2004. Weak faults – rotten cores. *Science* **303**, 181–2.

HÖLZEL, M., DECKER, K., ZÁMOLYI, A., STRAUSS, P. & WAGREICH, M. 2010. Lower Miocene structural evolution of the central Vienna Basin (Austria). *Marine and Petroleum Geology* **27**, 666–81.

JACKSON, C. A. L., GAWTHORPE, R. L. & SHARP, I. R. 2006. Style and sequence of deformation during extensional fault-propagation folding: examples from the Hammam Faraun and El-Qaa fault blocks, Suez Rift, Egypt. *Journal of Structural Geology* **28**, 519–35.

JAEGER, G. D. & COOK, N. G. W. 1979. *Fundamentals of Rock Mechanics*. London: Chapman & Hill Ltd., 515 pp.

JAMMES, S. & HUISMANS, R. S. 2012. Structural styles of mountain building: controls of lithospheric rheologic stratification and extensional inheritace. *Journal of Geophysical Research* **117**, B10403, doi: 10.1029/2012JB009376.

JANOSCHEK, W. R., MALZER, O. & ZIMMER, W. 1996. Hydrocarbons in Austria: past, present and future. In *Oil and Gas in Alpidic Thrustbelts and Basins of Central and Eastern Europe* (eds G. Wessely & W. Liebl), pp. 43–63. Geological Society of London, EAGE Special Publication no. 5.

KHALIL, S. M. & MCCLAY, K. R. 2002. Extensional fault-related folding, northwestern Red Sea, Egypt. *Journal of Structural Geology* **24**, 743–62.

KISSLING, R. 1993. Deep structure of the Alps – What do we really know? *Physics of the Earth and Planetary Interiors* **79**, 87–112.

KRÖLL, A. & WESSELY, G. 2001. Geologische Karte de Molassebasis. In *Geologische Themenkarten der Republik Österreich*, 1:200.000. Molassezone Niederösterreich und angrenzende Gebiete, **4** Themenkarten mit Erläut. Wien: Geologische Bundesanstalt.

KRONER, U., MANSY, J. L., MAZUR, S., ALEKSANDROWSKI, P., HANN, H. P. & HUCKRIEDE, H. 2008. Variscan tectonics. In: *The Geology of Central Europe: Vol. 1 Precambrian and Paleozoic* (ed. T. Mc Cann), pp. 665–712. Geological Society of London.

LACOMBE, O. & MOUTHEREAU, F. 2002. Basement-involved shortening and deep detachment tectonics in foreland of orogens: Insigths from recent collision belts (Taiwan, Western Alps, Pyrenees). *Tectonics* **21**(4), doi: 10.1029/2001TC901018.

LACOMBE, O., MOUTHEREAU, F. & ANGELIER, J. 2003. Frontal belt curvature and oblique ramp development at an obliquely collided irregular margin: geometry and kinematics of the NW Taiwan fold-thrust belt. *Tectonics* **22**(3), doi: 10.1029/2002TC001436.

LANKREIJER, A., BIELIK, M., CLOETINGH, S. & MAJCIN, D. 1999. Rheology predictions across the western Carpathians, Bohemian massif, and the Pannonian basin. Implications for tectonic scenarios. *Tectonics* **18**, 1139–53.

LEGRAIN, N., DIXON, J., STÜWE, K., VON BLANCKENBURG, F. & KUBIK, P. 2015. Post-Miocene landscape rejuvenation at the eastern end of the Alps. *Lithosphere* **7**, 3–13.

LENHARDT, W. A., ŠVANKARA, J., MELAICHAR, P., PAZDÍRKOVÁ, J., HAVÍŘ, J. & SÝKOROVÁ, Z. 2007. Seismic activity of the Alpine-Carpathian-Bohemian Massif region with regard to geological and potential field data. *Geologica Carpathica* **58**, 397–412.

LINZER, H.-G. 1996. Kinematics of retreating subduction along the Carpathian arc, Romania. *Geology* **24**, 167–70.

LINZER, H.-G., DECKER, K., PERESSON, H., DELL'MOUR, R. & FRISCH, W. 2002. Balancing lateral orogenic float of the Eastern Alps. *Tectonophysics* **354**, 211–37.

LINZER, H.-G., MOSER, F., NEMES, F., RATSCHBACHER, L. & SPERNER, B. 1997. Build-up and dismembering of a classical fold-thrust belt: from non-cylindrical staking to lateral extrusion in the eastern Northern Calcareous Alps. *Tectonophysics* **272**, 97–124.

LINZER, H.-G., RATSCHBACHER, L. & FRISCH, W. 1995. Transpressional collision structures in the upper crust: the fold-thrust belt of the Northern Calcareous Alps. *Tectonophysics* **242**, 41–61.

LIPPITSCH, R., KISSLING, E. & ANSORGE, J. 2003. Upper mantle structure beneath the Alpine orogen from high-resolution teleseismic tomography. *Journal of Geophysical Research* **108**, 2376, doi: 10.1029/2002JB002016.

MACEDO, J. & MARSHAK, S. 1999. Controls on the geometry of fold-thrust salients. *Geological Society of America Bulletin* **111**, 1808–22.

MAGNI, V., FACCENA, C., VAN HUNEN, J. & FUNICELLO, F. 2013. Delamination vs. break off: the fate of continent collision. *Geophysical Research Letters* **40**, 285–9.

MALAVIEILLE, J. 2010. Impact of erosion, sedimentation, and structural heritage on the structure and kinematics of orogenic wedges: analogue models and case studies. *GSA Today* **20**(1), doi: 10.1130/GSATG48A.1.

MANDIC, O. 2004. Foraminiferal paleocology of a subarine swell – the Lower Badenian (Middle Miocene) of the Mailberg Formation at the Buchberg in the Eastern Alpine Foredeep: initial report. *Annalen des Naturhistorischen Museums in Wien* **105**, 161–74.

MARSHAK, S. 2004. Salients, recesses, arcs, oroclines, and syntaxes: a review of ideas concerning the formation of map-view curves in fold-thrust belts. In *Thrust tectonics and Hydrocarbon Systems* (ed. K. R. McClay), pp. 131–56. The American Association of Petroleum Geologists, Tulsa, Memoir no. 82.

MÁRTON, E., GRABOWSKI, J., PLAŠIENKA, D., TÚNYI, I., KROBICKI, M., HAAS, J. & PETHE, M. 2013. New paleomagnetic results from the Upper Cretaceous red marls of the Pieniny Klippen Belt, Western Carpathians: Evidence for general CCW rotation and implications for the origin of the structural arc formation. *Tectonophysics* **592**, 1–13.

MÁRTON, E., KUHLEMANN, J., FRISCH, W. & DUNKL, I. 2000. Miocene rotations in the Eastern Alps – palaeomagnetic results from intramontane basin sediments. *Tectonophysics* **323**, 163–82.

MAURIN, J. C. & NIVIERE, B. 2000. Extensional forced folding and decollement of the pre-rift series along the Rhine graben and their influence on the geometry of the syn-rift

sequences. In *Forced Folds and Fractures* (eds J. W. Cosgrove & M. S. Ameen), pp. 73–86. Geological Society of London, Special Publication no. 169.

MAZZOLI, S., JANKOWSKI, L., SZANIAWSKI, R. & ZATTIN, M. 2010. Low-T thermochronometric evidence for post-thrusting (< 11 Ma) exhumation in the Western Outer Carpathians, Poland. *Comptes Rendus - Geoscience* **342**, 162–9.

MCKENZIE, D. 1978. Some remarks on the development of sedimentary basins. *Earth and Planetary Science Letters* **40**, 25–32.

MOLNAR, P. & TAPPONNIER, P. 1975. Cenozoic tectonics of Asia: effects on a continental collision. *Science* **189**, 419–26.

MOUTHEREAU, F., DEFFONTAINES, B., LACOMBE, O. & ANGELIER, J. 2002. Variations along the strike of the Taiwan thrust belt: basement control on structural style, wedge geometry, and kinematics. In *Geology and Geophysics of an Arc-Continent Collision, Taiwan, Republic of China* (eds T. B. Byrne & C. S. Liu), pp. 35–58. Geological Society of America, Boulder, Special Paper no. 358.

MOUTHEREAU, F., WATTS, A. B., & BUROV, E. 2013. Structure of orogenic belts controlled by lithospheric age. *Nature Geoscience* **6**, 785–9.

MUGNIER, J. L., BABY, P., COLLETTA, B., VINOUR, P., BALE, P. & LETURMY, P. 1997. Thrust geometry controlled by erosion and sedimentation: a view from analogue models. *Geology* **25**, 427–30.

MUÑOZ, J., BEAMUND, E., FERNÁNDEZ, O., ARBUÉS, P., DINARÈS-TURELL, J. & POBLET, J. 2013. The Ainsa Fold and Trust oblique zone of the central Pyrenees: kinematics of a curved contractional system from paleomagnetic and structural data. *Tectonics* **32**, 1142–75, doi: 10.1002/tect.20070.

NACHTMANN, W. & WAGNER, L. 1987. Mesozoic and early Tertiary evolution of the Alpine foreland in Upper Austria and Salzburg, Austria. *Tectonophysics* **137**, 61–76.

NEMCOK, M., POSPISIL, L., LEXA, J. & DONELICK, R. A. 1998. Tertiary subduction and slab break-off model of the Carpathian-Pannonian region. *Tectonophysics* **295**, 307–40.

NEUBAUER, F., GENSER, J. & HANDLER, R. 1999. The Eastern Alps: results of a two-stage collision process. *Mitteilungen der Österreichischen Geologischen Gesellschaft* **92**, 117–34.

NEUBAUER, F. & HANDLER, R. 1999. Variscan orogeny in the Eastern Alps and Bohemian Massif: how do these units correlate. *Mitteilungen der Österreichischen Geologischen Gesellschaft* **92**, 35–59.

NILFOUROUSHAN, F. & KOYI, H. A. 2007. Displacement fields and finite strains in a sandbox model simulating a fold-thrust-belt. *Geophysical Journal International* **169**, 1341–55.

NILFOUROUSHAN, F., PYSKLYWEC, R., CRUDEN, A. & KOYI, H. 2013. Thermal-mechanical modeling of salt-based mountain belts with pre-existing basement faults: application to the Zagros fold and thrust belt, southwest Iran. *Tectonics* **32**, 1212–26.

PEACOCK, D. C. P. & SANDERSON, D. J. 1991. Displacements, segment linkage and relay ramps in normal fault zones. *Journal of Structural Geology* **13**, 721–33.

PERESSON, H. & DECKER, K. 1997. Far-field effects of Late Miocene subduction in the Eastern Carpathians: E-W compression and inversion of structures in the Alpine-Carpathian-Pannonian region. *Tectonics* **16**, 38–56.

PERRIN, C., CLEMENZI, L., MALAVIEILLE, J., MOLLI, G., TABOADA, A. & DOMINGUEZ, S. 2013. Impact of erosion and décollements on large-scale faulting and folding in orogenic wedges: analogue models and case studies. *Journal of the Geological Society* **170**, 893–904.

PILLER, W. E., HARZHAUSER, M. & MANDIC, O. 2007. Miocene Central Paratethys stratigraphy – current status and future directions. *Stratigraphy* **4**, 151–68.

PLATT, J. P. 1986. Dynamics of orogenic wedges and the uplift of high-pressure metamorphic rocks. *Geological Society of America Bulletin* **96**, 1037–53.

QORBANI, E., BIANCHI, I. & BOKELMANN, G. 2014. Slab detachment under the Eastern Alps seen by seismic anisotropy. *Earth and Planetary Science Letters* **409**, 96–108.

RAMSAY, J. G. 1967. *Folding and Fracturing of Rocks*. New York: McGraw-Hill, 568 pp.

RATSCHBACHER, L., FRISCH, W., LINZER, H. G. & MERLE, O. 1991. Lateral extrusion in the Eastern Alps, 2. Structural analysis. *Tectonics* **10**, 257–71.

REBAÏ, S., PHILIP, H. & TABOADA, A. 1992. Modern tectonic stress field in the Mediterranean region: evidence for variation in stress directions at different scales. *Geophysical Journal International* **110**, 106–40.

REINECKER, J. & LENHARDT, W. A. 1999. Present-day stress field and deformation in eastern Austria. *International Journal of Earth Sciences* **88**, 532–50.

ROEDER, D. 2010. Fold-thrust belts at Peak Oil. In *Hydrocarbons in Contractional Belts* (eds G. P. Goofey, J. Craig, T. Needham & R. Scott), pp. 7–31. Geological Society of London, Special Publication no. 348.

ROYDEN, L. H. 1985. The Vienna basin: a thin-skinned pull-apart basin. In *Strike Slip Deformation, Basin Formation and Sedimentation* (eds. K. Biddle & N. Kristie-Blick), pp. 319–38. Society of Economic Paleontologists and Mineralogists, Special Publication no. 37.

RUH, J. B., KAUS, B. J. P. & BURG, J.-P. 2012. Numerical investigation of deformation mechanics in fold-and-thrust belts: influence of rheology of sigle and multiple décollements. *Tectonics* **31** TC3005, doi: 10.1029/2011TC003047.

SACHSENHOFER, R. F., BECHTEL, A., KUFFNER, T., RAINER, GRATZER, R., SAUER, R. & SPERL, H. 2006. Depositional environment and source potential of Jurassic coal-bearing sediments (Gresten Formation, Höflein gas/condensate field, Austria). *Petroleum Geoscience* **12**, 99–114.

SACHSENHOFER, R. F., KOGLER, A., POLESNY, H., STRAUSS, P. & WAGREICH, M. 2000. The Neogene Fohnsdorf Basin: Basin formation and basin inversion during the lateral extrusion in the Eastern Alps (Austria). *International Journal of Earth Sciences* **89**: 415–30.

SALAS, R., GUIMERÀ, J., MAS, R., MARTÍN-CLOSAS, C., MELÉNDEZ, A. & ALONSO, A. 2001. Evolution of the Mesozoic Central Iberian System and its Cainozoic inversion (Iberian Chain). In *Peri-Tethys Memoir 6: Peri-Tethyan Rift/Wrench Basins and Passive Margins* (eds P. A. Ziegler, W. Cavazza, A. H. F. Robertson & S. Crasquin-Soleau), pp. 145–85. Muséum National d'Histoire Naturelle, Paris, Memoir no. 186.

SAUER, R., SEIFERT, P. & WESSELY, G. 1992. Guidebook to excursions in the Vienna Basin and the adjacent Alpine-Carpathian thrust belt in Austria. *Mitteilungen der Österreichischen Geologischen Gesellschaft* **85**, 1–264.

SCHLUNEGGER, F. & KISSLING, E. 2015. Slab rollback orogeny in the Alps and evolution of the Swiss Molasse Basin. *Nature Communications* **6**, 1–10, doi: 10.1038/ncomms9605.

SCHMID, S. M., FÜGENSHCHUH, B., KISSLING, E. & SCHUSTER, R. 2004. Tectonic map and overall architec-

ture of the Alpine orogen. *Eclogae Geologicae Helvetiae* **97**, 93–117.

SCHRÖDER, B. 1987. Inversion tectonics along the western margin of the Bohemian Massif. *Tectonophysics* **137**, 93–100.

SEGHEDI, I., DOWNES, H., VASELLI, O., SZAKÁCS, A., BALOGH, K. & PÉCSKAY, Z. 2004. Post-collisional Tertiary-Quaternary mafic alkalic magmatism in the Carpathian-Pannonian region: a review. *Tectonophysics* **393**, 43–62.

SIBSON, R. H. 1983. Continental fault structure and the shallow earthquake source. *Journal of the Geological Socity of London* **140**, 741–67.

SIBSON, R. H. 1985. A note of fault reactivation. *Journal of Structural Geology* **7**, 751–4.

SIBSON, R. H. 1990. Rupture nucleation on unfavorably oriented faults. *Bulletin of the Seismological Society of America* **80**, 1580–604.

STEARNS, D. W. 1978. Faulting and forced folding in the Rocky Mountain foreland. In: *Laramide Folding Associated with Basement Block Faulting in the Western United States* (V. Matthews III, ed.), pp. 1–38. Geological Society of America, Memoir no. 151.

STRAUSS, P., HARZHAUSER, M., HINSCH, R. & WAGREICH, M. 2006. Sequence stratigraphy in a classic pull-apart basin (Neogene, Vienna Basin). A 3D seismic based integrated approach. *Geologica Carpathica* **57**, 185–97.

STRAUSS, P., WAGREICH, M., DECKER, K. & SACHSENHOFER, R. F. 2001. Tectonics and sedimentation in the Fohnsdorf-Seckau Basin (Miocene, Austria): from a pull-apart basin to a half-graben. *International Journal of Earth Sciences* **90**, 549–59.

SZANIAWSKI, R., MAZZOLI, S., JANKOWSKI, L. & ZATTIN, M. 2013. No large-magnitude tectonic rotations of the Subsilesian Unit of the Outer Western Carpathians: evidence from primary magnetization recorded in hematite-bearing Węglówka Marls. *Journal of Geodynamics* **71**, 14–24.

TARI, G. 2005. The divergent continental margins of the Jurassic proto-Pannonian Basin: implications for the petroleum systems of the Vienna Basin and Moesian Platform. In *25th Annual Bob. F. Perkins Research Conference: Petroleum Systems of Divergent Continental Margin Basins*. Society of the Sedimentary Geology, Gulf Coast Section, 955–86.

TAVANI, S., ARBUÉS, P., SNIDERO, M., CARRERA, N. & MUÑOZ, J. A. 2011. Open Plot Project: an open-source toolkit for 3-D structural data analysis. *Solid Earth* **2**, 53–63.

TAVANI, S. & GRANADO, P. 2015. Along-strike evolution of folding, stretching and breaching of supra-salt strata in the Plataforma Burgalesa extensional forced fold system (northern Spain). *Basin Research* **27**, 573–85.

THOMAS, D. W. & COWARD, M. P. 1995. Late Jurassic-Early Cretaceous inversion of the northern East Shetland Basin, northern North Sea. In *Basin Inversion* (eds J. G. Buchanan & P. G. Buchanan), pp. 275–306. Geological Society of London, Special Publication no. 88.

THÖNY, W., ORTNER, H. & SCHOLGER, R. 2006. Paleomagnetic evidence for large en-bloc rotations in the Eastern Alps during Neogene orogeny. *Tectonophysics* **414**, 169–89.

TRANSALP Working Group. 2002. First deep seismic reflection images of the Eastern Alps reveal giant crustal wedges and transcrustal ramps. *Geophysical Research Letters* **29**, doi: 10.1029/2001GL014911.

TURCOTTE, D. L. & SCHUBERT, G. 1982. *Geodynamics*. New York: Wiley.

TURNER, J. P. & WILLIAMS, G. A. 2004. Sedimentary basin inversion and intra-plate shortening. *Earth-Science Reviews* **65**, 277–304.

TWISS, R. J. & MOORES, E. M. 1992. *Structural Geology*. San Francisco: Freeman.

USTASZEWSKI, K., SCHMID, S., FÜGENSCHUH, B., TISCHLER, M., KISSLING, E. & SPAKMAN, W. 2008. A map-view restoration of the Alpine-Carpathian-Dinaridic system for the Early Miocene. *Swiss Journal of Geosciences* **101**, 273–94.

VERNANT, PH., NILFOROUSHAN, F., HATZFELD, D., ABBASI, M. R., VIGNY, C., MASSON, F., NANKALI, H., MARTINOD, J., ASHTIANI, A., BAYER, R., TAVAKOLI, F. & CHÉRY, J. 2004. Present-day crustal deformation and plate kinematics in the Middle East constrained by GPS measurements in Iran and northern Oman. *Geophysical Journal International* **157**, 381–98.

VONBLANCKENBURG, F. & DAVIES, J. H. 1995. Slab breakoff: A model for syncollisional magmatism and tectonics in the Alps. *Tectonics* **14**, 120–31.

WAGNER, L. R. 1996. Stratigraphy and hydrocarbons in the Upper Austrian Molasse Foredeep (active margin). In *Oil and Gas in Alpidic Thrustbelts and Basins of Central and Eastern Europe* (eds. G. Wessely & W. Liebl), pp. 217–35. Geological Society of London, EAGE Special Publication no. 5.

WAGNER, L. R. 1998. Tectono-stratigraphy in the Molasse Foredeep of Salzburg, Upper and Lower Austria. In *Cenozoic Foreland Basins of Western Europe* (eds A. Mascle, C. Puigdefàbregas, H. P. Luterbacher & M. Fernàndez), pp. 339–69. Geological Society of London, Special Publication no. 134.

WATTS, A. B. & BUROV, E. B. 2003. Lithospheric strength and its relationships to the elastic and seismogenic layer thickness. *Earth and Planetary Science Letters* **213**, 113–31.

WESSELY, G. 1987. Mesozoic and Tertiary evolution of the Alpine-Carpathian foreland in eastern Austria. *Tectonophysics* **137**, 45–9.

WESSELY, G. 1988. Structure and development of the Vienna Basin in Austria. In *The Pannonian Basin: a Study of Basin Evolution* (eds L. H. Royden & F. Horvarth), pp. 333–46. America Association of Petroleum Geologists, Memoir no. 45.

WESSELY, G. 2006. *Geologie der Österreichischen Bundesländer*. Geologische Bundesanstalt, Wien, 416 pp.

WHITE, N. J., JACKSON, J. A. & MCKENZIE, D. P. 1986. The relationship between the geometry of normal faults and that of the sedimentary layers in their hanging walls. *Journal of Structural Geology* **8**, 897–909.

WILLEMSE, E. J. M., POLLARD, D. D. & AYDIN, A. 1996. Three-dimensional analysis of slip distributions on normal fault arrays with consecuences for fault scaling. *Journal of Structural Geology* **18**, 295–309.

WILLIAMS, G. D., POWELL, C. M. & COOPER, M. A. 1989. Geometry and kinematics of inversion tectonics. In *Inversion Tectonics* (eds M. A. Cooper & G. D. Williams), pp. 3–15. Geological Society of London, Special Publication no. 44.

WITHJACK, M. O., OLSON, J. & PETERSON, E. 1990. Experimental models of extensional forced folds. *American Association of Petroleum Geologists Bulletin* **74**, 1038–54.

WITHJACK, M. O. & SCHLISCHE, R. W. 2006. Geometric and experimental models of extensional fault-bend folds. In *Analogue and Numerical of Crustal-Scale Processes*

(eds S. J. H. Buiter & G. Schreurs), pp. 285–305. Geological Society of London, Special Publication no. 253.

WÖLFLER, A., KURZ, W., FRIZT, H. & STÜWE, K. 2011. Lateral extrusion in the Eastern Alps revisited: refining the model by thermochronological, sedimentary, and seismic data. *Tectonics* **30**, TC4006, doi: 10.1029/2010TC002782.

XIAO, H. & SUPPE, J. 1992. Origin of rollover. *American Association of Petroleum Geologists Bulletin* **76**, 509–29.

ZATTIN, M., ANDREUCCI, B., JANKOWSKI, L., MAZZOLI, S. & SZANIAWSKI, R. 2011. Neogene exhumation in the Outer Western Carpathians. *Terra Nova* **23**, 283–91.

ZIEGLER, P. A., CLOETINGH, S., GUIRAUD, R. & STAMPFLI, G. 2001. Peri-Tethyan platforms: constraints on dynamics of rifting and basin inversion. In *Peri-Tethys Memoir 6: Peri-Tethyan Rift/Wrench Basins and Passive Margins* (eds P. A. Ziegler, W. Cavazza, A. H. F. Robertson & S. Crasquin-Soleau), pp. 9–49. Muséum National d'Histoire Naturelle, Paris, Memoir no. 186.

ZIEGLER, P. A., CLOETINGH, S. & VAN WEES, J. D. 1995. Dynamics of intra-plate compressional deformation: the Alpine foreland and other examples. *Tectonophysics* **252**, 7–59.

ZIEGLER, P. A., VAN WEES, J. D. & CLOETINGH, S. 1998. Mechanical controls on collision-related compressional intraplate deformation. *Tectonophysics* **300**, 103–29.

ZIMMER, W. & WESSELY, G. 1996. Exploration results in thrust and sub-thrust complexes in the Alps and below the Vienna Basin in Austria. In *Oil and Gas in Alpidic Thrustbelts and Basins of Central and Eastern Europe* (eds G. Wessely & W. Liebl), pp. 81–107. Geological Society of London, EAGE Special Publication no. 5.

ZOBACK, M. D. 2010. *Reservoir Geomechanics*. Cambridge, UK: Cambridge University Press, 449 pp.

Basin inversion in tectonic wedges: a comparative approach from analogue modelling and the Alpine-Carpathian fold-and-thrust belt

Tectonophysics 703–704 (2017) 50–68

Contents lists available at ScienceDirect

Tectonophysics

journal homepage: www.elsevier.com/locate/tecto

Basin inversion in tectonic wedges: Insights from analogue modelling and the Alpine-Carpathian fold-and-thrust belt

P. Granado [a,b,*], O. Ferrer [a,b], J.A. Muñoz [a,b], W. Thöny [c], P. Strauss [c]

[a] Institut de Recerca Geomodels, Universitat de Barcelona, Martí i Franquès s/n, 08028 Barcelona, Spain
[b] Departament de Dinàmica de la Terra i de l'Oceà, Universitat de Barcelona, Martí i Franquès s/n, 08028 Barcelona, Spain
[c] OMV AUSTRIA Exploration and Production GmbH, Trabrennstraße 6-8, 1020 Vienna, Austria

ARTICLE INFO

Article history:
Received 18 October 2016
Received in revised form 17 February 2017
Accepted 23 February 2017
Available online 27 February 2017

Keywords:
Analogue modelling
Sub-thrust basin inversion
Reactivation
Vertical load
Strain-softening

ABSTRACT

This work simulates the inversion and incorporation of sub-thrust segmented half-graben basins into tectonic wedges by means of sandbox analogue models. Segmented half-graben basins - striking at 90°, 45° and 15° to the extension direction - were created first, and then shortened using different angles for the basal detachment and topographic slope. A shallow viscous polymer layer located above the half-graben basin was included in one of the models. The experiments were analysed using time-lapse photography, topography laser scans and image-based 3D voxels. The results indicate a deformation sequence characterised by layer-parallel compaction, fault reactivation, thrust propagation and related folding. Fault reactivation was associated with the layer-parallel compaction accomplished by slip along the basal detachment, prior to and in between pulses of thrusting. Results reveal the fundamental control imposed by the vertical load of the tectonic wedge and its integrated strength profile in the inversion of sub-thrust basins. Results are compared to the Alpine-Carpathian fold-and-thrust belt.

1. Introduction

Extensional fault systems in rifted continental margins are systematically segmented by the occurrence of soft- and hard-liked transfer fault systems (e.g., Gibbs, 1984; Morley et al., 1990; Gawthorpe and Hurst, 1993). This segmentation arises from the interaction of fault growth processes with pre-existing crustal features that become reactivated upon rifting (e.g., Bartholomew et al., 1993; Faulds and Varga, 1998; Morley, 2010; Fossen et al., 2016). In this sense, structural inheritance may also play an important role during subsequent shortening stages. In collisional foredeeps, rifted continental margins are buried by foreland sedimentary systems and, ultimately, become overridden by advancing fold-and-thrust belts. With ongoing collision, compressive stresses can be transmitted into the foreland plate, causing the positive inversion of these deep-seated sub-thrust basins (Fig. 1) under compressional and/or transpressional stress regimes (e.g., Ziegler et al., 2001). Studies on fold-and-thrust belts such as the European Alpine system (e.g., Gillcrist et al., 1987; Williams et al., 1989; Huyghe and Mugnier, 1995; Muñoz, 2002; Mencos et al., 2015), the High Atlas (e.g., El Harfi et al., 2006), the Apennines (e.g., Scisciani, 2009), the Andes (e.g., Carrera and Muñoz, 2013) as well as numerical modelling works (e.g., Buiter et al., 2009; Nilfouroushan et al., 2013; Erdős et al., 2014), have illustrated that inversion of sedimentary basins is largely controlled by the inherited lithospheric architecture, including: (1) the physical properties of pre-existing fault systems and their orientation in relation to stress trajectories; (2) basin geometry and the physical properties of the stratigraphic infill; (3) basement type/s; (4) thermal history; (5) the integrated lithospheric strength profile and its variations through time (e.g., Ziegler et al., 2001). All these factors can be included in the concept of inheritance (e.g., Holdsworth et al., 2001).

The study presented here has been motivated by the recent interpretation of sub-thrust positive inversion structures below the Alpine-Carpathian fold-and-thrust belt (e.g., Granado et al., 2016; Fig. 2). The Höflein high (Fig. 3) is one of the largest hydrocarbon fields in the area and corresponds to a structurally complex basement high, poorly covered by available 3D seismic data. Similar sub-thrust structures are known to host large hydrocarbon reserves in other fold-and-thrust belts, bur their 3D structure and kinematics also remain poorly constrained due to deep burial and limited seismic resolution (e.g., Zimmer et al., 1996; Shiner et al., 2004; D'Adda et al., 2017). By controlling the modelling parameters, sandbox analogue models can provide structurally balanced and scaled solutions aiding in the interpretation process (e.g., Koopman et al., 1987; McClay, 1989, 1995, 1996; Buchanan and McClay, 1991, 1992; Sassi et al., 1993; Vially et al., 1994; Eisenstadt and Withjack, 1995; Storti and McClay, 1995; Brun and Nalpas, 1996; Roure and Colletta, 1996; Dubois et al., 2002;

* Corresponding author at: Institut de Recerca Geomodels, Universitat de Barcelona, Martí i Franquès s/n, 08028 Barcelona, Spain.
E-mail address: pablomartinez_granado@ub.edu (P. Granado).

http://dx.doi.org/10.1016/j.tecto.2017.02.022
0040-1951/

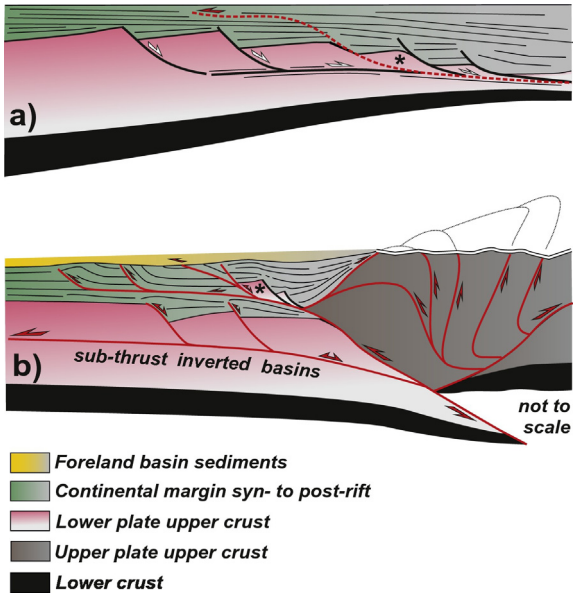

Fig. 1. a) Continental margin. b) Orogenic belt displaying extensional basins imbricated on a fold-and-thrust belt, and sub-thrust inverted basins.

Yamada and McClay, 2004; Eisenstadt and Sims, 2005; Panien et al., 2005; Del Ventisette et al., 2006; Bonini, 2007; Bonini et al., 2012; Di Domenica et al., 2014). In this work, the impact of the vertical load and the strength profile of tectonic wedges on the inversion of structurally segmented sub-thrust basins were investigated by means of sandbox models. For this matter, the experimental approach included the deformation of tectonic wedges using different basal detachment dips and topographic slopes (i.e., β and α angle, respectively) over a frictional basal detachment.

The analysis of the experimental results was focused on two models sharing the same tectonic wedge configuration, one with a shallow viscous detachment above the half-graben basin and one without it, aimed to represent end members of structural coupling. Insights into the geometry, the kinematics and the timing of basin inversion vs. thrust propagation were obtained. To aid in the interpretation of the experimental results, image-based 3D voxel reconstructions (see Dooley et al., 2009) were also carried out. Using longitudinal serial cross-sections as seeds, the technique allows correlating along-strike both the extensional and compressional architectures of the models by means of mutually-orthogonal virtual depth-slices and inline-sections. The experimental results are presented and compared to the Höflein high natural prototype, discussing the competing factors that may influence the role of inheritance in natural systems.

2. Geological framework

The Alpine-Carpathian fold-and-thrust belt is located in the transition between the Eastern Alps and the Western Carpathians (Fig. 2a) to the south of the Bohemian Massif (Fig. 2b). Beneath the fold-and-thrust belt, the former Middle Jurassic to Early Cretaceous rifted margin of the European plate is represented by the Lower Austria Mesozoic Basin (e.g., Wessely, 1987). Although structurally segmented, the basement fault array of the basin is dominantly NE-SW-striking and steeply SE-dipping (Fig. 2c). The basement fault system originated during the late stages of the Variscan cycle (e.g., Wagner, 1998), and since then, became reactivated in several episodes (e.g., Granado et al., 2016). Convergence between Adria and Europe led to the formation of an accretionary prism as the oceanic lithosphere of the European plate was subducted beneath the Adriatic plate. Upon continental collision, the Alpine-Carpathian fold-and-thrust belt developed from late Eocene to early Miocene by the N- to NW-directed overthrusting of the Adriatic plate and the accretion of the Alpine Tethys continental margin sequences onto the European platform (e.g., Decker and Peresson, 1996; Schmid et al., 2004; Beidinger and Decker, 2014). In NE Austria, the Lower Austria Mesozoic Basin and its crystalline basement were overthrust by this thin-skinned fold-and-thrust belt along the shale sequences of the uppermost post-rift and lowermost foreland sediments (e.g., Wagner, 1998; Beidinger and Decker, 2014). Thin-skinned thrusting was followed by the selective reactivation of the basement faults and the formation of new basement-involved thrusts between late early Miocene to earliest middle Miocene. The basement extensional faults and the basement-involved thrusts broadly share the same orientation as constrained by the seismic interpretation and 3D structural modelling carried out (Fig. 2c). The basement-involved shortening was responsible for the formation of the Höflein high and other inversion structures in the sub-thrust and the foreland (e.g., Granado et al., 2016; Fig. 2d).

The Höflein high (Fig. 3a) corresponds to the elevated footwall of the Höflein fault, which is constituted by three segments of distinct mean orientations (Fig. 3c): a Segment 1, dipping 70° towards 114° (i.e., NNE-striking); a Segment 2, dipping 76° towards 175° (i.e., E-W-striking); and a Segment 3, dipping 74° towards 136° (i.e., NE-SW-striking). Based on these orientations and the NW-directed direction of shortening in early Miocene (Beidinger and Decker, 2014), these three fault segments would have been at 15°, 45° and 90° to the shortening direction, respectively (Fig. 3). Interpretation from 3D depth-converted seismic data and well intersections has shown that the Alpine Basal Thrust is folded above the Höflein high. These observations indicate that the uplift was produced after thin-skinned thrusting and by the development of deeper, basement-involved thrusts. Based on this, Granado et al. (2016) interpreted the Höflein high as a harpoon structure (i.e., Williams et al., 1989) constituted by a mildly inverted extensional fault and an imbricate fan of basement-involved footwall shortcut thrusts. From middle Miocene onwards, lateral extrusion of the Eastern Alps towards the Carpathian embayment led to the collapse and burial of the orogenic wedge beneath the Pannonian basins system (Fig. 2a, d). This burial affected largely the fold-and-thrust belt and included parts of its foreland and wedge-top basin (e.g., Ratschbacher et al., 1991; Tomek and Hall, 1993; Fodor, 1995; Decker and Peresson, 1996; Huismans et al., 2001; Strauss et al., 2001; Horvárth et al., 2006; Hölzel et al., 2010).

3. Analogue modelling

3.1. Rationale

Despite the large amount of analogue modelling works on basin inversion to date, few have addressed the inversion of continental margins during the development of tectonic wedges (e.g., Bonnet et al., 2007). A non-cylindrical (i.e., 3D) approach was used for the experimental programme presented here. In such a way, and for the first time, the inversion and imbrication of segmented half-graben basins beneath and ahead of developing fold-and-thrust belts was simulated. Segmented half-graben basins were modelled first, and then shortened using different angles for the basal detachment and topographic slope. A shallow viscous polymer layer, located above the half-graben basin, was included in one of the models (Table 1). The methodology, materials' properties, scaling and the combination of analytical techniques used is this study are described in the following sections.

3.2. Experimental methodology

3.2.1. Set-up

The experimental programme was carried out at the *Geomodels Analog Modeling Laboratory* of the University of Barcelona. A similar set up to that described by Brun and Nalpas (1996), Smit et al. (2003), Schreurs et al. (2006), Graveleau et al. (2012) or Bonini et al. (2012) for physical

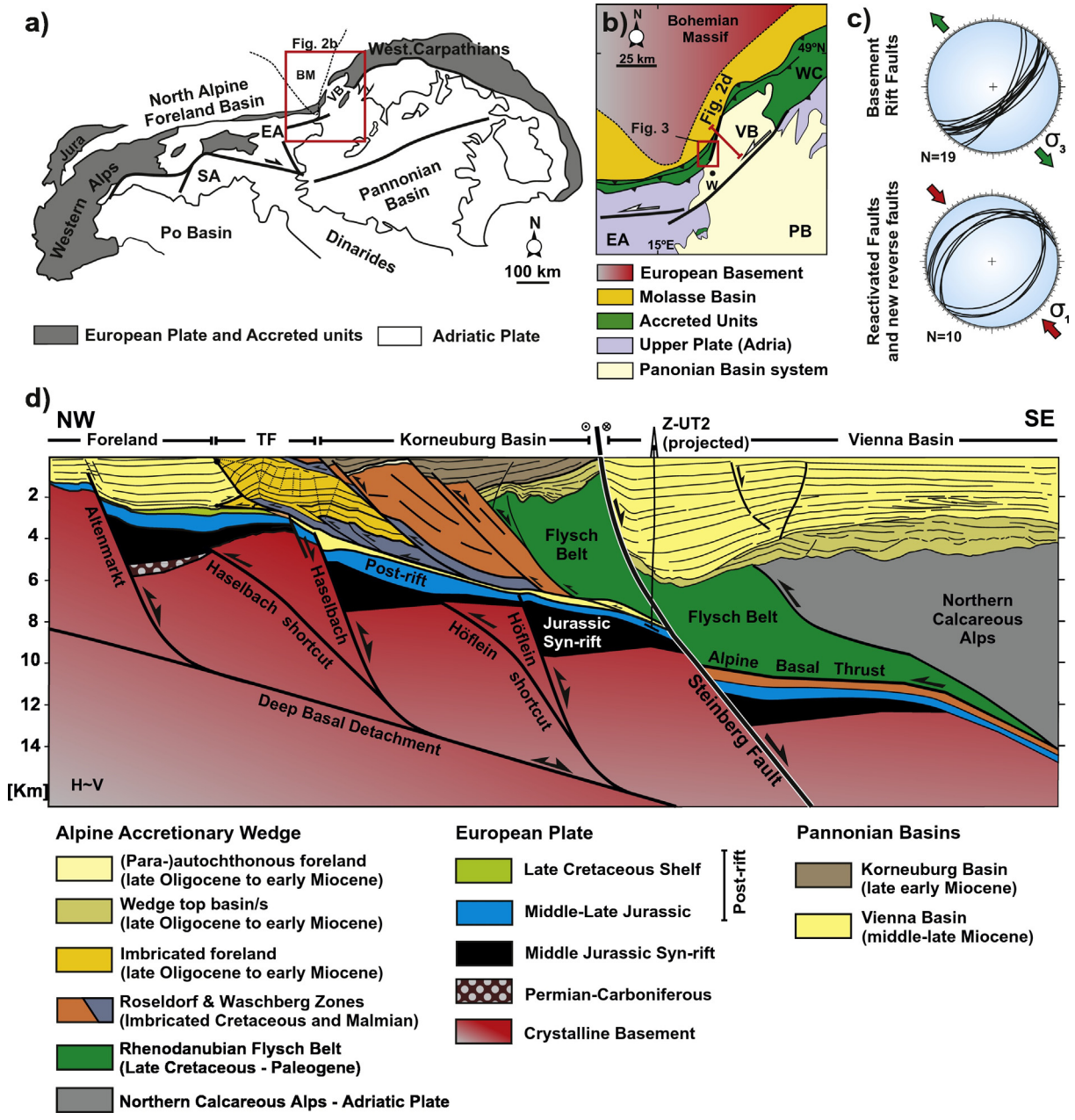

Fig. 2. Geological setting. a) Sketch of the Alpine-Carpathian-Pannonian tectonic framework (modified from Decker and Peresson, 1996). b) Simplified tectonic map of the Alpine-Carpathian Junction. c) Mean orientations of the Lower Austria Mesozoic Basin basement fault array. d) NW-SE-striking regional cross-section along the Alpine-Carpathian foreland, fold-and-thrust belt and the Pannonian basins (Korneuburg and Vienna basins). Modified from Zimmer et al. (1996), Beidinger and Decker (2014) and Granado et al. (2016). BM: Bohemian Massif; EA: Eastern Alps; PB: Pannonian Basin; PM: Para-Autochthonous Molasse; SA: Southern Alps; VB: Vienna Basin; W: Vienna; WC: Western Carpathians.

analogue experiments of brittle and brittle-ductile systems was used. The experimental rig consisted on two glass-sided walls, a fixed wall, and a moving backstop wall with pre-deformation dimensions of 75 × 50 × 6 cm^3. A strong plastic sheet was set at its base to simulate the basal detachment surface (Fig. 4). The plastic sheet was not deformed under the modelling conditions and maintained its length during the experiments. On top of the plastic sheet, a 2 mm-thick basal rigid plate with dimensions of 45 × 50 cm^2 was attached to the fixed wall (Fig. 4). This rigid plate was built with a non-rectilinear boundary inspired on the Höflein fault but aimed at providing a 3D component to the segmented extensional fault system. The rigid plate consisted on two segments oblique to the extension and shortening directions (i.e., one at 15° and another at 45°, such as segments 1 and 2 of the Höflein fault, respectively); the third fault segment perpendicular to both directions of deformation would correspond to the fault segment 3 (compare Figs. 3 and 4). Using a large rigid footwall block, or a rotating mechanical domino set up (Wernicke and Burchfield, 1982; McClay, 1989, 1995) was discarded to minimise the forced reactivation, and to allow for the 'free' deformation of the sandpack and the development of footwall shortcut thrusts by slip along the basal detachment (e.g., Panien et al., 2005; Bonini et al., 2012; Di Domenica et al., 2014).

3.2.2. Analogue materials and scaling

The models were constructed using modelling materials suitable to carry out simulations of upper crustal deformation (see Davy and Cobbold, 1991; Weijermars and Schmeling, 1986; Schellart, 2000; Lohrmann et al., 2003; Adam et al., 2005; Dell'Ertole and Schellart, 2013; Schellart and Strak, 2016). An extension rate of 1 cm/h was applied to all models given that the rheology of dry quartz sand is not strain rate dependent and that no proper estimates for the rate of

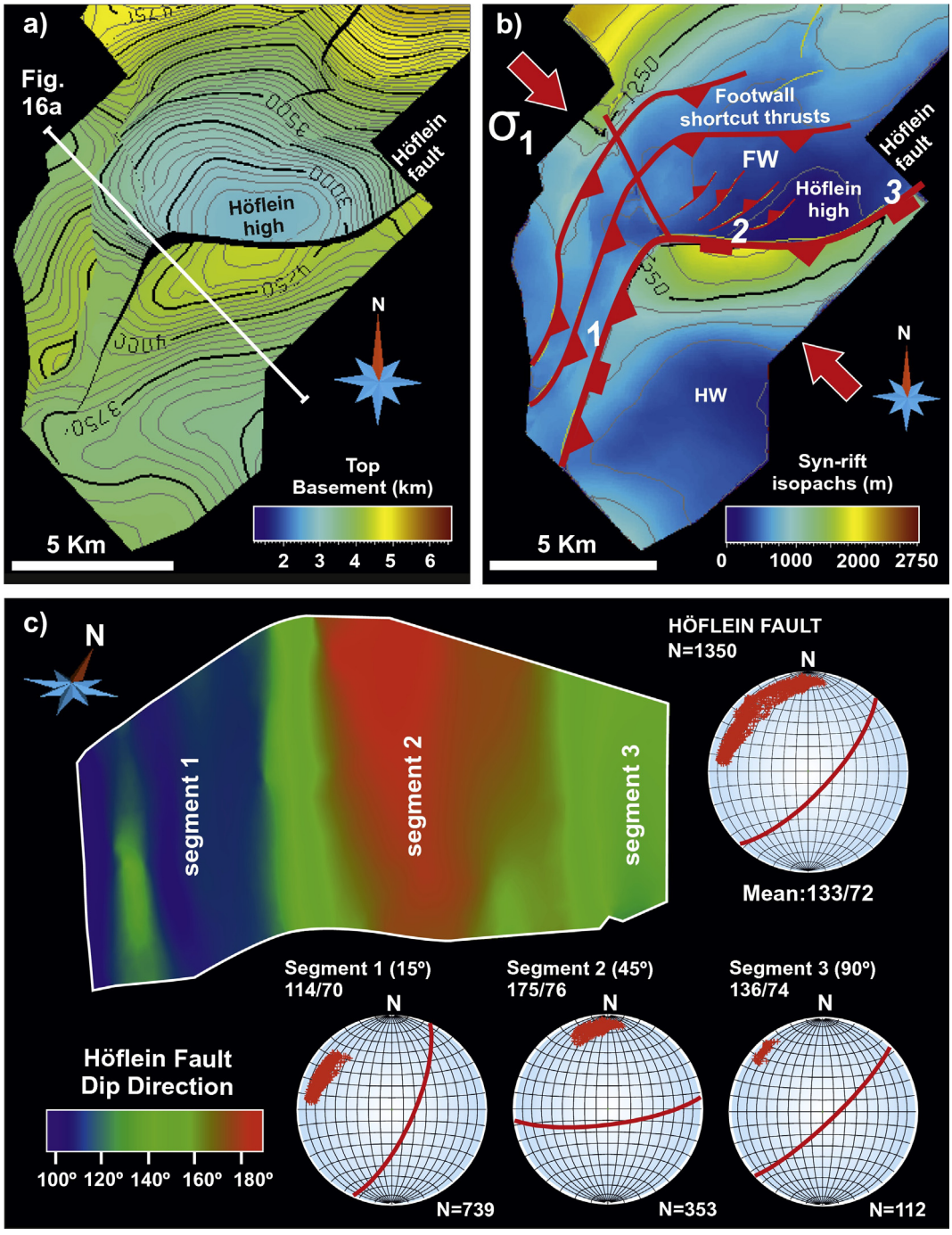

Fig. 3. 3D structure of the Höflein high and related fault segments. a) Top Basement structure map of the Höflein high. b) Syn-rift true stratigraphic thickness map of the Höflein half-graben. Numbers 1, 2 and 3 refer to the three fault segments individuated for the Höflein fault. c) Mean orientation of the Höflein fault and its three fault segments. See text for further details.

Jurassic rifting at the Lower Austria Mesozoic Basin are available. Based on the structural decoupling observed between thin-skinned thrust systems and sub-thrust basins, a strain-rate dependent polymer was used in one of the experiments carried out (see Table 1 and further explanations in the following). A 1.5 cm/h velocity of shortening was chosen after proper scaling using the polymer characteristics and the thrust

Table 1
Main parameters of the experimental programme.

	Basal detachment	Dip (β)	Shallow detachment	Topography slope (α)	Wedge (α + β)	Total extension	Extension rate	Total shortening	Shortening rate
Model 1	Frictional	0°	–	0°	–	5 cm	1 cm/h	–	–
Model 2	Frictional	0°	–	0°	0°	5 cm	1 cm/h	6 cm	1.5 cm/h
Model 3	Frictional	3°	–	32°	35°	5 cm	1 cm/h	15 cm	1.5 cm/h
Model 4	Frictional	3°	–	3°	6°	5 cm	1 cm/h	15 cm	1.5 cm/h
Model 5	Frictional	3°	–	0°	3°	5 cm	1 cm/h	15 cm	1.5 cm/h
Model 6	Frictional	3°	*Viscous*	0°	3°	5 cm	1 cm/h	15 cm	1.5 cm/h

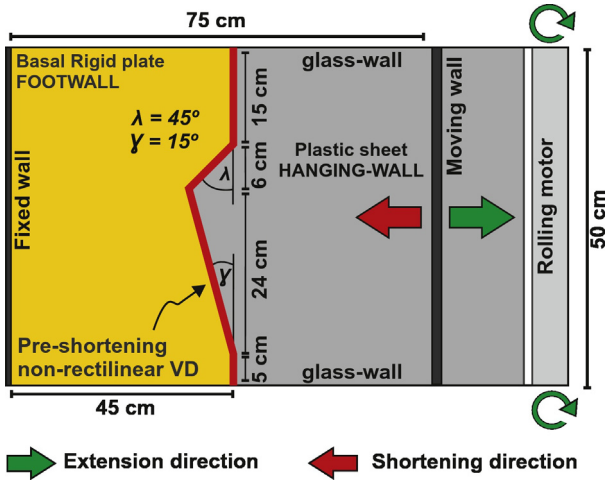

Fig. 4. Experimental set up. a) Top-view sketch of the experimental setup with the terminology used in this article. Note the 3 different segments of the rigid basal plate at 90°, 45° and 15° to the extension and shortening directions. Compare with Fig. 3c.

velocities estimated for the area by Beidinger and Decker (2014). The properties of the materials used and the scaling of the experimental programme are summarised on Table 2.

Dry well-sorted quartz sand with an average grain size of 250 μm, a mean coefficient of friction (φ) of 0.6, and an average angle of internal friction (ϕ) of ~34°, a bulk density of 1600 kg/m^3 and cohesive strength of around 55 Pascals was used. As demonstrated by Lohrmann et al. (2003) and Adam et al. (2005), sand displays an elastic/frictional plastic behaviour with transient strain hardening prior to transition to stable sliding. According to their works, the behaviour of dry quartz sand departs from the classically accepted Mohr-Coulomb rheology (e.g., Hubbert, 1951), but still remains a good mechanical analogue for modelling the brittle behaviour of upper crustal rocks. In particular, sand is considered to be a good analogue material to model settings where the frictional reactivation of faults happens to be mild (e.g., Eisenstadt and Sims, 2005).

The polymer used to replicate the shallow detachment of the thin-skinned fold-and-thrust belt was Rhodosil GUM FB from Bluestar Silicones, a transparent high-viscosity polydimethylsiloxane (see Dell'Ertole and Schellart, 2013). At the low velocities of deformation used in the analogue models presented in this study (Table 1), this polymer behaves as a nearly-Newtonian fluid with low yield strength and a stress exponent n of ~1 (e.g., Davy and Cobbold, 1991; Weijermars and Schmeling, 1986; Dell'Ertole and Schellart, 2013). This rheological behaviour is appropriate to simulate the natural deformation of salt or overpressured shale formations in upper crustal settings (e.g., Weijermars et al., 1993; Couzens-Schultz et al., 2003; Smit et al., 2003; Santolaria et al., 2015; Schellart and Strak, 2016). In comparison with the polymer detachment, the basal detachment constituted by the plastic sheet can be considered frictional as indicated by the dominant breaking-forward sequence of thrusting and the lack of any significant back-thrusting observed (e.g., Couzens-Schultz et al., 2003; Smit et al., 2003; Graveleau et al., 2012).

Table 2
Scaling parameters.

Parameter	Experiment	Nature	Model/nature
Length (L)	1 cm	1 km	1.10^{-5}
Gravity (g)	9.81 m/s^2	9.81 m/s^2	1
Density (ρ)	1.6 g/cm^3	2.6 g/cm^3	0.61
Dry quartz sand			
Density (ρ)	0.97 g/cm^3	2.2 g/cm^3	0.44
Polymer			
Viscosity (η)	1.18×10^4 Pa·s	5×10^{18} Pa·s	2.3×10^{-15}
Time (t)	1 h	258,270 yrs	4.42×10^{-10}
Velocity (V)	1.5 cm/h	5 mm/yrs	2.26×10^4

3.2.3. Procedure

A pre-deformational sandpack was built by pouring layers of even thickness of white-, blue- and black-coloured sand over the basal rigid plate and the plastic sheet. Sand layers of 0.4 cm thickness were laid to facilitate tracking of deformation (Fig. 5a). Subsequently, all models were subjected to 5 cm of extension parallel to the glass-sided walls of the rig at a constant rate of 1 cm/h. Deformation was carried out by a computer-controlled rolling engine that pulled the plastic sheet away from the fixed basal plate. This forced an asymmetric velocity discontinuity at the base of the sandpack and the consequent development of a half-graben (Fig. 5b). At the same time, the moving backstop wall was pulled by a worm screw attached as well to a computer-controlled engine. Both engines worked synchronously at the same rate to avoid differential shortening or extension of the sandpack. The accommodation space created during extension was filled with alternating layers of poured red-, white- and black-coloured sand simulating *syn*-rift deposits. Extension was halted every 30 min to add each new layer of syn-rift sand. The syn-rift sand was only poured inside the developing half-graben basin to fill the accommodation space created during each step of extension. For this, the top of the undeformed pre-rift layers was used as a regional reference of elevation. These steps were repeated until a total of 5 cm of extension were completed. Following extension, all models were covered with an even layer of orange-coloured sand to simulate a post-rift cover (Fig. 5b). This post-rift layer was used as a regional datum of elevation to assess the degree of shortening and uplift of the extensional basins during the subsequent phases of deformation.

For the shortening phase the rolling engine was locked and deformation was applied exclusively by pushing the backstop wall towards the 'undeformed foreland' at a constant velocity of 1.5 cm/h. For shortening, the first shortening model (i.e., Model 2) was kept horizontal whereas for the rest of the shortening experiments (i.e., Models 3 to 6) the deformation rig was tilted 3° towards the backstop moving wall (Fig. 5). In such a way, a series of distinct hinterland-thickening wedges were built by pouring brown and white layers of sand. The parameters changed for the modelling were: the dip of the basal detachment (β), the topographic slope (α), the wedge angle ($\alpha + \beta$), and the presence or absence of a shallow viscous detachment in an equivalent post-rift position. The models carried out and their characteristics are summarised on Table 1 and in Fig. 5. Although erosion and sedimentation are known to have a significant impact on the kinematics of tectonic wedges (e.g., Storti and McClay, 1995; Bonnet et al., 2007; Malavieille, 2010; Graveleau et al., 2012), these were omitted for the sake of simplicity.

3.2.4. Analysis

In order to keep record of the experiments during extension and shortening, time-lapse high-resolution digital photographs were taken from the lateral sides of the model, from an oblique point of view and from the top of the model at 15 s intervals. Videos from these time-lapse photos were generated for kinematic analysis of deformation (see online Supplementary material). A white-light scanner was also used to record the topographical evolution of the models. During extension, these scans were carried out after stopping the deformation rig and before adding each corresponding *syn*-rift layer (i.e., after each 0.5 cm increments of extension). During shortening, scans were made after stopping the rig and for each 3 cm deformation increments. At the end of each experiment, the models were preserved and then longitudinally sectioned at 3 mm spacing. A 4 cm wide section along each side of the experiments was discarded to remove any border effects. High-resolution photographs of the longitudinal cross-sections were then imported as seeds to generate 3D voxel models. Image-processing software was used to generate mutually orthogonal crosslines, inlines

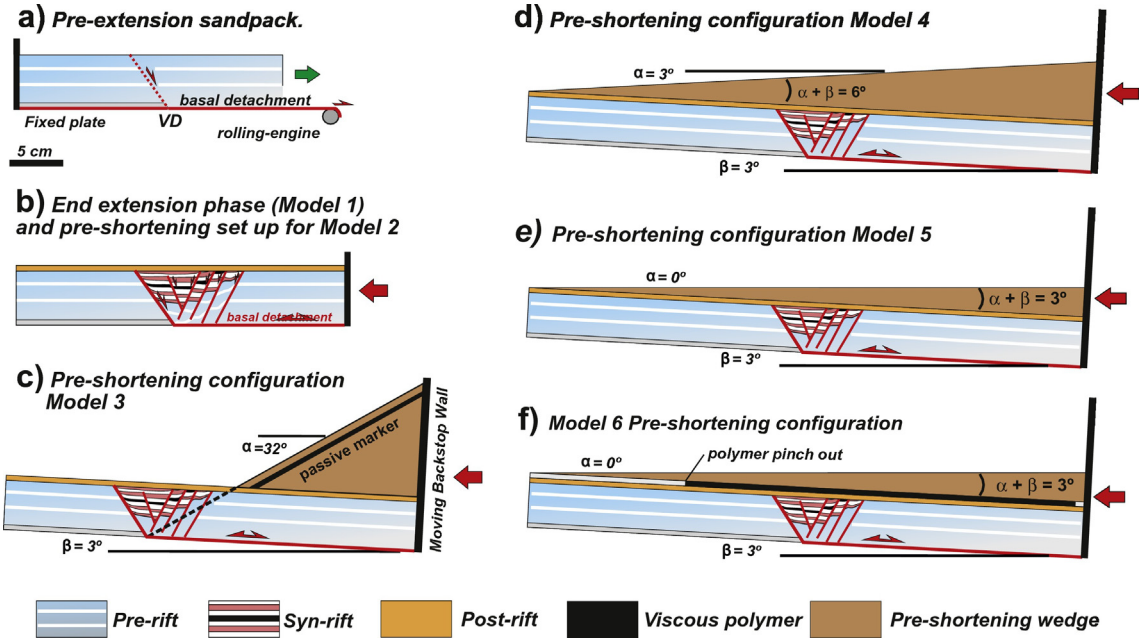

Fig. 5. Summary of the sandbox models set ups carried out in this study. a) Baseline extensional model set up previous to extension. b) Model 1 after 5 cm of extension. The results of Model 1 are also the pre-shortening configuration for shortening Model 2. c) Pre-shortening configuration for Model 3. d) Pre-shortening configuration for Model 4. e) Pre-shortening configuration for Model 5. f) Pre-shortening configuration for Model 6. See Table 1 for further details.

and depth-slices that allowed for better visualisation and interpretation of the experimental results.

4. Experimental results

4.1. Baseline extensional model results (Model 1)

A segmented half-graben basin was developed during the extensional deformation stage of each model. Time-lapse photography (see online supplementary material) has shown that during the earliest stages of extension a master border fault was developed above the velocity discontinuity. An early fault scarp developed above the segments at 90° and 15° to extension, whereas a monocline dipping into the half-graben was developed at the fault segment trending at 45° to extension (Fig. 6a). With ongoing extension, the monocline became breached, and the upward-propagating fault segments were linked along strike (Fig. 6b). Secondary faults, including antithetic and, to a lesser extent synthetic faults, grew as initially sinuous and isolated fault segments, trending parallel to the bisector of the normal to the extension direction and the corresponding velocity discontinuity segment. This is well illustrated by the synthetic fault that breached the monocline developed at the 45° segment. Initially isolated fault segments were developed on those fault segments at 90° and 15° to the extension direction, linking laterally with other isolated fault segments to produce less sinuous, longer strike faults (Fig. 6b). Overall, these faults grew migrating laterally from the 15° and 90° segments towards the 45° fault segment located in the central part of the sandbox model. The formation of additional antithetic faults always took place into the interior of the developing half-graben basin. As extension accumulated, the formerly developed antithetic fault systems progressively took less displacement and became abandoned. At the 45° segment, extensional relay ramps were generated in all the models (Fig. 6b). With continued extension, these relay ramps were eventually breached to form longer strike faults. Oppositely, the master border fault displayed a continuous activity during the extensional phase in all models, developing accommodation space immediately above the velocity discontinuity. This kinematic evolution was observed for all the models carried out in this study.

The internal 3D architecture of the segmented half-graben basin was additionally constrained by means of serial cross sections (Fig. 6c–e) and 3D image-based voxels (Fig. 7). Serial cross-sections have shown differences in regards of the number of faults and their spacing along strike (i.e., fault density): a total of 4 narrowly-spaced antithetic faults were developed at the 90° and 15° segments, whereas only 3 widely-spaced antithetic faults were developed at the central 45° segment. A synthetic fault was also developed at the central 45° segment and was responsible for the formation of a rider block (Fig. 6d). The developed antithetic faults were planar and showed similar cut-off angles at the 90° and 15° segments. Conversely, the antithetic faults developed at the 45° segment display a steepening, concave upwards geometry. The plan view geometry of the extensional basin is shown by a depth-slice (Fig. 7a) as a ribbon of *syn*-rift layers (i.e., red-, white- and black-coloured sand). These layers follow the shape of the basal rigid plate (see Fig. 4 for comparison with the deformation rig set up). Faults were revealed as thin linear features of coloured sand and correspond to the dragged sand layers produced by extension along discrete fault zones. The breached relays ramps and the breached monocline at the 45° fault segment are shown as patches of red- and white-coloured sand on the depth-slice (Fig. 7a). Three virtual inline sections (i.e., sections normal to the direction of extension; Fig. 7b-d) were generated from the 3D voxel and have shown the along-strike structural change of the basin from the footwall to the hanging-wall (i.e., sections from I–I′ to III–III'). For those inline-sections striking at low angles to the faults, the shallowly-dipping fault traces show the apparent dips of the extensional faults (Fig. 7b–d).

4.2. Shortening results

4.2.1. Shortening Model 2

This model consisted in the simulation of the inversion of a shallowly buried segmented half-graben basin by shortening the sandpack without any previous topography (i.e., $\alpha = 0°$) along a horizontal detachment (i.e., $\beta = 0°$). The pre-shortening configuration for Model 2 is shown in Fig. 5b. This set up allowed establishing a baseline model for comparison with the following ones. The total amount of shortening was 6 cm (i.e., slightly more than the amount of extension) and resulted in the formation of a pop-up anticline (Fig. 8) with no preferred structural vergence. The anticline was affected by surface-breaching faults which correspond to reactivated extensional faults (Fig. 8a), as well as

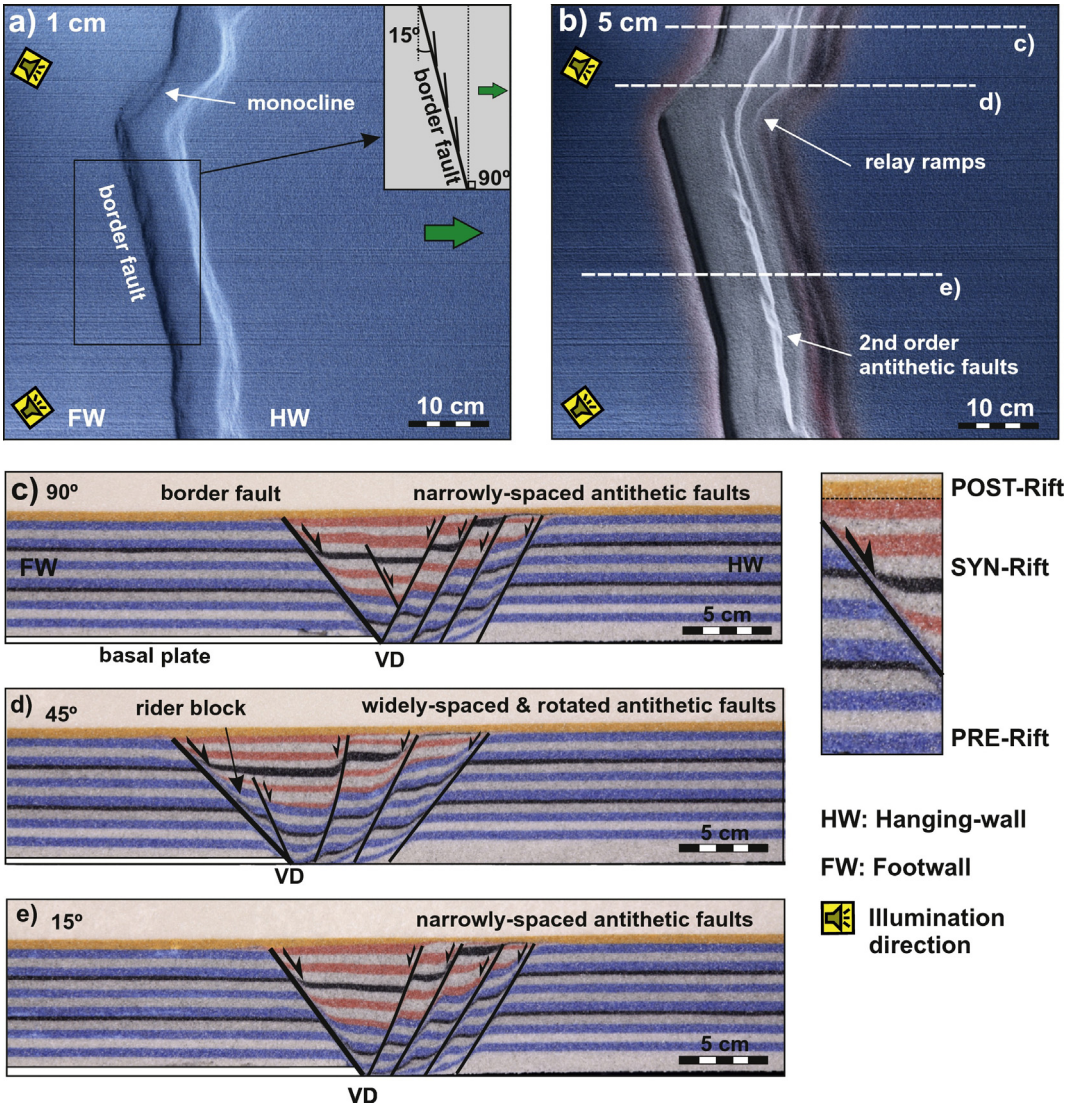

Fig. 6. Summary of results for baseline extension Model 1. Illumination is from the left. Shadowed areas are surface-breaching faults dipping to the right and illuminated areas are surface-breaching faults dipping to the left. a) Top view after 1 cm of extension. b) Top view after 5 cm of extension. c) Cross-section along the 90° segment. d) Cross-section along the 45° segment. e) Cross-section along the 15° segment. FW: Footwall. HW: Hanging-wall. VD: Velocity discontinuity.

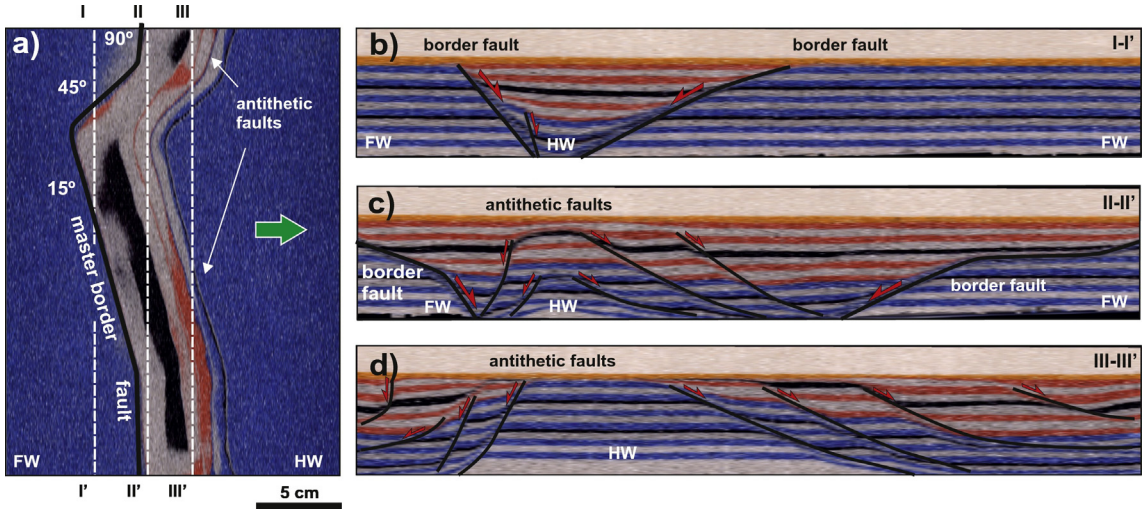

Fig. 7. Virtual sections extracted from the 3D voxel of Model 1. a) Depth-slice showing the top view geometry of the half-graben basin. b) Virtual inline passing by the tip of the extensional basin. c) Virtual inline passing along the central parts of the half-graben basin. d) Virtual inline passing by the 90° and the 15° segments. Shallow dips of the extensional faults are apparent dips. FW: Footwall. HW: Hanging-wall.

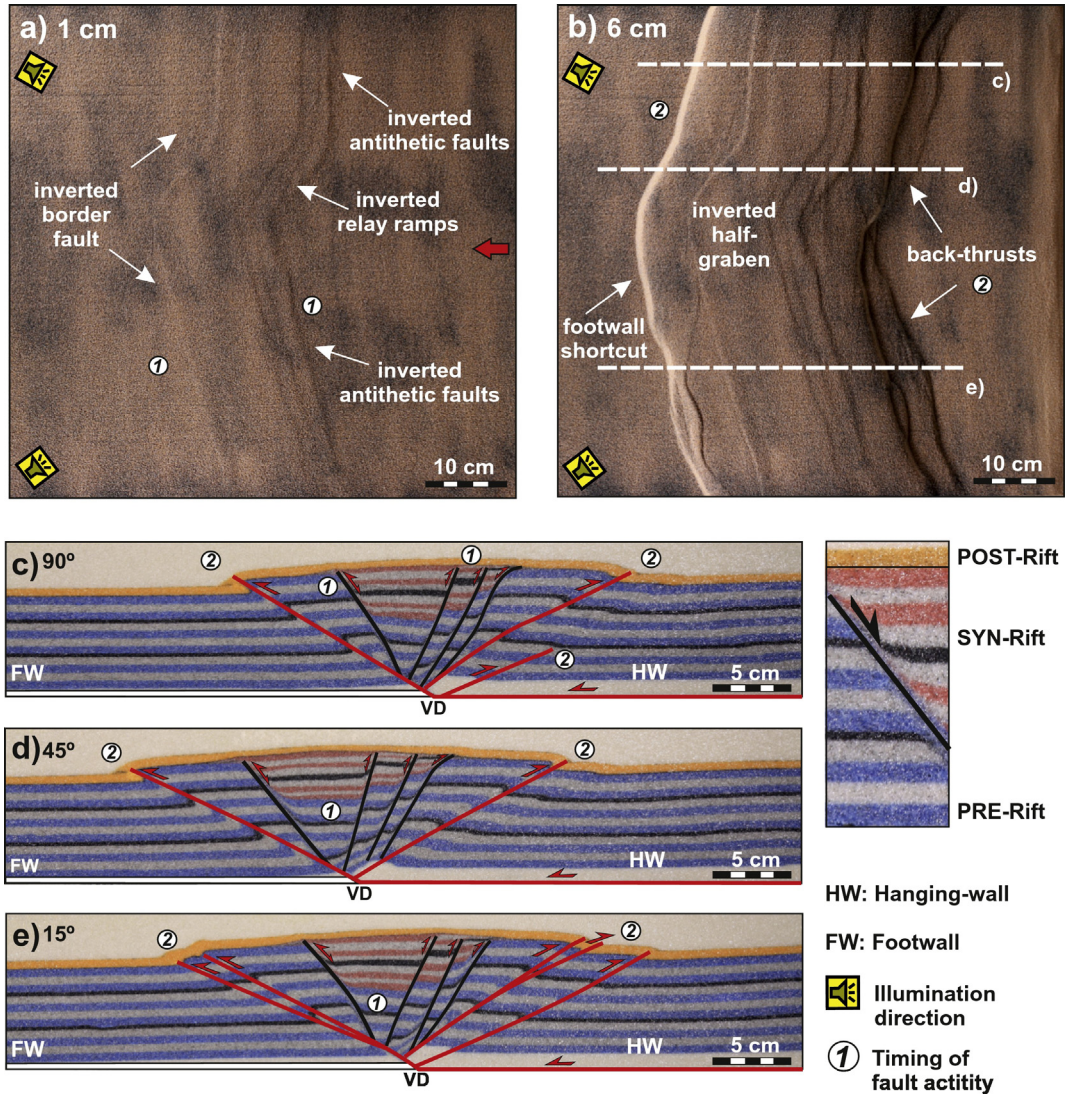

Fig. 8. Summary of results for Model 2. Illumination is from the left. Shadowed areas are surface-breaching faults dipping to the left, whereas illuminated zones are surface-breaching faults dipping to the right. a) Top view after 1 cm of shortening. b) Top view after 6 cm of shortening. c) Sliced cross-section along the 90° segment. d) Sliced cross-section along the 45° segment. e) Sliced cross-section along the 15° segment. Numbers indicate the relative timing of fault activity and basin inversion. FW: Footwall. HW: Hanging-wall.

two forward directed thrusts and two back-thrusts (Fig. 8a, b). On plan view, the developing pop-up anticline and the trace of the emergent thrusts and back-thrusts followed the shape of the underlying rigid plate. Serial vertical sectioning of the model has shown that the thrusts faults display a roughly linear geometry. No significant changes along strike in the structure were observed (Fig. 8c–e). These features indicate that the deformation results could have been partially controlled by the initial boundary conditions of the model.

Time-lapse photography was used to constrain the sequence of deformation (see online supplementary material). During the earliest stages of shortening, the moving backstop wall generated sliding along the basal horizontal detachment, producing the compaction of the sandpack up to the location of the velocity discontinuity. As revealed by time-lapse photography, the first structures to form developed after a certain degree of compaction, and then, folded the surface of the sandbox model (Fig. 8a). These surface-breaching structures are shown up as lighted and shadowed linear features. These early folds mimicked the shape of the previously developed extensional fault system, including the secondary antithetic faults and the breached relay ramps. Hence, these structures are indicative for the early reactivation of the extensional fault array. As shortening continued, deformation was taken up by displacement along back-thrusts and thrusts. The back-thrusts correspond to hanging-wall directed back-thrusts, whereas the thrusts correspond to footwall shortcut thrusts structures (e.g., McClay, 1989).

4.2.2. Shortening Model 3

This model consisted on the deformation of the segmented half-graben basin located ahead of a sand wedge with a topographic slope of $\alpha = 32°$. In contrast with the former model, the pre-shortening configuration included a hinterland-dipping basal detachment ($\beta = 3°$). The elevated slope was built to make it closely correspond to the internal friction threshold of the sand. The set up aimed at modelling the deformation of a near-critical wedge (i.e., in the verge of failure; see Chapple, 1978) so to test if and how the segmented half-graben was inverted and accreted to the toe of the wedge. The wedge was built onto the post-rift cover so as to pinch out in a linear fashion (i.e., at 90° to shortening direction) behind the segmented half-graben basin (Fig. 5c). The total amount of shortening was 15 cm (i.e., three times the value of extension).

Time-lapse photography allowed unravelling the sequence of deformation which is summarised on Fig. 9a and b (see online supplementary material). Similarly to Model 2, an initial phase of sand compaction took place by sliding along the basal detachment. This deformation phase was accompanied by the gentle inversion of the previously

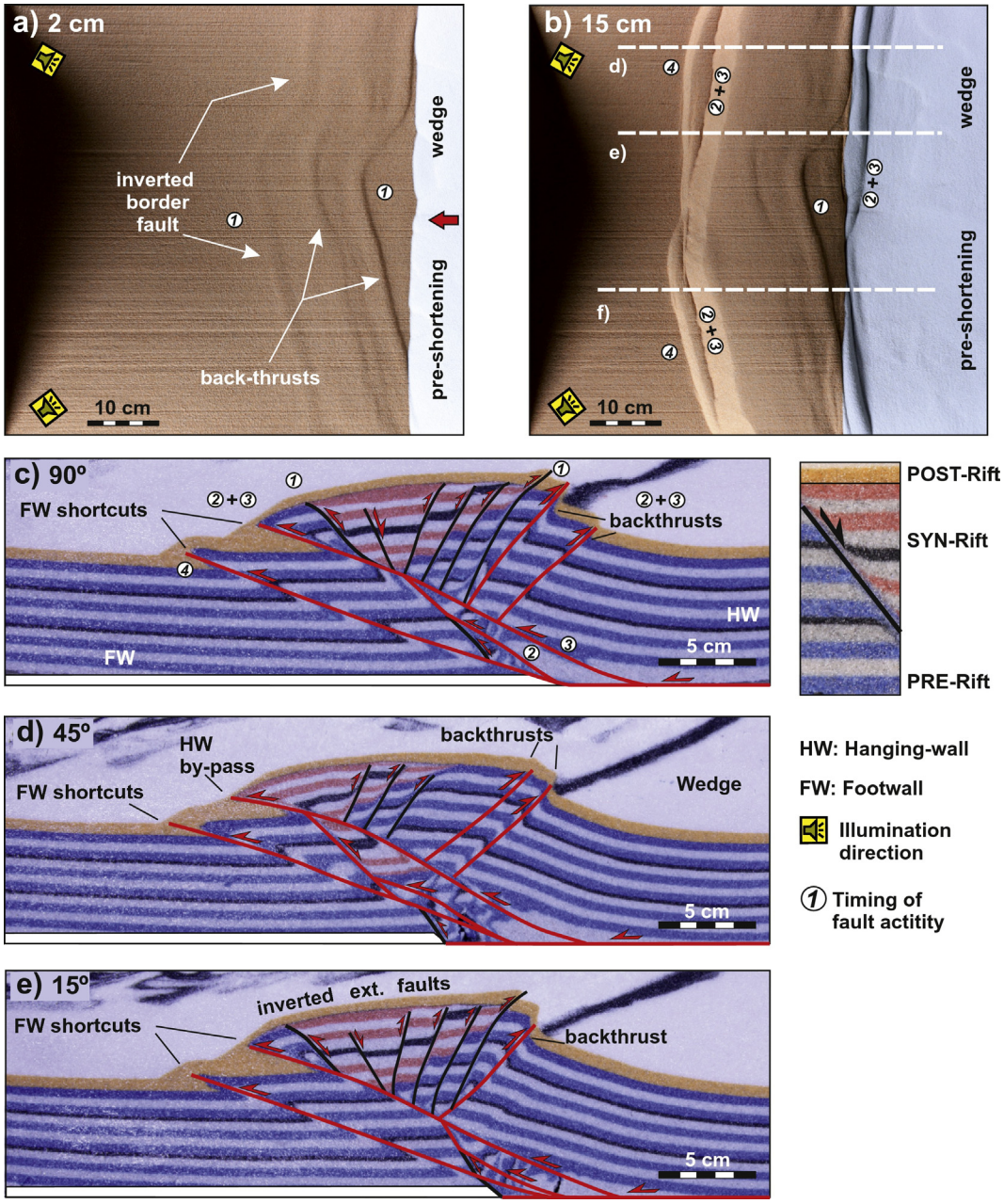

Fig. 9. Summary of results for Model 3. Illumination is from the left. a) Top view after 2 cm of shortening. b) End of experiment after 15 cm of shortening. c) Cross-section along the 90° segment. d) Cross-section along the 45° segment of the rigid basal plate. e) Cross-section along the 15° segment. Numbers indicate relative timing of thrust movement and basin inversion. FW: Footwall. HW: Hanging-wall.

developed extensional fault system (i.e., the master border fault and the antithetic faults) as shown by the formation of surface-breaching fault-propagation folds (Fig. 9a) above the underlying extensional fault system. Inversion was followed by emergent hanging-wall directed back-thrusts and foreland-directed thrusts which affected the pre-rift sand layers. Uplift along the foreland-directed thrusts led to the collapse of the thrust fronts by "mass-wasting". Although the overall kinematical evolution developed broadly in sequence towards the foreland, the cross-cutting relationships shown by serial cross-sectioning and time-lapse videos (see supplementary material) revealed out-of-sequence thrusting (i.e., thrusts #2 and #3; Fig. 9c) after the reactivation of the border extensional fault. The last deformation phase was represented by the formation of an emergent footwall shortcut thrust (i.e., thrust #4; Fig. 9b, c).

Cross sections have shown significant changes along the strike of the model. Thrust #3 developed as a footwall shortcut at the 90° and 15° fault segments, whereas it developed as a hanging-wall by-pass thrust towards the central parts of the sandbox (i.e., 45° segments). The by-pass thrust re-used the upper reaches of the border extensional fault (Fig. 9d), transporting and tilting the half-graben towards the foreland. The basin and its border fault were split in two in the central parts of the sandbox model, where it can be found in a hanging-wall and a footwall position (Fig. 9d). In the 90° and 15° segments, the inverted basin occurs imbricated on a hanging-wall position along with the master extensional fault (Fig. 9c and e).

4.2.3. Shortening Model 4

This model consisted on the deformation of the segmented half-graben basin along a hinterland dipping basal detachment ($\beta = 3°$), with a hinterland-thickening sand wedge covering the full stretch of the model. The sand wedge was built with a 6° thickening angle and a topographic slope $\alpha = 3°$ (Fig. 5d). After 15 cm of shortening, the deformed

tectonic wedged displayed three thrust sheets with associated surface-breaching fault-propagation folds (Fig. 10). Displacement along the hinterland thrust completely overrode the segmented half-graben basin. Time-lapse photography (see online supplementary material) and topography scans have shown a sequence of deformation characterised by a first stage of sand compaction associated to slip along the hinterland-dipping basal detachment. The deformation front of this early compaction phase migrated from the hinterland towards the foreland and arrived ahead of the half-graben basin. The border antithetic fault underwent mild reactivation by back-thrusting (i.e., back-thrust #1), developing a gentle fault-propagation fold. The early deformation front can be better appreciated on the topography scan (Fig. 10b) whereas the emergent back-thrust fault-propagation fold is better shown by time-lapse photography (Fig. 10a, c). Subsequent deformation was characterised by the development of a breaking-forward thrust system (i.e., thrusts #2, #3 and #4; Fig. 10e).

The longitudinal cross-sections revealed a broadly homogeneous along-strike structure dominated by a large thrust sheet associated with thrust #2. For this reason, the cross-section at 45° is shown as a representative section for the whole model (Fig. 10e). The next thrust to develop (i.e., thrust #3) propagated forward from beneath the segmented half-graben, splitting the master extensional fault and the *syn*-rift wedge in two. Displacement along thrust #3 also developed a fault-propagation fold with an associated back-thrust close to the surface. In the central parts of the sandbox, an emergent thrust front was developed (i.e., thrust #4), showing a top view shape parallel to the geometry of the basal plate (Fig. 10c, d). This last thrust propagated forwards in the central parts of the sandbox model but it is linked to thrust #3 towards the lateral ends of the sandbox, meaning that thrust #4 is a splay from thrust #3. Only the border antithetic fault underwent mild reactivation in this model.

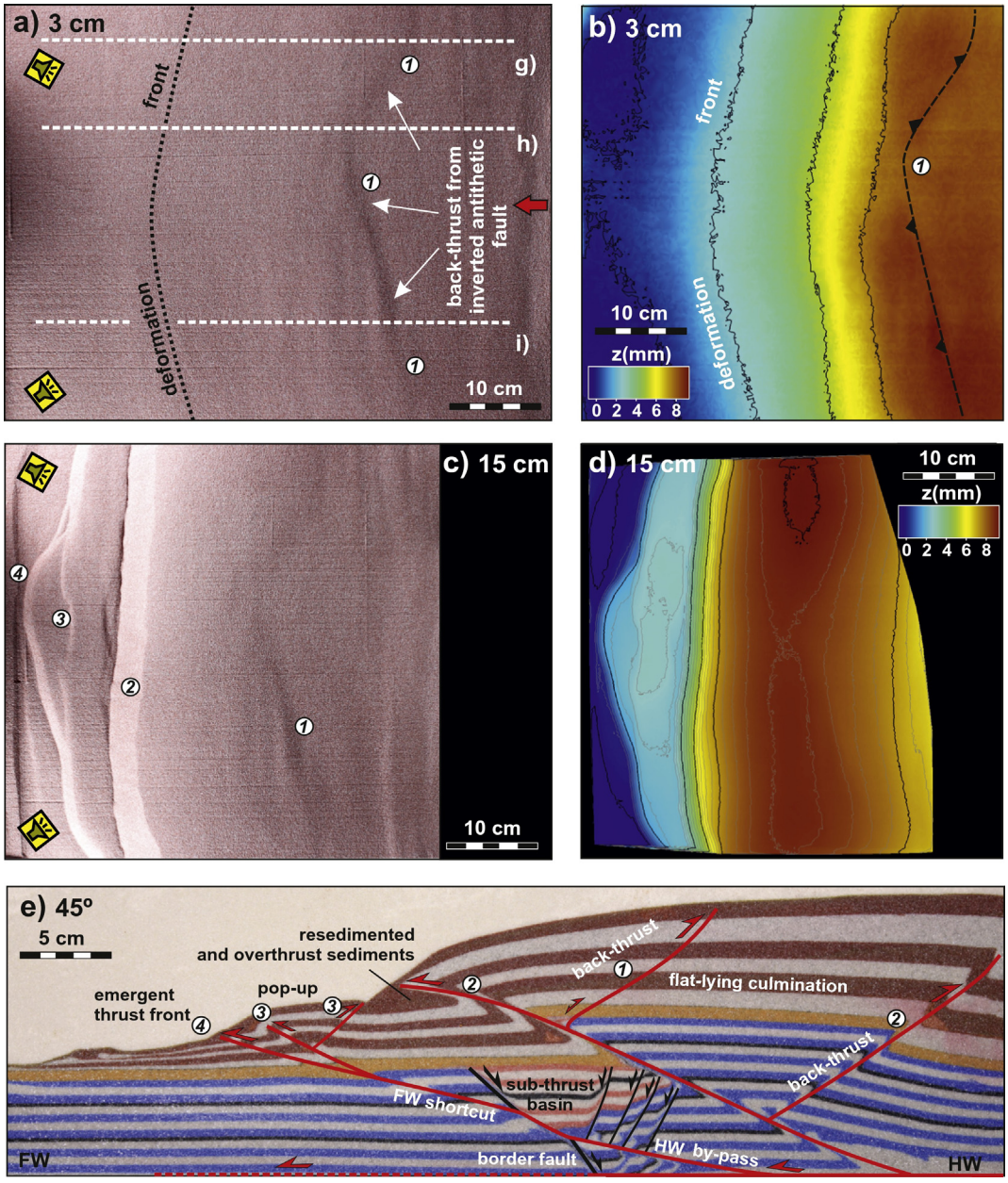

Fig. 10. Summary of results for Model 4. Illumination is from the left. A) Top view after 3 cm of shortening. b) Topography scan also reveals a bow-shaped deformation front developed ahead of the half-graben basin. c) Top view at the end of the experiment after 15 cm of shortening. d) Topography scan after the end of the experiment. e) Sliced cross-section along the 45° segment. Numbers indicate relative timing of thrust movement and basin inversion. FW: Footwall. HW: Hanging-wall.

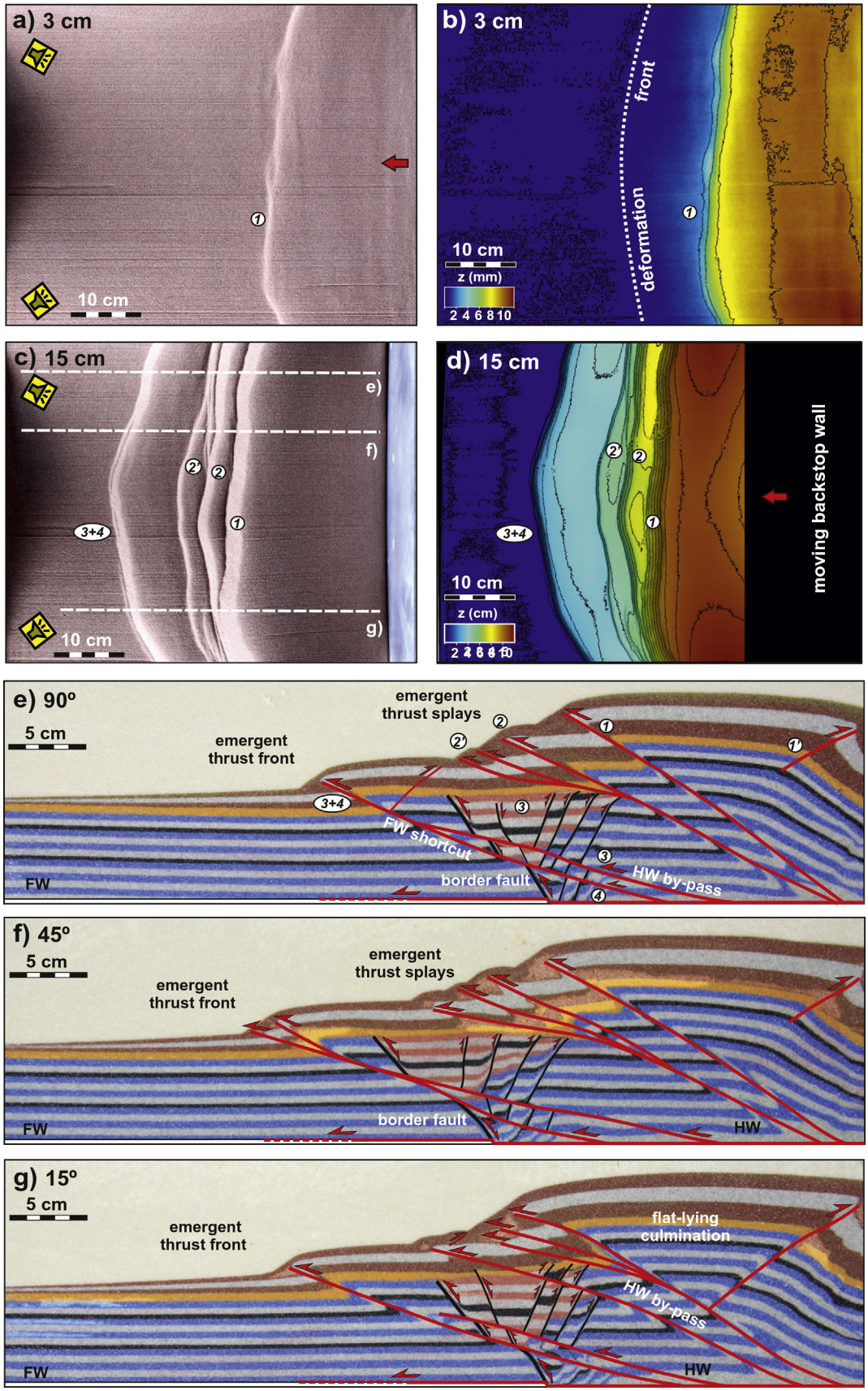

Fig. 11. Summary of results for Model 5. Illumination is from the left. a) Top view after 3 cm of shortening. b) Topography scan after 3 cm. c) Top view at the end of the experiment after 15 cm. d) Topography scan at the end of deformation. e) Cross-section by the 90° segment of the rigid basal plate. f) Cross-section passing by the 45° segment. g) Cross-section by the 15° segment. Numbers indicate relative timing of fault activity. FW: Footwall. HW: Hanging-wall.

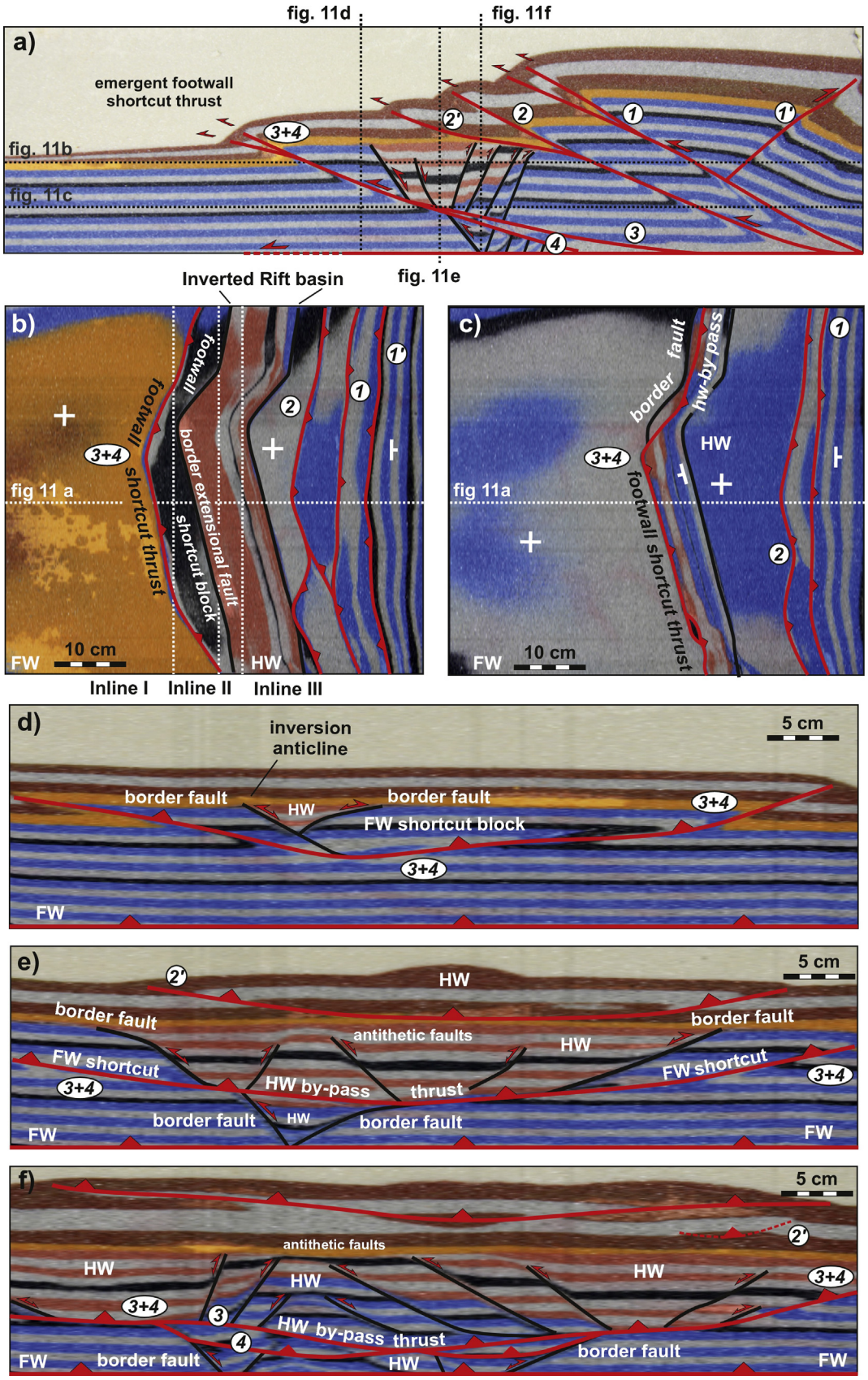

Fig. 12. Virtual sections extracted from the 3D voxel of Model 5. a) Cross-section for reference. b) Depth-slice using the undeformed post-rift unit (i.e., orange layer) as reference. c) Depth-slice taking the middle of the pre-rift sandpack showing the frontal thrust splitting the half-graben basin in two at the 45° and 90° segments. d) Inline-section showing the footwall shortcut block beneath the imbricated half-graben basin. e) Inline-section showing the imbricated half-graben basin over the hanging-wall by-pass thrust f) Inline-section showing the imbricated half-graben basin in a sub-thrust position. Numbers indicate relative timing of fault activity. FW: Footwall. HW: Hanging-wall.

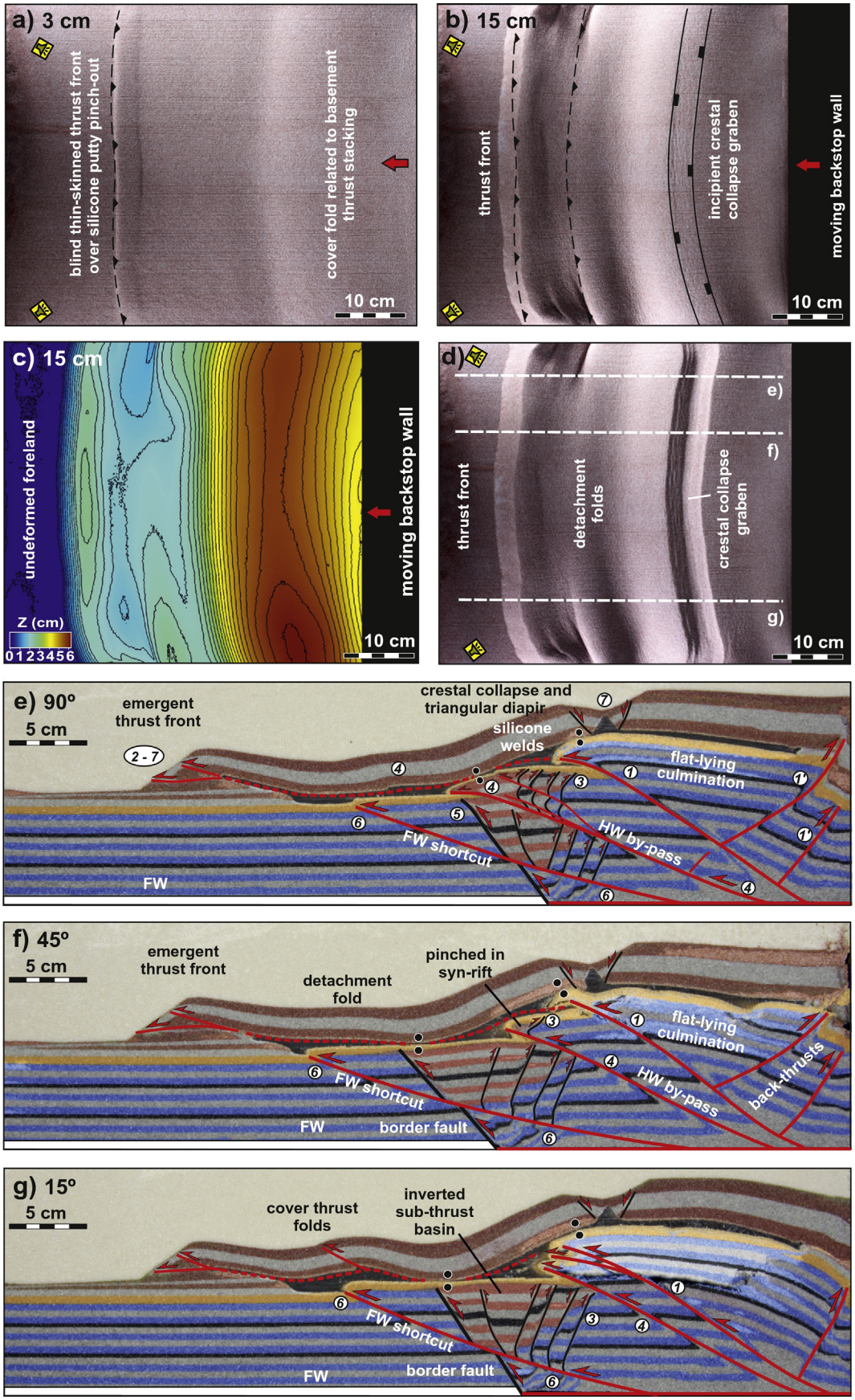

Fig. 13. Summary of results for Model 6. Illumination is from the left. a) Top view after 3 cm of shortening. b) Top view after 15 cm of shortening and c) its topography scan. d) Top view of the model after cessation of shortening. e) Cross-section by the 90° segment of the rigid basal plate. f) Cross-section by the 45° segment. g) Cross-section by the 15° segment. The numbers indicate the relative timing of fault activity. FW: Footwall. HW: Hanging-wall.

4.2.4. Shortening Model 5

This model consisted on the deformation of the segmented half-graben basin along a hinterland dipping basal detachment ($\beta = 3°$) with a sand wedge covering the full stretch of model. The wedge was built with no surface slope (i.e., $\alpha = 0°$). The pre-shortening configuration of the model is summarised in Fig. 5e. After 15 cm of shortening, time-lapse photography (see online Supplementary material), topography scans and serial cross sections (Fig. 11) showed that the sandbox model was deformed by a dominantly breaking-forwards sequence of thrusting. Time-lapse photography highlighted a significant amount of sand compaction by slip along the hinterland-dipping basal detachment prior to the nucleation of thrusts. Displacement along these thrusts formed several surface-breaching thrust faults and related splays. The compaction of sand by slip along the basal detachment formed a compaction front that advanced ahead of the location of the first emergent thrust front (i.e., thrusts #1 and #2 - #2′). This first sand compaction affected only those layers on the hanging-wall of the extensional basin. Further slip along the basal detachment generated additional compaction of sand ahead of the former compaction front, and in a similar fashion, before the nucleation of additional thrusts (i.e., thrusts #3 and #4). The first and second thrusts to form (i.e., thrusts #1 and #2 - #2′) are responsible for the main uplift of the wedge, whereas the last thrust system to develop (i.e., thrusts #3 and #4) imbricated the segmented half-graben basin, and widened the tectonic wedge (Fig. 11). Serial cross sections (Fig. 11e–g) showed that the first three thrust faults developed closely space apart, whereas the last thrust emerged further outboard.

Post-deformation vertical sectioning revealed the subtle reactivation of the extensional faults (i.e., the synthetic and antithetic faults; Fig. 11e–g) and back-thrusting affecting thrust sheet #1. The last thrust faults to form (i.e., thrusts #3 and #4) nucleated also from the rear of the sandpack but propagated through the half-graben basin hanging-wall and footwall. The extensional basin was split by these late thrusts into several segments and was imbricated along with a footwall shortcut block (Fig. 11e–g). In the light of the cross-sections and the lateral time-lapse photography, the sand compaction in between the development of thrusts #1-2-2′ and #3-4 seems to be the responsible for the mild inversion of the extensional fault system.

Virtual depth-slices were generated using the undeformed 'foreland' post-rift and pre-rift sand layers as a regional reference of elevation (Fig. 12a–c). The first depth-slice revealed the shape of uplifted half-graben basin, the plan view geometry of the frontal thrusts #3 and #4 and their imbricated footwall fault block. In a similar fashion to the 3D voxel of the baseline extensional model (Fig. 7), the imbricated half-graben basin displays its characteristic shape arranged in the three 90°, 45° and 15° segments. The footwall shortcut thrust displays kinked plan view geometry, with one larger linear segment parallel to the 15° segment of the border extensional fault, and a shorter sinuous segment striking oblique to the 45° and 90° segments. A deeper depth-slice using the undeformed pre-rift layers as an elevation datum (Fig. 12c) showed a thin slice of the lowermost part of the half-graben basin and its border extensional fault in a sub-thrust footwall position. The geometry of the footwall shortcut thrust is parallel to the trace of the segmented border fault. Virtual inlines generated from the 3D voxel were selected from the foreland towards the hinterland (Fig. 12d–f, respectively). These inlines show the geometry of the footwall shortcut block, along with a fragment of the former segmented half-graben. Gentle anticlines on the hanging-wall of the border fault are indicative for the mild inversion of the segmented extensional fault system. A thin sliver of *syn*-rift sediments in a footwall position is also revealed by these virtual inlines (Fig. 12e). Thrusts can be correlated along strike of the sandbox model and display a characteristic concave-upwards geometry.

4.2.5. Shortening Model 6

This model also consisted on the deformation of the segmented half-graben basin using the same wedge geometry as that of Model 5 (i.e., $\beta = 3°$ and $\alpha = 0°$), but included a 0.4 cm thick layer of viscous polymer. The polymer was laid pinching out in the foreland on a post-rift equivalent stratigraphic position (Fig. 5f). Total shortening was also 15 cm. As shortening started, a first thrust nucleated at the rear of the wedge (i.e., thrust #1) and transferred displacement forwards and upwards along a ramp-flat transition into the viscous polymer layer (i.e., thrust #2). In the early stages of shortening a broad cover anticline was developed above the rearmost thrust, whereas displacement along the viscous detachment formed an emergent thrust front at the polymer's pinch out (Fig. 13a). Further shortening was accommodated by a breaking-forward system of thrusts that affected the sub-polymer layers (i.e., thrusts #4 and #6). Conversely, deformation in the cover was represented by long-lasting deformation at the front, followed by out-of-sequence thrusting and related folding (Fig. 13b).

Contrary to the other shortening models, time-lapse photography has shown that no significant compaction of the sand wedge took place during the early deformation stages (see online Supplementary material). In addition, no evidences of fault reactivation and basin inversion were observed on the top view time-lapse photography during this early deformation. Gentle compaction of the sub-polymer layers took place only after a significant amount of shortening was accommodated by thrusting at the rear and shortening of the overburden along the viscous detachment. Topography scans have also revealed that uplift was mostly concentrated at the rear by the stacking of sub-polymer internal thrust sheets (Fig. 13c). This uplift was responsible for the development of an incipient crestal collapse graben above the frontal culmination of the thrust stack (Fig. 13d). On the other hand, shortening accommodated by the shallow detachment widened the tectonic wedge without generating significant uplift. After cessation of shortening, the uplifted hinterland underwent foreland-ward collapse of the cover units above the polymer layer (Fig. 13d). In this process, the overburden was not fully pierced by the flowing polymer as several welds were developed. These welds are located on top of the half-graben basin and on the frontal culmination of the hinterland thrust stack as shown by the cross-sections (Fig. 13e–g). Extension in the hinterland summit was accommodated by additional down-slope shortening and the associated reactivation of the cover thrust system.

Serial cross-sections have shown that mild inversion of the extensional fault system took place (Fig. 13e–g). Although fault reactivation was preferentially focused on the antithetic faults, the border and synthetic extensional faults were mildly reactivated as well. The observed cross-cutting relationships indicate that reactivation of the extensional faults took place before the imbrication of the segmented half-graben by the sub-polymer thrusts #4 and #6. At the light of the observations made, mild inversion of the extensional faults should have taken place by slip along the basal detachment prior to the break-forward propagation of thrusts #4 and #6. Thrust #4 propagated as a hanging-wall by-pass thrust, whereas thrust #6 propagated as a footwall shortcut thrust.

Virtual depth-slices and inline-sections were generated from the 3D voxel (Fig. 14). These sections illustrate further the geometry of the sub-polymer thrust system and the inversion-related structures. The most important observations derived from the voxel data are: in the upper parts of the model (Fig. 14b), the hanging-wall by-pass thrust

Fig. 14. Virtual sections extracted from the 3D voxel of Model 6. a) Cross-section for reference. b) Depth-slice taking the undeformed post-rift unit (i.e., orange layer) as reference. c) Depth-slice using the middle of the pre-rift sandpack as reference. d) Inline-section showing the inverted half-graben basin and the footwall shortcut block beneath the polymer detachment. e) Inline-section showing the imbricated sub-thrust basin. f) Inline-section showing thrust-stacking relationships and a large polymer weld. Numbers indicate the timing of thrust movement and basin inversion. FW: Footwall. HW: Hanging-wall.

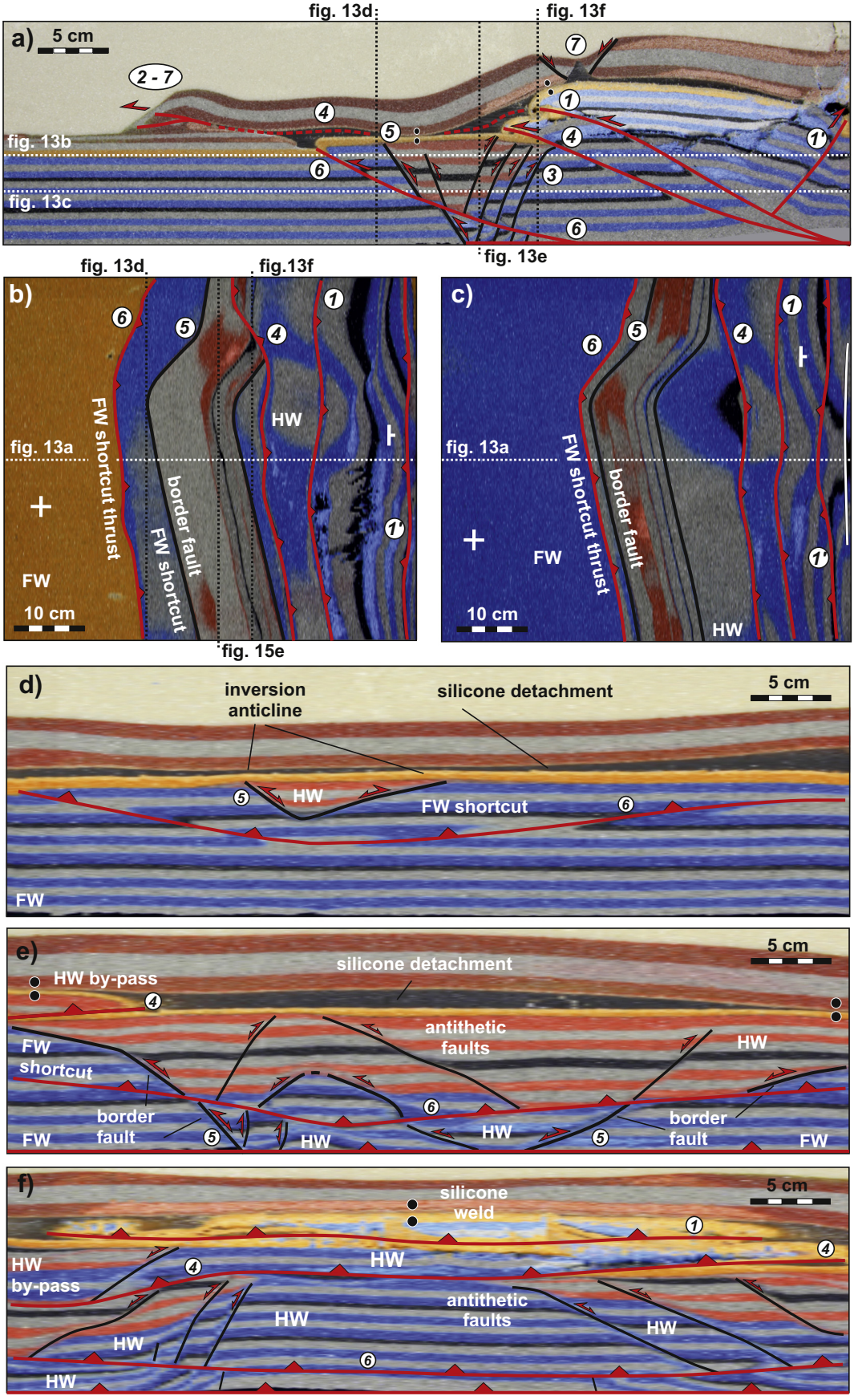
a)
5 cm
2 - 7
fig. 13b
fig. 13c
fig. 13d
fig. 13f
fig. 13e
b)
fig. 13a
FW shortcut thrust
border fault
FW shortcut
HW
FW
10 cm
fig.13f
fig. 15e
c)
fig. 13a
FW shortcut thrust
border fault
FW
HW
10 cm
d)
inversion anticline
silicone detachment
5 cm
HW
FW shortcut
FW
e)
HW by-pass
silicone detachment
5 cm
FW shortcut
antithetic faults
HW
border fault
FW
HW
f)
silicone weld
5 cm
HW by-pass
HW
antithetic faults
HW

(i.e., thrust #4) was only developed at the 90° segment. On the other hand, this thrust runs parallel to the 15° segment of the half-graben, and is oblique to the strike of the 45° segment. In the deeper sections (Fig. 14c), thrust #4 displays a rather linear strike. Thrust #6 developed as a footwall shortcut thrust parallel to the border extensional fault, particularly at the lower parts of the model (Fig. 14c). Inline sections have shown the concave-upwards geometry of the shortcut thrust block with a slice of the imbricated basin (Fig. 14d). Gentle hanging-wall anticlines above the reactivated border extensional fault can also be appreciated. A *syn*-rift repetition is observed associated with the hanging-wall by-pass thrust (i.e., thrust #4), being also located below the polymer detachment (Fig. 14e). The last inline also shows the stacking of thrust #1, #4 and #6 displaying repetitions of pre-rift on top of pre-rift and pre-rift on top of syn-rift. These sections also show the lateral terminations of thrusts sheets and related hanging-wall anticlines (Fig. 14f). Polymer welds have also been revealed above the half-graben basin (Fig. 14a, d), on top of the anticline associated with the hanging-wall by-pass thrust (Figs. 13e and 14e), and at the frontal culmination of the hinterland thrust stack (Figs. 13e and 14f).

5. Discussions

5.1. Extension on segmented half-graben basins

Extension above a segmented velocity discontinuity developed a through-going, segmented border fault along the whole width of the models. On the onset of extension, a fault scarp was formed above the 15° and 90° fault segments to the extension direction; conversely, a monocline was formed in between, over the fault segment striking at 45° to the extension direction. The initial development of secondary antithetic and synthetic extensional faults consisted on short and isolated arrays. As extension continued, antithetic faults lengthened by tip-propagation, forming relay ramps that were eventually breached and linked to form longer strike, through-going faults. Cross sections have shown different spacing and number of antithetic faults (i.e., fault densities) in the hanging-wall layers of the segmented half-graben (Figs. 6 and 7). A larger number of narrowly-spaced antithetic faults were developed at the 90° and 15° segments to the extension direction, whereas a lower number of steeper and widely-spaced faults developed at the central 45° segment. As shown by time-lapse photography, the extensional displacement along the border faults was continuously concentrated within dilatant but discrete deformation zones. Within these zones, sand grains underwent reorganisation and disaggregation, through rolling and translation by sliding along their contacts. This deformation mechanism is comparable to a particulate or granular flow (e.g., Fossen, 2010) and may have accounted for localised strain-softening. A similar deformation mechanism should be expected for the second order antithetic and synthetic faults.

5.2. Reactivation and inversion of segmented sub-thrust basins

The experimental set up provided a good comparison with natural collisional foredeep settings as it effectively simulated the steepening of fault systems in foreland plates as fold-and-thrust belts propagate. According to theoretical and field studies, the steepening of these faults should significantly impact their easiness for frictional reactivation,

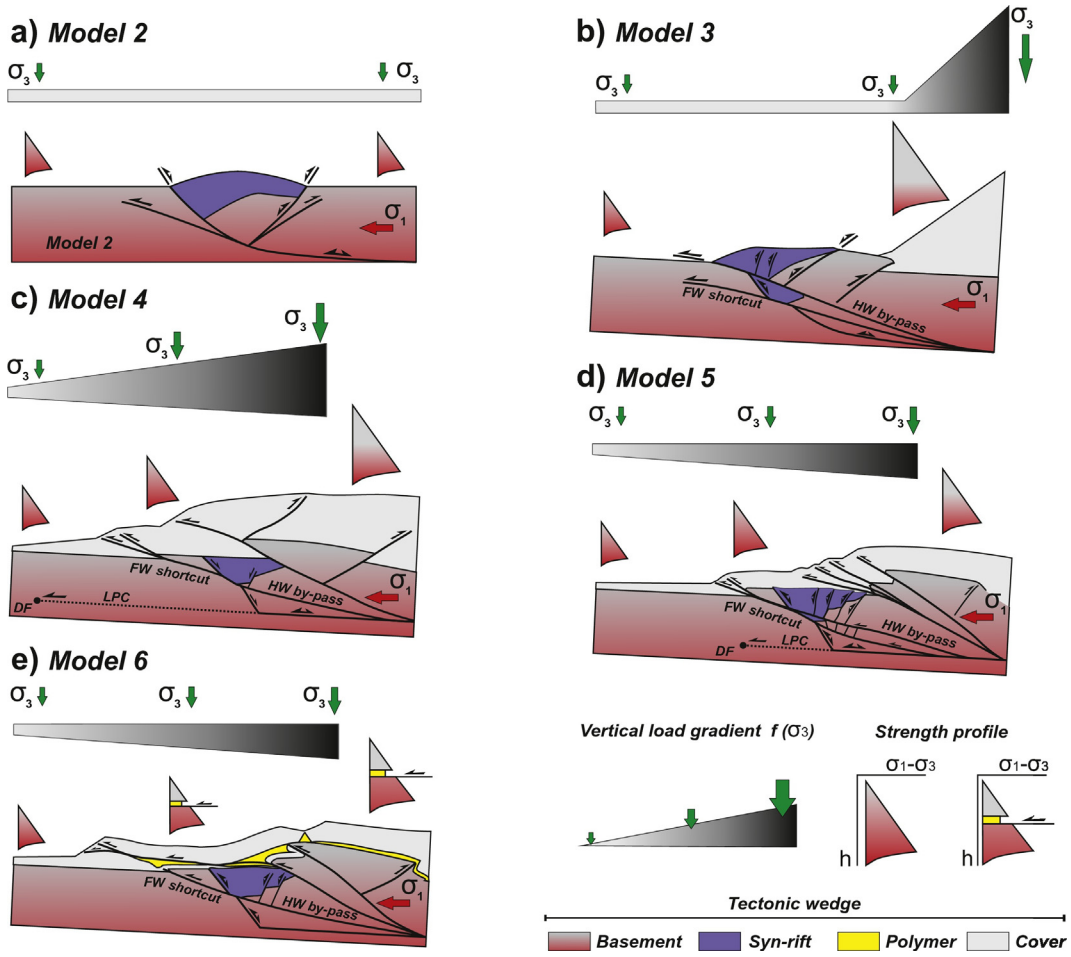

Fig. 15. Conceptual summary of the modelling results expressed as a function of the vertical load gradient of the wedge's minimum vertical compressive stress (σ3) and the integrated strength profile. DF: deformation front. LPC: layer-parallel compaction. σ1-σ3 = differential stress. h: wedge's thickness. FW: Footwall. HW: Hanging-wall.

particularly in a dip slip reactivation mode (e.g., Jaeger and Cook, 1979; Etheridge, 1986; Gillcrist et al., 1987). In this study, time-lapse photography has shown that, with the exception of Model 4, reactivation of the extensional fault system was mild but affected all models equally along strike, independently of their steep dips. In fact, no substantial differences on the easiness of reactivation regarding of the obliquity between the pre-existing faults (i.e., the 15°, 45° and 90° segments) and the direction of shortening have been found. The obtained modelling results are in disagreement with those reported by Brun and Nalpas (1996) stating the fundamental role of obliquity in the easiness for reactivation.

In all the shortening models, slip along the basal detachment produced different degrees of sand compaction before the onset of thrusting and in between pulses of thrust propagation. For granular analogue materials, Koyi et al. (2004) referred to layer-parallel compaction as the main modality of layer-parallel shortening. The shortening models carried out for this study have shown that the reactivation of the extensional fault system was associated with such layer-parallel compaction, also taking place before the onset of thrusting and in between thrust propagation pulses. The reactivation of the segmented extensional fault system may have been favoured by the dilatant nature of the inherited, strain-softened extensional fault zones. In this sense, Eisenstadt and Sims (2005) reported mild reactivation of a half-graben border fault in relation with the preservation of fault zone dilatancy. A localised loss in the frictional strength (i.e., strain-softening) associated with these discrete fault zones is the most reasonable way to explain how these were reactivated independently of their steep dips and their obliquity with the direction of shortening. In the models carried out, the footwall shortcut thrusts developed broadly parallel to the master border fault (see depth-slices in Figs. 12 and 14), and thus indicate a certain degree of control in the development of thrust systems imposed by the inherited fault zones.

Upon shortening, the models underwent different amounts of layer-parallel compaction, fault-reactivation, thrust propagation and thrust-related folding strictly as a function of the pre-shortening configuration of the tectonic wedge (Fig. 5). The distinctly tapered wedges (i.e., α and β angles) affected the reactivation and the incorporation of the sub-thrust basin by imposing a vertical-load gradient on the buried half-graben basins and by their integrated strength profile, which included the strain-softened extensional fault zones and the presence or absence of a shallow viscous detachment. More specifically, the post-rift equivalent 'stratigraphic' position of the viscous layer allowed for the decoupling of deformation between the segmented half-graben and its cover. When the half-graben basin was close to the surface (i.e., Models 2 and 3), inversion of the extensional fault system took place early in the deformation sequence (Figs. 8 and 9). In these two models, the absence of any substantial vertical load (Model 2) or a large vertical load gradient (Model 3) under a dominantly compressional stress field, favoured the reactivation of the extensional fault system during layer-parallel compaction and the earliest onset of thrust propagation, respectively (Fig. 15a, b). When the half-graben basin was covered by a thick wedge (i.e., Model 4, Fig. 10), only the border antithetic fault underwent very limited reactivation by back-thrusting (Fig. 15c). Although the layer-parallel shortening propagated ahead of the half-graben basin, it seems that the large vertical load imposed by the thick wedge hampered or avoided the reactivation the extensional fault array. On the other hand, when the half-graben basin was covered by a thin wedge (i.e., Model 5; Fig. 11), reactivation of the extensional faults took place late in the deformation sequence, following the breaking-forward propagation of thrusting (Fig. 15d). When the half-graben basin was covered by a thin wedge involving a viscous detachment (i.e., Model 6; Fig. 13), the propagation of thrusting was quickly transferred along a thrust flat towards the foreland overriding the half-graben basin (Fig. 15e). In Model 6, fault reactivation and basin inversion only took place after the propagation of deformation along the viscous polymer, and hence, later than in the other models.

5.3. Comparison to the Höflein high

A comparison between Model 6 and the Höflein high from the subthrust of the Alpine-Carpathian fold-and-belt (Fig. 16) has been carried out. Basin inversion in the Alpine-Carpathian fold-and-thrust belt took place in the latest stages of shortening, following the emplacement of a cover thin-skinned thrust system. In Austria, the shallow units of the strongly imbricated Rhenodanubian Flysch are folded into a broad open syncline whereas the Alpine Basal Thrust is folded into an open anticline over the Höflein high (Fig. 16a). These features indicate that the compressional reactivation of the faults in the crystalline basement took place after the emplacement of the shallow, thin-skinned thrust system. Model 6 showed a similar evolution as shown by a fast propagation of slip in the cover that overrode the half-graben along the viscous detachment. This was followed by basin inversion and thrust propagation in the layers beneath the viscous detachment, folding the cover thrust-related folds. In this model, the sequence of basement-involved deformation started with the mild inversion of the extensional fault system in relation with slip along the frictional basal detachment and the associated layer-parallel compaction. In a similar fashion to the natural prototype, reactivation of the inherited extensional fault system was mild, and much of the shortening was accomplished afterwards by the formation and propagation of a new thrust system in the form of footwall shortcut thrusts.

5.4. Inheritance in natural systems

The reactivation of inherited fault systems is inherent to the concept of basin inversion. In natural systems though, a series of competing geological processes may impact positively or negatively (i.e., enhance or decrease) the role of inheritance. In shallow crustal levels, reactivation is controlled by frictional processes which depend upon the cohesion,

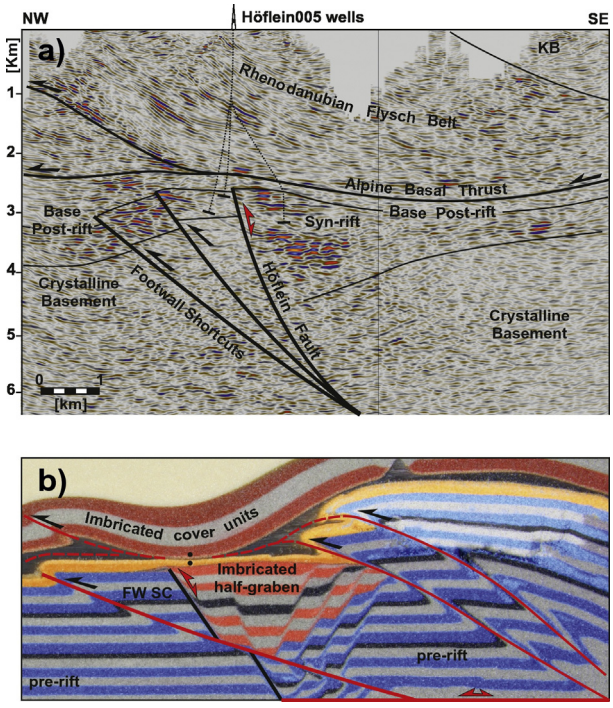

Fig. 16. Comparison between the Höflein high and results from Model 6. a) NW-SE striking seismic profile (i.e., approximately parallel to the direction of early Miocene shortening and perpendicular to the basement fault trend). See Fig. 3a for location of the profile. Wells are projected. KB: Korneuburg Basin. b) Cross-section along Model 6. FW SC: Footwall shortcut.

the coefficient of friction, fault orientation (i.e., amount of dip and direction of dip), as well as the pore-fluid pressure (Jaeger and Cook, 1979). Fault-weakening process involving chemical reactions between circulating fluids and the host fault-rocks can induce the formation of low-friction phyllosilicate-rich mineral assemblages (e.g., Gueydan et al., 2003). Therefore, fault-weakening may allow faults to sustain significant slip under theoretically anomalous orientations in respect to the active stress field (e.g., Colletini et al., 2009). These processes may seal faults but otherwise reinforce the role of inheritance, favouring their frictional reactivation. Alternatively, precipitation of hydrothermal fluids, quenching of melts, or widespread brecciation and fracturing within fault zones may favour their frictional lock-up by increasing the coefficient of friction and cohesion (e.g., Etheridge, 1986; Cox et al., 2001). These strain-hardening mechanisms may delocalise deformation and therefore reduce the role of inheritance in natural systems.

6. Conclusions

The experimental results indicate that the key parameters controlling the inversion of sub-thrust extensional basins are the wedges' vertical load and its pre-shortening integrated strength profile (Fig. 15). Large vertical loads hamper the inversion of deeply buried basins, whereas lower vertical loads or high vertical load gradients may favour the inversion of sub-thrust basins by fault reactivation and thrust propagation. Integrated strength profiles included the presence of discrete, strain-softened fault zones inherited from the extensional phases, as well as the presence/absence of viscous layers. The obliquity between the shortening direction and the orientation of pre-existing faults seemed less important than the vertical load distribution and the fault zone strength for the inversion of sub-thrust basins. Natural processes that modify the regional slope of tectonic wedges (i.e., such as erosion and sedimentation) should therefore have strong impacts on the likelihood and timing of sub-thrust basin inversion.

Fault reactivation occurred during layer-parallel compaction before and in between thrust propagation pulses associated with slip along the basal detachment of the system. Widespread, laterally extensive (i.e., post-rift) viscous layers may favour an early decoupling between cover and basement during shortening, with basin inversion taking place after the imbrication of cover units. A certain control imposed by the inherited extensional architecture in the formation of shortcut thrusts is also suggested by the results. Sandbox analogue modelling coupled with time-lapse photography, white-light topography scans, and serial sections from imaged-based 3D voxels have revealed as great tools for the better understanding of basin inversion in tectonic wedges.

Acknowledgements

This is a contribution of the Institut de Recerca Geomodels and the Geodinàmica i Analisi de Conques research group (2014SGR467SGR) from the Agència de Gestió d'Ajuts Universitaris i de Recerca (AGAUR) and the Secretaria d'Universitats i Recerca del Departament d'Economia i Coneixement de la Generalitat de Catalunya. The Geomodels Analog Modelling Laboratory was supported by a Scientific Infrastructure (UNBA08-4E-006) co-funded by the European Regional Development Fund of the *Ministerio de Ciencia e Innovación* of the Spanish Government and Statoil. PG acknowledges financial support, data supply and permission to publish from OMV Exploration and Production GmbH (Project FBG307451). Financial support from SALTECRES (CGL2014-54118-C2-1-R) project is also acknowledged. The final version of this manuscript benefited from the constructive reviews of Dr. João C. Duarte (Univ. of Lisbon), Dr. Stephane Dominguez (Univ. of Montpelier) as well as the Editor-in-Chief Dr. Philippe Agard (Univ. Université Pierre et Marie Curie, Sorbonne Universités, Paris). Modelling software Petrel by Schlumberger and Skua by Paradigm were used for seismic interpretation, 3D model building and analysis of laser-scanner data. Move restoration software by Midland Valley was used for cross-section construction.

Appendix A. Supplementary data

Supplementary data to this article can be found online at http://dx.doi.org/10.1016/j.tecto.2017.02.022.

References

Adam, J., Urai, J., Wieneke, B., Oncken, O., Pfeiffer, K., Kukowski, N., Lohrmann, J., Hoth, S., van der Zee, W., Schmatz, J., 2005. Shear localisation and strain distribution during tectonic faulting - new insights from granular flow experiments and high-resolution optical image correlation techniques. J. Struct. Geol. 27, 283–301.

Bartholomew, I.D., Peters, J.M., Powell, C.M., 1993. Regional structural evolution of the North Sea: oblique slip and the reactivation of basement lineaments. Petroleum Geology Conference series 4. Geological Society of London:pp. 1109–1112. http://dx.doi.org/10.1144/0041109.

Beidinger, A., Decker, K., 2014. Quantifying Early Miocene in-sequence and out-of-sequence thrusting at the Alpine-Carpathian junction. Tectonics 33, 222–252.

Bonini, M., 2007. Deformation patterns and structural vergence in brittle-ductile thrust wedges: an additional analogue modelling perspective. J. Struct. Geol. 29, 141–158.

Bonini, M., Sani, F., Antonielli, B., 2012. Basin inversion and contractional reactivation of inherited normal faults: a review based on previous and new experimental models. Tectonophysics 522–523, 55–88.

Bonnet, C., Malavieille, J., Mosar, J., 2007. Interactions between tectonics, erosion, and sedimentation during the recent evolution of the Alpine orogen: analogue modelling insights. Tectonics 26. http://dx.doi.org/10.1029/2006TC002048.

Brun, J.P., Nalpas, T., 1996. Graben inversion in nature and experiments. Tectonics 15, 677–687.

Buchanan, P.G., McClay, K.R., 1991. Sandbox experiments of inverted listric and planar fault systems. In: Cobbold, P.R. (Ed.), Experimental and Numerical Modelling of Continental Deformation: Tectonophysics. 188, pp. 97–115.

Buchanan, P.G., McClay, K.R., 1992. Experiments on basin inversion above reactivated domino faults. Mar. Pet. Geol. 9, 486–500.

Buiter, S., Pfiffner, O.A., Beaumento, C., 2009. Inversion of extensional sedimentary basins: a numerical evaluation of the localization of shortening. Earth Planet. Sci. Lett. 288, 492–504.

Carrera, N., Muñoz, J.A., 2013. Thick-skinned tectonic style resulting from the inversion of previous structures in the southern Cordillera Oriental (NW Argentine Andes). In: Nemčok, M., Mora, A., Cosgrove, J.W. (Eds.), Thick-skinned Dominated Orogens: From Initial Inversion to Full Accretion. 377. Geological Society of London, pp. 119–140 (Special Publication).

Chapple, W.M., 1978. Mechanics of Thin-Skinned Fold-and-Thrust Belts. Geol. Soc. Am. Bull. 89, 1189–1198.

Colletini, C., Niemeijer, A., Viti, C., Marone, C., 2009. Fault zone fabric and fault weakness. Nature 462:907–910. http://dx.doi.org/10.1038/nature08585.

Couzens-Schultz, B.A., Vendeville, B.C., Wiltschko, D.V., 2003. Duplex style and triangle zone formation: insights from sandbox analogue physical modelling. J. Struct. Geol. 25, 1623–1644.

Cox, S.F., Knacksedt, M.A., Braun, J., 2001. Principles of structural control on permeability and fluid flow in hydrothermal systems. In: Richards, J.P., Tosdal, R.M. (Eds.), Structural Controls on Ore Genesis. Reviews in Economic Geology, Reviews 14. Society of Economic Geologists Inc., Littleton, USA, pp. 1–22.

D'Adda, P., Longoni, R., Magistroni, C., Meda, M., Righetti, F., Cavozzi, C., Nestola, Y., Storti, F., 2017. Extensional reactivation of a deep transpressional architecture: insights from sandbox analogue modeling applied to the Val d'Agri basin (Southern Apennines, Italy). Interpretation 5 (1):SD55–SD66. http://dx.doi.org/10.1190/INT-2016-0078.1.

Davy, P., Cobbold, P.R., 1991. Experiments of shortening of a 4-layer model of the continental lithosphere. Tectonophysics 188, 1–25.

Decker, K., Peresson, H., 1996. Tertiary kinematics in the Alpine-Carpathian-Pannonian system: links between thrusting, transform faulting and crustal extension. In: Wessely, G., Liebl, W. (Eds.), Oil and Gas in Alpidic Thrustbelts and Basins of Central and Eastern Europe. 5. Geological society, London, pp. 69–77 (EAGE Special Publication).

Del Ventisette, C., Montanari, D., Sani, F., Bonini, M., 2006. Basin inversion and fault reactivation in laboratory experiments. J. Struct. Geol. 28, 2067–2083.

Dell'Ertole, D., Schellart, W.P., 2013. The development of sheat folds in viscously stratified materials in simple shear conditions: an analogue approach. J. Struct. Geol. 56, 129–141.

Di Domenica, A., Bonini, L., Calamita, F., Toscani, G., Galuppo, C., Seno, S., 2014. Analogue modeling of positive inversion tectonics along differently oriented pre-thrusting normal faults: an application to the Central-Northern Apennines of Italy. Geol. Soc. Am. Bull. http://dx.doi.org/10.1130/B31001.1.

Dooley, T.P., Jackson, M.P.A., Hudec, M.R., 2009. Inflation and deflation of deeply buried salt stocks during lateral shortening. J. Struct. Geol. 31, 582–600.

Dubois, A., Odonne, F., Massonnat, G., Lebourg, T., Fabre, R., 2002. Analogue modelling of fault reactivation: tectonic inversion and oblique remobilization of grabens. J. Struct. Geol. 24, 1741–1752.

Eisenstadt, G., Sims, D., 2005. Evaluating sand and clay models: do rheological differences matter? J. Struct. Geol. 27, 1399–1412.

Eisenstadt, G., Withjack, M.O., 1995. Estimating inversion: results from clay models. In: Buchanan, J.G., Buchanan, P.G. (Eds.), Basin Inversion. Geological Society of London Special Publication 88, pp. 119–136.

El Harfi, A., Guiraud, M., Lang, J., 2006. Deep-rooted "thick skinned" model for the High Atlas Mountains (Morocco). Implications for the structural inheritance of the southern Tethys passive margin. J. Struct. Geol. 28, 1958–1976.
Erdős, Z., Huismans, R.S., van der Beek, P., Thieulot, C., 2014. Extensional inheritance and surface processes as controlling factors of mountain belt structure. J. Geophys. Res. Solid Earth 119:9042–9061. http://dx.doi.org/10.1002/2014JB011408.
Etheridge, M.A., 1986. On the reactivation of extensional fault systems. Philos. Trans. R. Soc. A Math. Phys. Eng. Sci. 317:179–194. http://dx.doi.org/10.1098/rsta.1986.0031.
Faulds, J.E., Varga, R.J., 1998. The role of accommodation zones and transfer zones in the regional segmentation of extended terranes. In: Faulds, J.E., Stewart, J.H. (Eds.), Accommodation Zones and Transfer Zones: The Regional Segmentation of the Basin and Range Province. 323. Geological Society of America, Boulder, pp. 1–46 (Special Paper).
Fodor, L., 1995. From transpression to transtension: Oligocene-Miocene structural evolution of the Vienna Basin and the East-Alpine-Western Carpathian junction. Tectonophysics 242, 151–182.
Fossen, H., 2010. Deformation bands formed during soft-sediment deformation: observations from SE Utah. Mar. Pet. Geol. 27, 215–222.
Fossen, H., Fazli Khani, H., Faleide, J.I., Ksienzyk, A.K., Dunlap, W.J., 2016. Post-Caledonian extension in the West Norway-northern North Sea region: the role of structural inheritance. In: Childs, C., Holdsworth, R.E., Jackson, C.A.-L., Manzocchi, T., Walsh, J.J., Yielding, G. (Eds.), The Geometry and Growth of Normal Faults. 439. Geological Society, London. http://dx.doi.org/10.1144/SP439.6 (Special Publications).
Gawthorpe, R.L., Hurst, J.M., 1993. Transfer zones in extensional basins: their structural style and influence on drainage development and stratigraphy. J. Geol. Soc. 150 (6), 1137–1152.
Gibbs, A.D., 1984. Structural evolution of extensional basin margins. J. Geol. Soc. Lond. 141, 609–620.
Gillcrist, R., Coward, M.P.A., Mugnier, J.L., 1987. Structural inversion and its controls: examples from the Alpine foreland and the French Alps. Geodin. Acta 1, 5–34.
Granado, P., Thöny, W., Carrera, N., Gratzer, O., Strauss, P., Muñoz, J.A., 2016. Basement-involved reactivation in fold-and-thrust belts: the Alpine-Carpathian Junction (Austria). Geol. Mag. 153 (5-6), 1110–1135.
Graveleau, F., Malavieille, J., Dominguez, S., 2012. Experimental modelling of orogenic wedges: a review. Tectonophysics 538-540, 1–66.
Gueydan, F., Leroy, Y.M., Jolivet, L., Agard, P., 2003. Analysis of continental midcrustal strain localization induced by reaction softening and microfracturing. J. Geophys. Res. 108 (B2):2064. http://dx.doi.org/10.1029/2001JB000611.
Holdsworth, R.E., Stewart, M., Imber, J., Strachan, R.A., 2001. The structure and rheological evolution of reactivated continental fault zones: a review and case study. In: Miller, J.A., Holdsworth, R.E., Buick, I.S., Hand, M. (Eds.), Continental Reactivation and Reworking. 184. Geological Society of London, pp. 115–137 (Special Publication).
Hölzel, M., Decker, K., Zámolyi, A., Strauss, P., Wagreich, M., 2010. Lower Miocene structural evolution of the central Vienna Basin (Austria). Mar. Pet. Geol. 27, 666–681.
Horvárth, F., Bada, G., Szafián, P., Tari, G., Ádám, A., Cloetingh, S., 2006. Formation and deformation of the Pannonian Basin: constraints from observational data. In: Gee, D.G., Stephenson, R.A. (Eds.), European Lithosphere Dynamics. 32. Geological Society, Memoirs, London, pp. 191–206.
Hubbert, M.K., 1951. Mechanical basis for certain geological structures. Geol. Soc. Am. Bull. 62, 355–372.
Huismans, R.S., Podladchikov, Y.Y., Cloetingh, S., 2001. Dynamic modelling of the transition from passive to active rifting, application to the Pannonian Basin. Tectonics 20: 1021–1039. http://dx.doi.org/10.1029/2001TC900010.
Huyghe, P., Mugnier, J.L., 1995. A comparison of inverted basins of the Southern North Sea and inverted structures of the external Alps. In: Buchanan, J.G., Buchanan, P.G. (Eds.), Basin Inversion. 88. Geological Society of London, pp. 339–354 (Special Publication).
Jaeger, G.D., Cook, N.G.W., 1979. Fundamentals of Rock Mechanics. Chapman & Hill Ltd, London (515pp).
Koopman, A., Speksnijder, A., Horsfield, W.T., 1987. Sandbox models of inversion tectonics. Tectonophysics 137, 379–388.
Koyi, H.A., Sans, M., Teixell, A., Cotton, J., Zeyen, H., 2004. The significance of penetrative strain in the restoration of shortened layers—insights from sand models and the Spanish Pyrenees. In: McClay, K.R. (Ed.), Thrust Tectonics and Hydrocarbon Systems: AAPG Memoir. 82, pp. 207–222.
Lohrmann, J., Kukowski, N., Adam, J., Oncken, O., 2003. The impact of analogue material properties on the geometry, kinematics and dynamics of convergent sand wedges. J. Struct. Geol. 25, 1691–1711.
Malavieille, J., 2010. Impact of erosion, sedimentation, and structural heritage on the structure and kinematics of orogenic wedges: analogue models and case studies. GSA Today 20, 4–10.
McClay, K.R., 1989. Analogue models of inversion tectonics. In: Cooper, M.A., Williams, G.D. (Eds.), Inversion Tectonics. 44. Geological Society of London, pp. 41–62 (Special Publication).
McClay, K.R., 1995. The geometries and kinematics of inverted fault systems: a review of analogue model studies. In: Buchanan, J.G., Buchanan, P.G. (Eds.), Basin Inversion. 88. Geological Society of London, pp. 97–118 (Special Publication).
McClay, K.R., 1996. Recent advances in analogue modeling: uses in section interpretation and validation. In: Buchanan, P.G., Nieuwland, D.A. (Eds.), Modern Developments in Structural Interpretation, Validation and Modelling. 99. Geological Society of London, pp. 201–225 (Special Publications).
Mencos, J., Carrera, N., Muñoz, J.A., 2015. Influence of half-graben basin geometry on the subsequent post-rift sedimentation and basin inversion: the Organyà Basin and the Bóixols thrust sheet (south Central Pyrenees). Tectonics 34:1452–1474. http://dx.doi.org/10.1002/2014TC003692.
Morley, C.K., 2010. Stress re-orientation along zones of weak fabrics in rifts: an explanation for pure extension in 'oblique' rift segments? Earth Planet. Sci. Lett. 297: 667–673. http://dx.doi.org/10.1016/j.epsl.2010.07.022.
Morley, C.K., Nelson, R.A., Patton, T.L., Munn, S.G., 1990. Transfer zones in the East African rift system and their relevance to hydrocarbon exploration in rifts (1). AAPG Bull. 74 (8), 1234–1253.
Muñoz, J.A., 2002. Alpine Tectonics I: the alpine system north of the Betic Cordillera tectonic setting; the Pyrenees. In: Gibbons, W., Moreno, T. (Eds.), The Geology of Spain. Geological Society, London, pp. 370–385.
Nilfouroushan, F., Pysklywec, R., Cruden, A., Koyi, H., 2013. Thermal-mechanical modelling of salt-based mountain belts with pre-existing basement faults: application to the Zagros fold and thrust belt, southwest Iran. Tectonics 32:1212–1226. http://dx.doi.org/10.1002/tect.20075.
Panien, M., Schreus, G., Pfiffner, A.O., 2005. Sandbox experiments on basin inversion: testing the influence of basin orientation and basin fill. J. Struct. Geol. 27, 433–445.
Ratschbacher, L., Frisch, W., Linzer, H.G., Merle, O., 1991. Lateral extrusion in the Eastern Alps, 2. Structural analysis. Tectonics 10, 257–271.
Roure, F., Colletta, B., 1996. Cenozoic inversion structures in the foreland of the Pyrenees and Alps. In: Ziegler, P.A.H., Horvath, F. (Eds.), Peri-Tethys Memoir 2: Structure and Prospects of the Alpine Basins and Forelands, 170. Mémoires Muséum National d'Histoire Naturelle, Paris, pp. 173–209.
Santolaria, P., Vendeville, B.C., Graveleau, F., Soto, R., Casas-Sainz, A., 2015. Double evaporitic décollements: influence on pinch-out overlapping in experimental thrust wedges. J. Struct. Geol. 76, 35–51.
Sassi, W., Colletta, B., Balé, P., Paquereau, T., 1993. Modelling of structural complexity in sedimentary basins: the role of pre-existing faults in thrust tectonics. Tectonophysics 226, 97–112.
Schellart, W.P., 2000. Shear test results for cohesion and friction coefficients for different granular materials: scaling implications for their usage in analogue modelling. Tectonophysics 324, 1–16.
Schellart, W.P., Strak, V., 2016. A review of analogue modelling of geodynamic processes: approaches, scaling, materials and quantification, with an application to subduction experiments. J. Geodyn. 100, 7–32.
Schmid, S.M., Fügenshchuh, B., Kissling, E., Schuster, R., 2004. Tectonic map and overall architecture of the Alpine orogen. Eclogae Geol. Helv. 97, 93–117.
Schreurs, G., Buiter, S.J.H., Boutelier, D., Corti, G., Costa, E., Cruden, A.R., Daniel, J.-M., Hoth, S., Koyi, H.A., Kukowski, N., Lohrmann, J., Ravaglia, A., Schlische, R.W., Withjack, M.O., Yamada, Y., Cavozzi, C., Delventisette, C., Elder Brady, J.A., Hoffmann-Rothe, A., Mengus, J.-M., Montanari, D., Nilforoushan, F., 2006. Analogue benchmarks of shortening and extension experiments. In: Buiter, S.J.H., Schreurs, G. (Eds.), Analogue and Numerical Modelling of Crustal-scale Processes. 253. Geological Society of London, pp. 1–27 (Special Publication).
Scisciani, V., 2009. Styles of positive inversion tectonics in the Central Apennines and in the Adriatic foreland: implications for the evolution of the Apennine chain (Italy). J. Struct. Geol. 31, 1276–1294.
Shiner, P., Beccacini, A., Mazzoli, S., 2004. Thin-skinned versus thick-skinned structural models for Apulian carbonate reservoirs: constraints from the Val d'Agri Fields, S. Apennines, Italy. Mar. Pet. Geol. 21, 805–827.
Smit, J.H.W., Brun, J.P., Sokoutis, D., 2003. Deformation of brittle-ductile thrust wedges in experiments and nature. J. Geophys. Res. 108. http://dx.doi.org/10.1029/2002JB002190.
Storti, F., McClay, K., 1995. Influence of syntectonic sedimentation on thrust wedges in analogue models. Geology 23 (11), 999–1002.
Strauss, P., Wagreich, M., Decker, K., Sachsenhofer, R.F., 2001. Tectonics and sedimentation in the Fohnsdorf-Seckau basin (Miocene-Austria): from a pull-apart basin to a half-graben. Int. J. Earth Sci. 90, 549–559.
Tomek, Č., Hall, J., 1993. Subducted continental margin imaged in the Carpathians of Czechoslovakia. Geology 21, 535–538.
Vially, R., Letouzey, J., Benard, F., Haddadi, N., Desforges, G., Askri, H., Boudjema, A., 1994. Basin inversion along the North African Margin: the Saharan Atlas (Algeria). In: Roure, F. (Ed.), Peri-Tethyan Platforms Editions Technip, Paris, pp. 79–120.
Wagner, L.R., 1998. Tectono-stratigraphy in the Molasse Foredeep of Salzburg, Upper and Lower Austria. In: Mascle, A., Puigdefàbregas, C., Luterbacher, H.P., Fernàndez, M. (Eds.), Cenozoic Foreland Basins of Western Europe. 134. Geological Society of London, pp. 339–369 (Special Publication).
Weijermars, R., Jackson, M.P.A., Vendeville, B.C., 1993. Rheological and tectonic modeling of salt provinces. Tectonophysics 217, 143–174.
Weijermars, R., Schmeling, H., 1986. Scaling of Newtonian and non-Newtonian fluid dynamics without inertia for qualitative modelling of rock flow due to gravity. Phys. Earth Planet. Inter. 43, 316–330.
Wernicke, B., Burchfield, B.C., 1982. Models of extensional tectonics. Inaugural meeting of the Canadian Tectonics Group. 4, pp. 105–115.
Wessely, G., 1987. Mesozoic and Tertiary evolution of the Alpine-Carpathian foreland in eastern Austria. Tectonophysics 137, 45–49.
Williams, G.D., Powell, C.M., Cooper, M.A., 1989. Geometry and kinematics of inversion tectonics. In: Cooper, M.A., Williams, G.D. (Eds.), Inversion Tectonics. 44. Geological Society of London, pp. 3–15 (Special Publication).
Yamada, Y., McClay, K.R., 2004. 3-D analog modelling of inversion thrust structures. In: McClay, K.R. (Ed.), Thrust Tectonics and Hydrocarbon Systems. AAPG Memoir 82, pp. 276–301.
Ziegler, P.A., Cloetingh, S., Guiraud, R., Stampfli, G., 2001. Peri-Tethyan platforms: constraints on dynamics of rifting and basin inversion. In: Ziegler, P.A., Cavazza, W., Robertson, A.H.F., Crasquin-Soleau, S. (Eds.), Peri-Tethys Memoir 6: Peri-Tethyan Rift/Wrench Basins and Passive Margins Mém. Mus. Nat. Hist. Nat. 186, pp. 9–49.
Zimmer, W., Wessely, G., Wessely, G., Liebl, W., 1996. Exploration results in thrust and sub-thrust complexes in the Alps and below the Vienna Basin in Austria. Oil and Gas in Alpidic Thrustbelts and Basins of Central and Eastern Europe. 5. Geological Society, London, pp. 81–107 (EAGE Special Publication).